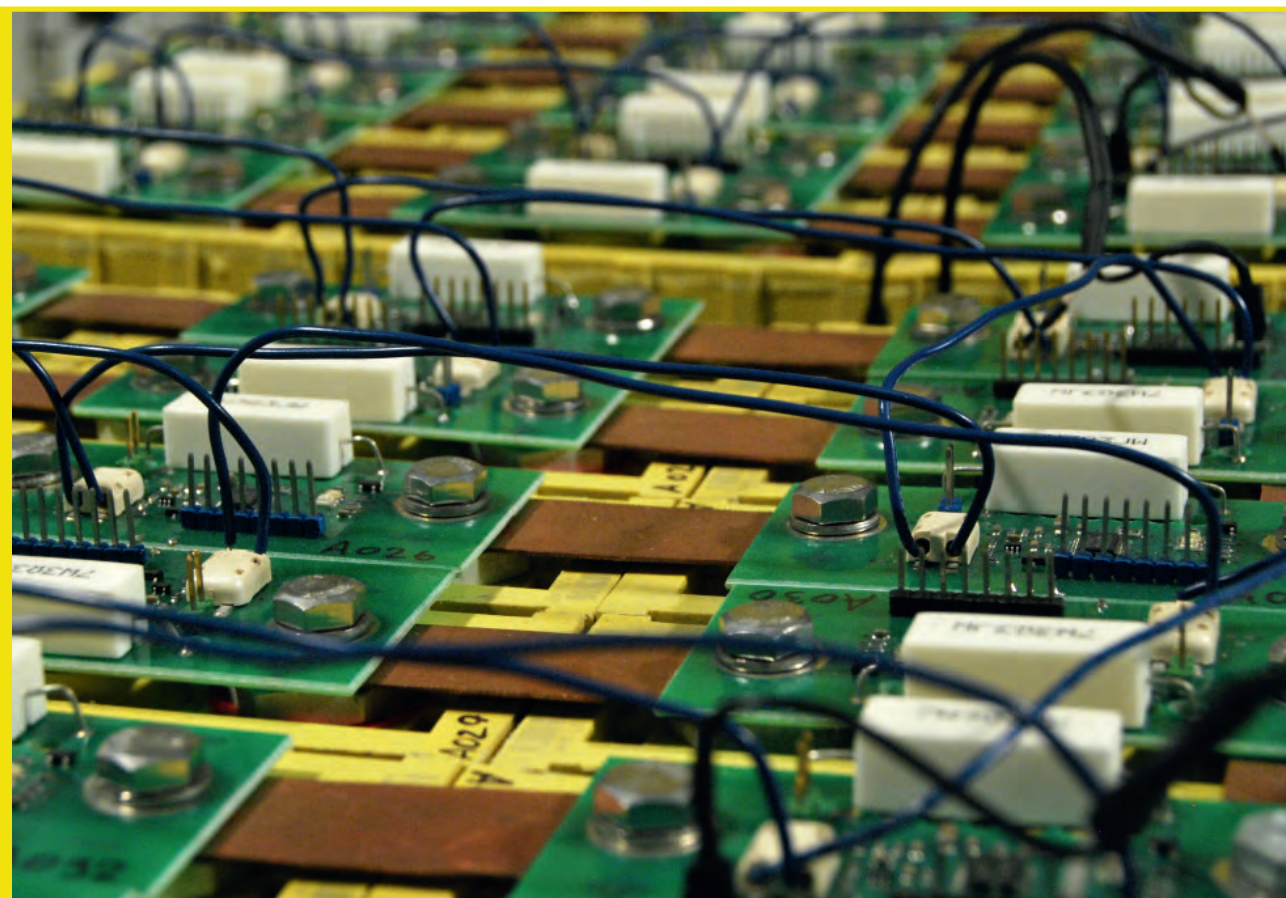


**Kristaps Vītols**

**RESEARCH AND DEVELOPMENT OF BATTERY  
PACKS AND THEIR BALANCING METHODS  
FOR PERSONAL MOBILITY VEHICLES**

Doctoral Thesis



**RIGA TECHNICAL UNIVERSITY**  
Faculty of Electrical and Environmental Engineering  
Institute of Industrial Electronics and Electrical Engineering

**Kristaps Vītols**

Doctoral Student of Study Programme “Computerised Control of Electrical Technologies”

**RESEARCH AND DEVELOPMENT OF  
BATTERY PACKS AND THEIR BALANCING  
METHODS FOR PERSONAL MOBILITY  
VEHICLES**

**Doctoral Thesis**

Scientific supervisor  
Professor Dr. sc. ing.  
Ilja Galkins

RTU Press  
Riga 2022

## ACKNOWLEDGEMENT

I dedicate this work to my family which provided generous support and inspiration throughout whole research process.

This work has been supported by the European Social Fund within the project “Support for the implementation of doctoral studies at Riga Technical University”



This work has been supported by the European Social Fund project “„Development of the Academic Personnel of Riga Technical University" No. 8.2.2.0/18/A/017

## **ABSTRACT**

This Work is devoted to research and development of vehicle traction batteries and their management systems. As the battery technology is reaching maturity, personal mobility vehicles are becoming more popular. Within this Work, three battery systems have been developed: two for personal mobility vehicles and one for stationary energy storage.

To achieve the set goals, existing vehicle battery packs were analyzed as well as the lithium-ion technology itself. Research of battery cell balancing scientific literature was carried out and a novel three group classification has been proposed. Two of the reviewed balancing methods were selected for further analysis, prototype design and experimental verification. The two methods were: switched resistor balancing method and multi secondary winding transformer method. After successful initial testing, both methods were combined in one new mixed two-layer balancing topology, which is capable to improve balancing performance of reference switched resistor balancing topology under favorable conditions. The developed balancing prototypes have been implemented in lithium-ion batteries both for research project purposes and for educational processes.

The Doctoral Thesis has been written in English. It consists of an Introduction; 7 Chapters; Conclusion; 86 figures; 7 tables; 5 appendices; the total number of pages is 165, including appendices. The Bibliography contains 220 titles.

## ANOTĀCIJA

Šis Darbs ir veltīts transportlīdzekļu bateriju un to pārvaldības sistēmu izpētei un izstrādei. Attīstoties bateriju tehnoloģijai, aizvien populārāki kļūst individuālās mobilitātes transportlīdzekļi. Šī darba ietvaros tika izveidotas trīs bateriju sistēmas: divas individuālās mobilitātes transportlīdzekļiem un viena stacionārajai enerģijas uzkrāšanai.

Lai sasniegtu rezultātus, Darba ietvaros tika analizētas esošās transportlīdzekļu bateriju sistēmas, kā arī pati litija jonu bateriju tehnoloģija. Tika veikta bateriju elementu balansēšanas metožu izpēte, balstoties uz kuru, tika izveidota šo metožu klasifikācija. Izmantojot apgūtās bateriju balansēšanas metodes, tika analizētas, praktiski izveidotas un pārbaudītas divas metožu realizācijas: šuntējošā rezistora balansēšanas metode un vairāku sekundāro tinumu transformatora balansēšanas metode. Abas metodes tika apvienotas vienā jaunā jauktā divpakāpju balansēšanas-lādēšanas risinājumā, kurš pie labvēlīgiem apstākļiem ir spējīgs uzlabot vispārējo baterija balansēšanas veikspēju attiecībā pret vienkāršu šuntējošā rezistora balansēšanu. Izveidotie balansēšanas risinājumi tika pielietoti litija jonu bateriju darbināšanai, gan pētniecības projektu, gan mācību procesa ietvaros.

Promocijas darbs ir uzrakstīts angļu valodā, tajā ir ievads, 7 nodaļas, secinājumi, literatūras saraksts, 86 attēli, 7 tabulas, 5 pielikumi, kopā 165 lappuses, ieskaitot pielikumus. Literatūras sarakstā ir 220 nosaukumi.

# CONTENTS

---

ACKNOWLEDGEMENT .....	2
ABSTRACT .....	3
ANOTĂCIJA .....	4
CONTENTS .....	5
INTRODUCTION.....	8
Main hypothesis and objectives .....	9
Hypothesis.....	9
Objectives.....	9
Means and methods of research .....	9
Scientific novelties .....	9
Practical novelties .....	10
Practical application of research results .....	10
Dissemination of research results.....	10
1. ANALYSIS OF ELECTRIC VEHICLE BATTERIES.....	12
1.1. Light-duty vehicles.....	12
1.2. Buses and trucks.....	15
1.3. Personal mobility vehicles .....	15
2. LITHIUM-ION BATTERY TECHNOLOGY INVESTIGATION .....	19
2.1. Construction .....	19
2.2. Operation.....	21
2.3. Types of Li-ion chemistries.....	21
2.4. Discharging .....	23
2.5. Charging.....	27
3. ANALYSIS OF BATTERY MANAGEMENT SYSTEMS .....	30
3.1. Battery balancing methods .....	33
3.2. Dissipative balancing methods.....	35
Dissipative fixed resistor balancing .....	35
Switched resistor balancing.....	36
3.3. Selective charge/discharge methods.....	42
Pack reconfiguration based .....	42

Multi converter .....	43
Selective charging balancing .....	44
3.4. Charge transfer methods.....	45
Capacitor based charge transfer methods .....	45
Inductor based charge transfer methods.....	48
Transformer-based charge transfer methods .....	54
3.5. Summary of balancing methods.....	63
4. INVESTIGATION OF INDIVIDUAL CELL TESTING METHODS .....	65
4.1. LFP cell testing.....	65
Capacity testing .....	65
Open circuit voltage testing.....	66
Two-cell discharge test.....	67
4.2. 18650-size cell testing .....	69
Capacity dispersion analysis .....	69
Impedance analysis .....	75
5. THE DEVELOPMENT OF A BATTERY CONFIGURATION FOR A PMV .....	82
5.1. Wheelchair Concept .....	82
5.2. Market analysis of powered wheelchairs .....	82
5.3. Market analysis of battery cells.....	83
5.4. Analysis of battery voltage selection .....	88
Analysis of series and parallel configuration .....	88
Impact of nominal voltage on traction motor.....	88
Analysis of drive converter semiconductor losses .....	90
Analysis of battery charger efficiency versus nominal voltage .....	92
Discussion of nominal voltage for battery pack.....	93
6. CELL BALANCING SYSTEM DEVELOPMENT AND VERIFICATION.....	95
6.1. Development of cell module 1 .....	95
Development of the circuit.....	95
Development of data transfer .....	99
Development of the microcontroller program.....	100
Evaluation of cell module 1.....	102
6.2. Cell module 2 .....	104

Improvements.....	104
ADC calibration .....	105
Levelling Out the ADC Measurements .....	106
Slope Equalization of the ADC .....	108
6.3. Cell module 3 .....	110
6.4. Development of the master module .....	113
Hardware .....	113
Communication .....	114
6.5. Testing of the developed switched resistor balancing system.....	115
7. DEVELOPMENT OF ADVANCED CELL BALANCING.....	119
7.1. Development of multi-secondary winding transformer balancing.....	119
Operation.....	119
Testing.....	121
7.2. Energy Efficiency with Passive Balancing .....	122
7.3. Test of battery efficiency with mixed two-layer balancing.....	123
7.4. Discussion on performance of mixed two-layer balancing.....	124
CONCLUSIONS .....	126
Author's publications .....	128
Appendix 1 .....	131
Appendix 2 .....	133
Appendix 3 .....	139
Appendix 4 .....	140
Appendix 5 .....	142
REFERENCES.....	152

# INTRODUCTION

The recent advances in the commercial electric vehicle (EV) sector by the major automotive industry members are quite obvious. Steadily more and more electric vehicles are appearing on the market and on the streets of Latvia as well [1]. Conventional internal combustion engines are shifting toward electric technologies by introducing hybrid technologies where additional electric motors with their battery packs are added to the vehicle to improve the performance. It seems that electric vehicles could one day come back to be every day standard means of transportation while being energy efficient and climate conscious. The major driving force behind this is the goal to achieve sustainable economy and environmental neutrality – to stop the climate change by reducing greenhouse gas emissions [2][3].

The electric vehicle portfolio is additionally expanded by electric personal mobility vehicles (PMV). As the name implies, these vehicles are intended to provide means of transportation for a single individual. The visibility and availability of PMVs is greatly increased by companies providing short- or long-term leasing of e-scooters and e-bicycles in many countries.

In Latvia e-mobility is developing as well. Riga Technical University is shifting towards fully electric vehicle fleet: more than a dozen EVs have been purchased and are successfully utilized. A local rallycross vehicle designer and manufacturer OSC led by engineer and designer Andris Dambis has been developing racing electric vehicles and electric public transport minibuses [4]. Another notable example is the Blue Shock Race team which is developing high performance electric race karts [5].

The key to all this progress is the advent of modern lithium-ion (Li-ion) battery technology. It began in the beginning of '90s, when it was used in portable consumer gadgets and applications. The initial batteries had relatively high capacity albeit at low charge/discharge rates. Gradually, the technology diversified to support higher discharge rates and improved operational temperature which in turn improved safety: such cells were used in power tools. As the various chemistries of Li-ion technology matured in capacity, safety, lifespan, cycle life and manufacturing cost it became feasible to use them in the previously mentioned electrical vehicles.

However, Li-ion batteries still have one considerable drawback: safety – they must not be overcharged/over-discharged and their temperature must be within operational limits. A violation of these rules can lead to permanent damage to the battery, a fire or even explosion. A battery management system (BMS) is required for every Li-ion battery pack to keep its operational variables within set limits. A disconnect switch can be used in the simplest BMS when a battery is approaching a critical state. In larger multi-cell batteries, an additional circuit is used keep cells equally balanced to optimize the performance of the whole pack. There is a wide variety of such battery balancing circuits or methods in research literature. Different advantages and disadvantages can promote one or other balancing method for a particular application.

The initial motivation for this thesis is to design a battery pack for an ongoing electric kart educational project – a personal mobility vehicle in a broader sense. To fulfil this goal, battery technology must be reviewed and tested. A suitable BMS must be designed. The testing of

battery performance can yield valuable information for BMS balancing method selection. Further, balancing methods could be combined to improve cumulative performance or at least minimize individual drawbacks.

## **Main hypothesis and objectives**

### **Hypothesis**

The balancing performance of a battery management system can be improved by combining two different balancing methods into a two-layer balancing solution.

### **Objectives**

1. To analyse present electric vehicle battery systems.
2. To investigate lithium-ion battery technology and analyse present battery balancing methods.
3. To perform investigative testing of lithium-ion cells.
4. To utilize obtained knowledge to design a battery pack for a small electric vehicle.
5. To develop a custom two-layer balancing system.

### **Means and methods of research**

*MS Excel* has been extensively used for calculations and data processing, especially for statistical analysis. *Matlab* was used for data processing, visualization, and measurement process automation – instrumentation control scripts were designed and executed. *HxD hex editor* software was used to obtain raw data from memory cards which were used for cell data logging. *LTspice* has been used for preliminary simulations of various parts of designed circuits.

During the development, testing and experimental verification, a variety of laboratory equipment was used in different configurations. The list of used equipment includes various power supplies, oscilloscopes with assortment of probes, a thermal imaging camera, a battery impedance meter, electronic loads, precision power analyser and several multimeters.

A few models of MSP430 family microcontrollers were used throughout this project. Both *IAR Embedded Workbench* (mostly in assembly language) and *Code Composer Studio* (mostly in C language) to program and debug microcontrollers. *Orcad Capture, Layout and PCB editor* was used for most PCB design. Occasionally, *Altium designer* was used as well. Experimental PCBs were manufactured in-house using PCB milling while proven board manufacturing was outsourced.

### **Scientific novelties**

1. Switched resistor and multi-secondary winding transformer balancing methods has been combined for the first time to produce a two-layer balancing solution.
2. A novel battery balancing categorization is proposed which groups existing methods into dissipative methods, selective charging/discharging methods, and charge transfer methods.
3. A statistical analysis of unused cell parameters has been presented which indicate small differences in parameters which in turn justify the use of switched resistor balancing.

### **Practical novelties**

1. An analysis process of battery voltage and configuration selection process has been provided for a wheelchair personal mobility device.
2. A fully modular switched resistor balancing board with daisy-chain data exchange has been developed.
3. Procedure and hardware have been developed to calibrate both cell voltage and temperature measurements of developed balancing boards.

### **Practical application of research results**

1. The developed switched resistor balancing board (version 2) has been implemented in a 20-cell battery pack for an electric kart.
2. The developed switched resistor balancing solution (version 3) has been implemented in a 144-cell battery pack for a DC microgrid battery energy storage system.
3. The provided battery design process has been used to develop a battery pack for a power-assisted wheelchair. The pack prototype has been equipped with a battery management system and case/housing combo which permits easy battery pack replacement.

### **Dissemination of research results**

There are 33 author's publications in total and a chapter of one book. The following 13 publications are presented in the Doctoral Thesis:

1. R. Zemnieks and **K. Vitols**, "Automation of Battery Impedance Measurement Using Matlab," in *2020 IEEE 61st Annual International Scientific Conference on Power and Electrical Engineering of Riga Technical University, RTUCON 2020 - Proceedings*, 2020.
2. **K. Vitols** and A. Podgornovs, "Impact of battery cell configuration to powered wheelchair drive efficiency," *Arch. Electr. Eng.*, vol. 69, no. 1, pp. 203–213, 2020.
3. **K. Vitols** and E. Grinfogels, "Battery Batch Impedance Analysis for Pack Design," in *2019 IEEE 7th IEEE Workshop on Advances in Information, Electronic and Electrical Engineering (AIEEE)*, 2019, pp. 1–5.
4. **K. Vitols**, E. Grinfogels, and D. Nikonorovs, "Cell Capacity Dispersion Analysis Based Battery Pack Design," in *2018 6th IEEE Workshop on Advances in Information, Electronic and Electrical Engineering (AIEEE)*, 2018, no. 1, pp. 1–5.
5. **K. Vitols** and E. Poiss, "Development of Electric Scooter Battery Pack Management System," in *2018 IEEE 59th International Scientific Conference on Power and Electrical Engineering of Riga Technical University (RTUCON)*, 2018, pp. 1–5.
6. **K. Vitols** and A. Podgornovs, "Concept of cost-effective power-assist wheelchair's electrical subsystem," in *2017 5th IEEE Workshop on Advances in Information, Electronic and Electrical Engineering (AIEEE)*, 2017, pp. 1–4.
7. **K. Vitols**, "Efficiency of LiFePO<sub>4</sub> battery and charger with a mixed two level balancing," in *2016 57th International Scientific Conference on Power and Electrical Engineering of Riga Technical University (RTUCON)*, 2016, pp. 1–4.
8. **K. Vitols**, "Efficiency of LiFePO<sub>4</sub> Battery and Charger with Passive Balancing," in *AIEEE 2015*, 2015.

9. **K. Vitols**, “Lithium ion battery parameter evaluation for battery management system,” in *2015 56th International Scientific Conference on Power and Electrical Engineering of Riga Technical University (RTUCON)*, 2015, pp. 1–4.
10. **K. Vitols**, “Design considerations of a battery pack - DC grid interface converter,” in *2015 IEEE 5th International Conference on Power Engineering, Energy and Electrical Drives (POWERENG)*, 2015, vol. 2015-Septe, pp. 476–479.
11. **K. Vitols** and I. Galkin, “Evaluation of cell balancing solution with a custom energy measurement device design,” in *2014 55th International Scientific Conference on Power and Electrical Engineering of Riga Technical University, RTUCON 2014*, 2014.
12. **K. Vitols**, “Redesign of passive balancing battery management system to active balancing with integrated charger converter,” in *2014 14th Biennial Baltic Electronic Conference (BEC)*, 2014, pp. 241–244.
13. **K. Vitols**, “Design of an embedded battery management system with passive balancing,” in *2014 6th European Embedded Design in Education and Research Conference (EDERC)*, 2014, pp. 142–146.

# 1. ANALYSIS OF ELECTRIC VEHICLE BATTERIES

## 1.1. Light-duty vehicles

Light-duty (category M1) electric vehicles and hybrid electric vehicles (ICE vehicles with traction batteries) are gradually replacing conventional internal combustion engine vehicles. Major automotive manufacturers are investing heavily in both development of new EV models and battery technologies. It is well known that the battery performance is the main bottleneck of rapid overall EV adoption. EV battery key performance indicators are price, capacity, energy density, life, safety and charging time. The first three indicators are basically the same as the goal of the manufacturer is to equip a vehicle with the highest capacity battery – energy density sets the limit of physical size while price sets the limit on profitability of the overall vehicle model. Majority of early EVs had fairly small capacity battery packs to reduce the price associated with battery. Only high-performance premium EVs had tens of kWh of energy which granted driving range seemingly comparable to ICE vehicles albeit at an increased price. As batteries evolved through the preceding decade in terms of technology and mass production, they have become more available at decreased cost which allows implementation of higher capacity battery packs. For example, the small city car *Volkswagen e-up!* initially in year 2012 had only an 18.7 kWh battery pack which provided 130 km of range. The current version of *e-up!* uses a 32.3 kWh battery which is capable of up to 260 km of driving range [6]. Notably, both versions have approximately the same price – an indication that manufacturer has found solution to decrease battery price per kWh. However, the transition to electric vehicles was initiated by hybrid vehicles. *Toyota Prius* being the first production HEV. It was first delivered in 1997 and since then has been sold in millions of units promoting benefits of electric traction. The first versions of *Prius* used NiMH chemistry battery pack with advanced BMS to maintain optimal battery energy level and long lifespan by controlling temperature and SoC. In 2016 *Toyota* started producing a plug-in version of *Prius*. It featured a significantly larger Li-ion battery pack (4.4 kWh) which encouraged the use of electric-only driving mode – essentially running *Prius* PHEV as an EV. Now, as the Li-ion technology is advancing and price is decreasing, new *Prius* (not plug-in) models are offered with Li-ion chemistry battery packs as well [7]. *Toyota Prius* certainly had a significant impact on electric traction and battery familiarization. Soon after the success of *Prius*, many other car makers followed with their HEVs and PHEVs.

One could argue that modern mass-produced EV era begun in 2010 (2009 in Japan) with advent of *Mitsubishi iMiEV* which was equipped with a 16 kWh Li-ion battery. In the same year another Japanese OEM launched its EV as well: the successful *Nissan Leaf* is still being produced in its second generation. It had a 24/30 kWh Li-ion battery while the new version is equipped with a 40 kWh LIB which is made of 192 NMC pouch cells [8]. BMS PCBA images from amateur teardowns indicate that custom labeled ASICs are used for cell monitoring and balancing [9]. It is probable that switched resistor balancing is used with a single 430  $\Omega$  shunting resistor per cell. Given that cells are arranged in 96S2P configuration, it can be calculated that each cell pair has approximately 116 Ah capacity – the shunting resistor provides less than

10 mA of current for this cell pair. A miniscule 0.000084 A/Ah current is selected to do the balancing.

A notable early EV from European Union OEMs is the *i3* hatchback produced by *BMW*. It was introduced in 2013 and it still is into production. Its battery is made of high-capacity prismatic NMC Li-ion cells at 22, 33 and 42.2 kWh capacities. The battery is divided in modules and each module consists of 12 series connected cells with a module management board [10]. *LTC6801* independent multicell battery stack fault monitor IC and *LTC6802-2* multicell addressable battery stack monitor IC from *Linear Technologies* (now *Analog*) are used to monitor voltages and temperatures of the cells and perform switched resistor balancing [11]. The board also has an *MC9S12P* family microcontroller from *NXP*. 2512-size 56 $\Omega$  surface mount resistor is used to balance each cell. At 4.2 V the balancing current is 75 mA or 0.00125 – 0.000625 A/Ah (depending on the used cells) – significantly more than that of *Nissan Leaf*.

An interesting market penetrating approach was used by American electric vehicle manufacturer *Tesla* – it used (and still uses) top-down disruption strategy. In 2008 it started to series produce its first EV – the *Tesla Roadster* which was a two-seat roadster with somewhat high performance for an electric vehicle of the day [12]. The *Roadster* used a battery pack made of 6831 consumer-grade 18650-sized Li-ion cells arranged in 99S69P configuration [13]. The total capacity was approximately 53 kWh and it was divided among 11 battery modules [14]. According to *Tesla*'s technical report, each module was equipped with a monitoring PCB which used CAN Bus communication to transmit battery data to the central management controller board. The pack was liquid cooled to provide high performance and safety.

By making the high-performance *Roadster*, *Tesla* gained positive attention as an EV manufacturer whose product radically differed from the “glorified electric golf carts” of the time. *Tesla* used investor's trust and spent a few years to develop its next EV: the *Model S* – an expensive liftback sedan characterized by its business/premium look and the best EV performance: sports car acceleration and long driving range [15]. Again, *Tesla* used ubiquitous 18650-size battery cells from *Panasonic*, presumably Li-ion NCA type. According to amateur teardowns, a nominal 85 kWh (The usable capacity of the pack was decreased to 83.5 kWh to improve battery life span) battery pack was made using 96S74P cell configuration producing approximately 400 V when fully charged [16]. The 74 cells in parallel are referred to as the brick. Six bricks are series connected to make a module and 16 modules are further series connected to make the battery pack. Each module is equipped with a local battery management board which is built around *BQ76PL536A* battery monitor and secondary protection IC from *Texas Instruments* [17]. This IC supports up to 6 cells, can measure voltage of each cell, have inputs for two thermistors, uses SPI interface to communicate with host and other monitor ICs (from other modules). It also performs cell balancing using switched resistor method. *BQ76PL536A* controls an external transistor in SOT-23 package to connect four 1206 size 158  $\Omega$  resistors to the required cell. From this, it can be calculated that 106 mA balancing current (at cell voltage 4.2 V) is used to balance 244 Ah “cell” (brick made of 76 cells) hence just 0.00043 A/Ah balancing current proportion is used which indicates that *Tesla* is quite confident in the uniformity of cells of the battery pack.

After successful launch of *Model S*, *Tesla* together with *Panasonic* announced building of a battery gigafactory (with annual produced volume higher than 1 GWh, usually tens of GWh) to produce batteries locally for its own consumption. The gigafactory started operation in 2016 and have fully exploited the benefits of economies of scale by providing 18650-size cells to make battery packs which costs less than 200 € per kWh. The success of *Tesla* and *Model S* gave a clear indication that EV business has potential and promoted other OEMs to launch their own EV models. To exploit premium vehicle sector even more (and attract investors funding) *Tesla* designed another even more expensive premium EV: the *Model X* in form of a SUV which is being delivered since 2015. Both *Model S* and *Model X* share the same battery cells. *Model X* has been available with battery packs from 75 to 100 kWh.

Building upon knowledge from previous designs, in 2017 *Tesla* finally launched an EV that was marketed as sort of “affordable” for most new vehicle buyers: the *Model 3* which is a four-door sedan. The battery for this EV is available in range from 50 kWh to 75 kWh and it is made using custom designed Li-ion NCA 2170-size cells. The pack is made from just four series connected modules: two modules are larger and other two smaller to fit the shape of the battery pack [18]. This construction trend to decrease number of modules indicates maturity and reliability of battery technology – if modules do not fail then there is no need to make them replaceable/repairable. Each module is equipped with a BMS board – the four of them are daisy chained together and connected to a high-voltage system controller board – master BMS. Each module BMS board is populated with two pairs of custom labeled IC which presumably perform cell monitoring and balancing. An independent report claims that two-level active balancing is implemented using the same pair of custom ICs at both module level and battery pack level. However, judging from the available images of the BMS board, it could be utilizing switched resistor balancing as well, using external resistors mounted on the bottom layer and internal transistor switches of the larger LQFP IC package. This thought is supported by the seeming similarity to LTC6813-1 battery monitor IC made by *Analog Devices* which can perform passive balancing (switched resistor) for up to 18 cells [19]. It can provide up to 200 mA balancing current, however the available low resolution images of the management board prohibit further analysis [20].

In 2020 *Tesla* started to deliver its *Model Y* – a compact crossover EV which is based on almost the same traction and energy storage system as *Model 3* [21]. Taken all together, *Tesla* managed to make a successful EV manufacturer image and has built a considerable knowledge base in less than two decades. However, time will tell whether *Tesla* and its strategy are good for the long term as other vehicle OEMs will launch their fleets of EVs.

To summarize, light-duty EVs are mostly using Li-ion batteries with NMC chemistry, except for *Tesla* which uses Li-ion NCA chemistry [22]. It must be noted that the large Chinese EV market is somewhat specific – a significant part of EVs use LFP chemistry especially buses [23]. The reviewed non-scientific materials indicate that switched resistor balancing is used to equalize cells of the battery pack. Balancing current has a wide range: from just 84  $\mu$ A to 1.25 mA per Ah of a cell. Low balancing current indicates OEM’s confidence in overall cell quality and minimal parameter variation. Interestingly, commercial battery management ICs are being used in EVs. It could be that in initial EV models OEMs are not fully confident in

their battery related skills hence it is safer to use third party battery management ICs. However, as the knowledge will increase one can expect that battery packs of future EVs will have more custom designed BMS controllers to suit specific needs.

## 1.2. Buses and trucks

The adaption of commercial electric trucks has not been as successful as light passenger EVs. The main reason is range and initial costs – both are directly related to the battery pack. Short range delivery trucks/vans have existed for several decades to perform deliveries inside cities and suburban neighborhoods. A special case is electric forklifts – due to no exhaust gases they can be used indoors (factories, warehouses) and hence have a well-established market [24]. Historically, lead-acid batteries have been the dominant source of energy [25] although recent advances in LIBs (reduction of costs) could change this situation. In recent designs, LIBs are being implemented in heavy-duty trucks, for example the vehicle models of company *E-Force One AG* uses NMC LIBs with capacities higher than 300 kWh [26]. A major player in EV business is Chinese OEM company *BYD* which is known for extensive use of LFP batteries in its EVs [27]. It produces electric cars, buses, forklifts and trucks [28]. One of its highest performing trucks – *Class 8 BYD 8TT* is equipped with 409 kWh battery and while the truck weighs almost 12 tonnes, it can transport more than 35 tonnes of cargo [29]. *BYD* is supplying electric busses to European markets with worldwide production of over 45000 units [30]. Well known vehicle OEM *Mercedes-Benz* has developed its own electric bus: *eCitaro* – in its starting version it is using a 292 kWh NMC LIB made of 37 Ah prismatic cells arranged in 12 cells per cell module. 15 cell modules are used to make a battery module – the number of battery modules can be increased to improve the range of the bus.

The company plans to gradually shift to solid-state batteries which will eventually be upgraded with additional fuel cell range extender to achieve 400 km range [31][32]. A locally notable vehicle is the *Opportunity charge M2 electric minibus*. This 18-seat passenger electric bus built on *Mercedes-Benz Sprinter* platform is a result of local electric vehicle development project. To achieve fast charging time and long life a 552V / 444 kWh LTO battery was implemented together with custom inverted pantograph charging connection [33]. Overall, probably due to substantially smaller market and being a sort of niche product, it was impossible to find information about bus and truck BMS structure and cell balancing approach.

## 1.3. Personal mobility vehicles

A variety of different “smaller-than-typical-car” electric vehicles exist on the market. Here they are combined under personal mobility vehicles – PMVs. In EU, a part of these vehicles is in the L category which include mopeds, motorcycles, motor tricycles and quadricycles. Generally, motorcycles and motor tricycles are two-wheel and three-wheel vehicles whose maximum speed is higher than 45 km/h while speed of mopeds and quadricycles is less than 45km/h and maximum continuous rated power does not exceed 4 kW. An exception is heavy quadricycles whose power is no more than 15 kW. An electric bicycle becomes a moped if its

maximum continuous rated power is more than 0.25 kW or its top speed is higher than 25 km/h when electric power is used [34]. Given EU regulation does not include power/speed definitions for such vehicles as vehicles for physically handicapped, competition vehicles, pedestrian controlled vehicles, off-road vehicles, self-balancing vehicles and vehicles without at least one seating position – the popular electric scooters. All these vehicles are manufactured with electric drives and battery packs.

Among two wheeled vehicles, electric bicycles and scooters are the most popular. Electric bicycles or ebikes are available as produced models or as kits which can be installed on conventional bicycle. Two main components are the battery and the drive. Drive motor can be installed in two locations: the most popular is hub motor (front or back wheel) while alternative is the mid-drive where motor is integrated with crankset. The battery pack can be installed in various locations: integrated into the frame, tube mounted or on/in the rear rack. Most of major manufacturers produce 36 V battery packs using Li-ion chemistries. Although the nominal voltage range is much broader ranging from 12 V up to 72 V. The typical voltages are 24 V, 36 V and 43 V which is used by *Bafang*. Rarer voltages are 12 V, 25 V, 29 V, 37 V [35]. Smaller manufacturers provide customized battery packs with significantly higher voltages: 48 V, 52 V, 60 V and 72 V [36] although according to EN19194 standard of cycles and electric road vehicles with power less than 250 W the voltage can be only as high as 48 V. While information about cells are not available from most OEMs, in some cases it is indicated that the battery is made of 18650-sized NMC cells. Online amateur teardowns indicate that 18650-size is predominantly popular [37]. Alternatively, 26650- and 20700/21700-sizes and LFP chemistry is used. The energy content of reviewed battery packs varied from 200 Wh to 750 Wh with distinctive groups at 400 Wh and 500 Wh. From the simplistic battery marketing materials and teardown videos it can be found that BMS is built with switched resistor balancing with balancing at the top (full charge). The functions of BMS varies from OEM to OEM but they include the rudimentary ones with addition of more complex data logging and probably some SoH estimation. While some battery packs have built-in charge indicators, they are also wired to a so-called display unit which basically is a miniature control center which provides graphical status/performance information of the whole system to the user. UART, CANbus, SMBus and Bluetooth are some of interfaces used to exchange information between the battery and other components [38].

Electric scooters differ from electric motorcycles by the position of the driver: a scooter has a step-through chassis with footrest platform, while a motorcycle has a “filled” chassis – the driver has to mount a motorcycle by swinging one leg over the chassis. Typical ICE scooters are equipped with a seat underneath which the engine is located. Kick scooters are relatively simple mechanical devices without a seat. As the name implies, the propelling force is provided by the drivers/rider’s physical power. Both ICE scooters and kick scooters have recently evolved into electric scooters. The ones which are equipped with a seat are better suited for higher top speeds, while majority of urban personal transportation electric scooters are seatless and require the driver to be standing. These electric scooters are often marketed with max speed not exceeding 25 km/h to fall into sport equipment category – not governed by Road Traffic Safety Directorate.

Market analysis of electric seat-less kick scooters shows a wide variety of models with different capabilities. Major online store *Banggood* offers 101 electric scooters while the offer of *Amazon* is not as categorized and yields around 240 electric articles which include proper electric scooters, their parts, unicycles, self-balance boards, hoverboards, hovershoes, three wheeled scooters, onewheels and even underwater electric scooters and other personal electric transport vehicles. The offer of 16 dedicated online stores was analyzed to obtain specific information regarding a total of 238 electric kick scooter’s models and their clones. A major group of reviewed scooters is intended for the aforementioned sport equipment category – 49 scooters have max speed 25 km/h, while 43 have even lower max speed. Low speed scooters have groups at 8 km/h and 16 km/h – these scooters are intended for children as the max weight of the driver is limited to around 50 kg. A wide variety of scooters exist above 25 km/h threshold. Majority are in the 25 – 65 km/h assortment while 20 of reviewed models have even higher top speeds reaching maximum at 120 km/h. Reasonably, as the top speed increases so does the performance of motor and battery. The slowest scooters are equipped with a single 90-200 W chain drive motor. Series connected sealed lead acid batteries can be found among these models to supply 12 to 24 V at capacities in 100 – 200 Wh range. In more expensive models, state-of-art brushless hub motors and 36 V Li-ion batteries can be found with capacities as high as 200 Wh. The 25 km/h group is mostly equipped with front or rear hub motor rated at 250 – 350 W. Batteries are composed of 18650-sized Li-ion cells at pack capacities ranging from 150 Wh to 300 Wh at 36 V in most cases. It is probable that cell chemistry is NMC. High speed scooters still use the same 18650-sized cells (when information is available) at higher capacities and voltages. The max speed can be as high as 120 km/h while 35 – 160 km range is achieved using 48 – 72 V battery packs at 300 – 3000 Wh capacities. Model distribution vs top speed is shown in Fig. 1.1, battery capacity is shown in Fig. 1.2 and battery voltage is shown in Fig. 1.3.

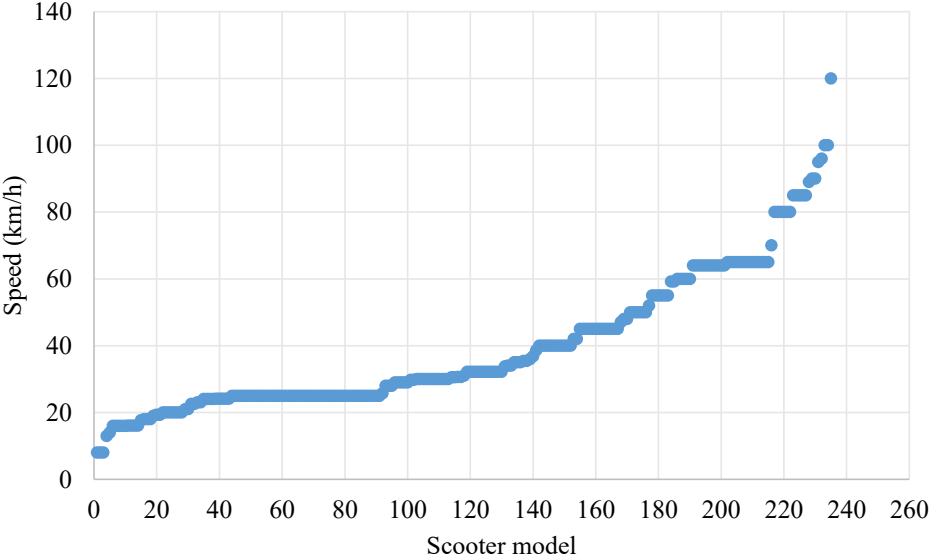


Fig. 1.1. Top speed distribution of reviewed electric seat-less kick scooters.

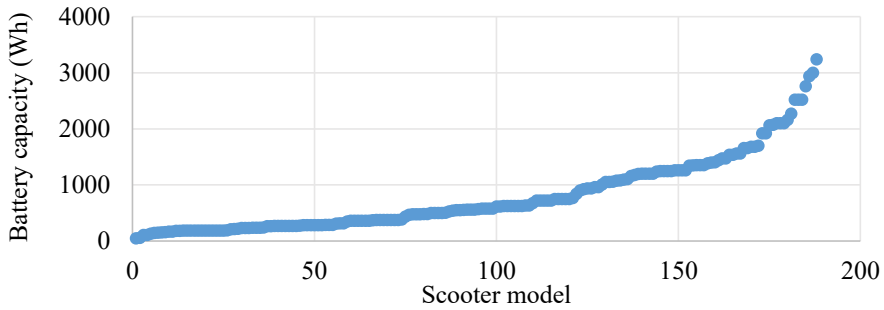


Fig. 1.2. Battery capacity distribution of reviewed electric seat-less kick scooters.

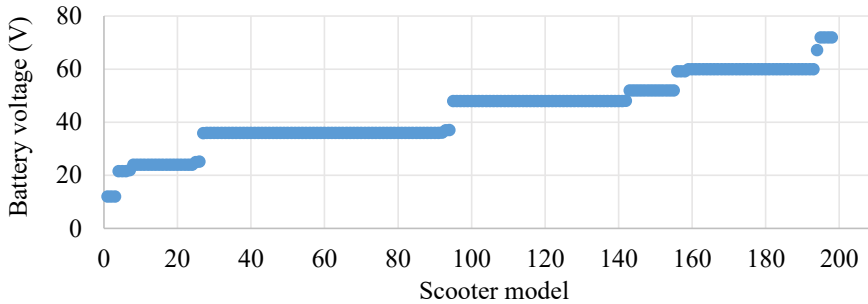


Fig. 1.3. Battery nominal voltage distribution of reviewed electric seat-less kick scooters.

Similarly, as with other vehicles, it is cumbersome to obtain reliable information about battery construction and battery management system. Through repair videos [39] and spare part images it was found that *Xiaomi M365* uses *bq7693003* battery monitor IC from *Texas Instruments* which means that given model uses switched resistor balancing with 0805-size resistors – low balancing current. In some occasions it is mentioned that scooter is equipped with a Bluetooth communication to transfer battery parameters to smart phone. Most likely this feature is integrated in the BMS.

To summarize and conclude this chapter, it is obvious that battery EVs of all kinds use lithium-ion batteries. Majority of batteries are of NMC and NCA chemistries while in some specific cases LFP and even LTO chemistries are used. One of the objectives of this chapter was to provide insight in cell balancing methods used in various EVs. Unfortunately, vehicle manufacturers do not provide information about their BMS. The only usable information was amateur and professional EV battery teardowns as well as spare part images. From the available information it was concluded that switched resistor balancing method is used predominantly. Even in large battery packs (20 – 100 kWh) small surface mount resistors are used to dissipate excessive energy at currents less than 1 mA. This brings up questions: are cells produced at such qualities that mismatch is miniscule, have battery pack design evolved so far that uniform conditions exist for all cells, is cell energy mismatch a real problem, are there requirements for higher rate/shorter time balancing? To answer these questions, more literature regarding lithium-ion batteries and balancing methods must be analysed.

## 2. LITHIUM-ION BATTERY TECHNOLOGY INVESTIGATION

The lithium-based rechargeable batteries were last to enter the battery market. Notable rechargeable battery chemistries which predate lithium-ion are lead-acid, nickel-cadmium, nickel-metal hydride and molten-salt batteries [40]. During the last decades lithium-ion battery (LIB) technology has evolved quickly, overtaken significant part of the market and the total worth of related technologies is expected to grow in the future [41]. As the name implies, the chemical element lithium (Li) is the key component of every lithium-based battery: primary or secondary, metal or ion variety. Lithium is the lightest metal with one of the lowest electrode potentials hence it fulfils requirements for a high-performance battery. However, lithium is highly reactive: it aggressively reacts with water and oxygen from air – both lead-acid and NiMH chemistries uses electrolyte with water hence lithium-based batteries needs a new type of electrolyte. Studies in lithium electrochemistry was already done as early as in the second decade of 20th century. However, the research and development of lithium batteries took off only in 1970s – the first rechargeable lithium battery prototype was demonstrated in 1976. The first commercially available non-rechargeable (primary) lithium battery was already sold in the same decade. It took a couple of decades for the rechargeable battery – it was commercialized in 1990 [42]. Initial models used metallic lithium anode (negative electrode) with titanium disulfide cathode (positive electrode) but it was noticed that this construction under certain circumstances and cycling can grow so called dendrites – treelike structures which extend from anode, pierce separator layer and cause an internal short circuit which causes venting with flame, fire or explosion. It was found to be difficult to prevent dendrite growth in lithium metal batteries hence research was shifted to another lithium battery type: lithium-ion battery, in which there is no metallic lithium and only lithium ions are used transfer and store charge [43].

Rechargeable LIBs became available in year 1990 with key advantage: higher specific energy density than other available battery chemistries. Gradual development of new cathode materials adjusted LIB technology for most requirements of portable applications from highest energy density smartwatches and cell phones to high current hand tools and long life EV batteries. Additionally, less expensive LIB chemistries were developed for stationary applications. It is estimated that total LIB market is in the 30-billion-euro range and it is expected to increase fourfold in this decade [41]. LIBs constitute approximately 60% of all automotive batteries. Over the 30-year period of commercialization, LIBs have become a dominant battery technology with room for improvement. This technology has changed our lives by enabling personal portable devices and now it is a key-enabler for EVs. In 2019 three researchers were awarded Nobel prize in chemistry for the development of lithium-ion batteries [44].

### 2.1. Construction

Li-ion cell construction is fairly complex if compared to simplistic lead-acid cell. The basic essential components are the same: two electrodes, electrolyte and a separator. For basic

functionality, electrolyte has to be able to transfer lithium ions and at the same time it should not react with those highly reactive ions. While the electrolyte of lead-acid and NiMH cells is rather simplistic inorganic water-based liquid, the electrolyte of li-ion cells is a non-aqueous organic carbonate-based liquid which contains some sort of lithium salt or mixture of salts to provide some free lithium ions for energy transfer. The electrolyte is flammable which adds to the overall safety issues of the LIB technology.

The separator layer has the same basic function – prevent contact of electrodes (internal short circuit) while providing free path for the ion flow. In general, it is made of porous polymer material which can be internally composed of different layers of plastic (polypropylene, polyethylene and others) with additives to provide additional safety by blocking short circuit currents and decreasing flammability. From the cell performance perspective, separator layer is an unwanted element of the cell as it does not contribute to the actual electrochemical reaction. It adds dead weight and volume which in turn decreases volumetric and gravimetric energy density. For this reason, it is desirable to make this layer as thin as possible – some cells can have separator thickness of around a dozen micrometres and constitute just a few percent of the total mass of the cell [45].

A li-ion cell is made as an ion transfer cell in which both electrodes can accept and store Li ions. During charging/discharging these ions are transferred from one electrode to the other. This operational principle is known as the rocking chair. At this point it must be emphasized that a Li-ion cell can be made using a variety of different electrode materials. There are six most prevalent material combinations which result in six types of Li-ion cells. For description of cell construction, the most popular construction will be used: the negative electrode (anode) is made of graphite; the positive electrode (cathode) is made of lithium and some other metal/s oxide. Both anode and cathode active materials are selected to provide the required capacity, current and life. Electrodes can have some additives to improve current carrying capability. Additionally, both electrodes are bonded to current collectors (passive material) – high conductivity metal conductors used collect electrons from active material and provide path to the external connection of the cell. In some cell constructions the current collector metal is actually a part of the external connector. Aluminium for positive electrode and copper for negative electrode is a common current collector material choice as both metals have high conductivity, adequate electrochemical stability and are easily available.

The case of a cell is another contributor of passive material. Li-ion cells are being manufactured in all shapes according to the application requirements. In most situations, the internal structure of a cell is made as a jelly roll. First each electrode-current collector combination is made as a sheet roll then both electrodes and separator layer are combined by rolling all layers into one roll. Finally, the electrolyte is filled. Naturally, the resulting roll is of cylindrical shape hence the most effective (from manufacturing perspective) cell shape is cylindrical. In case of pouch/flat and prismatic cell shapes, the jelly roll is pressed and processed into required shape and then encapsulated in casing. Alternatively, a cell can be made of individual material sheets which are stacked together to produce flat cells – this process is more expensive and time consuming than jelly roll process [46].

## 2.2. Operation

The basic operation of li-ion cell is simple: positively charged lithium ions flow from negative electrode to positive during discharge and vice versa during charging. At the same time, during discharge electrons travel through the external circuit from negative electrode to positive and from positive to negative during charging. At fully discharged state the porous structure of negative graphite electrode is empty (without Li ions) and oxidized (without electrons) while the positive electrode is fully reduced to metal (lithium and others) oxide. The situation is reversed when the cell is fully charged: negative electrode structure is filled with lithium ions taken from the positive electrode. Corresponding chemical reactions are given in Fig. 2.1.

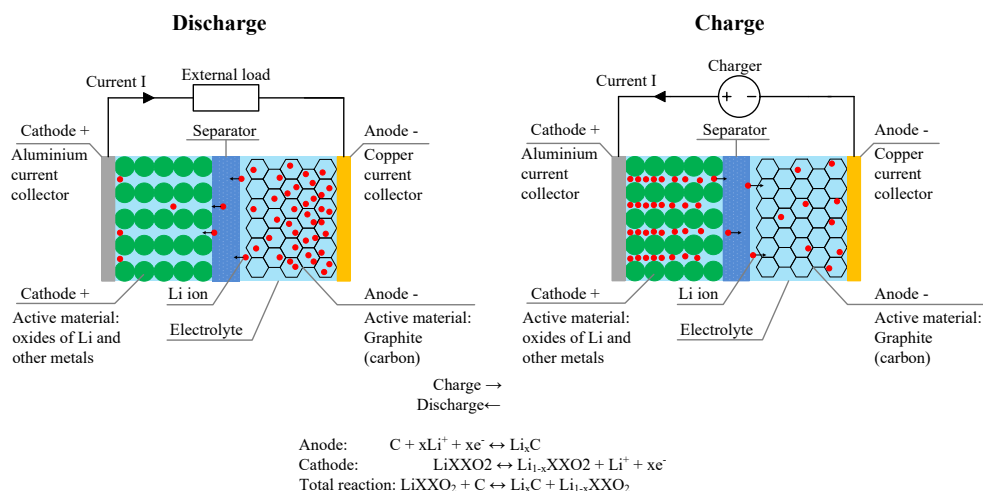


Fig. 2.1. Generic chemical reactions of a Li-ion cell.

## 2.3. Types of Li-ion chemistries

As previously noted, there are six common Li-ion chemistries. They differ according to the materials used in both electrodes. The widest variety is for the positive electrode (cathode) which can have five compositions: LCO, LMO, NMC, NCA and LFP. These three letters are abbreviations of the main chemical components of the active material. LCO and LMO are among the first commercially available Li-ion chemistries. Their composition is straightforward: L stands for lithium, C stands for cobalt, M stands for manganese and O stands for oxide/oxygen. Therefore, LCO Li ion cell has lithium cobalt oxide ( $LiCoO_2$ ) cathode (positive electrode) and LMO cell has lithium manganese oxide ( $LiMn_2O_4$  or  $Li_2MnO_3$ ) cathode. It gets a little bit complicated with NMC and NCA where N is nickel, C is cobalt, M is manganese and A is aluminium. In the names of these two materials lithium (L) and oxide (O) parts are omitted to maintain three-letter format. Therefore, NMC is lithium nickel manganese cobalt oxide ( $LiNiMnCo_2$ ) and NCA is lithium nickel cobalt aluminium oxide ( $LiNiCoAlO_2$ ). Finally, in LFP L stands for lithium, F for iron (from Latin: *ferrum*) and P for

phosphate. Therefore, the cathode of LFP chemistry is made of lithium iron phosphate ( $\text{LiFePO}_4$ ). In all these five chemistries only the cathode (positive electrode) was the variable. The anode material in all five types remained the same: graphite. The remaining type is LTO where L is for lithium, T is for titanium and O is for oxide/oxygen. Due to some chemical nomenclature rules this material is called lithium titanate ( $\text{Li}_2\text{TiO}_3$ ). Titanate material is used to replace the graphite in anode. For some confusion, the cathode of an LTO cell can be made of LMO or NMC material. Additionally, the performance of these types is changing as battery technology is advancing. For example, NMC is a popular type for EVs. It used to have 1:1:1 ratio between nickel, manganese and cobalt hence an extended name was NMC111. Then chemistry was improved to reduce cobalt content (an expensive conflict mineral) and new NMC622 type modification was introduced. It is expected that NMC811 material will be available and become mainstream in near future. The key difference between these variations is the increase in gravimetric energy density.

To summarize, each of six basic types have their specific characteristics: cost, energy density, specific power, safety, life span, temperature range even the voltage. A graphical representation of some different features is given in Fig. 2.2. From this, one significant conclusion can be drawn: the name “Li-ion battery” is quite generic – the true performance is revealed when the exact type of chemistry is known. To continue the confusion, a term lithium polymer (Li-poly, LiPo) battery exists. Despite the rumours that Li-poly is some special battery type, it is a type of Li-ion battery which has a sort-of solid electrolyte. In a Li-poly battery, the common liquid electrolyte of a traditional Li-ion battery is replaced with a gel-like electrolyte. In practice, majority of Li-ion cells have some additives and improved separator structure to confine liquid electrolyte thus essentially making Li-poly cells. These cells are mainly made in pouch format. A different variation is the solid-state Li-ion – as the name implies, the electrolyte is made fully solid thus making it possible to produce cells thinner than 1 mm. Fully solid-state Li-ion technology is still in research and development stage, however it promises higher charge/discharge rates, longer lifecycles, higher energy density while being safer and less expensive. Most likely all promises will not be carried out but announcements from developer companies indicate that solid-state batteries will become commercially available during this decade [47]. Progress in solid-state technology is intertwined with development of lithium-sulphur (Li-S) battery. Li-S battery could be the next breakthrough in energy density however it heavily relies on functional solid-state technology [48]. A closer future is improved anode materials for existing chemistries. The common graphite anode can be replaced by silicon material which can store significantly more Li ions resulting higher energy density. However, silicon anode cannot provide required cycle life. Both materials are being combined to achieve both features. Advances in carbon materials promise improvements in battery chemistry. One novel carbon allotrope is graphene which excels in high electrical and thermal conductivity – both features can be used to improve performance of traditional graphite-based anodes [49][46][45][50].

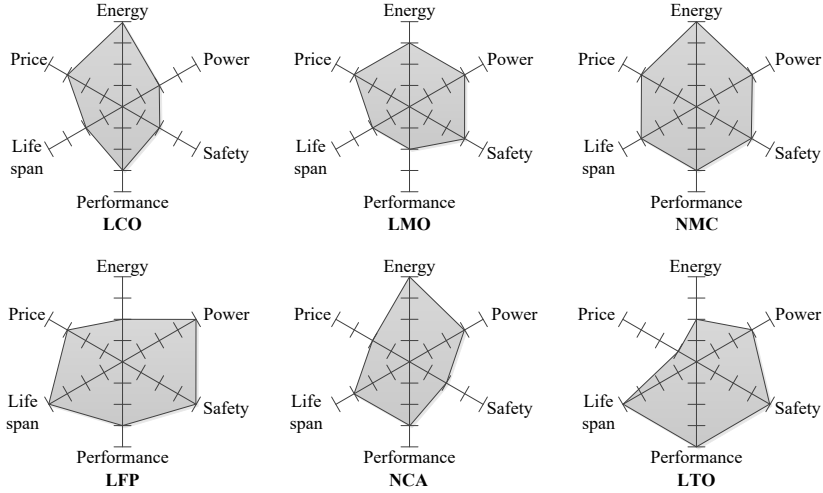


Fig. 2.2. Characteristics of common Li-ion types.

## 2.4. Discharging

All LIBs are characterized by relatively low self-discharge and no memory effect as opposed to the NiMH chemistry which requires occasional full discharge. In case of LIBs, full discharge is to be avoided to maximize battery lifespan. Depth of discharge (DoD) can be calculated using (2.1.):

$$DoD = \frac{I_{DCH} \cdot t_{DCH}}{C_{nom}} \cdot 100\%, \quad (2.1)$$

where  $DoD$  – discharged capacity, %;

$I_{DCH}$  – discharge current, A;

$t_{DCH}$  – discharge time, h;

$C_{nom}$  – nominal capacity, Ah.

Often state of charge (SoC) is used as inverse of DoD. Generally, both are interchangeable (2.2.) and (2.3.):

$$DoD = 100\% - SoC, \quad (2.2)$$

$$SoC = 100\% - DoD, \quad (2.3)$$

As for most batteries, the discharge rate affects the voltage of the cell – at high rates the voltage will drop more, in some cases it is beneficial to decrease the cut-off voltage to achieve a desired end DoD. In most LIBs the discharge curve (vertical axis represents battery voltage while horizontal axis represents SoC or DoD) is linear with a drop at the final stage of discharge (90-100% DoD) when discharged at low rate. However, as the rate is increased, the drop at high DoD becomes flatter while the voltage drops faster at the opposite end of the curve, at low DoD (Fig. 2.3). The discharge performance is heavily affected by the temperature of the cell – in Fig. 2.3 the 6.6C rate curve does not reach 2.0 V cut-off voltage because temperature of the cell has risen to the max limit. The nominal curve is given at 20, 23 or 25 °C. At 45 °C ambient

temperature, the voltage curve of the cell is increased by less than 100 mV, hence increased temperature minimally affect voltage under discharge. The situation is different if ambient temperature is decreased. At 0° C the voltage of a cell can a couple hundred mV lower (Fig. 2.4). At negative temperatures the voltage decreases further limiting the discharge rate – if rate is too high the voltage drops below cut-off voltage and discharge should be terminated. This effect is somewhat mitigated if cell is operated at moderate discharge rate – due to internal losses the cell can self-heat and thus improve its performance. For most Li-ion types the available capacity rapidly decreases at low temperature (below -15 °C). However, there exists a wide variety of different types and special purpose battery models which are designed to operate at high rates or low temperatures.

It can be said that the type of chemistry plays a critical role in the discharge performance. The most obvious initial difference is the nominal voltage (Fig. 2.5). It is commonly assumed that a single Li-ion cell has 3.6 V nominal voltage although 3.7 V are prevalent as well – these values are for the dominant group of LCO, LMO, NMC and NCA. On top of these two numbers, values around them can exist as well, for example, *LG Chem* produces 18650-size *INR18650MJI* cell (NMC type) whose datasheet’s nominal voltage is 3.635 V [51]. However, 3.6 and 3.7 V values are close together and difference is not critically important in most cases.

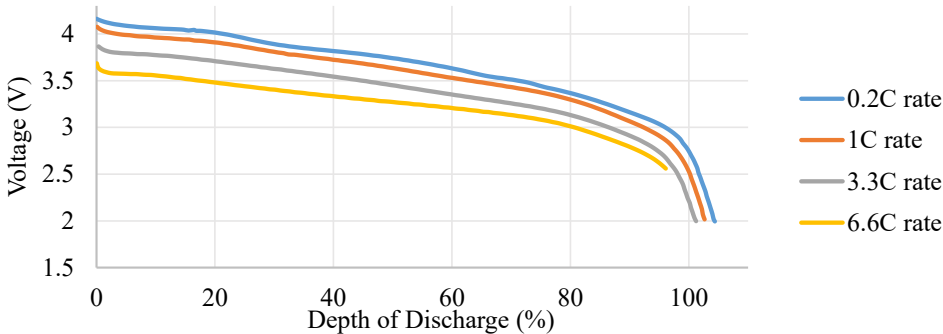


Fig. 2.3. Voltage curves of a single NMC Li-ion cell at different discharge rates [52].

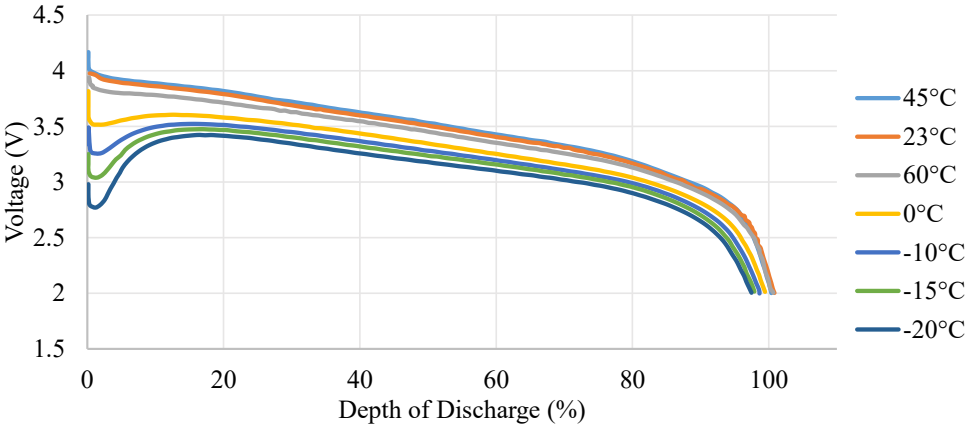


Fig. 2.4. Voltage curves of a single NMC cell at different ambient temperatures [52].

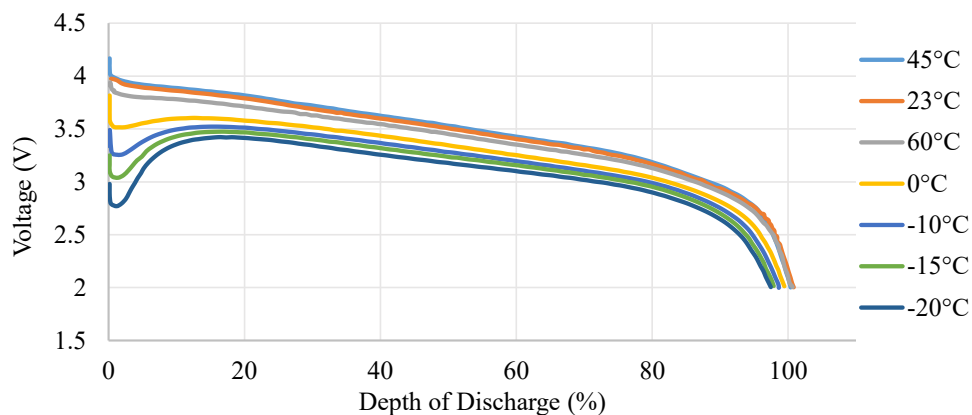


Fig. 2.5. Generalized voltage curves of single Li-ion cells of various chemistries.

LCO is rated at 3.6 V with 3.0 V optimal discharge cut-off. This type is known for its high gravimetric energy density and hence used in space/weight critical applications like mobile phones and laptops. The specific power is poor: discharge rate should not exceed 1C. LCO can be considered as an energy cell – used in applications where high energy is more important than high power. High rates and overcharging can lead to thermal runaway. LCO was one of the initially successful chemistries, but now the high price of cobalt and low safety has made this older type obsolete, putting more focus on NCA and NMC chemistries.

LMO is rated at 3.7 V with the same 3.0 V optimal discharge cut-off although the minimal voltage can go as low as 2.5 V. The energy density is considerably lower than LCO however this type is capable of much larger discharge rates. The recommended discharge rate remains the same – 1C (for max life) but max rate can go as high as 10C or even 30C for brief periods. This high specific power density makes LMO a good choice for power tools and other high-rate devices. High current can be achieved due to more stable manganese-based cathode structure – this type is safer than LCO. Thermal runaway would occur at much higher temperature. Unfortunately, lower energy density is not the only drawback – cycle rate is lower than that of LCO. Drawbacks have been minimized in NMC chemistry which combines features of both cobalt and manganese, making LMO less relevant.

NMC can be rated at 3.6 to 3.7 V depending on the exact materials and proportions of the cathode. The discharge cut-off varies from 2.7 to 3 V with 2.5 V as the absolute minimum. NMC is considered to be the leading LIB chemistry with ability to produce cells with both high energy and power at good cycle life. Gravimetric energy density is more than 200 Wh/kg and discharge rates up to 2C are achievable. For example, the *US18650VTC6* cell made by *Sony* has 3.6 V nominal voltage and 3 Ah rated capacity at weighting 46.6 g [52]. This translates to 10.8 Wh energy storage and 231 Wh/kg gravimetric energy density. At the same time this cell has 5C (15 A) continuous discharge rate. Depending on various additives and construction, NMC is used in power tools, hobby electronics, EVs and industrial applications. More than 60 % of all LIBs are NMC and adoption in EVs is more than 50%. The use of manganese improves safety at higher discharge rates however NMC is not considered to be the safest and highest power chemistry.

NCA has 3.6 V nominal voltage and cut-off at 2.5 V if max discharged capacity is required (100 % DoD). It was introduced at the end of 20th century as a replacement for unsafe LCO chemistry. This type is regarded as high energy with good power capability and long life, additionally EV manufacturer *Tesla* together with battery manufacturer *Panasonic* has proven that battery packs with price less than 200 € per kWh can be manufactured using cylindrical NCA cells [20][53]. NCA chemistry does not provide as discharge rate as NMC, the limit is in 2C to 3C range. Additional drawback is the inherently lower safety and easier thermal runaway. These negative effects can be controlled if proper battery and thermal management system is used.

LTO and LFP chemistries significantly differ from the previous two cobalt and manganese chemistries. The nominal voltage of an LFP cell is 3.2 V while the cut-off varies from 2.0 to 2.5 V depending on the model and mode of operation. If longer life is desired, then cut-off voltage should be increased to 2.8 V. The discharge curve is very flat at rapid voltage curves at both ends, hence making it harder to estimate SoC. Despite the low cost of materials, LFP cells are rather expensive because of low gravimetric energy density. The advantages are high power, high safety and long life under specific discharge conditions. Safety includes chemical and thermal stability as well as some tolerance to overcharge and short circuit. For example, *A123 Systems* manufactures *AMP20MIHD-A* flat pouch cell which has 19.6 Ah at 3.3 V nominal voltage (higher than usual 3.2 V) [54] at gravimetric energy density of 131 Wh/kg which is low if compared to NMC or NCA types. However, this cell can be discharged 363 A current which translates to 18C rate. Additionally, the manufacturer claims that this cell model will retain 90% capacity after 3000 cycles at 100 % DoD. LFP chemistry is popular in China for EVs, industrial applications and utility level energy storage.

LTO is characterized by even lower nominal voltage ranging from 2.2 to 2.4 V. The minimum discharge cut-off is at 1.5 V while in some models it is recommended to stop discharging when voltage decreases to 1.85 V. The relatively low nominal voltage is the greatest disadvantage of this chemistry. Energy of a cell can be calculated by multiplying capacity (Ah) with nominal voltage (2.4.):

$$E_{nom} = V_{nom} \cdot C_{nom} , \quad (2.4.)$$

where  $E_{nom}$  – nominal energy, Wh;

$V_{nom}$  – nominal voltage, V;

$C_{nom}$  – nominal capacity, Ah.

At same capacity and significantly lower voltage the resulting energy and volumetric/gravimetric energy density will be low. This further translates to high initial cost per kWh of the battery pack – the highest among all LIBs. Otherwise, LTO has some significant advantages. Both charging and discharging rates are high: typically quoted discharge rates are up to 10C with 30C pulses. Pulse (10 seconds) current capability of actual high-power optimized models can be as high as 75C. The cycle life is measured in several thousands and if reduced DoD range is used then cycle life can extend to tens of thousands of cycles. Additionally, the operational temperature range is wide and thermal stability is high making LTO the safest Li-ion chemistry. For a practical example, *Leclanche* manufactures *LT34* LTO

cell with 34 Ah capacity at 2.2 V weighting 1080 g [55]. Simple calculation yields that gravimetric energy density is just 70 Wh/kg – less than high performance NiMH chemistry can provide. However, this cell can be discharged at 6C and 10C in pulses at temperature range from  $-20$  to  $+55^{\circ}$  C. Additionally, at 100 % DoD cycling it is rated for 15000 cycles while 80 % DoD cycling will extend cycle life to 20000 cycles. Given parameters make LTO suitable for large EVs (bus, tram, train) and stationary energy storage which requires high charge and discharge rates.

## 2.5.Charging

In general, the CCCV charging method is used to charge LIBs similarly to lead-acid chemistry. Hence, there are two main charging phases: the faster constant-current phase and the slower constant-voltage phase as shown in Fig. 2.6. If a battery is deeply discharged (below minimum voltage) then a pre-charge phase should be introduced before full current CC phase. The pre-charge current should be 10 % or less than the nominal charging current (given in the datasheet) of the battery. Once the voltage of the battery is higher than minimal discharge voltage, charger can switch to full current charging in CC phase. In normal operation, pre-charge phase should be omitted as BMS (battery management system) has to prevent deep discharge and associated damage to the LIB. However, if the battery voltage is indicating deep discharge then pre-charge should be carried out to pre-condition both electrodes for effective lithium ion transport. Immediately applying a full current (or even worse fast-charge current) to a deeply discharged LIB can result in additional heating (risk of thermal runaway and associated danger) and permanent damage to the electrodes [56].

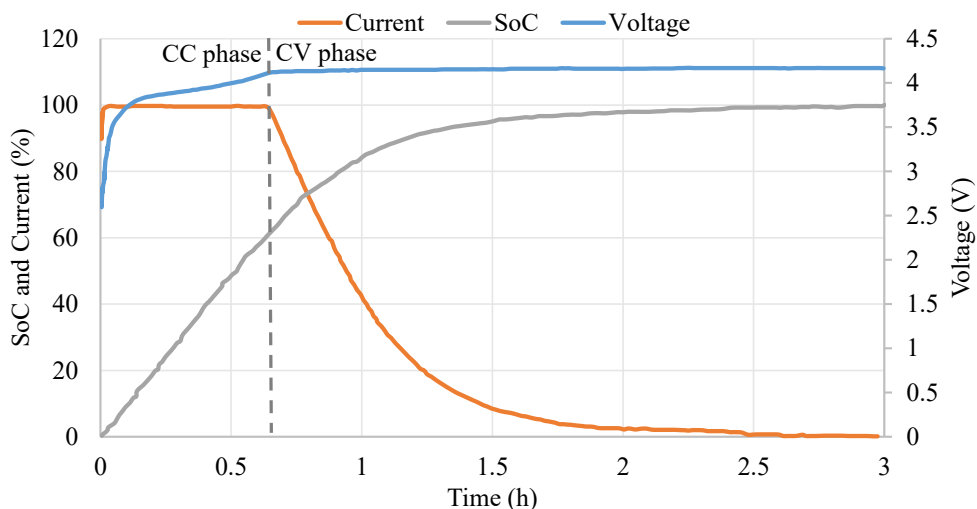


Fig. 2.6. Charging curves of an NMC Li-ion cell. Current is expressed in percent where 100 % represents 1C rate.

Most of the charge to the battery is delivered during the CC charging phase. The controllable parameter is current. The standard charging rate commonly is 0.5C which results in

approximately 2 to 2.5 hour 0 – 100 % battery charging (including CV phase). Older Li-ion chemistries were quite sensitive to charging current – higher rates would result in metallic lithium plating on electrodes, electrode expansion (package deformation) and overall performance deterioration. In worst case it would result in thermal runaway and venting with flame. Progress of technology and development of new types (NMC, NCA) have resulted in more robust cells with higher allowable charging rates. Now, faster charging can be achieved by using 1C or even 2C rates. However, fast charging has its limits. In standard charging, most time of charging is spent in CC phase, when battery is charged to 80 – 90 % SoC. CC phase is terminated when charging voltage level is reached and charging transitions to CV phase during which the remaining charge is delivered to the battery. Charging during CV phase happens much slower due to ever decreasing current. When high rate is used in CC phase, the charging voltage limit is reached much faster due to cell heating and resistive drop (seen as voltage increase) similar to that of discharge curve (at high discharge current battery voltage drops, at high charge current voltage steps up). As a result, less charge is transferred to the cell, for example just 60 – 80 % or even less. The remaining charge must be delivered in the slower CV phase. The other issue with fast charging is temperature rise. Both resistive losses and ionic conductivity losses produce heat which increase temperature of the battery. When max temperature threshold has been reached, charging current must be decreased hence fast charging transitions to standard charging. This problem can be alleviated if proper thermal management is used for the battery pack. A quality cooling system can keep temperature low (well below max limit, preferably not more that around 30 °C) to allow fast charging while avoiding performance degradation. For some battery models, active cooling can allow to increase charging current even higher to achieve faster charging time. In general, it is commonly assumed that EV fast charging (CC phase) can charge battery only to 80 % SoC level [57].

Both LFP and LTO chemistries have some charging advantages. As LFP is thermally more stable it can be charged with 3C rate if proper temperature monitoring is used. The charging performance of some LTO cell models is dramatically different. While typical charging rates can be as high as 6C, cells with 10C and 60C pulse charging capability are available on the market. Some of such cells can be charged to 80 % SoC in just 6 minutes [58].

The CC phase ends and transition to CV phase happens once the voltage of the cell reaches charging voltage limit. For LCO, LMO, NMC and NCA chemistries, the charging voltage is 4.2 V. Charging to a higher voltage will result in small addition to the capacity however the cell will degrade faster, and the safety risks increase dramatically. Some high-energy optimized cells can be charged to 4.3 V however in automotive applications the charging voltage is lowered to improve battery lifespan (available/usable battery capacity is lower than the nominal battery capacity) [59]. Lower charging voltage naturally results in lower max SoC hence it is an easy method to decrease used capacity range. As previously noted, decreased used capacity (never fully charged, never fully discharged) increases cycle life. Additionally, keeping a Li-ion cell at its maximum voltage (same as charging voltage) stresses the internal structure which leads to overall degradation. Lowering max voltage reduces this internal chemical stress and promotes longer calendar life [60]. Again, LFP and LTO max charging voltage is significantly different, same as nominal voltage. Depending on the exact chemistry LFP max charging

voltage can be in 3.65 – 4 V range. 3.65 V is the dominating voltage level while 4 V in some datasheets will be given as the absolute maximum level after which damage is imminent. LTO cells can be charged to 2.8 – 3 V level – significantly less than other graphite anode-based LIBs.

The charging (SoC increase) speed gradually decreases during CV phase as the current rate declines. In standard charging, CC phase lasts less than 1 hour while CV phase can be in the range of 1 to 2 hours. As previously noted, majority of charge is delivered to the battery during the short CC phase while the long CV phase delivers remaining fraction. If it is required to fully charge a battery the additional step of cell balancing can increase charging time. The charging is terminated when charging current decreases below cut-off limit. This limit traditionally is 10 – 3 % of the 1C rate. Charging cut-off conditions are not always provided by the battery manufacturer, hence there is some engineering freedom. Additionally, charging timeout can be introduced as well. For example, the datasheet of *US18650VTC6* cell (manufactured by *Sony*) states CCCV charging to 4.2 V at 2.5 A (0.5C) with 2.5 h cut-off - a current cut-off limit is not specified [52]. The timeout criterion can be helpful when the battery reaches its end of life. In some cases, the self-discharge/leakage current increases as the battery ages. If the leakage current is higher than current cut-off level, then battery charging current will never decrease below set cut-off and charger will indefinitely continue charging the battery. A timeout can prevent this situation.

Charging is affected by temperature. Cell/battery datasheets provide information about ambient temperature for three situations: discharge, charge and storage. Traditionally one would expect that storage temperature range is the broadest. It is not so in case of LIBs. For short term storage (less than a month) it is the same as discharge operating temperature whose range can be –20 °C to +60 °C. As the storage time increases, ambient temperature should be kept within –20 °C to 25 °C range to maintain calendar life. Temperature during charging must be in 0 to 45 °C range, preferably below 30°C. Already under 10°C standard charging rate should be decreased to 0.25C. It is generally assumed that LIBs should not be charged if temperature is below 0 °C – if temperature is lower, ion mobility is restricted and charging will cause deformation of electrodes, which in turn will degrade performance and safety due to plating of metallic lithium. Both the LIB and the charger should be equipped with temperature monitoring to perform charging only if temperature is within safe operation range. If a battery will be required to be charged at freezing temperatures (an EV in northern countries where the winter temperatures are well below 0 °C), then battery pack has to be equipped with thermal management which can provide heating. Of course, the temperature of the LIB will rise on its own during charging due to internal losses – BMS has to prevent temperature rise above operating point. Temperature can be controlled by controlling current or by using active thermal management. It can be noted that charging temperature can vary from model to model and from chemistry to chemistry. Again, LTO excels in operation at low temperatures. An LTO *LT34* pouch cell made by *Leclanche* can be both discharged and charged at temperatures ranging from –20 °C to +55 °C [55]. Research laboratories are working on improvements for all Li-ion chemistries to allow charging at temperatures below freezing point. There are reports that some LIBs (non-LTO) can be charged at freezing temperatures albeit at very low rates.

### 3. ANALYSIS OF BATTERY MANAGEMENT SYSTEMS

LIBs and even single lithium-ion cells require an obligatory BMS which can have a variety of functions. The main task of a BMS is to maintain a safe operation of the battery – the safety of LIBs has always been an issue which requires special care. The functions can be divided in four groups: protection, monitoring, estimation and balancing. Safety essentially is protection. Some cells have some inherent safety features, such as overpressure, short circuit and thermal protection. Overpressure is implemented as a valve which will open when the internal pressure of a cell reaches critical level. Short circuit protection can be made as an internal fuse or a PTC resistive element whose resistance increases if its temperature gets too high – this acts as thermal protection as well. As these three mechanisms are parts of a cell, they do not constitute a BMS which is made using a set of external elements [61].

In simplest single cell batteries, the BMS (sometimes called cell/battery protection circuit) can be realized as a single printed circuit board which is equipped with a control logic (microcontroller, ASIC or analog), some measurement circuitry and switch elements. The control element uses measurement circuit to measure cell voltage, current and temperature. The measured voltage is processed to provide undervoltage (UV) and overvoltage (OV) protection. UV condition happens when the cell is being deep discharged. OV condition happens when the cell is overcharged. To prevent both of these damaging conditions, the control logic opens switch elements to stop further discharge or charging. Switches can be implemented as integrated elements of an ASIC, as discrete semiconductors (MOSFETs for example) or as electromechanical switches like relays or contactors. The same switches can be used to stop short circuit current (SC) and over current (OC). The SC condition happens when cell current is higher than absolute maximum rating. The OC condition happens when cell current is higher than rated nominal level for prolonged period. For example, some cell can have a pulse/peak current rating of 20 A at 10 seconds. If the current is 20 A for longer period than 10 seconds, then OC protection should be activated. In some cases, cell manufacturer limits pulse current depending on the cell temperature hence OC protection is often implemented together with thermal protection – high current naturally causes cell's temperature to rise. When temperature hits some set threshold (over temperature condition (OT)), current must be terminated. Both charging and discharging can be prohibited if temperature is out of safe operation area. This adds under temperature (UT) condition which is particularly important to prevent charging if temperature is below 0 °C. When implemented on cell level, these basic protection functions can be realized using small printed circuit boards. For example, the abundant 18650 size cell can be purchased in two variants: unprotected and protected. The unprotected variant is the basic cell with built-in PTC and vent features. The protected variant is equipped with an additional cell protection PCB (18 mm in diameter) which is attached to one side of the cell and the whole package is covered with plastic insulation. The resultant cell is a few millimetres longer as opposed to the unprotected one which is 65 mm long. A small protection board is incorporated in even the smallest pouch cells to provide at least minimal protection. In simplest form, the protection board can lack logic circuits and switches. A resettable fuse (for example PPTC) could be used instead.

The same protection features are implemented on battery pack level as well. Naturally, the complexity of the BMS increases with number of cells. In a multi-cell pack, parameter monitoring can be separated as a distinctive function. Designated front-end integrated circuits are being manufactured to fit most battery pack requirements. These ICs perform individual cell voltage measurements, pack voltage measurements, pack current measurements and temperature measurements. Some safety actions can be implemented in the monitoring ICs while others are performed by central controller. Front-end monitoring ICs are equipped with some sort of communication protocols to transfer obtained values to higher level controllers. In large battery packs (such as EVs) the battery is split in modules and each module can have its own module management board which transfers individual cell data to the central BMS board where it is processed, and appropriate actions are taken. Some new variables are generated at the pack level: max and min cell voltage, pack voltage, max and min temperature. These values can be further used not only for basic protection functions but for estimation of various performance indicators and cell balancing. Current monitoring can have its own board or at least IC. Shunt or Hall-effect sensors are used to measure instant values which can be used locally for fast short circuit protection or sent to central controller for advanced processing. For large high-performance packs, thermal management becomes an important issue as proper temperature conditions can greatly expand life span of LIBs [62]. Thermal management system can be a part of overall BMS. Battery packs can be actively cooled (or heated) – temperature of coolant medium and its flow must be monitored as well. BMS monitoring functions might include data logging of all mentioned measured parameters and additional ones like total cycles, max and min discharge levels, total delivered energy and other time and charge related variables.

The central BMS controller uses data from monitoring circuits to implement safety and protection functions. Additionally, data is used to calculate and estimate various performance indicators which can be further used to govern the pack or sent to higher level controllers and user interface. From overall vehicle system perspective, SoC estimation is one of the most important functions as it provides information about the remaining available proportion of charge. There are various SoC estimation algorithms depending on battery chemistry and application. Traditional input parameters are current which is being integrated over time (known as coulomb counting) and voltage of the pack which in turn depends on the instantaneous current value and temperature. As the battery ages, the inner parameter values change and SoC estimator must adapt to those changes. Additional information can be obtained from battery electrochemical impedance spectroscopy (EIS), which in some cases can provide direct information about SoC and in others it can aid to determine other parameters. It must be noted that SoC provides estimate in percent of nominal capacity and not the actual available energy. When the battery is new, 100 % SoC indicates that full rated energy is available, however as the battery ages, the capacity decreases thus after some years of operation the SoC of a fully charged battery will be 100 % but the actual energy might be just 80 % of what it was when the battery was new. This brings to another battery performance indicator: the state-of-health (SoH). In simplest form, SoH indicates how much the capacity of the battery has degraded. It can be estimated by dividing actual capacity by nominal rated capacity. The result

is expressed in percent. A 100 % SoH indicates that battery is new – this number will gradually decrease as the battery ages. SoH can be defined differently: it can represent the remaining useful life (RUL) of the battery. In this case the estimation becomes a lot more complex as it takes into consideration the impedance change (using EIS), the cycle life (in form of cycle counter) and other parameters like self-discharge. The result can be expressed in percent, remaining total storable energy or even remaining days before failure. Another parameter to estimate is the state-of-power (SoP) or simply available power. The available power depends on the ambient temperature, temperature of pack and SoC [63]. It indicates how much power for how long time can be discharged. This parameter is important in systems where future activity (high discharge rates) can be and has to be planned.

These previously described BMS function groups (protection, monitoring, estimation) to some extent are common for all high-performance/high-cost/high-reliability applications and battery chemistries. The last function – balancing, is not obligatory for most battery chemistries (although it can be used in all), however it is essential for LIBs. Lead-acid and NiMH chemistry cells can be balanced by trickle charging; however, it is not allowed for Li-ion chemistries, hence external circuits must be introduced to provide balancing. The balancing function is used to keep all cells of a battery at the same charge level although typically, balancing keeps cells at the same voltage level. There are two reasons for cell mismatch. The first one is that all cells are not created equal – manufacturing differences affect capacities, leakage and other parameters of individual cells. The other cause of misbalance stems from usage and ageing – temperature gradient, interconnection structure and just plain ageing can cause cells to develop different capacities, OCV curves and leakage over time. When all cells of a battery pack are perfectly balanced, the available capacity is maximal. However, if one cell is at lower SoC, it decreases the SoC of the whole pack – it will be the first cell to reach discharge cut-off threshold and hence the battery is rendered empty although other cells still have usable charge. This is the case where the weakest link determines the strength of the chain. Additionally, when a misbalanced pack is charged and a single cell is misbalanced at higher SoC, it will reach full voltage faster. If charging is continued, this cell will be overcharged with all damaging consequences. Hence charging must be stopped when any of the cells of a battery pack reach full voltage.

BMS and its functions can extend further. As mentioned, thermal management can be a part of BMS, especially if active temperature control is used: forced air or liquid cooling/heating. In EVs charging is controlled by the BMS as it has information about charging voltage, current and can provide temperature and safety control. BMS has communication interface to the main vehicle control system. Some sort of charger is usually implemented in an EV and in some cases the charger is a part of the battery pack. EV batteries are equipped with fuses and set of contactors: for work current and precharge. Smaller batteries can have some human machine interface (HMI), for example a set of LEDs, to indicate remaining charge. All of these features are controlled by the BMS.

### 3.1. Battery balancing methods

Over the years of battery management system development many different methods to balance the cell voltages or states of charge have been proposed. Quite often these methods of cell balancing are categorized in two groups: passive and active balancing. In some articles passive balancing methods are the ones that dissipate excess energy as heat. A traditional passive balancing method is to use a resistor in parallel with each cell to perform balancing at the cost of energy wasted as heat. On the other hand, active balancing methods are intended to remove charge from higher SoC cells and transfer it to cells with lower SoC. Traditionally some circuit with controllable switches and capacitors or inductors is used to transfer energy between cells with as little heat losses as possible. In some literature active balancing includes switched resistor balancing – probably because controllable switches are used to connect or disconnect resistors. However, here passive and active categories will not be used. A direct replacement would be dissipative and non-dissipative balancing. Here it is proposed to further split the non-dissipative group in selective charge/discharge methods and charge transfer methods as shown in Fig. 3.1.

The proposed categorization of balancing methods is not completely unique and unheard of – previously many researchers have done worked on balancing method classification and published their results in various articles. As mentioned above, quite often the classification of methods begin by splitting all methods in active and passive (dissipative) groups [64][65][66][67][68]. In literature, passive methods include variations of dissipative balancing topologies and the overcharge method. Active balancing group includes almost everything else under different naming: capacitor-based methods, inductor-based methods, transformer-based methods, converter based methods. There are some interesting classification proposals, each with some benefits.

In [69] charge equalizers are primarily divided by their control architecture: centralized or individual cell control. For centralized control a central controller is monitoring all cells and their equalization circuits (switched capacitor, transformer with multiple secondary windings) while for individual cell control type each cell is equipped with some local control activate energy transfer from cell to cell or from pack to cell using shunting or various converter-based methods.

Another approach is to classify active methods based on the energy flow among the cells: cell to cell, cell to pack, pack to cell and combination of cell to pack to cell [68][69]. This classification does not promote individual elements (capacitors, inductors, transformer) or converter types which makes it a universal and effective tool to distinguish balancing methods based on the actual charge transfer functionality which is required for cell balancing in different applications.

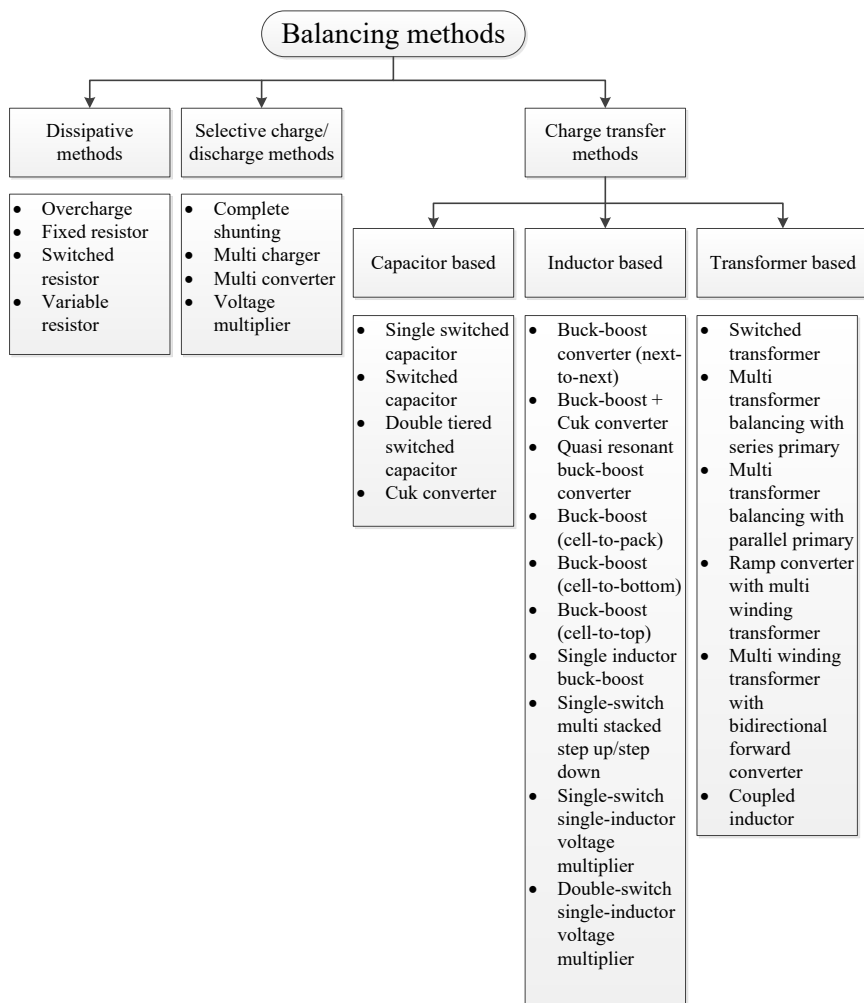


Fig. 3.1. Categories of balancing methods.

Some researchers for classification distinguish only some major groups based on the converter/method type. The types are shunting, shuttling and energy converter where shunting traditionally is some sort of dissipative method although in [70] buck-boost and boost converter is among shunting methods. Shuttling methods are related to various circuits that utilize capacitors to transfer energy between cells [65][71][70][72]. The energy converter group most often consists of converters based on switched transformers, multiple transformers, shared transformers, flyback structure, forward structure, buck-boost, multiple inductor converters, Cuk converter, ramp converter, full-bridge, resonant and quasi-resonant converters [73]. Often a major group is dedicated just to capacitive energy transfer methods (shuttling) such as single switched capacitor, switched capacitors, double-tiered capacitors [74][72][71].

The proposed category classification (Fig. 3.1) can be compared to the described classifications of other authors. Here the dissipative methods branch is exclusively devoted to

methods that convert any excessive charge to heat by using resistance of electronic elements or by applying overcharge. Selective charge/discharge group corresponds to auxiliary charger and complete shunting methods while the major branch of charge transfer methods is the largest group that incorporates capacitive shuttling and transformer/inductor converter-based methods.

### 3.2. Dissipative balancing methods

At least three main dissipative balancing methods can be distinguished: trickle charging, fixed resistor balancing and switched resistor balancing. The use of trickle charging to balance cells voltages could be regarded as a true passive balancing method because it involves no additional circuitry. Some types of cells can be brought to light overcharge regarded as trickle charge to equalise the voltages of the cells of the battery. One example is lead-acid batteries that can be trickle charged in the final state of charging. When being trickle charged the water in battery electrolyte is split to oxygen and hydrogen. Both gases could be vented or returned back to water using catalytic additives. The main result is that this process turns the energy delivered to the overcharged cell into heat while the other series connected cells can continue to charge until all cells reach full voltage. Additionally, trickle charge makes up for the energy lost as self-discharge. For this reason, trickle charge is sometimes referred to as float charging. While small strings (as the cell count of the string increases, the energy lost during trickle charging increases exponentially) of lead-acid and nickel metal hydride cells can be balanced using trickle charging, the lithium-ion chemistries are not capable to accept virtually any overcharge. This is because the full lithium-ion cell voltage is close to the electrolyte breakdown voltage. The electrolyte is non-aqueous and can be flammable which leads to more danger if the cell is being overcharged.

#### Dissipative fixed resistor balancing

The other group of dissipative balancing methods utilize external resistors to dissipate the extra energy which would otherwise lead to cell overcharge. The simplest form of resistor balancing is to just connect a resistor in parallel to each cell of the string (Fig. 3.2). All resistors are constantly discharging all of the cells. If a cell has higher voltage, then the current through resistor will be increased as well. The result is a balanced battery pack with minimal development and components costs. The actual balancing efficacy of balancing process (time required to equalize cell voltages) depends on the parameters of resistors: the resistance sets the balancing current from one side and the rated power limits it from the other side. As the balancing current increases so does the dissipated power – at some point the issues of thermal management becomes significant. However, the main disadvantage is the high energy loss. The balancing power  $P_{bal}$  per cell is given in (3.1.) where  $V_{cell}$  is cell's voltage while  $R_{bal}$  is the resistance of the balancing resistor.

$$P_{bal} = \frac{V_{cell}^2}{R_{bal}}. \quad (3.1.)$$

Since the resistors are always connected to the cells, they are constantly discharging the battery pack whether it is being charged, discharged or in stand-by. The result is similar as if the battery pack had increased self-discharge. Another disadvantage is that this method can bring the cell energy/voltage levels only down thus justifying this method only during battery

pack charging. The permanently connected resistor balancing could be used for all cell types but in practice it is used rarely due to the high permanent energy loss.

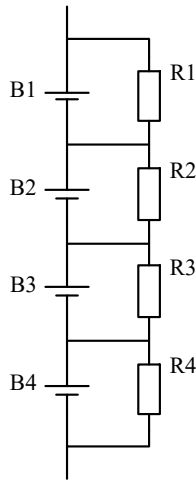


Fig. 3.2. Dissipative fixed resistor balancing circuit.

### Switched resistor balancing

The most commonly used balancing method is switched resistor balancing which is referred to as bypass resistive shunting, resistive current shunting, charge shunting and dissipative resistor shunting as well. If the switches are implemented as transistors driven by cell voltage comparators then the topology is regarded as analog shunt equalization [75]. In [67] it is grouped under active balancing methods as some control is done to organize the balancing process while review articles [66][65][76] group it under passive methods because of the dissipative action. The basic balancing operation remains the same as for the previously described dissipative fixed resistor balancing – removing the excess charge from the target cell through passive, resistor, element until the charge matches those of the lower cells of the pack or a reference state of charge. The difference is that the resistors can be disconnected from the cells to prevent the additional unnecessary cell discharge. A simplified schematic of the balancing topology is shown in Fig. 3.3.

This type of dissipative balancing with switched shunting resistor is a common balancing method because of its reliability and simplicity [66][65][67][76]. The basic dissipative resistor balancing circuit topology can work in two modes, continuous mode and detecting mode. In continuous mode the resistor switches of all cells are controlled by the same signal, that sets the switches on or off at the time. In detecting mode each switch is controlled separately according to the state of the cell it is connected to and to the commands of the master controller if any. The switched resistor balancing can be designed to operate without a master controller. In such a case each cell is equipped with the same circuit that can measure the parameters of the particular cell and connect the resistor if necessary. The main advantage of this mode is that there is no complex control and cell balancer module circuit is still very simple. However, without a central master module there is no data exchange and overall parameter measurement

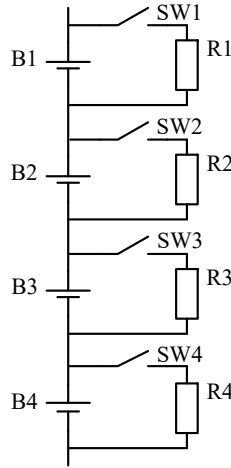


Fig. 3.3. Switched resistor balancing topology.

which can provide information of battery pack parameters, improve charging process and improve the balancing process itself. If a master module is used, then the basic cell balancer functions are the same with additional function of communication to send cell voltage and temperature information and receive commands from the master module. The cell balancer can still be partially autonomous as it can switch on the bypass circuit according to the upper or lower cell voltage levels which are programmed by the master module. The master module itself grants many benefits as it is an essential part of the battery management system while just having cell balancing modules would be a partial management system – one that does simple balancing without any cell protection or state estimation.

Switched resistor balancing can be used for both top and bottom balancing. For bottom balancing, prior to battery assembly all cells are connected in parallel and thus equalized according to their open circuit voltages. As the name implies for bottom balancing the cells are equalized to match their empty state – at their bottom state of charge. For top balancing all cells are equalized so that during charging they all reach 100 % SoC at the same time despite the differences in their respective capacity.

While both types of balancing could be used, the top balancing is traditionally more preferred. It is also called charging balancing. In this mode the charging current  $I_{cell}$  of each cell can be determined using (3.2.) where  $I_{chg}$  is the total charging current,  $V_{cell}$  is voltage of the cell  $R_{bal}$  is the resistance of the balancing resistor and  $R_{on}$  is the resistance of the switch which can be similar to the  $R_{bal}$ .

$$I_{cell} = I_{chg} \cdot \frac{V_{cell}}{R_{bal} + R_{on}} \quad (3.2.)$$

Part of the charging current is diverted to balancing resistor. Bottom balancing has a drawback that after each battery cycle the total SoC and each cell individual SoC is brought to 0 %. If the battery pack is not soon charged again then the cells of the battery might go into over discharge because of self-discharge and some current draw due to the connected balancing circuit. Additional disadvantage is that the battery pack is discharged to 100 % depth of

discharge every cycle which according to the lead-acid and lithium-ion battery manufacturers decreases the cycle life of the battery. The lower the depth of discharge the more cycles the battery will operate. For top balancing all of the cells are at their 100 % SoC after every charge cycle which could be considered as minor drawback as fully charging a lithium-ion battery tends to decrease its lifetime.

In reality the cells of a battery pack will each have a slightly different capacity which results in a situation that a top balanced battery pack is considered empty once the cell with the lowest capacity reaches 100 % DoD. All of the other cells will not reach the empty state. However, in practice in most cases the battery pack is not discharged totally as it would be a bit troublesome for the user of the particular cell phone, laptop or especially electric vehicle. As the battery is not fully discharged every cycle, it will have more cycle life if compared to a battery that is fully discharged during each use. During charging a top balanced battery pack will charge slower due to cell balancing taking place but throughout this process some charge will be stored in the cells which later translates to longer battery runtime. During discharge of a bottom balanced pack, once a single cell will reach empty cut-off voltage the pack will not supply any more current to the load, but instead will just discharge the remainder of pack's energy without any extension of the battery runtime.

One could argue that for both top and bottom balanced packs some part of the balancing could be carried out during middle region of battery discharge. While theoretically it would be possible in practice the OCV versus SoC curve for lithium-ion batteries is very flat and it would be difficult to precisely measure the SoC of cells just by measuring the cells voltage which additionally is affected by the load current – different cell internal impedances can create significant errors. Traditionally the end of charge and end of discharge regions are used to determine which cells are out of balance because in these regions tens of millivolts can account for a single percent of SoC. For these aforementioned reasons the top balancing is preferred for switched resistor balancing.

The losses of top balanced switched resistor balancing method can be analysed analytically. When charging the pack, balancing power loss  $P_{loss}$  is zero while no balancing resistor is activated – this amounts for most of time of the charging procedure if cells are equal and closely balanced. During charging, once the first cell reaches full voltage/balancing voltage ( $V_{bal}$ ), its balancing resistor is activated and charging current is decreased to match the balancing current (3.3.) (an idealized case):

$$I_{chg} = I_{bal}. \quad (3.3.)$$

As a result, the SoC of given cell does not change while balancing losses appear according to (3.4.):

$$P_{cell\_loss} = V_{bal} \cdot I_{bal}. \quad (3.4.)$$

Gradually, more cells reach balancing voltage, and add to the total power loss which can be calculated using (3.5.). Eventually  $n-1$  cells are full and just one cells is being charged –  $P_{loss}$  is at max value and can be calculated using (3.6.). The charging current is reduced to zero (charging is stopped) once the last cell reaches full voltage hence  $P_{loss}$  becomes zero as well.

$$P_{loss} = \sum_{i=1}^{n_{bal}} P_{cell\_loss\_i} \quad (3.5.)$$

$$P_{loss\_max} = (n-1) \cdot V_{bal} \cdot I_{bal} \quad (3.6.)$$

The balancing power loss is a discrete function as can be seen in 20-cell battery example in Fig. 3.4. The power loss gradually increases in steps from zero to its max value when 19 cells ( $n-1$ ) are full/being balanced. The duration of each step is related to cells SoC mismatch during charging operation.

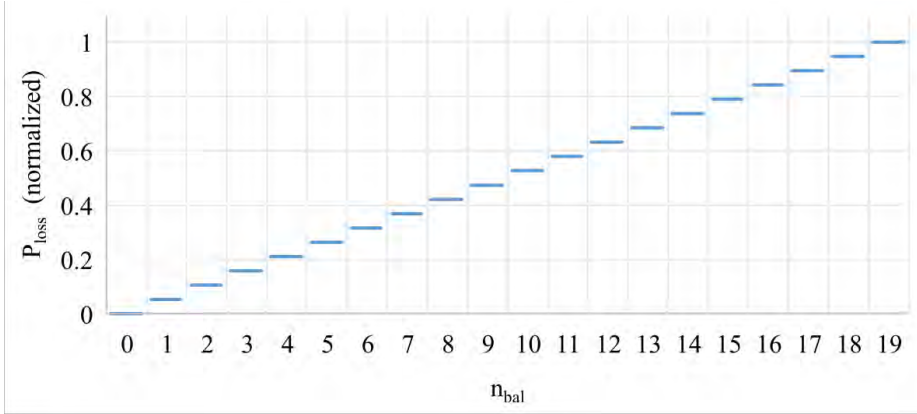


Fig. 3.4. Balancing power loss of a 20-cell battery.

The total energy loss during balancing operation is more useful variable as it can be easily compared to total energy loss of other balancing methods. Generally, balancing energy loss  $E_{loss}$  is an integral of balancing power loss (3.7.):

$$E_{loss} = \int_0^{full} P_{loss}(t) dt, \quad (3.7.)$$

where  $E_{loss}$  – total balancing energy loss, Wh;  
 $P_{loss}(t)$  – balancing power loss function, W;  
 $full$  – time at which balancing is stopped, s.

The integration interval is from the beginning of balancing operation to the end when last cell reaches its full voltage. As the  $P_{loss}(t)$  is a discrete function then  $E_{loss}$  can be expressed as a sum of individual  $P_{loss}$  levels (3.8.):

$$E_{loss} = \sum_{x=1}^{n-1} (x \cdot V_{bal} \cdot (\Delta C_{x+1} - \Delta C_x)), \quad (3.8.)$$

where  $E_{loss}$  – total balancing energy loss, Wh;  
 $n$  – total number of cells;  
 $V_{bal}$  – balancing voltage, V;  
 $\Delta C$  – capacity difference, Ah.

$\Delta C$  is specific to every cell – it shows the relative difference in capacity in respect to the previous cell and the one which is being balanced. For the first cell  $\Delta C_1=0$  and each next  $\Delta C_x$  value can be calculated as difference between previous  $C_{x-1}$  and given cell's  $C_x$  value. If  $\Delta C$  value span and distribution is narrow then resulting  $E_{loss}$  will be small. Equation (3.8.) can be used to calculate energy losses of a 20-cell battery with normal cell capacity distribution at different capacity variations. Fig. 3.5 shows the obtained graph. 10 sets of random normal distribution capacities were generated for each of capacity variation points from 0.5 % to 4 %. The line shows average energy losses while dots mark the max and min losses of performed calculations. If capacities of battery cells have normal distribution, then balancing losses will increase linearly with increase in cell capacity variation.

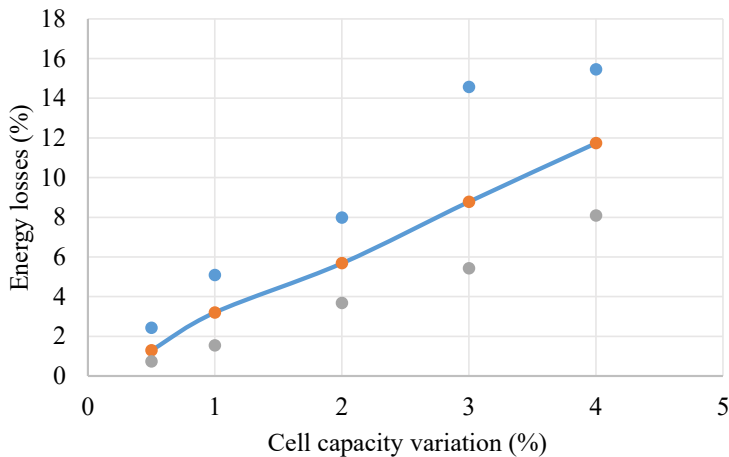


Fig. 3.5. Energy loss of a 20 cell battery with switched resistor balancing at different cell capacity variation levels.

Despite the overall criticism of inefficient operation, there are multiple scientific publications that utilize variations of the switched resistor balancing. In one case a special smart FET with current protection is used as the switch and resistor with local balancing control thus simplifying the circuit design and overall control [77]. In [78] and [79] switched resistor balancing with relay switches or analog-controlled Darlington transistors is regarded as suitable for use in aerospace products.

Application specific integrated circuits have been developed by major manufacturers to perform cell monitoring and balancing. One of such commercial solutions is the *DS2751* chip from *Maxim Integrated*. The chip performs single cell current, voltage and temperature measurements. The obtained results can be sent to a central controller using *Dallas* 1-wire interface. If current measurement is made, then the chip performs current accumulation to estimate the remaining charge in the cell. *Zanithic Technologies* has provided a solution for high cell count battery pack. Two optocouplers are used to isolate the communication line and a third optocoupler is used to drive a switched resistor for balancing purpose [80]. The drawbacks of this solution are: high optocoupler count increases costs; chip with integrated temperature measurement sensor might not be placed at the hottest spot of the cell; the cell unit cannot

perform balancing on its own – it has to receive a command from a master controller to switch on or to switch off the resistor.

Alternative product is offered by *Texas Instruments* in the form of *bq29312* and *bq2084* devices. These devices are designed to perform the various functions of a battery management system. One of the chips is used to measure and balance the cells while the other performs measurements of the whole battery pack and estimates the SoC. As this system is designed for portable equipment the battery cannot exceed 8 cells in size. *bq29312* uses internal switched resistor balancing while *bq78PL114* device uses active balancing using *PowerPump* technology which essentially is buck-boost balancing [81]. However, this device currently is discontinued and replaced by *bq34z100*, *bq77908* and *bq77910* which use only switched resistor balancing. It can be concluded that the active balancing solution was not enough profitable, or the technology has some significant flaws. The more simple *bq76PL536* switched resistor balancing integrated circuits are used in [82] where balancing is done according to both cell voltage and SoC estimation. Authors claim that the result is an improved balancing performance with reduced balancing time due to balancing during all charging time and not only when cells reach full voltage.

An integrated experimental resistor balancing solution is presented in [83]. While the traditional method is to use a switch element for the connection of shunting resistor, here a set of two operational amplifiers are used to control a PMOS device in the active region. The PMOS with series resistor is connected in parallel to each cell of the pack. The operational amplifiers use charging current signal and cell voltage signal to set balancing current level through PMOS. The solution is simulated using 0.35  $\mu\text{m}$  technology and authors claim that it can provide sufficient balancing as the balancing current is set by the charging current of the whole pack.

Authors of series of articles [71],[68] and [84] propose the use of a MOSFET operated in saturation mode as the combination of switch and shunting resistor. For the cell balancing units, a MOSFET is connected in parallel to each cell. A microcontroller generates PWM signal that is low pass filtered and used to drive the gate of the MOSFET. The current of the MOSFET has to be measured to achieve stable shunting operation. The main advantage of this balancing method is that a constant and variable shunting current is provided by just one element. The disadvantages include the need of current feedback for stable operation and more complicated heat management if compared to resistor shunting. The same authors have done work to research the balancing methodology. The proposed cell management system uses average cell voltage to determine which cell should be shunted to equalize the battery pack thus decreasing the balancing time.

Traditionally switched resistor balancing is regarded as an inefficient method and many other methods are proposed as better alternatives [66][65][67][70][64]. However, as previously indicated multiple commercial products are available and are actively implemented in battery pack design. Battery pack performance has to be evaluated in depth to understand whether simple switched resistor balancing is responsible for considerable losses, or it can be successfully used to maintain a good performance of battery pack.

### 3.3. Selective charge/discharge methods

In this work, the group of non-dissipative balancing methods is intended to transfer charge from fuller cells to the empty ones unlike the dissipative methods where the redundant charging energy was wasted as heat. This group can be further split in selective charge/discharge methods and charge transfer methods. The selective charge/discharge methods can be divided in three main parts: multi charger, complete shunting and multi converter methods.

The simplest method to charge a battery pack without any balancing could be the selective multi charger balancing. A separate charger is used for each cell to perform selective charging. Once the particular cell is full, the charger is disconnected. This method can be used if the cell count of the battery is small. This method was used to charge the kart's battery pack when six series connected lead-acid batteries were used for each pack. Six laboratory bench power supplies were used to charge six batteries. The main drawback of such method is obvious: a charger is required for each battery – for high cell count battery packs it would be quite impossible to add a charger for each cell. Additionally, this method performs balancing only during charging and special control system or manual control is required to perform the individual cell/battery charging.

#### **Pack reconfiguration based**

As the name implies, pack reconfiguration methods change the connections of the cells to avoid charging or discharging particular cells or fragments of strings. These methods are sometimes named complete shunting methods. Two similar reconfiguration methods are presented in [85] and [86] where two power switches are used to bypass a selected cell (Fig. 3.6) that is typically degraded if compared to others. The authors of [85] have continued their work in [87] where the self-reconfiguring battery pack is equipped with a dedicated constant current adaptive voltage (CCAV) bidirectional DC/DC converter used for charging and discharging. [87] and [86] differ that in one case a single MOSFET is used per switch while for the other a set of two MOSFETs are used for each fully controllable bidirectional switch. The authors of [88] propose to use a diode and a thyristor for each switch which in their research yielded satisfactory results. The pack reconfiguration method has been used in [89] to reconfigure high power battery modules instead of single cells thus achieving higher efficiency and lower system costs while still keeping some reconfiguration flexibility. The reviewed articles used semiconductor switches while in some cases it could be a reasonable choice to use relays to add additional safety when the relays are open. In some cases, the relays could be more efficient if compared to semiconductor switches. The mentioned methods provide certain functionality while both charging and discharging. As all balancing methods, pack reconfiguration methods have some disadvantages. One of the disadvantages to be noted is that half of the shunting switches are always conducting the charging/discharging current – switch resistance is added to the battery internal resistance and thus there are additional conduction losses. If the battery pack is intended for high power applications, then there is a need for high current shunting switches which can significantly increase both the costs and the size of the battery pack. Quite often it can be difficult to add additional series switches. Another drawback

is related to the nominal voltage of the battery pack. When a cell is being shunted the voltage of the battery pack decreases by the voltage value of the particular cell. This is disadvantageous if the load is sensitive to the battery voltage. Additionally, the battery charger is required to be able to charge the battery pack a decreased voltage which means that the charger becomes an integrated part of the battery energy storage system. However, in this regard, the main advantage of complete shunting is that this method is capable to provide good functionality of the battery pack even if one or several cells of the stack are damaged to the point where they can be regarded as open circuit.

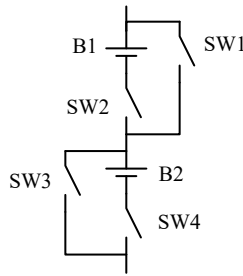


Fig. 3.6. Complete shunting balancing topology.

### Multi converter

A more advanced type of shunting method is the group of multi converter based balancing methods. Typically, these converters are regarded as full-bridge multilevel converters or modular multilevel converters. The basic principle is that each cell [90] or a group of cells [91] is equipped with a bidirectional converter (typically a full-bridge converter) and the outputs of the converters are series connected to build the series string of the battery (Fig. 3.7). By controlling the individual converters each cell can be selectively charged, discharged or completely bypassed if needed. The current of each cell can be controlled independently as opposed to the pack reconfiguration methods. One of the special advantages is that this system can be used as the main converter – the cascaded H-bridge multilevel inverter. The inverter can be used to supply motors [92][93] or to be connected to the grid [90][94][91]. This feature is of great importance as multilevel converters can provide improved voltage waveform with lower harmonic content [91]. However, the main challenges of this method utilization is related to two aspects. First, each cell (or cell group) needs an individual converter which complicates the design of battery pack. As each converter consists of semiconductor switches, there is additional losses – mostly conduction losses. If a MOSFET H-bridge topology is used, then the additional conduction losses  $P_{cond}$  (battery is supplying full voltage without balancing) can be calculated using (3.9.) where  $n$  is number of converters,  $I_{bat}$  is battery current and  $R_{DSon}$  is MOSFET on-state resistance.

$$P_{cond} = n \cdot I_{bat}^2 \cdot 2R_{DSon} \quad (3.9.)$$

As noted in [90] the use of underutilized MOSFETs leads to additional losses to the overall system. The other main challenge of this balancing method is related to control. First it has to

estimate the SoC of each cell, which is more complicated if compared to other methods because the charge/discharge current is different for each cell. Some specific pseudo-OCV measurement methods have been done in [90] with good results. Second, it has to control all cell converters to both provide the necessary power and voltage waveform to the load and at the same time to maintain good balance of the cell's SoC by selectively using the individual cells. The reviewed articles have achieved good performance of cell SoC balancing even being able to balance cells with 45 % capacity difference [90]. The authors of [93] have done additional work to analyse the heating and cooling effects of multilevel converter based cell balancers and have concluded that temperature deviation of the cells can lead to premature ageing of battery pack and that multilevel converter based cell balancing can be effectively used to not only to balance the SoC of the cells but balance the temperatures of the individual cells as well which comes as additional advantage of such balancing method. It must be emphasized that this balancing method is a promising solution because it has two functions: balancing and multilevel converter. One could argue that multilevel functionality is the best part while the cell balancing is just a convenient feature.

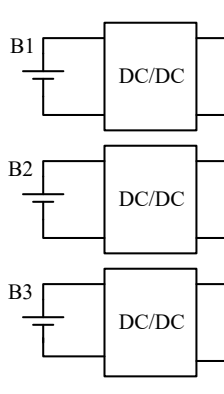


Fig. 3.7. Multi converter balancing topology.

### Selective charging balancing

In [95] a method to selectively charge a battery pack is presented. A forward converter with one output is used as the charging source. Then a switch selector block is used to select an individual cell to be charged. Two MOSFETs and two diodes are required to connect a cell. For a  $n$  cell stack,  $2n+2$  MOSFETs and  $2n$  diodes are required. The proposed system performs pulse charging as only a single cell of the pack is charged simultaneously. The balancing of the cells is achieved by varying charging time of individual cells – cells are equalized only during charging. Additionally, this particular charging system is designed to provide pulse discharging to improve battery lifetime. Authors of [96] has improved the charger system even more to provide a single stage power factor correction at the charger converter input. Overall this method could be used for low cell count battery packs while for larger packs the complexity of switch selector block and wiring can become too sophisticated.

### 3.4.Charge transfer methods

#### Capacitor based charge transfer methods

The basic idea and the most common type of capacitor-based charge transfer is to connect a capacitor to one of the cells of the stack using a matrix of switches as shown. The capacitor will charge to the particular cell's voltage. Then the capacitor is connected to the next cell of the stack. If the next cell has lower voltage, then the cell will be charged from the capacitor. If the next cell has higher voltage, then the capacitor will be charged to a higher voltage. Continuously a capacitor or capacitors are connected to corresponding cells of the pack thus transferring energy from the cells with higher voltage to the cells with lower voltage.

Arguably the most basic method is named (single) switched capacitor balancing method as it uses a single capacitor and set of switches to transfer energy (Fig. 3.8). Alternatively this method is called flying capacitor charge shuttling method [65] or single switched capacitor equalizer. One of the main advantages of this method is that in its most basic form it requires very little control and measurement circuits. Basically, the balancing circuit can be operated continuously by relatively slowly circulating the capacitor connections. Eventually the voltage of the cells will be equalized by charge shuttling through the capacitor. The circuit and control are simple as is the implementation. This method can transfer energy to any cell of the stack without additional steps but for this task additional measurement and control circuitry is required. The disadvantages include low equalizing capability if the number of cells is high [77][97], poor modularity [70], additional measurement circuitry and complex control required if equalization speed is to be improved [66], high current stress as the capacitor is directly connected to a cell, high switch count [98] as the circuit requires SPDT and SPST bidirectional switches which usually are implemented using two transistors. In some references the switch elements are noted as relays [73]. Some of the disadvantages can be overcome by using a more complex switch matrix-power converter-electric double layer capacitor (EDLC) topology. Switch matrix is used to selectively connect a cell to the converter which discharge overcharged cell to an EDLC, in the next phase, EDLC is discharged and switch matrix is used to charge an undercharged cell. While the system is more complex and expensive, it can achieve higher balancing rates and reach 90 % efficiency [99].

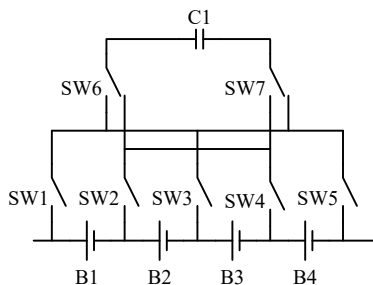


Fig. 3.8. Single switched capacitor balancing topology.

A method that is usually considered higher performing uses a capacitor per two cells. The topology is shown in Fig. 3.9. This method often is called switched capacitor balancing method

[100], capacitor shuttle balancing method or charge shuttling [101][102]. It can be seen that the previous method is often called the same. In some cases, the two methods are distinguished by adding word “Single” to the method that uses a single capacitor [72]. It must be noted that generalized literature review shows that this method could be the first capacitor-based balancing method [103]. The total capacitor count is  $n-1$  where  $n$  is cell count. The circuit uses only bidirectional SPDT switches and switch count is the same as the cell count. This method can transfer energy from one cell to the next (next-to-next balancing) thus a major disadvantage is the low equalization speed and poor efficiency if the mismatched cells are far apart in the stack. However, a significant advantage over the single capacitor version is the easy modularization feature [67]. The equalization time of this method can be improved by adding one extra capacitor and a set of switches which allow to connect this capacitor to the first and last cells of the stack [97] thus making a full balancing loop. The proposed upgrade has limited usability as it decreases modularity and requires switches that have voltage rating higher than that of the stack. Another way of improving the balancing speed is to disconnect capacitors from one another. As a result the charge transfer can be properly controlled to increase energy efficiency and decrease balancing time down to 5 times [104]. However, it must be noted that for this topology each capacitor is equipped with a set of two SPDT switched thus increasing circuit complexity, size and control requirements.

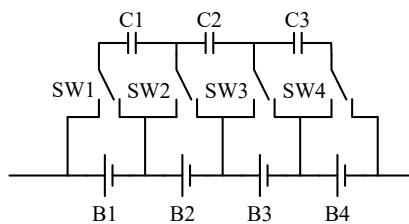


Fig. 3.9. Switched capacitor balancing topology.

The switched capacitor method can be designed to be double-tiered. Occasionally the methods are distinguished by adding terms single-tiered or double-tiered at the beginning of methods names. In [72] this method is named double-tiered capacitive shuttling method. The additional capacitors permit energy transfer between cells that have one cell in between as shown in Fig. 3.10. The second tier decreases both voltage equalization time and energy losses. A deeper balancing reveals additional advantage of lower switch current stress and lower sensitivity to parameter variation [105]. The same source reveals that if the capacitances of both tiers are large, then the benefits of the second tier become poor. Eventually the same authors published an article in which an in-depth analysis of the circuit that reveals the effects of parameter variation. Such parameters as capacitor capacity, switching frequency and switch resistance plays an important role in energy efficiency and speed of equalization. The analysis shows that there is an optimal crossover frequency and switch resistance that permits the best functionality for this method [106].

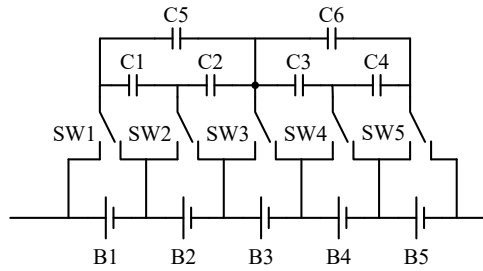


Fig. 3.10. Double tiered switched capacitor balancing topology.

A variation of switched capacitor method can be used to implement battery modularization. If a battery consists of a long string of cells, such as BEV or HEV, where cell count approaches or breaches a hundred of series connected cells, some balancing methods can become hard to implement and ineffective. One way of solving this problem is to modularize the pack, so that each module has a comfortable number of cells. Each module can be balanced separately. One additional balancer is required to balance between modules. For example, switched capacitor balancing can be used to balance voltages within a module. The same topology can be used to balance the voltages of the modules – each module is regarded as a cell for the module balancing system layer. From layer perspective this method is similar to double tier switched capacitor balancing topology. This approach can improve balancing time while increasing complexity, size and costs [107][108]. Additional benefits include effective utilization of well-known balancing methods of small battery packs, good flexibility and a chance to use different balancing topologies for internal module and whole pack equalization.

Previously reviewed capacitor-based charge transfer methods used capacitors as plain intermediate charge storage devices. Quite different approach is to use a capacitor as the central energy transfer element in a power electronics converter. One such example is a Cuk converter balancing topology [109][72]. The balancing topology is shown in Fig. 3.11. The topology can transfer energy between two series connected cells in either direction. This is a disadvantage if the energy is to be transferred between cells that are far apart as the system performance drops as more individual cell equalizers are utilized to balance a single cell. Capacitor  $C1$  is used as an intermediate energy storage container. For a  $n$  series connected cells there are required  $n+1$  individual cell equalizers. The main advantages of this method are good modularity, full duty cycle operation and if the  $L1$  and  $L2$  inductors are coupled, then there is no current ripple at converter input/output which improves overall performance. It has been researched that fuzzy logic control can be used to decrease cell equalization time by 32 % [110][111][112].

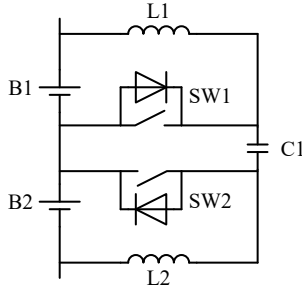


Fig. 3.11. Cuk converter based balancing topology.

### Inductor based charge transfer methods

The next group of charge transfer methods is based on converters implementing inductors as the main intermediate charge storage device. One of the most popular inductor based balancing topologies is buck-boost converter based topology [113][82] which is also named *PowerPump* [114], cell to cell PWM controlled converter [67], buck-boost chopper [115], PWM controlled shunting [70], bidirectional current pump [116] and bidirectional non dissipative current diverter [117]. The basic topology with two individual cell equalizers is shown in Fig. 3.12. This method is performing charge transfer from cell-to-cell between cells that are next-to-next connected. An individual cell equalizer is connected to a pair of cells thus for  $n$  series connected cells there are  $n-1$  cell equalizers required. It can be noted that this method is similar to that on the Cuk converter based. If compared, buck-boost based topology has disadvantages of high current ripple and narrow duty cycle variation for balancing operation. However, this method requires only one inductor and no capacitor per individual cell balancer which makes it cheaper, smaller and easier to design and implement.

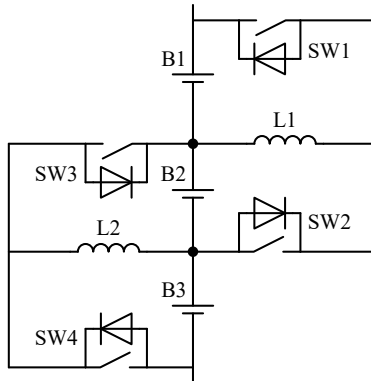


Fig. 3.12. Buck-boost (next-to-next) based balancing topology.

From the reviewed charge transfer methods, only for this method a commercial product has been found in the form of *Texas Instruments bq76PL102* integrated circuit [114] and an application note using *Freescale Semiconductor* parts [118]. However, it must be noted that this product is not recommended for new designs and the manufacturer recommends replacing

it with a switched resistor based balancing topology. This indicates that there are some profound problems with charge transfer balancing market. Nevertheless, this method is quite popular as one of the most basic solutions to perform charge transfer balancing. It can be operated at 50 % duty cycle without feedback to provide a sort of sensor less solution [119]. However, if operated at 50 % duty cycle, the balancing current is determined by the two cell voltage differences and parasitic elements of the circuit which means that is difficult to predict the current value and thus design the circuit. If as typically, cells have small voltage mismatch then the balancing current will be low, and the balancing will be slow. First, to maintain current control a cell voltage or inductor current feedback is required which increases the system complexity and costs. Second, often the duty cycle is limited below 50 % to operate at discontinuous conduction mode to decrease the switching losses [73][117][114]. In both cases the duty cycle is slightly higher or lower than 50 % which makes a narrow control signal window.

The same buck-boost converter concept can be used to design a multiphase interleaved converter balancing topology [120]. The main difference from Fig. 3.12 is that the top switch connects inductor to the positive pole while the bottom switch connects the same inductor to the negative pole of the battery pack. In this topology, each inductor-top switch-bottom switch combination is regarded to as a multiphase converter leg. The duty cycle of each transistor is fixed and calculated according to the voltages of two corresponding strings of cells. The fixed duty cycle operation permits natural cell balancing control method. In [120] a prototype was tested and it was able to achieve 100 mV standard deviation among 8 cell battery pack. Apparently, more care should be taken to select a proper duty cycle. The same article demonstrates coupled inductor version as well – the benefits are decreased costs and size of the balancer circuit. The proposed method is fairly simple and easy to implement however if a battery with high cell count would be used then high voltage switching elements would be required, and wiring could become troublesome.

The buck-boost based balancing topology can be combined with previously mentioned Cuk converter based balancing topology to provide good balancing performance while the topology is operated at 50 % duty cycle without feedback and heavy use of BMS [121]. Another topology upgrade is presented in [122], where additional capacitor and inductor is added to the cell balancer to form a resonant tank and thus provide quasi-resonant zero current switching which can decrease MOSFET losses by more than 96 % and increase the overall balancing efficiency by up to 30 %. The proposed topology uses variable PWM control from the main BMS. The same buck-boost method can be redesigned to use a double buck-boost convert for each individual cell balancer – further improvement is to combine both inductors to form a transformer. As revealed in [115], while the circuit has more elements, it increases balancing performance by decreasing equalization time, improving efficiency and apparently decreasing the size of the passive components due to lesser filtering requirements – the transformer-inductor solution provides practically ripple free balancing currents. Some research has been done to implement buck-boost topology in two layer balancing of battery pack where one balancing method is used to equalize cells within a sub pack while another topology equalizes voltages of the sub packs [123] thus achieving faster and more efficient equalization.

The buck-boost converter circuit can be used to design other cell balancing topologies as well. The development of a buck-boost based sort of cell-to-pack balancing topology is covered in [124][125][126]. In all three articles, individual cell balancers (in articles labeled as sub-circuits) consisting of a diode, switch and an inductor are used. This topology actually only partially is a cell-to-pack method as it can transfer energy from a generic cell up the stack in [124] and [126] while the energy is transferred down the stack in [125]. Different combinations of sub-circuit elements determine the energy transfer direction. Obviously for the first cell in [124] and [126] a different sub-circuit is required as it has to transfer balancing energy down the stack. The same is true for the last cell in [125] – here all cells share the same sub-circuit but an additional boost converter is connected in parallel to the output of bottom sub-circuit to transfer energy from a storage capacitor to the whole pack. The storage capacitor is charged whenever any cell is redistributing its charge. As this method uses an additional boost converter, it occasionally is regarded to as boost shunting method [67][70]. The circuits of both variants are shown in Fig. 3.13 and Fig. 3.14. These circuits have the advantage of a modular design; however, they require one special module for the first/last cell. The elements for the first/last sub-circuit have extra voltage stress as they connect the first and last cell which can be a serious disadvantage in battery packs with high number of cells such as electric vehicles and grid energy storage systems. This balancing can be effectively implemented in smaller battery packs such as required in laptops. The cell-to-top topology has an obvious advantage over cell-to-bottom topology as it does not require additional converter (boost converter) to redistribute charge from the temporary storage capacitor  $C1$  which decreases the performance of the system. Both circuits require central control to measure all cells voltages and drive switches to perform charge removal of individual cells which adds to the complexity of these methods. The authors of both topologies claim that this dynamic balancing method can provide quick and effective equalization. In [73] these topologies are compared to other popular methods and it is concluded that they are among the best, while being highly modular, low volume and easy wiring. The same paper states that the main drawback is high cost due to many components.

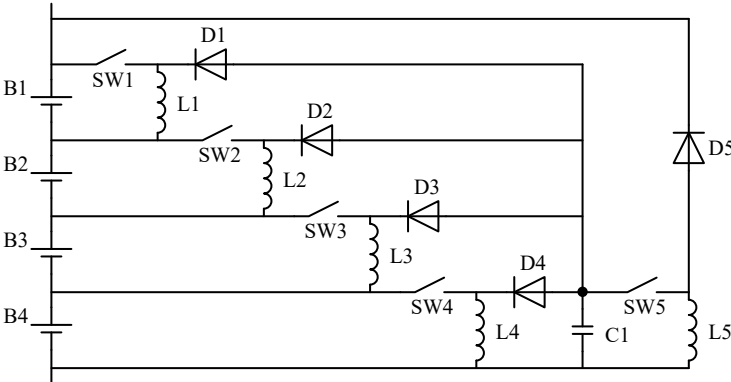


Fig. 3.13. Buck-boost (cell-to-bottom) based balancing topology.

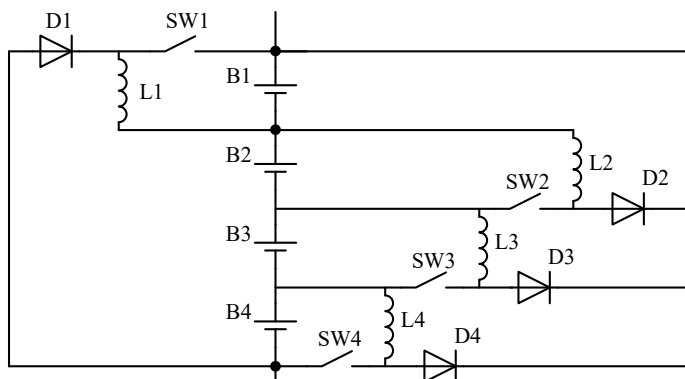


Fig. 3.14. Buck-boost (cell-to-top) based balancing topology.

Another buck-boost based balancing topology is presented in [127][128][129] by multiple authors. In other balancing reviews this topology is regarded to as single inductor buck-boost or shunt inductor method [67][109][66]. As the name implies, this method uses a single inductor and a matrix of switches and diodes to perform bidirectional energy transfer from cell to cell as shown in Fig. 3.15. Here each switch is a semiconductor device – usually a MOSFET. Additional diodes from  $D1$  to  $D6$  are required to achieve only single direction current conduction. The circuit requires  $2n$  switches and  $2n-2$  diodes as the switching elements if  $n$  is the number of cells to be balanced. This adds to costs and lower efficiency of this balancing topology.

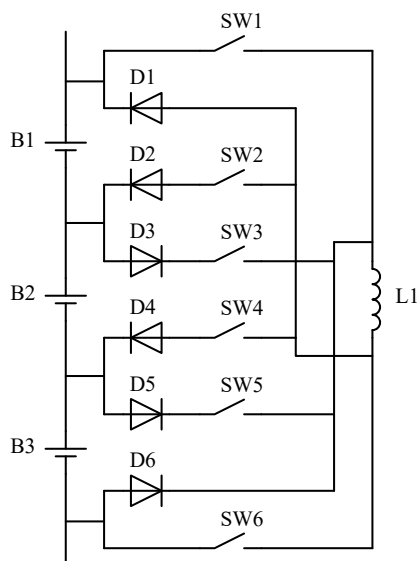


Fig. 3.15. Single inductor buck-boost based balancing topology.

A similar topology with different operational principles is presented in [130]. Here a single inductor and a matrix of switches with additional diode and two switches is used to transfer

energy from cell to pack. The article reports successful balancing of a four-cell battery pack but no further performance investigation is carried out.

One more balancing method that here is added to the group of inductor-based charge transfer methods is the single switch equalization charger method. As presented by the authors of multiple articles [131][132], this method is based on stacked buck-boost converters or voltage multiplier. In other reviews this method is regarded to as the voltage multiplier method [67] since main work is done on this variant. In [67] the original topology is split in two parts: current source charger and a voltage multiplier with additional switch. However, the original articles state that the voltage multiplier portion have no switches while the input portion has an inductor-based power converter. The layout of the multi stacked boost can change per topology used for the buck-boost converter [131][132]. SEPIC, Zeta, Cuk [131], boost, buck-boost and derived isolated power converter topologies can be used for both variants. While the name of the topology uses term buck-boost, in fact it should be step up-step down, as it can use (and uses) any converter that can perform this functionality. This topology can be used to distribute energy during charging which makes it member the selective charging methods.

The first version of single switch equalization is based on multi stacked SEPIC converters while the original articles refers to it more generally – multi stacked buck boost converter [131][132]. The topology is shown in Fig. 3.16. The particular figure represents a 4-cell stack that is charged using the equalizer circuit which is based on multi stacked SEPIC converters. The authors have done mathematical analysis which proves that passive element variations have no effect on the equalization performance. Experimental testing reveals that the prototype can equalize cells with different initial condition and cells with different capacities. Constant power – constant voltage charging method can be used with this topology. The main advantage is obvious – the topology has only one switch and no distributed measurement system is required to control the energy flow to individual cells. However, it can be difficult to obtain the SoC of a particular cell and to control the balancing currents of individual cells. No analysis has been done to estimate the possibility of application for high cell count battery pack.

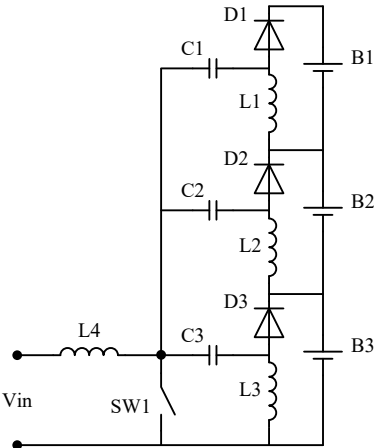


Fig. 3.16. Single-switch multi stacked step-up/step down balancing topology based on SEPIC converter.

A more advanced single-switch equalization utilizes voltage multiplier. The concept is proposed by the same previous authors in [133] and [134]. While the proposing authors name this topology as single-switch single-inductor equalization charger using a voltage multiplier [134], in review this balancing method is labelled as voltage multiplier method with a current input [67]. As the original name implies, this topology uses a single switch and a single inductor as opposed for the stacked converter version reviewed previously. Voltage multiplier is used to equalize voltages of the cells (Fig. 3.17). The advantages are obvious – the circuit contains only one magnetic component thus decreasing the size of the board and quite possibly the costs as well. The control of the charging equalization remains the same and constant input current - constant voltage control is used to charge the cells. Deeper analysis reveals that this topology is capable for relatively low charging power but if the switch-inductor input cell is replaced with an isolated converter then the topology can be used to redistribute the charge within the battery pack thus operating as standalone cell balancing system. Both simulation and experimental validation have been performed and for equalization of three cells with different initial voltage, the final standard deviation was approximately 5 mV which is sufficiently low [133].

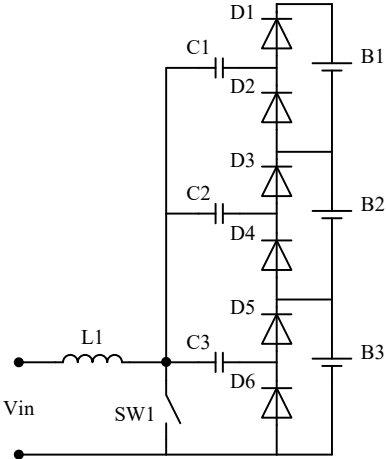


Fig. 3.17. Single-switch single-inductor voltage multiplier balancing topology.

The single-switch topology can be further advanced to create a topology named: double-switch single-inductor resonant cell equalizer using a voltage multiplier [135]. A series resonant inverter is used for the equalizer input side (input cell) while the multiplier remains the same as in previous version. The half bridge is connected to the negative side of the bottom cell while and to the positive side of the top cell (Fig. 3.18). In [135] the operation of the topology is analysed to reveal that for the equalization energy is taken from the cells with higher voltages and delivered to the ones with lower voltages without any feedback. This topology is functioning as a true cell voltage equalizer as opposed to the previous two versions, which partially are used for selective charging as well. Additional benefit comes in form of increased efficiency due to resonant operation (zero voltage switching) although no efficiency estimation was provided for the single-switch versions. An experimental prototype provided evidence that

the topology can equalize six electric double layer capacitor cells down to 5 mV deviation from both voltage-balanced and voltage-imbalanced conditions with maximal efficiency of approximately 50 %. However, this double-switch variant has drawbacks as well – the operation relies on correct inductor and frequency calculation; the topology is not as modular as previous versions due to additional connection between top and bottom cells of the battery stack.

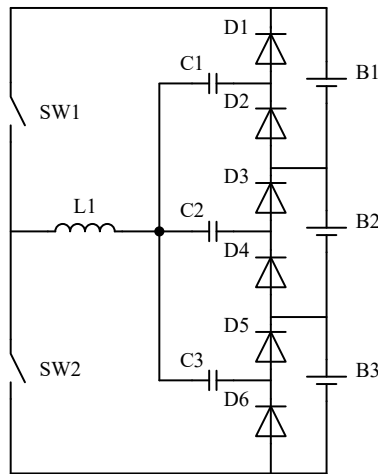


Fig. 3.18. Double-switch single-inductor voltage multiplier balancing topology.

### Transformer-based charge transfer methods

The final cell balancing method group sums up different methods that utilize a transformer to perform charge transfer and/or charging with balancing. Some of methods that utilize coupled inductors are included in this group as well.

To continue from the previous group, voltage multiplier balancing technology can be used with so called “isolated input cell” – inverter with a transformer at the input of the multiplier. One such voltage equalizer is presented in [136] where the voltage multiplier is driven by a forward-flyback resonant inverter. The inverter is fed from the battery pack thus it is capable to equalize cell voltages during both charging and discharging. A similar approach with different functionality is presented in [137] where the equalization function is an additional function of a SEPIC converter which is used to charge the battery pack. A node from the SEPIC converter is used to drive a series-resonant voltage multiplier. A transformer is required to decouple the required power signal thus one could argue whether this method actually is a transformer-based charge transfer method. In both cases the efficiency is improved by resonant circuits which provide some sort of soft switching conditions for the transistors.

As presented in [65], most transformer based methods can be further grouped in three groups: switched transformer, multiple transformer and shared transformer methods. There are some methods that does not group nicely or could be grouped in more than one group. One example is the previously reviewed voltage multiplier-based methods.

The main characteristic features of a switched transformer balancing method are a single transformer with single primary and secondary winding and a switch matrix that is used to

connect to a desired cell. This method can provide uni- or bi-directional energy flow, thus it can be designed for cell-to-pack, pack-to-cell or for both balancing modes. An example of pack-to-cell method is presented in [138] and [139] where a flyback converter is fed from the battery pack while the output is connected to one of the cells using a matrix of selection switches. This circuit can operate with high efficiency but requires continuous control as voltages of individual cells need to be monitored to decide which cell should be charged. One of the most problematic part of this topology is the switch matrix. Not only voltage ratings of switches increase with cell count, but additional problem is associated with driving of the selection switches. The modularity depends on the voltage ratings of the selection switches. The topology was implemented using a single, non-modular board in all of the reviewed articles. Block diagram representation of the basic topology is shown in Fig. 3.19.

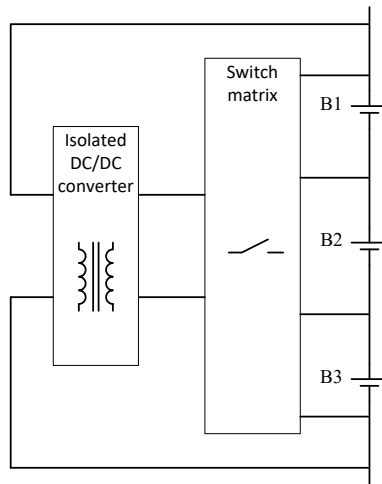


Fig. 3.19. Block diagram of switched transformer balancing topology.

The same block diagram suits energy transfer in other direction: cell-to-pack. A particular design is presented in [140] where the input of a flyback converter is connected to a particular cell using a set MOSFETs and diodes. The output is connected to the poles of the battery pack. Particular interest is taken in designing gate drive circuits for the cell selection switches. Bidirectional converter functionality is achieved by using bidirectional switches for both primary and secondary side of the flyback converter [141]. Thus the balancing topology is able to perform both cell-to-pack and pack-to-cell equalization. Additional improvement is to use a center tapped secondary winding to reduce required switches in the switch matrix. Solid state relays can be used for the switch matrix if the cell switching has low frequency [76]. The converter block can be realized as multiple converters to reduce circuit size and improve balancing performance. Smaller first-stage converters are used to equalize a group of cells while a second-stage converter is used to distribute energy between multiple first-stage converters [69][142]. The use of multiple converters can relief component voltage stress in high cell count batteries. Also, it improves modularity of the balancing topology. The main advantages of switched transformer balancing topologies are the high efficiency and simplest magnetic components among transformer-based methods. Traditionally these methods have poor

modularity, fairly sophisticated control and measurement circuitry. High active component count could be regarded as one of drawbacks as well. However, various improvements have been made to improve modularity and overall performance.

The next group – multiple transformer balancing methods, do not use a switch matrix, but utilizes a set of transformers – traditionally a transformer per cell. As most transformer based balancing topologies, these methods can be used to perform cell-to-pack [143], pack-to-cell [144][145][146][147] and bidirectional energy transfer [117]. Occasionally some of these methods are grouped as DC/DC converter methods, when each transformer is the central part of an individual converter sharing central control [143].

Pack-to-cell methods are usually designed based on low power flyback converters although other types of converters can be used as well. The primary side of the transformer is connected to construct a typical flyback converter while the secondary side of the transformer is rectified and connected to one cell Fig. 3.20. A center tapped secondary with resonant half-bridge circuit can be used to connect to two cells to decrease the required number of transformers and improve the overall efficiency by using soft switching [144]. Quite often the primary side has only one converter power switch shared by all transformers –  $S_4$  in Fig. 3.20. Transformer selection switches are required to select which of the multiple transformers is to be used for energy transfer. All of the primary sides are connected in one of two ways: parallel or series. In series connection (Fig. 3.20 (a)), all of the primary windings are connected in series and each transformer winding has a parallel switch that can shunt it, thus the central control can select which transformer is to be used for energy transfer [144][146]. In parallel connection (Fig. 3.20 (b)), one end of all windings is connected to a common node while other end is connected to a different node through individual switches which can be controlled to select one of the transformers [145][147]. The transformer selections switches can be implemented using solid state relays or using discrete MOSFETs to construct bidirectional switches although bidirectionality is not always required.

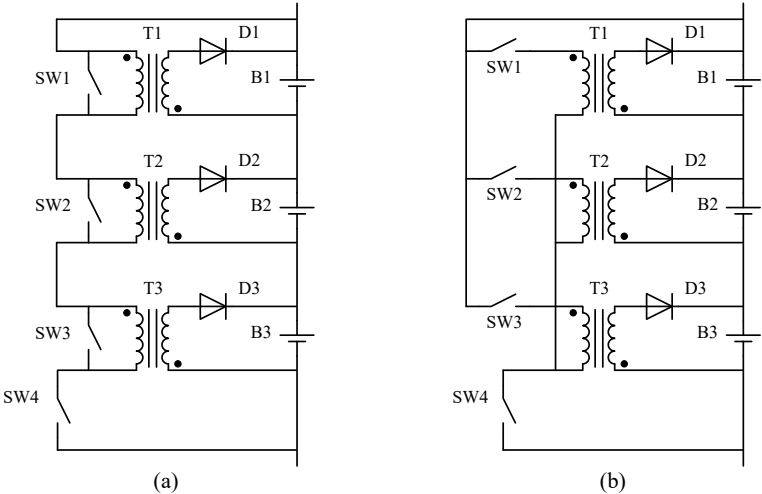


Fig. 3.20. Pack-to-cell multi transformer balancing topology based on flyback converter with (a) series primary windings (b) parallel primary windings.

Further advanced topologies include variations to improve modularity or overall size. A pack-to-cell topology with series primaries and flyback converter is upgraded in [145] to provide improved modularity. The whole battery pack is split in smaller sub-packs. A typical multi transformer balancing topology as shown in Fig. 3.20. Circuit (a) is used to balance cells within the sub-pack. Additional transformer is used per sub-pack in parallel with the primaries of the balancing topology. The secondary windings of the additional transformers are connected in parallel. Thus, the switching of the flyback converter power switch not only transfers energy from the sub-pack to a selected cell but additionally energy is transferred to another sub-pack through the additional transformers. It must be noted that each additional transformer has only two windings and electrical connection is made to transfer energy. The construction of each sub-pack is the same thus the balancing topology can be easily expanded to add more sub-packs, improving the modularity of the multi transformer balancing topology.

Typically, multi transformer balancing topology suffers from the fact that many of the elements experience full pack voltage which is especially troubling for high voltage battery packs. Elements with high rated parameters are larger and more expensive. In [143] this problem is addressed by proposing a two-stage cell balancing scheme. The given multi transformer balancing method utilizes a low power flyback converter per cell to transfer energy in a cell-to-pack manner. The only difference from typical single-stage methods is that the outputs of all converters are connected to a storage capacitor – this part make the first stage. The second stage consists of a more powerful flyback converter that is designed to step-up storage capacitors voltage to deliver its energy back to the battery pack. The proposed scheme is reported to have good balancing capability while operating with high efficiency due to low voltage stress. The overall size of the balancing system is decreased and modularity is improved.

In review literature multi transformer methods are mostly regarded to as expensive/satisfactory, complex, large/satisfactory while the advantages are high power, average speed and good modularity [67][70][66]. It can be estimated that the main source of disadvantages is the transformers – expensive and large components which are used extensively for multi transformer topologies.

Finally, the shared transformer methods. These methods can be further divided in two parts: with distinct primary winding and other variants. As this group name “shared transformer methods” implies, a single transformer is used for the balancing. A single transformer was used for the switched transformer balancing as well, here however, the shared transformer, in most cases, has multiple outputs with dedicated cell connections – similar as in the case of multi transformer methods. One can discuss that this group combines switched and multi transformer methods to bring together the benefits (or drawbacks) of both.

Shared transformers methods with distinct primary windings are the main branch with designs patented tens of years ago [148][149]. This type of shared transformer method is commonly referred to as multi-winding transformer method as the main transformer has multiple secondary windings – one for each cell or one for a pair of cells. Other versions of shared transformer methods do not group together well thus they will be reviewed individually.

Fig. 3.21 shows a reference version of a multi-winding transformer balancing topology that supplies primary side converter directly from the pack while a winding and a diode is used to transfer energy to each cell. One can imagine that the power topology could be that of a flyback or forward converter with multiple isolated outputs – each connected to a single cell [149]. References [150][149][151][152] are often cited as the reference for this type of topology. These publications come from the same research group and it proposes the given topology, but with additional DC/DC converter to feed the primary circuit of the multi-winding transformer. The DC/DC converter could be fed from the battery pack or from the DC-link of the charger. Significant emphasis is put on the design of transformer as it is the most complex and limiting component of the topology. Coaxial winding transformer design is proposed to limit and control parasitic parameters while providing relatively easy manufacturing. However, the complexity transformer usually is mentioned as the main drawback of multi-winding topologies [65][109]. The balancing time is relatively low as the secondary diodes are conducting only part of the period.

Interleaved active clamp flyback converter could be used to address multiple issues related to the traditional flyback converter design [153]. The proposed converter uses constant frequency and duty cycle to simplify control and zero voltage switching to reduce switch voltage stress and improve peak efficiency to 88 %. The use of two identical transformers could be considered as the main drawback. The construction of the system is quite complex but it can significantly decrease voltage difference among cells and increase discharge time. Another improvement to the traditional method (Fig. 3.21) flyback converter is to use dedicated circuitry to perform forced cell selection as opposed to natural selection as discussed before [154]. In the proposed approach, MOSFETs are used to replace the secondary side rectification diodes. An auxiliary transformer with multiple output windings is used to provide power to control rectification MOSFETs. Additional selection switches are used to select which of the MOSFETs are connected to the auxiliary transformer. This method has fewer switching elements than the ones which use additional switches to selectively block cell charging. The experimental testing has revealed that this method can provide outstanding equalization performance due to precise delivery of balancing energy to the weakest cell at the cost of complex selection circuitry. Additionally, the BMS is required to monitor the voltage of each cell to actually select the weakest cell.

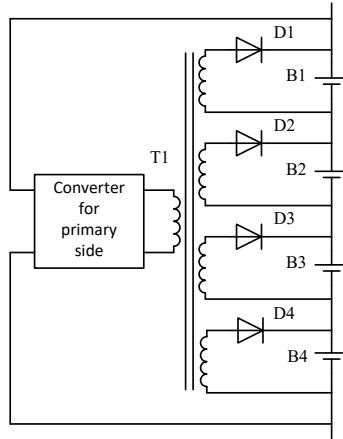


Fig. 3.21. Multi-winding transformer balancing reference topology.

One of the simplest shared transformer/multi-winding transformer method in literature is labeled as ramp converter method due to the current shape in the primary winding of the transformer [155]. This method performs pack-to-cell/s energy transfer. The topology is shown in Fig. 3.22. Primary side of the transformer is fed from the whole pack using a type of series loaded resonance converter half bridge circuit [155][156][157][158]. Such primary side converter produces flux in both directions and bipolar voltage is available on the secondary windings as opposed to the reference one where the output voltage is unidirectional. A secondary winding with two diodes is used to transfer energy to two cells – one halfwave is rectified using one diode and one cell is charged while other halfwave charges the other cell. Obviously, there is an advantage that only half of secondary windings are required as opposed to reference topology. However, there is a disadvantage because all cells are divided into two groups and those two groups are balanced separately. Achieving balance for a single out of balance cell would take more time as if compared to situation when all cells are balanced simultaneously.

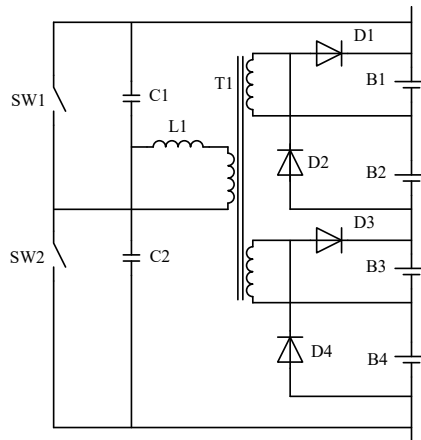


Fig. 3.22. Ramp converter with multi winding transformer balancing topology.

A similar circuit to Fig. 3.22 is proposed in [159] where the secondary side is the same while a full bridge circuit is used for the primary side. 50 % duty cycle is used to achieve simple control and partial soft switching to improve performance. The charge current is limited by the leakage inductance of the transformer. The benefits over the previously reviewed ramp converter is that there is practically no control for the primary side – the switches are operated at fixed frequency and duty cycle for the whole period of cell balancing.

Another variation of primary side is presented in [160] where a class-E inverter is used to drive the primary winding. Such configuration uses zero voltage switching for the single switch which is switched at 50 % duty cycle thus high efficiency and simple control is achieved at low cost. However, the balancing currents of individual cells are not controlled, and the typical problem of different balancing voltages arises due to mismatch in parameters of secondary windings. The work of [160] is further advanced in [161] where a different rectification method is used for the secondary side. The previously introduced single-winding-two-diode rectification is replaced by double single-winding-two-diode scheme. Now two windings and four diodes are used to rectify both half waves and perform simultaneous charge balancing of both odd and even cells. The benefit is that there is no double voltage drop in the rectifier as each winding provides the correct polarity to be rectified using a single diode thus the efficiency is kept at the same level while the balancing time is decreased. On the other hand, twice the number of windings is required which complicates the construction of the transformer even further. The use of this method is considered to be used to balance battery modules (sub-packs) thus this method is related to multistage balancing.

The functionally most advanced multi-winding transformer balancing topology (based on Fig. 3.21 reference) is presented in [162][163] where the diodes of the secondary side are replaced with semiconductor switches to provide bidirectional energy flow through the balancing multi-winding transformer. The converter of the primary side is realized as a flyback while each cell on the secondary side is effectively equipped with an individual flyback converter that can transfer energy out of the cell while the diode of the switch is used as rectifier of the primary side converter to transfer energy to the cell. Both top and bottom balancing can be used to provide the shortest equalization time. Part of the topology can be adapted to provide cell voltage scanning using the transformer as a multiplexer [162]. Cell's voltage values are essential for this topology to provide a precise energy delivery from the overcharged cells and to allow cell balancing by capacity. This reveals the main drawback – complexity. There are  $n+1$  ( $n$  is cell count) power switches which are to be controlled for proper operation – the control of the prototype has not been described but it definitely is quite sophisticated. Each cell needs to be monitored for both voltage and capacity. The proposed design uses one secondary winding per cell thus the transformer is as complex as the reference design. The modularity could be described as poor/weak. However, both simulations and experimental validation prove that this topology can increase the usable energy of the battery by as much as 15 %. The best results were achieved if capacity balancing was used instead of the simpler voltage balancing.

Two alternative bidirectional multi-winding balancing topologies were found in literature. Both of them are designed with only secondary windings. The winding count is the same as cell count. Basically, each cell is equipped with an individual converter. This improves modularity;

however, all windings should still be placed on the same core, making it impractical for larger battery packs. In [164] each of converters is designed as a bidirectional forward converter and thus the switch count also is same as cell count (Fig. 3.23). While the previous group could perform all types of charge transfer, this topology performs only cell-to-cell transfer. Particular topology has limited controllability – BMS can select from which cell energy is transferred to the transformer. From transformer energy is naturally transferred to the cell with the lowest voltage. This topology has been tested during charging performing as charging current shunting method. A variation of this topology is presented in [165] where all switches share the same drive signal which results in simple control. The topology acts to equalize cell voltages however, there is no results to indicate equalization speed which could be slow in the case of similar cell voltages due to no cell voltage measurement feedback. Each converter is equipped with additional capacitor to achieve soft switching and decrease losses. The reported efficiency is above 90 %.

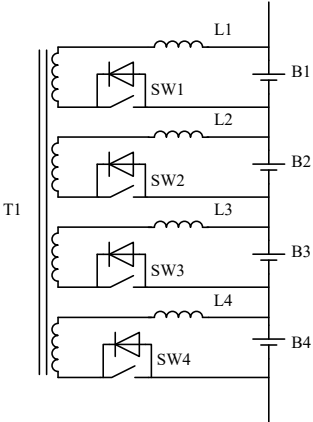


Fig. 3.23. Multi winding transformer with bidirectional forward converter balancing topology.

There are some multi winding transformer topologies which are derived from buck-boost balancing topology. In general, inductors of each buck-boost balancing block are coupled in the form of a multi winding transformer, so this group can be labeled as coupled inductor balancing topologies. Operation of such topology for six cell balancing is analyzed and explained in [166]. Traditional buck-boost type topology is used to transfer energy to neighbor cell while flyback-mode operated multi winding transformer is used to transfer energy to further cells. This method is capable to perform cell-to-cell balancing. Single winding and two bidirectional switched are required per cell pair. Despite the simplicity of the topology, the control is complex while modularity is poor mainly due to the transformer design. Source claims that proposed topology has advantage of relatively small size due to good utilization of transformer windings in both flyback and buck-boost operation. Further advance of the same principle topology is proposed in [167] where each buck-boost balancing block is equipped with auxiliary resonant cells to achieve zero voltage zero current transition of main switches. It is possible to reduce size of the circuit due to reduced losses. Additionally, the circuit (Fig. 3.24) presented in [167] uses single

MOSFET switches as opposed to circuit in [166] where a pair of MOSFETs are used for each bidirectional switch. Still the switch count is high –  $2n$  switches and  $n$  diodes are required. Additionally, each resonant cell has 2 capacitors and 2 inductors. It is obvious that the control of topology increases due to the control of auxiliary resonant cells. In [168] this issue is addressed by more advanced solution where just a single auxiliary resonant cell is used to provide zero voltage zero current switching for all main switches through multi winding transformer coupling. For this topology  $n+2$  switches and 2 diodes are required. The resonant cell uses 2 capacitors and an inductor. The inductor count remains high due to a series inductor for each main switch. 100 kHz switching for experimental verification and 1 MHz switching is considered for future to decrease the size of passive components. Still the control remains fairly complicated as a DSP is required to perform associated calculations.

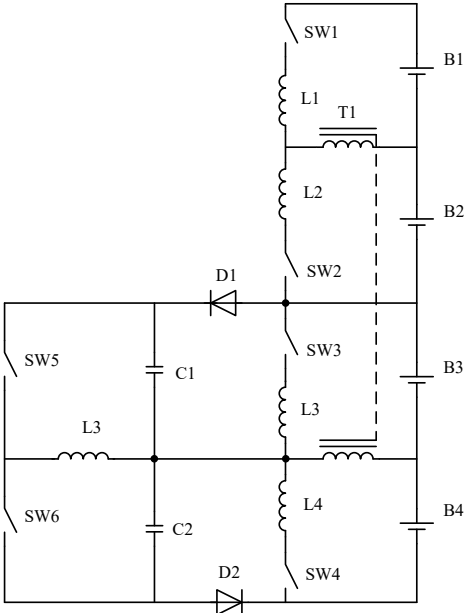


Fig. 3.24. Coupled inductor buck-boost/flyback balancing topology with resonant cell.

A topology design that bears some similarity to buck-boost topology and uses coupled inductors is presented in [169][170][171][172][173] by the same research group. Due to use of asymmetrical half-bridge circuits this topology is named modular balancing bridge. Good modularity can be considered as the main advantage of this topology. Modularity is achieved using off-the-shelf four winding inductors.  $n/2$  inductors,  $n$  MOSFETs and  $n$  diodes are required for this circuit which provides good overall cost. Topology is presented in Fig. 3.25. Two multi winding inductors ( $T1$  and  $T2$ ) are shown with open windings – these are to be used to further extend topology by adding more cells. Energy transfer between inductors is achieved by direct connection of inductor windings – the same effect could be achieved by using a single core with required number of windings. Despite multiple inductors required for high cell count stacks, the performance is still similar to that of a single shared transformer. Multiple control methods

are described and analyzed. Circuit control can get complicated and parasitic elements might decrease efficiency for high voltage battery packs – voltage rating of inductors can be a source of additional concern.

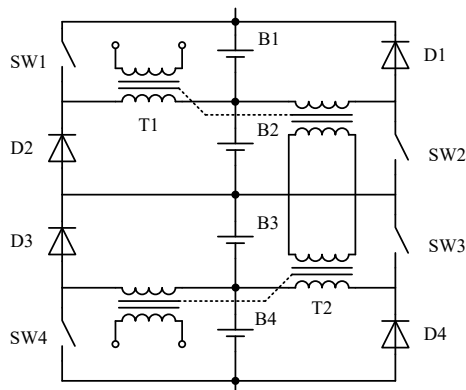


Fig. 3.25. Modular balancing bridge.

### 3.5. Summary of balancing methods

Previous sub sections provided an overall review of various balancing methods presented mostly in research articles. It must be emphasized that this list is not concluding – during the making of this review new articles with relevant topologies have been published.

One of the conclusions from this review is that often the common motivation in most of charge transfer methods articles is that dissipative balancing is inefficient and should be avoided [99][119][136]. This motivation assumes that balancing will be performed once the cells have high SoC mismatch. Up to 0.5 V voltage [119] and 42 % SoC [74] mismatch is used to validate proposed balancing circuits. However, in practical battery packs cells are balanced during every charging procedure which in turn minimizes cell voltage mismatch at the end of next discharge [174]. It is often written that charge transfer methods can have significantly higher power transfer capabilities and these circuits can balance cells that have high mismatch during discharge. In practice to perform balancing while the battery is being used is a demanding task if the battery must provide high power (traction applications) as the balancing circuitry must transfer nominal battery current to compensate for cell which are fully discharged while other cells still has some remaining charge. This brings to the fact that cell voltage is not a good indicator of SoC for cell balancing purposes, especially if the pack is reaching its end of life. Most of balancing methods actually perform cell voltage balancing as opposed to actual cell charge balancing [163]. The goal of a high-performance balancing system is to maintain all cells at the same SoC level, however, by balancing according to cell voltage, cells can have different SoC levels at the same voltage because of different ageing process which leads to different actual charge capacities. The reasons for cell voltage balancing are that it is a lot easier to just measure each cell's voltage and fresh cells should not have higher capacity mismatch than 3 % (typical information from manufacturers datasheets [175]) which is relatively easy to balance. Test results in [174] show that for up to 500 cycles the charge/discharge efficiency of

a balancer-less multi-cell battery is practically the same as if the battery would be equipped with balancing circuit – this adds to the conclusion that switched resistor balancing is eligible even for modern battery packs.

Another relevant conclusion is about multi-layer or multi-stage balancing – this concept is poorly researched. Some proposals are presented in [143] and [69] where small DC/DC converters are used to balance cells within a battery module while a more powerful DC/DC converter is used to transfer energy from the small converters to the whole battery pack. In [143] the same converter topology is used for both stages while [69] presents more advanced solution where a switch block is used to connect to cells and energy transfer is possible among the first stage balancing converters (the small ones). Similar work has been done in [108] and [107] where a balancing topology is used to perform balancing of individual cells and additionally perform balancing of cell modules. Here the proposed term is modularized balancing as the battery is divided in modules where dedicated balancing circuits transfer energy between them. This approach improves the performance of cell-to-next-cell balancing topologies such as switched capacitor topology. From the research perspective the most interesting concept is provided only in [123] where different balancing topologies are used for each layer or stage. Such dual-balancing or mixed-balancing approach can effectively be used to gain on advantages of different balancing topologies. This concept should and will be investigated here in more detail.

## 4. INVESTIGATION OF INDIVIDUAL CELL TESTING METHODS

As the goal of this thesis project is to design and implement a battery pack with BMS for a small vehicle, the first experimental step is to obtain measurement data regarding individual cells. The execution of this step is divided into two parts. Due to material and measurement equipment availability, LFP prismatic 40 Ah cells were tested initially. As new material (cells) became available, NMC/NCA 18650-size cylindrical cells were tested to obtain data about capacity and impedance dispersion within one batch. The obtained data will be used to characterize cells and verify performance whether given cells are suitable for designated application. Additionally, measured data can be further used to implement battery status estimation in BMS. The final measurements of cylindrical cell capacity and impedance are useful for cell sorting to alleviate requirement for the balancing system.

### 4.1.LFP cell testing

Cell availability determined the execution of these experimental measurements. The first available cells were *WB-LYP40AHA* produced by *Winston battery / Thunder Sky Winston*. Alternative model names are *TSWB-LYP40AHA* and *TS-LFP40AHA*. The chemistry is LFP. The case is prismatic and made of plastic with screw holes for both terminals. The parameters of the cell are: 40 Ah capacity at 3.2 V nominal voltage. The operation voltage spans 2.8 V to 4.0 V. Manufacturers operator manual state that the maximum working voltage range is 2.7 to 4.0 V [176] and smaller range should be used to improve cycle life [177]. The continuous discharge current is 3C while charging current is 0.5C. At 80 % DoD the cell is expected to last for 5000 cycles [178]. The online datasheet has very limited information about the nominal performance of the given model – nor capacity nor nominal voltage are included in the datasheet hence experimental measurements can provide reliable and useful information.

#### Capacity testing

For the first test, the capacity of nine cells were measured at different charging voltages. Cells were charged to three levels: 3.6, 3.7 and 3.8 V. Charging was terminated once charging current was less than 1 % of nominal (0.4 A). Then cells were rested for 24 h. The discharge current was set to 10 A and cut-off voltage was set to 3.0 V. *EA-EL 3400-25* electronic load was used in battery test mode to discharge cells and obtain capacity measurement. The obtained capacity readings are shown in Fig. 4.1. The average capacity at 3.8 V is 40.93 Ah, at 3.7 V it is 40.12 Ah and at 3.6 V it is 40.07 Ah. The difference between 3.8 V and 3.6 V charging is 2.08 % which could be considered small. Since the decreased operational voltage range improves cycle life, it is beneficial to use smaller charging voltage. It can be added that given nine cells have noticeable capacity difference. More cells should be tested for a proper capacity dispersion analysis; however, the number of available cells was restricted at the time of given test.

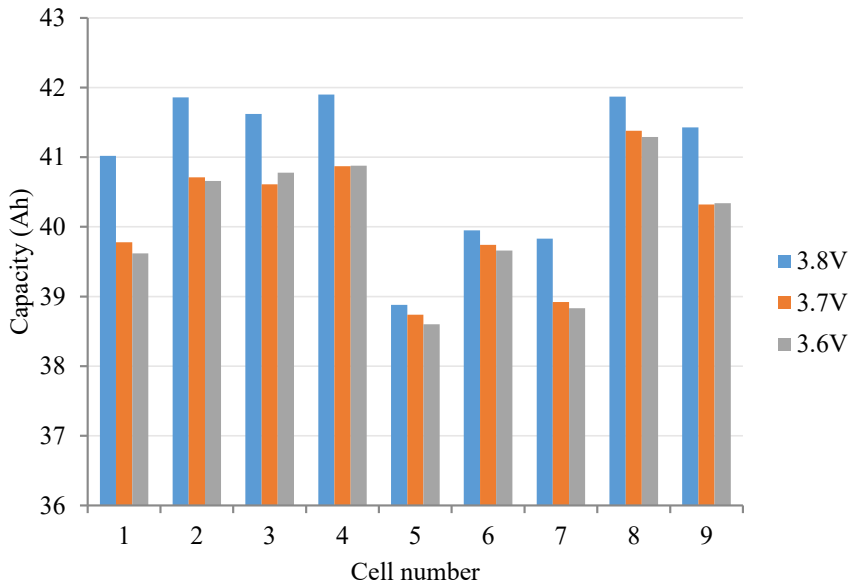


Fig. 4.1. Capacity of 9 LFP cells at different charging voltages.

#### Open circuit voltage testing

For the next test, the same nine cells were tested for open circuit voltage (OCV). Initially cells were charged in parallel to 3.8 V until total current was less than 3.6 A. Then cells were relaxed in parallel for 12 h. The OCV was measured during discharge which was done in 5 Ah steps. The cell was relaxed for 2 h after each step and then OCV voltage was measured using *Agilent UI252B* multimeter. The discharge was stopped if voltage decreased below 2.8 V – some additional voltage difference at 40 Ah point is the result.

The obtained OCV graph is shown in Fig. 4.2. After charging and relaxation, for the first point (0 Ah) all cells were at 3.6 V  $\pm$  1 mV. It can be seen that all readings are well grouped however at 10 Ah discharge and after 25 Ah discharge some voltage difference is noticeable. At 10 Ah max difference is 7.4 mV, at 25 Ah it is 4.9 mV, at 30 Ah it is 10.4 mV, at 35 Ah it is 16.3 mV and at final 40 Ah it is 33.7 mV.

OCV variation can cause errors in SoC estimation. LFP chemistry is well known for its flat discharge OCV curve – in Fig. 4.2 it can be seen that from 5 Ah to 35 Ah the cell voltage decreases only by 118 mV. If rephrased, 75 % change in SoC corresponds to 11.8 % change in cell voltage (if cell's full voltage swing is 1 V (3.8 V to 2.8 V)). Further, 1 % of SoC corresponds to 1.57 mV – clearly given cell voltage difference will cause significant SoC estimation error if only voltage is used to determine SoC. Voltage hysteresis and polarisation will cause additional error, hence coulomb counting, temperature and EIS can and should be added to improve SoC estimation to reasonable level (at least 1 % accuracy) [179][180].

The obtained graph indicates that if cell balancing is done during end-phase of charging then there is relatively small change in charged capacity per mV of cell's voltage hence there is no need for high resolution measurements of battery's cells volages.

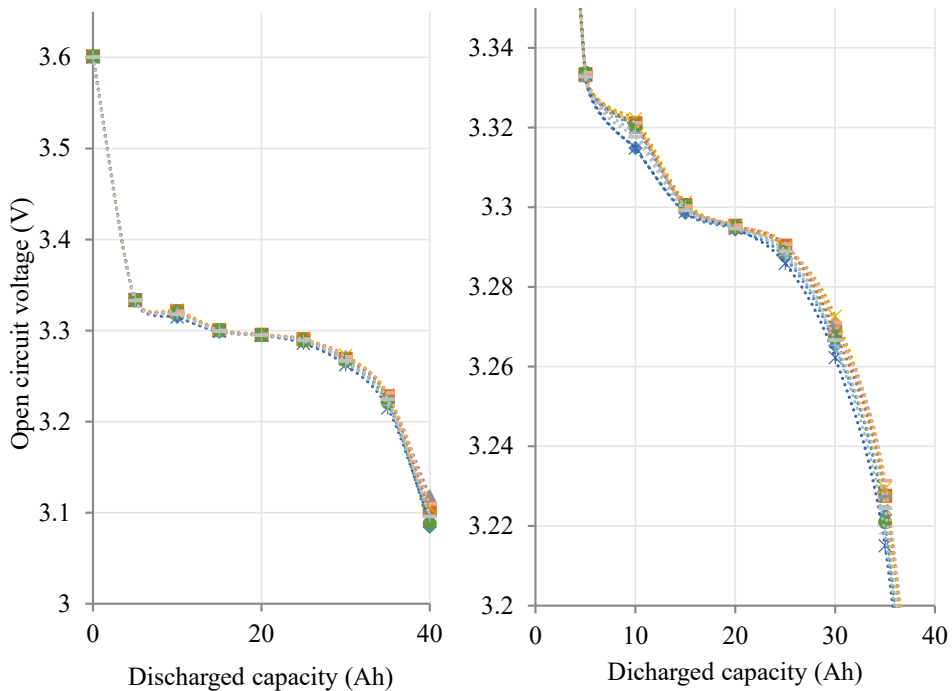


Fig. 4.2. OCV of 9 LFP cells. Left: full span. Right: zoom-in on central region.

### Two-cell discharge test

Out of curiosity, another discharge test was done. Two cells were selected, charged to 3.8 V and balanced in parallel then relaxed for 24 h independently. For the test, both cells were connected in series and a discharge with 20 A current was done until one of cells reached 2.8 V. The voltage of each cell was periodically registered and obtained graph is shown in Fig. 4.3. The initial voltage of both cells was 3.707 V. Already after 4 minutes of discharge each cell has different voltage: first cell is at 3.206 V while second cell is at 3.212 V. For 99 minutes (80 % of total discharge time) the voltage difference is almost the same. Then during next 20 minutes the voltage of second cell decreases faster and it reaches cut-off level (2.800 V) after 124 minutes while the first cell is still at 2.842 V level. The discharged capacity was 41.33 Ah. The discharge of first cell was continued individually and additional 2 minutes were required to reach 2.800 cut-off limit – this corresponds to 0.67 Ah. The key finding is that cell voltage at one point cannot predict voltage at another, distant, point. In this test, initially the first cell seemed weaker as its voltage was 6 mV smaller, however at the end of discharge, first cell's voltage was 42 mV higher and it actually stored additional 0.67 Ah. This finding shows that if cell balancing is done throughout all cell operation then only single point voltage should not be used to select cells with excessive charge – in this case, the second cell would be additionally discharged to match voltage of the first cell – it would incorrectly lead to loss of total capacity as second cell would reach cut-off even faster. A simple solution is to perform balancing only at the end-phase of charging procedure.

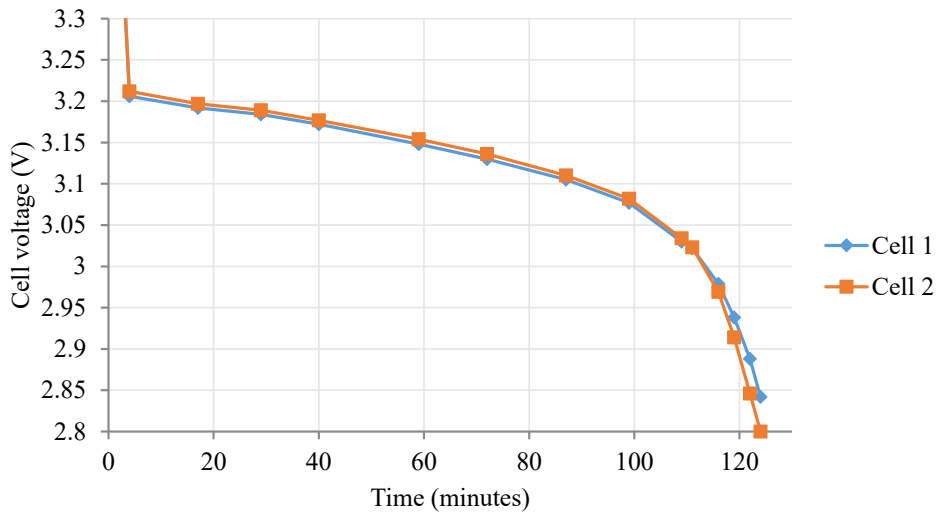


Fig. 4.3. Voltages of two series connected cells during a discharge.

Additional tests were done to verify or estimate performance of given LFP cells. These tests include cell charge-discharge efficiency, thermal performance at up to 3C charge/discharge current levels. Some tests were carried out to clarify the cell OCV relaxation time at different SoC levels and after different discharge current patterns. The results of these tests are not directly relevant; hence they are omitted from this section.

## 4.2.18650-size cell testing

A set of 18650-size cells became available during the latter period of this thesis-project. Four 83 cell batches of 18650-size cells were purchased as part of a research project to develop a customizable power-assist wheelchair. Cells were selected to suit the requirements of the wheelchair battery pack specification – it was decided to use 18650-size cells due to wide variety and high abundance. Due to space restrictions, a single cell had to have at least 3 Ah of capacity. An extended selection process is reviewed in section 5.3. Finally, the local availability played a role and four models from different manufacturers were selected and purchased. The basic specification of these models is given in Table 4.1. In the manufacturer’s specifications [51][52][175][181] there are some confusions, for example some provide *nominal* (smaller) and *rated* capacity (larger) while others give *rated* (in between), *minimum* and *typical* (larger) – here the one which was smaller but not minimal was used. Overall, even these seemingly large manufacturers provide inadequate cell datasheets. Often charge/discharge cycles are estimated from graphs, same as max discharge current while charge current is often given for *standard charge* conditions.

Table 4.1

Basic specification of the tested 18650-size cells

Manufacturer	Model	Capacity, Ah	Nominal voltage, V	Cycle life	Cut off voltage, V	Max discharge current, A	Charge current, A
Sony	US18650VTC6	3.13	3.6	500	2.5	20	3
LG Chem	INR18650MJ1	3.5	3.635	400	2.5	10	1.7
Samsung SDI	INR18650-35E	3.35	3.6	500	2.65	8	1.7
Panasonic	NCR18650GA	3.3	3.6	300	2.5	10	1.475

### Capacity dispersion analysis

The initial capacity of all 332 (4×83) cells was measured to obtain information about capacity dispersion within the batches. First, each cell was precharged to 4.1 V using a laboratory power supply. The constant current level was set to 1 A. Afterwards, the charging was finalized using a battery charger evaluation board *bq24171EVM-706-15V* from *Texas Instruments*. This board was used to charge cells with the current specified in Table 4.1 to 4.2 V level. The charging was automatically terminated once the charging current level reached 10 % of the set charge rate. Once a cell was charged, within 15 minutes it was connected to an *Elektro-Automatik EA-EL 3400-25* electronic load which has battery test mode with time and capacity counter. Then the cell was discharged in constant current mode until cell’s cut off voltage was reached. All cells were discharged with the same 2.3 A current. Capacity reading was recorded once cut-off voltage was reached. After full discharge, the cell was charged to 30 – 50 % state of charge level for storage. The setup that was used for capacity measurement is shown in Fig. 4.4.



Fig. 4.4. Capacity measurement test equipment.

Statistical methods ((4.1.) – (4.4.)) were implemented to analyze the obtained measurements. In calculations, each measured value was denoted as  $x$  while the sample size was denoted as  $n$ . The resultant variables are seen in Table 4.2. There is a difference between the cell models. Starting with the mean ( $\mu$ ) values (calculated using (4.1.)) which show that on average battery cell capacity are different from nominal. Standard error ( $SE$ , calculated using (4.2.) and (4.3.)) shows approximate fluctuations around the mean values, which is relatively small for all models but in comparison it is largest for the *INR18650MJI* cells. Sample variants or the dispersion of the sample of the data set showed how much the data can be varied. With all four models this value is small which means that cell capacities are similar and stable. The average deviation from the average measurement on the data set is shown by standard deviation, this is close to zero for all four models however it is at least two times larger in case of *INR18650MJI*. Going through all the measurement for the cell capacity the range was calculated percentage wise to show how the values of each model could differ. Again, for *INR18650MJI* the range of the capacity value can differ a maximum up to 5 %, which is slightly higher than the 3 % range given by the manufacturer. For *US18650VTC6* the range was only 2.03 % and for *INR18650-35E* the range of the capacity values can differ 2.31 % while for *NCR18650GA* the values differed in 2.74 % range. This data shows that within all models except *INR18650MJI* choosing any random cells for one battery the difference between the cells will never be greater than 3 percent. It can be assumed that in these cases the application of resistive balancing during charging process would not generate high energy losses. To assure that the experiment was conducted precisely with no outliers the calculations were done under the empirical rule, that 99 % of the data should be in the three standard deviation range. For all four batteries the empirical rule was the definitive outcome so the experiment can be considered valid and accurate.

Table 4.2

Calculated Statistical Variables of Cell Capacity

	VTC6	MJ1	35E	GA
Mean ( $\mu$ )	2.955	3.205	3.240	3.324
Standard error (SE)	0.00135	0.00349	0.00197	0.0022
Median	2.954	3.209	3.242	3.321
Mode	2.953	3.213	3.243	3.321
Standard deviation ( $\sigma$ )	0.0123	0.0318	0.0179	0.02
Sample variance ( $S^2$ )	1.522e-4	1.011e-3	3.214e-4	4.000e-4
Range % of value of mean	2 %	5 %	2 %	3 %
Range	0.06	0.173	0.075	0.091
Minimum	2.927	3.088	3.199	3.286
Maximum	2.987	3.261	3.274	3.377
Confidence level (95.0 %)	0.0027	0.0069	0.0039	0.0044

$$\mu = \frac{\sum x}{n}, \quad (4.1.)$$

$$\sigma = \sqrt{\frac{\sum (x-\mu)^2}{n-1}}, \quad (4.2.)$$

$$SE = \frac{\sigma}{\sqrt{n}}, \quad (4.3.)$$

$$S^2 = \frac{\sum x^2 - \frac{(\sum x)^2}{n}}{n-1}, \quad (4.4.)$$

where  $\mu$  – mean value;

$\sigma$  – standard deviation;

$SE$  – standard error;

$S^2$  – sample variance.

To show more visual comparison of the models, a box and whisker plot is shown in Fig. 4.5. It shows the average measured values including bottom and top quartiles of the data set and their fluctuations. In the figure it clearly shows that cells capacity of *US18650VTC6*, *INR18650-35E* and *NCR18650GA* are more stable with lower fluctuations than what was found in model *INR18650MJ1*.

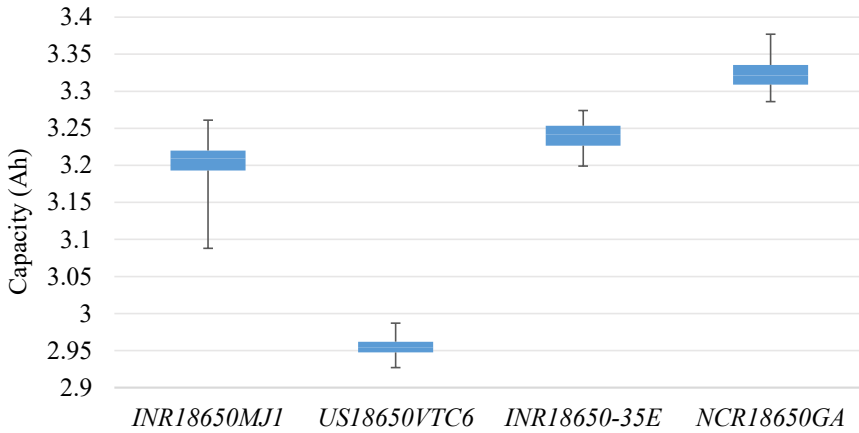


Fig. 4.5. Box-whiskers plot for comparison of different capacities of selected cell models.

In Fig. 4.6 all of the 83 measurements of each cell capacity are shown as a scatter plot around their linear projected values. For *US18650VTC6* measurement values are spaced relatively close with regards to the linear projection on either side. To calculate further the probability of optimal similarities within randomly selected cells of the battery, regression analysis was conducted on all four types. In the regression analysis all tendencies of the data are made visible, these can be seen in the constructed graph in Fig. 4.7. Residual plots show the difference of observed values and the predicted value. The values should be scattered around the line evenly on both sides as it is for all four models. Line fit plot shows how stable the data is and how it varies throughout the sample size. Fig. 4.7 allows for the slight differences of *INR18650MJ1* to be seen.

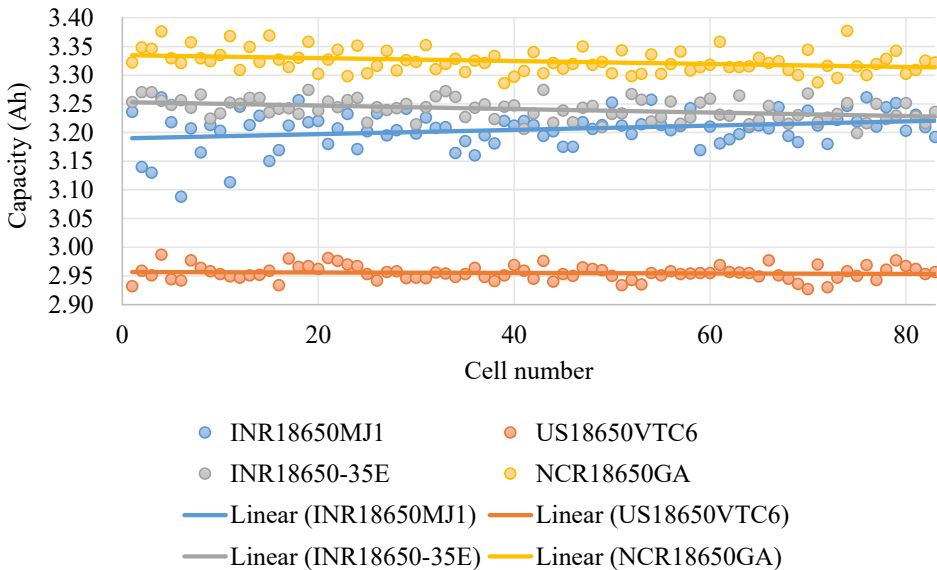


Fig. 4.6. Scatter plot of all capacity values with projected linear lines.

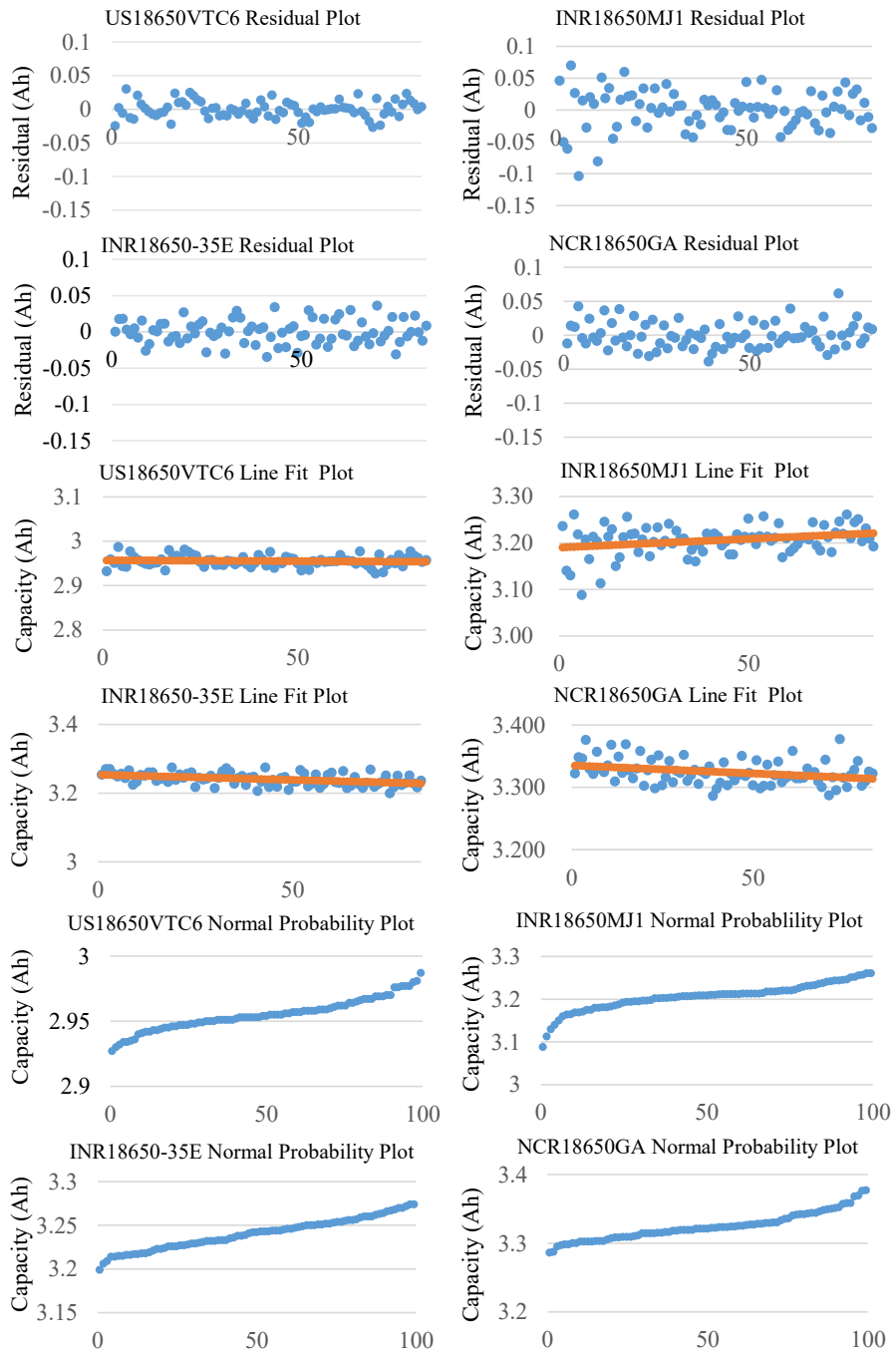


Fig. 4.7. Constructed Residual plots, Line fit plots and Normal probability plots in Regression analysis for all measured capacities.

Normal probability plot (Fig. 4.7) shows the tendency of the data being normally distributed, it identified outliers skewness and kurtosis the best outcome from the probability plot is that of *INR18650-35E*. The tendencies shown throughout the regression analysis indicate that all data sets are more less normally distributed. Normal distribution plot has been constructed for all four data sets of capacities – it is shown in Fig. 4.8.

All models are symmetrical on either side of the middle point, however the closest to the normal distribution plot line was the *US18650VTC6*. After finding all of the tendencies of the data sets it is possible to calculate the probability of randomly selecting cells to be within a 3 percent range – typical manufacturer's tolerance. The probability of choosing any four *INR18650MJI* random cells and having a 3 % range in cell capacity values is 89.26 %.

Additional calculations were made regarding the option what would be the best optimal battery cell pack of 28 cells when selecting the cells of each battery type knowing the measured data. The results are with an amazingly small range of capacity difference between the cells of the pack. For *INR18650MJI* the optimal chosen working capacity would be 3.210  $\pm$  0.006 Ah (The cell capacity would be within 0.187 % range). For *US18650VTC6* the optimal chosen working capacity would be 2.955  $\pm$  0.004 Ah (The cell capacity would be within 0.135 % range). For *INR18650-35E* the optimal chosen working capacity would be 3.243  $\pm$  0.007 Ah (The cell capacity would be within 0.231 % range). And for *NCR18650GA* the optimal chosen working capacity would be 3.323  $\pm$  0.006 Ah (The cell capacity would be within 0.181 % range). By comparing the randomly chosen battery back with specifically chosen one, the difference in the range and the precision of the battery pack capacity is more than ten times larger. If the goal would be to get a pack with maximal capacity (irrelevant capacity range) then capacities for each type would be 2.967 Ah, 3.236 Ah, 3.259 Ah and 3.344 Ah respectively.

Another interesting estimation is the likelihood of obtaining a 28-cell battery pack with certain cell capacity range by random cell selection. For *US18650VTC6*, *INR18650-35E* and *NCR18650GA* capacity mismatch range is below 3 % while probability to obtain 3 % range from *INR18650MJI* cells is just 1.9 %. The probability of 2 % cell capacity range mismatch is 66.2 % for *US18650VTC6*, impossible for *INR18650MJI*, 18.5 % for *INR18650-35E* and 7.6 % for *NCR18650GA*. It was calculated that the probability to obtain a battery pack with cell capacity range below 1 % is less than 0.1 % or impossible for all cell models.

To conclude, the performed measurements and consecutive statistical analysis indicate that in two of the given four cases cell mismatch is within 3 %. This 3 % figure is sometimes indirectly provided by the manufacturer in the cell datasheet. For example, the datasheet provides two capacity indicators: nominal and minimum – often the difference between the two are around 3 %.

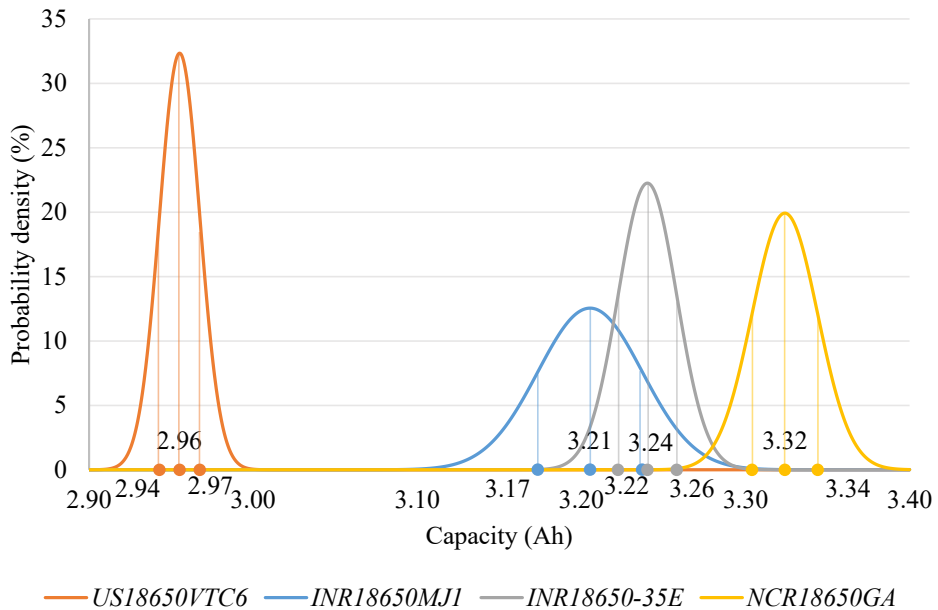


Fig. 4.8. Normal Distribution plots of measured cell capacities.

In case of *INR18650MJI* cell capacity, some of the measured cells were outside of 3 % range. There is approximately 10 % chance that randomly selected cells will have capacity mismatch higher than 3 %. In this particular case the explanation could be related to the fact that the given cells were manufactured more than a year prior to the given testing. Calendar ageing might have caused differential capacity decrease among the cells. Measured capacity of *INR18650MJI* cells was 3.2 Ah while the nominal capacity is 3.5 Ah – approximately 0.3 Ah might have been lost due to calendar ageing. It must be noted that manufacturer’s defined capacity estimation method was not used for the measurements.

Initial 3 % capacity mismatch is lower than that which is traditionally provided as the motivation for active balancing circuit application. Measurements and statistical calculations prove that a battery from fresh cells will have capacity mismatch range lower than 3 %. One can estimate that 3 % mismatch could be easily handled using traditional switched shunting resistor balancing method.

It is of great importance to note that this research was done using fresh cells with no cycle ageing. This research should be continued by ageing all cells using same conditions and periodically performing cell capacity measurements to obtain statistical data about whole group capacity dispersion evolution. While such research would be beneficial for this thesis project, it would take too much resources (time and equipment) hence it was omitted.

### Impedance analysis

The previous capacity test was used to sort available cells to produce optimal battery packs with minimal capacity difference among cells. Capacity measurement is a time-consuming

process as it requires charging (up to 2.5 hours) and discharging (more than 1 hour) of each cell. Another battery parameter is measurable faster – the impedance. In industry impedance of batteries and cells is being measured at 1 kHz. This measurement takes seconds and can reveal information about cell/battery connections – thus faulty cells can be removed [182]. A more informative impedance measurement is electrochemical impedance spectroscopy (EIS) where impedance is measured across different frequencies. As revealed in literature analysis EIS can be used for various purposes including SoC, SOH and life estimation [179], [183]–[188], internal temperature estimation [186], [189] and battery failure estimation [190], [191]. EIS can be used to detect cell mismatch both during initial sorting [182] and throughout battery life [180]. A good overview of EIS technology and requirements for utilization in on-board battery packs is given in [192] where EIS analysis is promoted for battery second-life evaluation. A battery impedance meter became available during the latter period of this thesis-project, hence it was decided to measure impedance of all 332 18650-size cells to verify correlation between capacity and impedance – if strong correlation is found then much faster impedance measurements could be used to sort cells prior to battery pack assembly. Additionally, same as capacity measurements, initial impedance could be compared to future impedance measurements of aged cells to reveal cell aging effects, improve cell models and generally characterize cells in future research.

A methodology was developed for the procedure of impedance measurement. Each cell was initially charged to 4.1 V at 1 A using a laboratory power supply. Three cells were charged simultaneously for time optimization. Then each cell was given final charging using a battery charger evaluation board *BQ24171EVM-706-15V* operating in CC-CV mode. The board was configured to charge one cell to 4.2 V with 1 A. The charging was stopped once current decreases below 10 % of set value.

After charging the cell was relaxed for at least 30 minutes. Then impedance was measured using a *Hioki BT4560* battery impedance meter. The impedance was measured at four frequencies: 1, 10, 100 and 1000 Hz. A warm-up measurement was performed at 0.9 Hz. The impedance meter measured given variables: impedance ( $Z$ ), reactance ( $X$ ), resistance ( $R$ ), phase angle ( $\Theta$ ) and cell voltage ( $V$ ). All of these variables at given frequencies were combined in a single measurement CSV file and saved on a PC.

The impedance measurements were performed at 100 % SoC, at 1 Ah (~70 % SoC) and 2 Ah (~30 % SoC) discharge level. Hence, impedance was measured at three charge levels for each cell. The discharge was done using an electronic load *EA-EL 3400-25* from *Elektro Automatik*. A cell switching board was designed to automatically perform discharge of seven cells. A *Beagle Board Black* single board computer was used to interface the switching board to a PC running a *MATLAB* script to control the discharge process. The same script was used to control the electronic load to discharge exactly 1 Ah as well. The measurement setup is shown in Fig. 4.9.



Fig. 4.9. Impedance measurement setup. From left: laboratory power supplies, electronic load, impedance meter, cell switching board, PC for control and measurement storage.

After doing the experiment and gathering all the data about battery resistance at different frequencies and on different charge levels, calculation and analysis were made. During the measurements over 4000 valuable descriptive data entries were gathered. In the calculation and analysis, different statistical methods were used. For all these different data sets specific statistical calculations were made. The main factors that were calculated for these data sets were mean, standard error, median, Standard deviation, Sample Variance, Range, Confidence Level and Fluctuation against the mean. Also, for the data sets normal distribution plots were distributed and compared.

To show visual data set of cell impedance measurements, a plot off all the measurements was constructed at one frequency level but for all three charge levels as can be seen in Fig. 4.10. In this scatter plot it is seen that higher impedance levels will occur at 100 % charged level with some very few exceptions. But the lines for  $-1\text{ Ah}$  and  $-2\text{ Ah}$  are similar and the levels are changing between the 83 measured cells. This plot also reveals a significant variation between one cell set at a certain charge level.

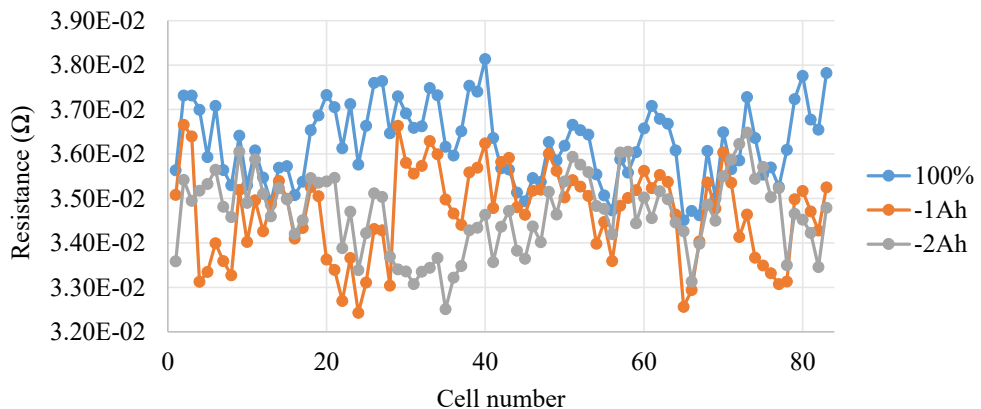


Fig. 4.10. Impedance (R) measurement results of *INR18650-35E* cells at 100 %, 1 Ah and 2 Ah discharge level.

Fig. 4.11 shows a plot of *INR18650-35E* impedance measurements at 100 % charged level but at five different frequencies: 0.9 Hz, 1 Hz, 10 Hz, 100 Hz and 1000 Hz. Table 4.3 presents statistical parameters which are calculated from measured values. The plot and the table shows some patterns: the higher the frequency in which the cell is tested or measured, the more stable impedance outcome correlates to the frequency. It can be seen that at low frequency the resistance part of the impedance becomes dominant. The fluctuation in the measurements varies from 2.6 % to 5 %. There is a 2.4 % difference in the variation comparing cell impedance measured in 1000 Hz than measured in 0.9 Hz or 1 Hz. This could mainly be because of the cell warming up and reaching some higher unusual peak values.

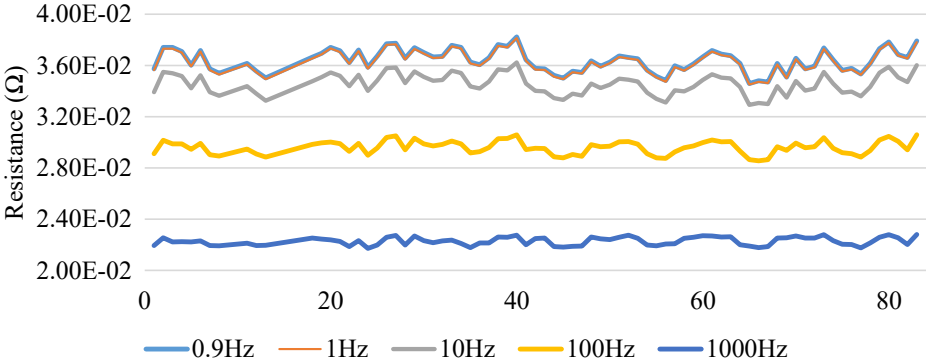


Fig. 4.11. Impedance of *INR18650-35E* cells at different test frequencies and 100 % state of charger.

Table 4.3

Calculated statistical parameters of measured *INR18650-35E* impedance values

	0.9 Hz	1 Hz	10 Hz	100 Hz	1000 Hz
Mean	0.036329	0.036245	0.034506	0.029573	0.022264543
Standard Error	9.44E-05	9.43E-05	8.71E-05	5.71E-05	3.53027E-05
Median	0.036263	0.036185	0.034508	0.029581	0.022263
Standard Deviation	0.00086	0.000859	0.000794	0.00052	0.000321622
Sample Variance	7.39E-07	7.38E-07	6.3E-07	2.71E-07	1.03441E-07
Range	0.003642	0.003629	0.003309	0.002033	0.0011491
Minimum	0.034586	0.03451	0.032922	0.028555	0.0216513
Maximum	0.038228	0.038139	0.036231	0.030588	0.0228004

To see the patterns in different cells, 4 different cell models were measured and compared at different states of charge and frequencies. In the Table 4.4 data sets are gathered and analyzed for all battery types at 100 % charge level and 1 Hz frequency. As it is seen in the Fig. 4.12 plot the measurement results are quite different because the batteries have different parameters. The stability and variance of the battery sets can be analyzed. The variance in the battery sets varies between 5 % and 10.6 %, it's a 5.6 % difference and in values the fluctuations varies in the smallest 0.03624 Ω +/- 0.0018 Ω to largest 0.0507 Ω +/- 0.00537 Ω. The fluctuation for all

the cells varies in  $0.00357 \Omega$  difference. Confidence intervals and Deviation is low, which shows that all the data sets are closely related and there are no error outliers.

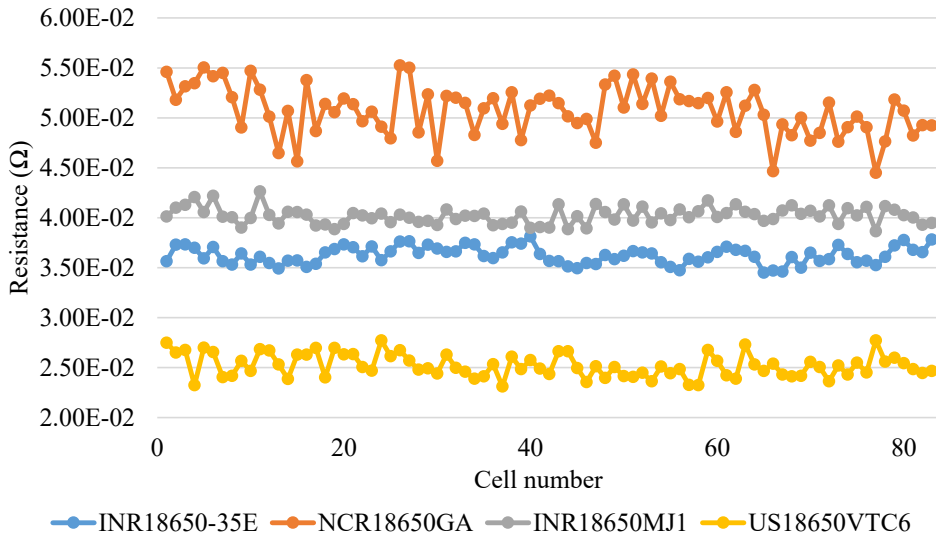


Fig. 4.12. Impedance results of all cell models when measured at 1 Hz and at 100 % state of charge.

Table 4.4

Calculated statistical parameters of measured impedance values at 100 % SoC and 1 Hz

	<b>35E</b>	<b>GA</b>	<b>MJ1</b>	<b>VTC6</b>
Mean	0.036245	0.050746	0.040216	0.025208
Standard Error	9.43E-05	0.000268	9.01E-05	0.000127
Median	0.036185	0.051017	0.040196	0.025047
Standard Deviation	0.000859	0.002445	0.000821	0.001157
Sample Variance	7.38E-07	5.98E-06	6.74E-07	1.34E-06
Range	0.003629	0.01073	0.003986	0.004605
Minimum	0.03451	0.044507	0.038643	0.02312
Maximum	0.038139	0.055237	0.042629	0.027725

The obtained results were compared to the results of previous experiment where the capacities of the same cells were measured and analyzed [193]. The comparison is done to see if there is any correlation between impedance and capacity variation.

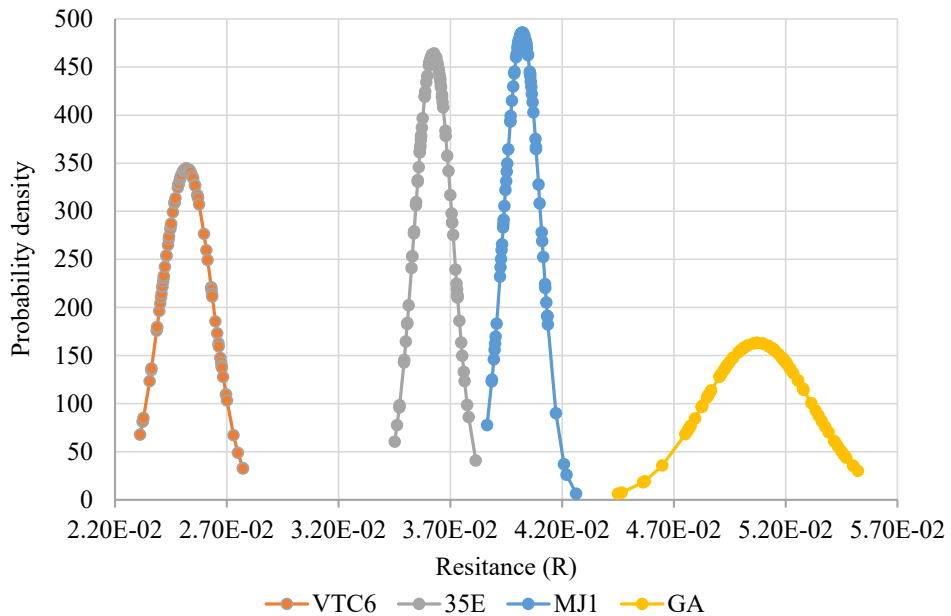


Fig. 4.13. Normal distribution plot of impedance (resistance) for 4 different cell models.

In Fig. 4.13 the normal distribution for impedance (resistance) measurements for the same four cell models are shown. The forms of the distributions are symmetric and similar to each other without skewness to any side. Normal distributions of Fig. 4.13 and Fig. 4.8 can be compared. Calculations regarding the correlation between the normal distributions of capacity and impedance were made and the results are that measurements in both sectors – capacity and impedance are very closely correlated distribution wise. Correlation in distribution varies from 95 % to 98 % throughout the model types. That shows that both Capacity and Impedance measurements throughout the data are stable and with a very high level of normal distribution in both aspects.

Seeing that both measurement types are normally distributed, the direct correlation between Capacity and Impedance can be calculated in each model of cells and between each individual cell. The results are shown in Table 4.5. Two cell models show that there are 20 % or more correlation between cell Capacity and Impedance change. *INR18650MJ1* shows an 11 % correlation and *NCR18650GA* showed only 1 % correlation.

Table 4.5

Correlation Calculation between each battery cell measurement comparing Capacity and Impedance in 4 different types of batteries

Correlation	US18650VTC6 Capacity	INR18650MJ1 Capacity	INR18650-35E Capacity	NCR18650GA Capacity
US18650VTC6 impedance	22 %			
INR18650MJ1 impedance		11 %		
INR18650-35E impedance			20 %	
NCR18650GA impedance				1 %

Performed measurements and consecutive statistical analyses indicate different things. The fluctuations in impedance of cells are a bit higher than fluctuations in the capacity measurements. Fluctuations in impedance in these cell models vary from 5 % to 10.6 % depending on the models. Fluctuations in the Impedance goes lower if the frequency is raised. Looking at one specific cell model raising frequency from 1 Hz to 1000 Hz lowered the fluctuations from 5 % to 2.6 %, which is a great improvement. Comparing measured data with the gathered Capacity measurements, both are perfectly normally distributed and strongly correlated distribution wise. The calculated straight correlation between capacity and impedance proved to be moderate in case of *US18650VTC6* and *INR18650-35E* while in case of *INR18650MJ1* and *NCR18650GA* the correlation is weak. From this, it can be concluded that impedance measurements are not applicable to direct cell sorting according to capacity. However, as noted in scientific literature, impedance measurements can be used estimate other cell parameters and thus they could be sorted, for example, according to their *health* – this approach could become relevant in future when used EV batteries will be applied for second-life applications.

## **5. THE DEVELOPMENT OF A BATTERY CONFIGURATION FOR A PMV**

This part of the doctoral thesis is a result of project activity during which a specialized battery pack was designed for a PMV: a powered wheelchair. Quite often wheelchairs are described as a specific niche product that is experiencing market growth due to the ageing populations in the developed countries [194][195]. It is only logical that seniors of developed countries are requesting functional, high performance equipment to prolong quality lifestyle [196]. While wheelchairs are a product designed for specific customer base, historically they have been designed to improve the life quality for people with various disabilities that most often are not related to ageing and related aspects [197]. Such disabilities can be the result of injuries, infections and various illnesses. While a senior would require a powered wheelchair to assist travel because of fatigue and age-related illnesses, injury and other illnesses may require a more specific wheelchair design – it could be a simpler version or a more complex, centred on the human-machine interface design.

### **5.1. Wheelchair Concept**

The main goal of the project was to develop a power-assist wheelchair that would be cost-effective and thus available to a wider user spectrum. The set points are as follows: the prototype must be cost-effective; it is to be power-assist type; it can be propelled using only manual power; it can be propelled using only electric power; the drive must be able to perform recuperative braking to increase energy efficiency; the prototype wheelchair must be portable, in worst case it can be dismantled for transportation purposes; the battery pack must be removable by the user which is sitting in the wheelchair; the battery pack should have an on-board charger; the battery pack should have a stand-alone charger; the battery status information should be available to the user using smart phone app; the wheelchair should have various control methods using different human machine interfaces. The wheelchair concept is to use two symmetric standalone drives with dedicated battery ports and battery packs. Prototype wheelchair development consists of three branches: mechanical subsystem, control subsystem and electrical subsystem. The developed battery and its charger are part of the electrical subsystem. From the drive perspective it was defined that its power consumption will be 320 W at max.

### **5.2. Market analysis of powered wheelchairs**

For the first step to design a new battery energy storage system, the market of available existing products was analysed. 34 electric wheelchairs from three online stores [198][199][200] were used for the analysis. The first conclusion is that all the reviewed wheelchairs used sealed lead-acid batteries. 20 models used 24 V nominal voltage while only 14 used 12 V nominal voltage for the battery pack. Both voltages are to be expected as lead-acid batteries typically are manufactured at 12 V nominal voltage. In most cases wheelchairs

with 12 V battery had less range and smaller max speed if compared to 24 V battery versions. If 12 V and 24 V systems are compared then 24 V systems at same power levels have less losses due to smaller currents. Smaller currents also add to simpler motor driver design thus 24 V battery voltage is preferred over the 12 V. Historically 24 V lead-acid battery has been a popular choice due to low cost and excellent availability [201] [202][203].

The next important point of analysis is battery capacity. Naturally, battery capacity is strongly related to the travel distance. However, as this analysis show, this correlation is not the same for all wheelchair models. The analysed wheelchairs had travel distance ranging from 8.4 km to 40.2 km. Here capacity is expressed in *Wh* (watt-hour) as opposed to common *Ah* (ampere-hour) because packs have different voltages. Among the reviewed products, the lowest capacity was 144 Wh which was enough to provide 16.1 km to 20.6 km travel distance. The highest capacity of 1800 Wh was for a wheelchair that was specified to have travel range of 40 km. This information is not quite relevant when evaluating pack capacity requirements as the max travel distance of 40.2 km was achieved using a pack with 864 Wh capacity. A better parameter to evaluate the capabilities of commercial products is a type of efficacy which here is expressed as *Wh/km* – required energy to travel 1 km. This parameter varied from worst 60 Wh/km to best 7 Wh/km. Obviously, this difference is high and requires an explanation. One point is that wheelchairs have max speed ranging from 5.6 km/h to 15 km/h. Higher speed requires more power and sturdier chassis construction which adds to weight which in turn adds to energy consumption. Second point is complicated to analyse objectively as it is related to wheelchair comfort level. Generally, if the wheelchair has more comfort, most likely it will be heavier – more energy required to travel 1 km. Finally, wheelchair with the highest efficacy was labelled as portable, leading to the fact that it is relatively light – weighting approximately 64 kg. Again, energy consumption to move less mass is low if compared to a wheelchair that weights 119 kg (efficacy 60 Wh/km). One additional point is that the small portable wheelchair had regenerative braking functionality which adds to the energy usage efficacy [204] – the prototype wheelchair should have this feature as well. The average efficacy among the analyzed wheelchairs was 24 Wh/km and this value was used to perform initial calculations. The prototype wheelchair should have range of at least 20 km. Previous efficacy assumption leads to a battery pack with 480 Wh capacity. In research articles [194][195][196][205] batteries with capacities ranging from 10 Ah to 17 Ah are used to travel distances from 10 km to 26 km depending on user weight and assistance level. It can be estimated that the selected 480 Wh (20 Ah @ 24 V) capacity is a conservative value which in future could be optimized. As the prototype will be equipped with two replaceable batteries, it was decided to design each battery with around 300 Wh capacity [206].

### **5.3. Market analysis of battery cells**

Once the analysis of commercial alternatives was finished, the obtained information was used to further develop the BES system concept for the wheelchair prototype. The wheelchair prototype was designed for easy use for all types of disabilities and it should be as portable as

possible. One of the goals was to design a replaceable battery pack that can be replaced by the wheelchair user.

One of the options was to use a set of commercially available lead-acid batteries (4 batteries with dimensions 100×100×150 mm) to achieve the previously required 480 Wh capacity at 24 V bus voltage. In this case there would be just a single battery for both drives. The total volume and weight of such battery pack would be 6 L and 16.3 kg. It most likely would not be easy to lift and manipulate a battery pack with such weight for any person in a sitting position. Additionally, typical wheelchairs have no space where to locate a battery with such volume so that it can be accessed by the user while sitting in the chair.

A state-of-art option was to use lithium-ion technology for the battery prototype. The project required a physical prototype to be built, hence it was essential to select battery cells which can actually be purchased. Additionally, the experimental nature of the prototype could benefit from a cell form factor which is abundantly available in different models from different manufacturers. A decision was made to design the battery using 18650-size cells as they are readily available in wide variety of models.

Two online shops [207][208] were used to collect information about 18650-size cells. A total of 115 shop articles were analysed. The complete list is given in Appendix 4. First, 29 articles of cells with added protection circuits were removed. Such cells are intended for use as single cell rechargeable batteries in various consumer products. Multi cell batteries are constructed using plain unprotected cells. The remaining 86 articles constituted models manufactured by four manufacturers: *Sony*, *LG Chem*, *Samsung SDI*, and *Panasonic/Sanyo*. 54 models remained after removal of articles with same models. 29 models had 3.6 V nominal voltage which can be considered typical. The voltage of the remaining were higher than 3.6 and less than 3.78 V in one case. Higher voltage would be beneficial as a cell would store more energy however, the most important parameter is the capacity: distribution graph of all models capacity is shown in Fig. 5.1. It can be seen that capacity is distributed proportionally among the models with several lowest values of 1500 mAh and one highest value of 3500 mAh.

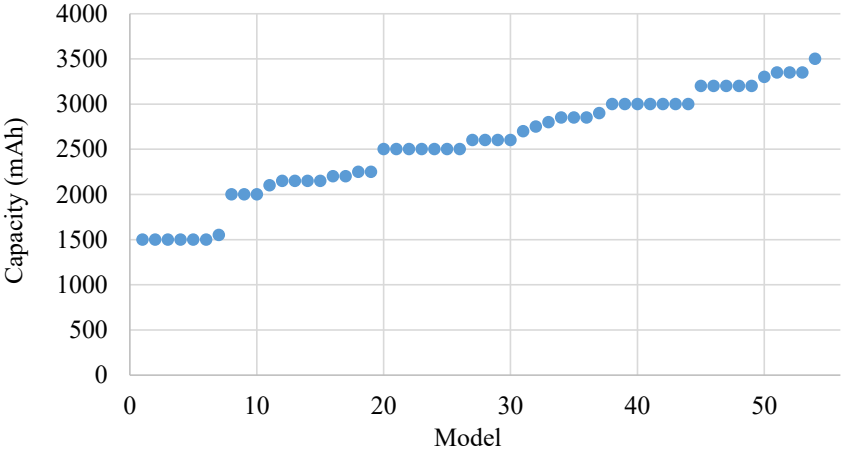


Fig. 5.1. Capacity distribution of analysed cells.

The cell weight distribution graph is shown in Fig. 5.2. The min weight is 43 g, the max is 50 while the average is 46.7 g. The distribution seems linear and one could assume that higher capacity cells will weigh more. However, if weight is plotted according to each cells capacity, as in Fig. 5.3 then there is a high variability of weight among same capacity cells. For example, a 1500 mAh cell can weigh from 43 to 48 g, while 3000+ mAh cells can weigh from 46.5 to 50 g. At 48 g one cell can be rated at 1500 mAh while another is at 3300 mAh. From this it can be concluded, that as long as the cells' standard size remains the same, the weight is not a dominant parameter for filtering suitable models – one should initially consider other parameters.

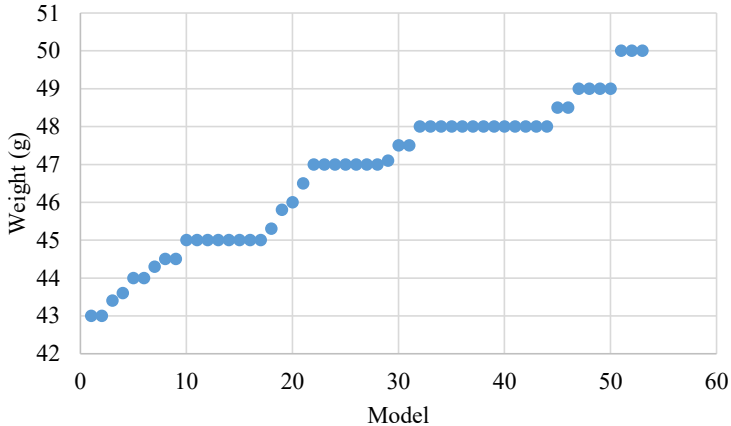


Fig. 5.2. Weight distribution of analysed cells.

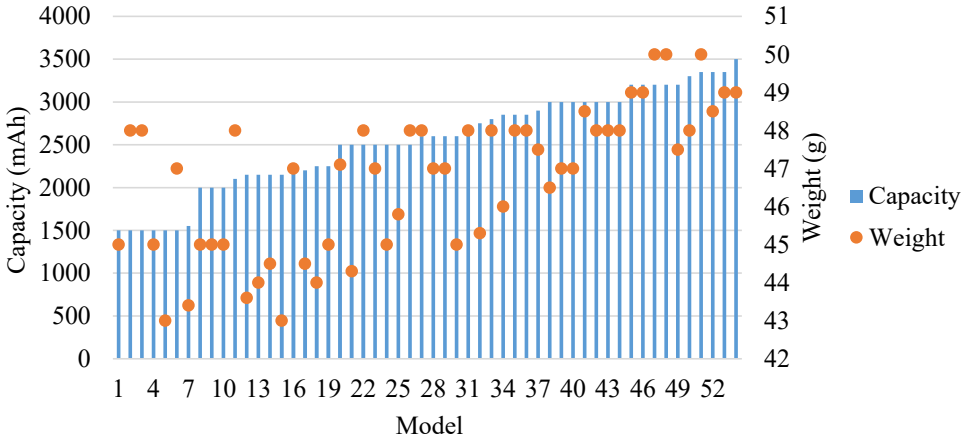


Fig. 5.3. Cell capacity and weight.

At this point, capacity was used to estimate which of the available cells are best suited for the application. Expression (5.1.) was used to calculate the number of required cells ( $n_{cell}$ ) for

battery to meet the 300 Wh goal.  $E_{total}$  is the energy capacity of the battery,  $U_{cell}$  is the nominal voltage of a cell and  $C_{cell}$  is the nominal capacity of a cell.

$$n_{cell} = \frac{E_{total}}{U_{cell} \cdot C_{cell}} \quad (5.1.)$$

The required cell count varies from 24 to 56 cells. Higher cell count results in heavier, larger and more expensive battery pack, hence an arbitrary value was selected to remove part of the models from further analysis – 21 models remained after removal of packs with more than 30 cells.

Next, cycle life was analysed. The cycle life varied from 100 to 500 cycles. In case of most models, the cycle life was rated at three values: 250 – 6 models, 300 – 27 models and 500 cycles for 18 models. The battery is a critical part of all EVs, hence it should provide max capacity and max cycle life. The perspective cell model list was further reduced by eliminating cells with cycle life smaller than 500 cycles. 9 models remained for further analysis.

Further analysis concerns charge/discharge current capability of each model. For all models, max charging current was rated as 1C or less, resulting in range of 1.45 to 3.2 A. Among all of the analysed models, were few had charging rates higher than 2C. The discharge current had broader variation ranging from 2.75 to 20 A which corresponds to 1C to more than 6C. As previously determined, the pack will have at least 25 cells to meet the energy requirement. These cells will be arranged in some configuration as parallel connection would yield too low voltage and series connection would yield too high voltage of 105 V (5.2.)

$$U_{pack\_max} = U_{cell\_max} \cdot n, \quad (5.2.)$$

where  $U_{pack\_max}$  – max voltage of a pack, V;

$U_{cell\_max}$  – max voltage of a cell, V;

$n$  – number of series connected cells;

As discussed in further sections, the max voltage of given application should be kept below 36 V, which results in 10 series connected cells if 3.6 V nominal voltage is used for the calculation. This in turn means that given 25 cells will be split into 3 parallel branches (extra cells would be added to make all branches identical). At estimated 320 W power, less than 9 A would be drawn from the battery or less than 3 A from each cell – this discharge current can be provided continuously by almost any of the filtered cell models – just one was filtered out. This conclusion is valid for any configuration. It should be noted that a cell model with larger discharge current overhead might perform better in long term due to slower aging.

In this analysis the final step is to examine charging current, weight and cost. The charging current for the filtered models varies from 0.5C to 1C which has a significant impact on the charging time although fast charging is not achieved. Additionally the prototype was designed so that the battery can be easily replaced alleviating the need for fast charging. Weight of the remaining models is in 46 to 50 g range: 4 g cell difference will result in 100 g difference of a total pack. The absolute weight difference is not large, albeit not insignificant – it should be considered if all other selection criteria are at a tie. Once technically restrictive criteria are

met, it is time to consider financial criterion: the cost. First, the price of a 300 Wh battery can be calculated using (5.3.):

$$Cost_{pack} = Cost_{cell} \cdot n_{cell}. \quad (5.3.)$$

Then a figure of merit (*FOM*) can be calculated to estimate which model provides more capacity per euro using (5.4.):

$$FOM = E_{pack} / Cost_{pack}. \quad (5.4.)$$

The results of both calculations are shown in Table 5.1. The highest *FOM* is for a battery made of 30 INR18650-MG1 cells. Despite the same capacity costs varies dramatically: from 92.70 € to 169.00 €. It must be noted that cell costs were taken from an online store, hence they can be different in other stores and change with time. From the cost perspective, the best case is the *NCR18650B*. This model additionally has the lowest cell count (25 cells) which produces lightest and smallest battery. The cost difference between two best models is insignificant: just 1.45 €. *NCR18650B* has a slight disadvantage of lower charging current which might increase charging time. To conclude, any of model of the given list would suffice from electrical engineering perspective, however in the actual project local availability played a major role. Additionally, multiple models should be obtained to test actual performance in the specific prototype conditions. As seen in the next section, the nominal voltage and battery configuration can play a role in cell model selection.

Table 5.1

Comparison of perspective battery cell models

Model	Capacity, mAh	Voltage, V	Discharge, A	Charge, A	Weight, g	Cost, €	Pack cells	Pack capacity, Wh	Pack weight, g	Pack cost, €	FOM
INR18650-MG1	2850	3.62	10.0	2.9	46.0	3.09	30	310	1380	92.70	3.34
NCR18650B	3350	3.6	6.4	1.6	48.5	3.65	25	302	1213	91.25	3.30
NCR18650A	2900	3.6	3.8	1.5	47.5	3.45	29	303	1378	100.05	3.03
INR18650-35E	3350	3.6	8.0	2.0	50.0	4.25	25	302	1250	106.25	2.84
INR18650MH1	3200	3.67	10.0	3.1	49.0	4.25	26	305	1274	110.50	2.76
NCR18650GA	3300	3.6	10.0	1.7	48.0	4.59	26	309	1248	119.34	2.59
US18650VTC6	3000	3.6	20.0	3.0	46.5	5.75	28	302	1302	161.00	1.88
INR18650-32E	3200	3.65	6.4	3.2	50.0	6.50	26	304	1300	169.00	1.80

## 5.4. Analysis of battery voltage selection

As previously explained, the use of small capacity (<4 Ah) standardized size cells gives a degree of freedom when designing a battery pack. Such cells can be arranged in various configurations to produce different voltages. This results in the necessity to assess the impact of battery configuration on other drive system components: a drive converter, motor and battery charger – a battery driven approach [209][210]. A list of set-goal parameters from the development project were used as the initial data for the design of the battery: determine the required number of cells and their connections which sets the nominal supply voltage and current.

### Analysis of series and parallel configuration

If the preliminary number of cells and their model have been selected, then one can select nominal voltage of the pack. An all-parallel configuration would produce 3.6 V while series connection would produce nominal 90 V. Using (5.5.) one can calculate battery losses ( $P_{batt\_loss}$ ) which depends on battery current ( $I_{batt}$ ) and battery internal resistance ( $R_{bat}$ ).

$$P_{batt\_loss} = I_{batt}^2 \cdot R_{batt} \quad (5.5.)$$

Current depends on produced power and voltage which in turn depends on cell configuration. Equation (5.6.) on the left shows current calculation for series connection while calculation on the right produces current for parallel connection.

$$I_{batt} = \frac{P_{batt}}{U_{cell} \cdot n_{cell}}, \quad I_{batt} = \frac{P_{batt}}{U_{cell}} \quad (5.6.)$$

Each cell of the battery has its own internal resistance ( $R_{cell}$ ). Equation (5.7.) on the left produces total battery resistance for series connection while the right calculation produces resistance of parallel connection.

$$R_{batt} = R_{cell} \cdot n_{cell}, \quad R_{batt} = \frac{R_{cell}}{n_{cell}} \quad (5.7.)$$

If (5.6.) and (5.7.) are inserted in (5.5.) then the left side of (5.8.) describes battery losses for series connection while the right side for parallel connection.

$$\frac{P_{batt}^2 \cdot R_{cell} \cdot n_{cell}}{U_{cell}^2 \cdot n_{cell}^2} = \frac{P_{batt}^2 \cdot R_{cell}}{U_{cell}^2 \cdot n_{cell}} \quad (5.8.)$$

Equation (5.8.) is linear since  $P_{batt}$  and  $U_{cell}$  can be considered constant for this calculation. This means that battery losses do not depend on cell interconnections. From this perspective one could use any cell interconnection scheme. However, resulting nominal battery voltage can have effect on the efficiency and other parameters of remaining drive elements.

### Impact of nominal voltage on traction motor

The wheelchair design includes two motors – one for each rear wheel. Each motor is to be driven by an individual drive converter and battery pack. Motors will be designed as permanent magnet synchronous motors. The nominal voltage of the motor can be adjusted to match the

one provided by the battery; thus an analysis of the motor design must be made to find the optimal voltage.

Basic motor specification values are the rated active power, rotational speed and voltage. The choice of voltage determines the required current to obtain the torque and power of the motor. The first step of the analysis is to select the values of electromagnetic loads – induction in the air gap  $B\delta$ ,  $T$  and linear load  $A$ . The linear load is determined by the current of all armature winding turns per unit length of the stator circumference (5.9.):

$$A = \frac{2 \cdot m \cdot \omega \cdot I_a}{\pi \cdot D}, \quad (5.9.)$$

where  $m$  – number of phases;  
 $\omega$  – angular frequency, rad/s;  
 $I_a$  – armature current, A;  
 $D$  – stator diameter, m.

The induction in the air gap is chosen so that the induction in the teeth does not exceed 1.4 - 1.8 T, and the linear load should be no more than 40 A/m [211].

However, for estimating electrical losses in the conductors with the known cross section it is recommended to use this value as the current density (5.10.):

$$j_a = \frac{I_a}{S_{wwoi}}, \quad (5.10.)$$

where  $j_a$  – armature current density, A/mm<sup>2</sup>;  
 $S_{wwoi}$  – wire cross section without insulation, mm<sup>2</sup>.  
 It is proportional to the magnitude of the linear load:  $A \sim j_a$ .

Distributed and concentrated armature windings were considered. Conductors laid in the groove are unevenly spaced across its cross section, leaving unfilled spaces. This circumstance must be considered when determining the dimensions of the slot. If the slot is filled with a round conductor, then it can be calculated (5.11.):

$$k_{fill} = \frac{n_{sl} \cdot d_{wwi}^2}{S_{sli}}, \quad (5.11.)$$

where  $k_{fill}$  – slot fill factor;  
 $n_{sl}$  – number of slot wires;  
 $d_{wwi}$  – wire diameter with insulation, mm;  
 $S_{sli}$  – insulated slot cross section, mm<sup>2</sup>.

Calculation of the fill factor gives a value of 0.785. However, a value of 0.75 is considered the most realistic for concentrated single-layer windings. The slot filling factor varies in the aisles of 0.65-0.68 for distributed windings.

When a wire is divided into elementary conductors, the fill factor drops sharply and is compared with the factor for distributed windings. However, maintaining a single conductor increases the frontal parts of the windings by increasing the allowable bending radius.

For reasons of manufacturing technology, concentrated windings are made with division into layers horizontally. The second variant with vertical winding separation [212] makes it possible to reduce the frontal parts and increase the slot filling, however, such windings are more labor-intensive in manufacturing. A slot fill factor was analyzed using conditions: constant dimensions of the motor at given power rating; constant torque. Nominal voltage is the variable parameter. For low rotational speed motors, linear load is recommended to be no more than 14.0 A/m [213]. Exceeding the linear load will reduce the efficiency of the motor and use of materials. In turn, the slots of the motor remain unchanged and if the voltage is reduced then it is impossible to place the wire in the slot of the motor. The analysis confirmed that a motor can be designed if the nominal voltage is in the range of 18 V to 36 V. A slot fill factor limits motor design as shown in Fig. 5.4

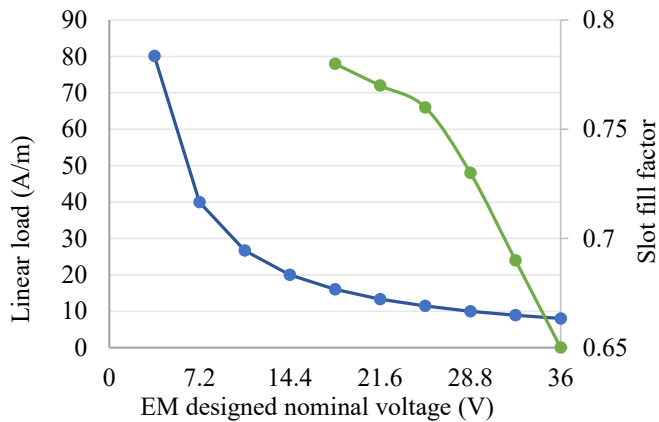


Fig. 5.4. Calculated linear load (grey) and armature slot fill factor (black).

### Analysis of drive converter semiconductor losses

A typical converter topology choice is a voltage source inverter which will be directly fed from the battery pack. The nominal voltage of the battery pack has direct impact on the electrical parameters of the inverter. If a converter will consume 320 W from the battery pack and the battery can be designed to have nominal voltage from 3.6 V to 36 V then there will be 89 A to 9 A nominal input current ( $I_{nom}$ ). An analysis of commercially available switches has been performed to estimate switch losses versus nominal battery voltage. Silicon n-channel MOSFETs which are actively produced were used for the analysis. For each nominal voltage level (of total 10 levels) semiconductors were first filtered to have at least the required current level and minimal breakdown voltage must be at least two times higher than that of the fully charged battery pack. In most cases at least a dozen switches were selected to perform power loss calculation according to [214]. Typical buck converter signal waveforms were used to simplify calculations. Conduction losses  $P_{con}$  were calculated using (5.12.) where  $R_{DSon}$  is the drain-source on-resistance at 10 V gate-source voltage and  $I_{nom}$  is the nominal current.

$$P_{con} = R_{DSon} \cdot I_{nom}^2 \quad (5.12.)$$

Switching losses  $P_{sw}$  are calculated using (5.13.) where  $E_{on}$  is the energy loss per turn-on,  $E_{off}$  is the energy loss per turn-off and  $E_{Mrr}$  is the energy loss of reverse recovery of the diode. 100 kHz switching frequency  $f_{sw}$  was used for all calculations.

$$P_{sw} = (E_{on} + E_{off} + E_{Mrr}) \cdot f_{sw} \quad (5.13.)$$

$E_{on}$  is calculated using (5.14.) where  $U_{full}$  is full charging voltage,  $I_{nom}$  is nominal current,  $t_{ri}$  is rise time of current and  $t_{fu}$  is fall time of voltage.  $E_{off}$  is calculated in a similar manner except that  $t_{ri}$  is replaced by  $t_{fi}$  (current fall time) and  $t_{fu}$  is replaced by  $t_{ru}$  (voltage rise time).

$$E_{on} = U_{dd} \cdot I_{nom} \cdot \frac{t_{ri} + t_{fu}}{2} + Q_{rr} \cdot U_{full} \quad (5.14.)$$

The voltage rise and fall times were calculated according to (5.15), where gate-drain capacitance (CGD) value was obtained from the datasheet capacitance variation graph. Datasheet current rise ( $t_{ri}$ ) and fall ( $t_{fi}$ ) times is far from an optimal, a better approach would be to use rise and fall times which are calculated using methods given in [215] and [216].

$$t_{fu} = (U_{full} - R_{DSon} \cdot I_{nom}) \cdot R_g \cdot \frac{C_{GD}}{U_{Dr} - U_{plateau}} \quad (5.15.)$$

Calculations were performed on several switches with lowest  $R_{DSon}$  value, several switches with lowest total gate charge value, and on several switches with lowest figure-of-merit value which is multiplication of  $R_{DSon}$  and total gate charge values. After initial examination of the results several more switches were hand-picked to find the ones with lowest losses. The obtained loss calculation results are given in Fig. 5.5. A total of 10 loss groups were obtained – one for each battery voltage level in 3.6 V steps. Only five lowest loss switch models are presented in the figure to provide estimation of the best-case situation. It can be concluded that above 7.2 V nominal voltage, the configuration of the battery pack has no impact on the losses of the drive’s semiconductor switches.

The same MOSFET models were used to provide the 50-point cost graph shown in Fig. 5.6. The line presents the average for each voltage group. It can be concluded that battery configuration does not strongly affect the costs of MOSFETs for a drive converter if nominal voltage is above 7.2 V.

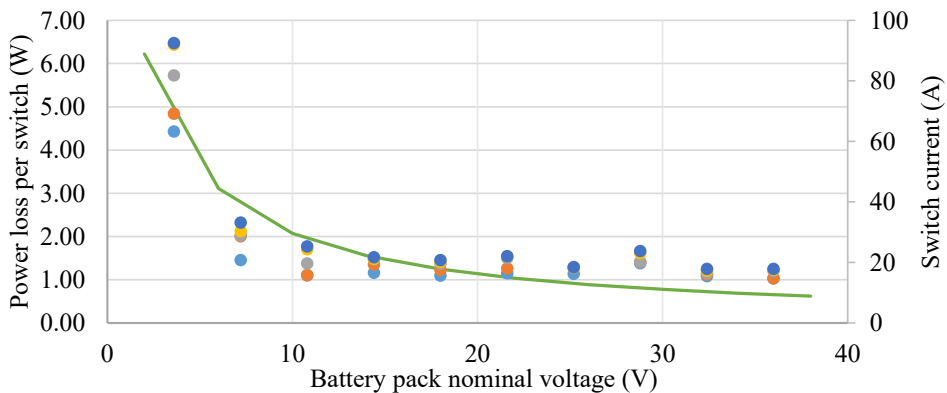


Fig. 5.5. Calculated power loss (dots) and current (line) per switch at different nominal battery voltages.

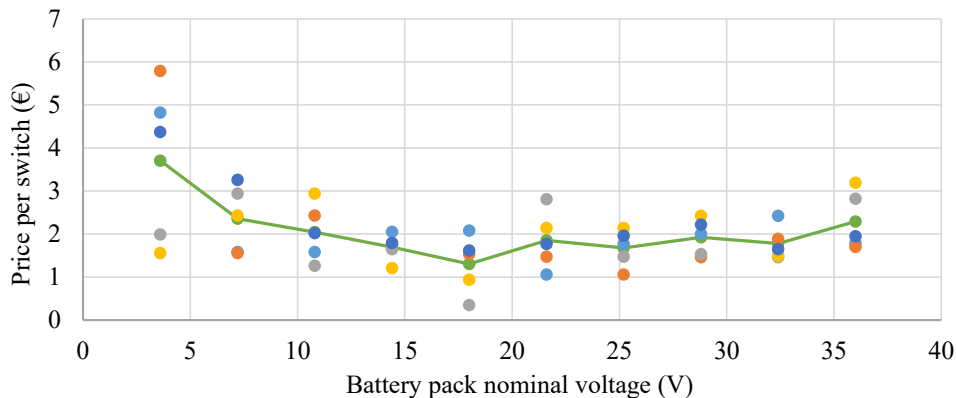


Fig. 5.6. Price of selected MOSFETs (dots) and average price (line) at different battery pack nominal voltages.

### Analysis of battery charger efficiency versus nominal voltage

One of the goals of the project was to design such a charging device which can simultaneously charge both battery packs. It is intended to use multi-converter isolated SEPIC (single-ended primary inductance converter) topology as shown in Fig. 5.7 and proposed in [217]. Generally, a charger could be designed to any battery specification, however, for this project the charger should be small in size to accomplish onboard charging while being housed in one of the armrests. Losses should be minimized to reduce charger cooling requirements hence loss calculation was performed. The AC side losses of the converter does not change if the output power remains constant – the nominal charging power is 350 W per battery. The design and component selection of the DC output side depends on the output voltage and current. As can be seen in Fig. 5.7, there are four identical SEPICs. Each of them has two outputs. One output is connected to the first battery while the other is connected to the second battery – converters are connected in parallel and they share a common set of output filter capacitors. Two outputs naturally operate to split output power between both batteries: the battery with lower voltage will receive more power while the other battery (with higher voltage) will charge slower. The remaining secondary side power component is a rectifier diode which will be replaced with a synchronous rectification MOSFET (metal-oxide-semiconductor field-effect transistor).

The selected MOSFETs of the previous section can be used in a synchronous rectification mode for the charger. The top 5 MOSFETs of each voltage were used to calculate losses of the charger output side. Even if just a single empty battery is connected to the charger it should be charged with 350 W – the power of each converter would be one quarter of total or 87.5 W. This power was used to calculate nominal current values of the rectifier switch at different battery nominal voltages. The obtained current levels and power losses per switch are presented in Fig. 5.8. It can be concluded that for battery voltage from 7.2 V to 36 V the losses are similar, and any voltage can be used as the nominal. A small exception is 28.8 V, where losses are higher due to the use of 80 V MOSFETs, which have higher  $R_{DSon}$  value than 60V MOSFETs, which were used for 18 – 25.2 V nominal voltage calculations.

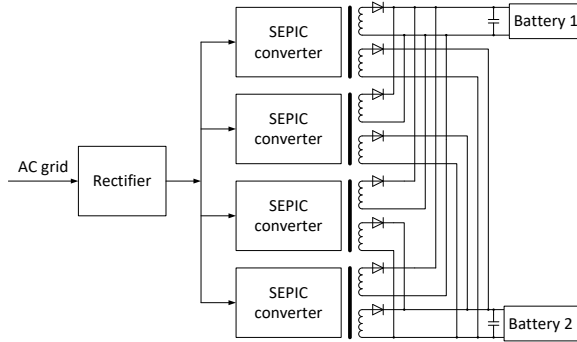


Fig. 5.7. Proposed layout of charger configuration

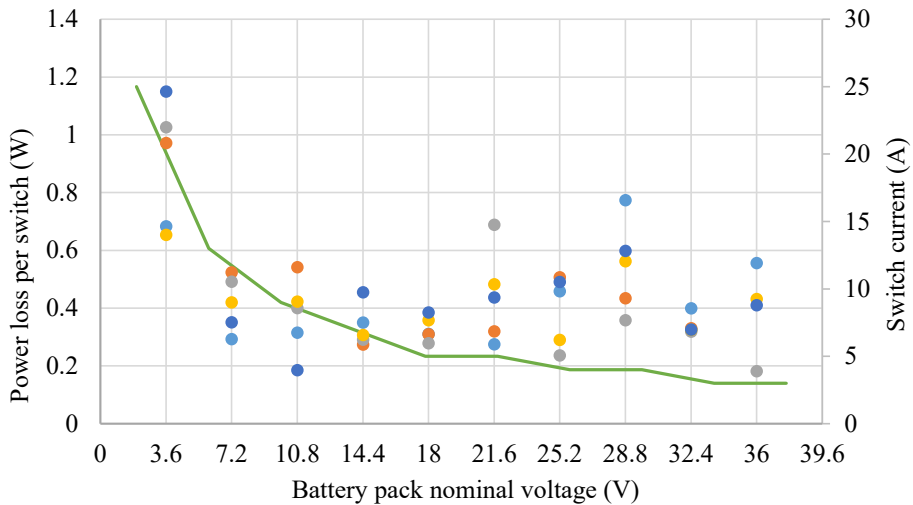


Fig. 5.8. Calculated power loss (dots) and current (line) per rectifier switch at different nominal battery voltages

### Discussion of nominal voltage for battery pack

The previous sections evaluated how power losses of a motor, drive converter and battery charger change with respect to nominal voltage. The semiconductor loss calculation of a drive converter and battery charger revealed that if the battery voltage is selected to be higher than that of a single cell, the losses become almost constant (see drive losses in 0). The small MOSFET cost variation does not have significant impact on the selection of nominal voltage. The motor design calculations revealed that the voltage of the battery pack should be higher – at least 18 V to reach reasonable slot fill factor value.

The battery pack would optimally consist of 25 cells (as established in the previous section). Integer 25 produces very few configuration combinations, hence if some flexibility is to be achieved, another cell number should be used. 28 is the next higher integer which produces more configurations. Additionally, a 28 cell pack will be suitable to use 6 of the previously selected cell models – it allows some redesign and field test comparison in the same battery

size. The standard describing wheelchair battery packs sets the maximum nominal voltage to 36 V [218] albeit it covers only lead-acid based batteries and the limit is given for the charger. A standard covering lithium-based battery technology for wheelchairs (ISO/AWI 7176-31) is currently under development. In the case of Li-ion cells full charge voltage would reach 42 V if 10 cell series (10S) configuration is used to produce 36 V nominal voltage. This configuration would require 3 parallel cells (3P) for each level to achieve required capacity and symmetry at all levels thus the final configuration would be 10S3P and it would require 30 cells in total. Additional two cells would increase total costs and size of the battery – a disadvantage. Table 5.2 summarizes all configurations if a minimum of 28 cells at 3.6 V each is used. Four configurations use 28 cells. 1S28P and 2S14P configurations are to be avoided due to a high nominal current and resulting converter losses as indicated by the calculations of the drive converter section. A full charge voltage of 9S4P and 10S3P configurations exceeds 36 V – for safety, these configurations should be avoided as currently there is no standard describing a wheelchair’s lithium-based battery. This leaves 4S7P and 7S4P configurations. 4S7P should not be used because a 14.4 V nominal voltage is not suitable for the motor design which requires the voltage to be higher than 18 V. 7S4P configuration is the best choice as the nominal voltage is high (current is low) and while losses and price of semiconductors are relatively low. 5S5P – a 25 cell configuration would be marginally sufficient for motor requirements and it would lack the possibility to switch to other (smaller capacity) cells and would not be backwards compatible with 12V-based lead-acid battery systems – this is an additional feature of 7S4P configuration. To conclude, it was decided that 7S4P configuration is best suited for the project needs as it provides good performance and flexibility at the cost of 3 extra cells.

Table 5.2

Parameters of battery pack at different cell configurations

Nominal voltage (V)	Full voltage (V)	Current (A)	Battery configuration	Required cells	Drive losses	Charger losses	MOSFET price
3.6	4.2	88.9	1S28P	28	High	High	High
7.2	8.4	44.4	2S14P	28	Average	Average	Average
10.8	12.6	29.6	3S10P	30	Low	Average	Average
14.4	16.8	22.2	4S7P	28	Low	Low	Low
18	21	17.8	5S6P	30	Low	Low	Low
21.6	25.2	14.8	6S5P	30	Low	Average	Average
25.2	29.4	12.7	7S4P	28	Low	Low	Low
28.8	33.6	11.1	8S4P	32	Low	Average	Average
32.4	37.8	9.9	9S4P	36	Low	Low	Average
36	42	8.9	10S3P	30	Low	Average	Average

## 6. CELL BALANCING SYSTEM DEVELOPMENT AND VERIFICATION

The key goal of this thesis project is to develop a balancing system which can be used in PMVs battery packs. As described in previous sections, small EVs tends to use battery packs with relatively low voltages: from 12 V up to 72 V which corresponds to 3S – 20S cell connection for 3.6 V cells and 4S – 23S connection for 3.2 V cells. As indicated in previous section, if sufficiently large number of cells are available then it is possible to sort them to match capacity at fraction of percent while random selection will result in around 3 % difference. If this small capacity difference corresponds to cell charge mismatch during battery usage, then switched resistor balancing could be selected as an appropriate balancing method due to low cost and complexity. Hence, this section is devoted to developing a modular cell balancing solution which is based on switched resistor method. Additionally, a way to improve efficiency and balancing speed using a transformer-based charge transfer is explored – both balancing methods are integrated to develop a novel multi-stage balancing method.

As revealed in next section, given balancing system is developed for balancing of batteries consisting of 40 Ah prismatic LFP cells – the same cells which were used in some of the tests of previous section. Due to large size of cells and since both poles are nearby and on the same plane it was decided to develop a highly modular balancing solution – a single balancing board per cell, with a central control board.

### 6.1. Development of cell module 1

The design process of a cell module can be divided into two parts: design of hardware and software. The first part might seem simple because of the rather plain balancing topology. Yet still careful design considerations had to be made to make the module power and cost efficient – even for a small battery pack a number of modules will be needed which leads to the issue of keeping the production costs as low as possible.

The first prototype was created to obtain some sort of a result as quickly as possible. The development was divided in three parts: development of the circuit – designing the circuit and PCB around certain cost and space limitations; development of data transfer – already early on it was decided to use a data transfer which would require a simple hardware part and probably a more complex software part; development of the microcontroller program – writing a software that would perform both cell balancing and data communication.

#### Development of the circuit

The circuit of the cell balancer module was designed in *Cadence OrCAD Capture* software. Schematic is shown in Fig. 6.1. The main blocks of the module are the microcontroller and the cell shunting elements.

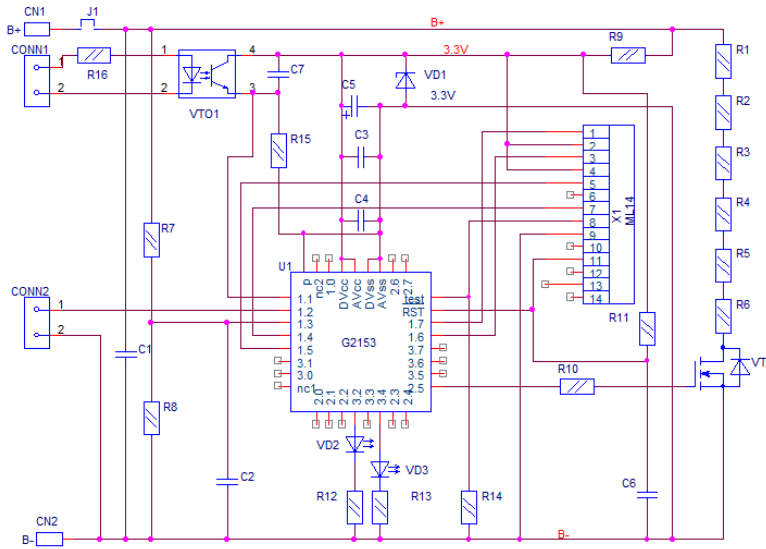


Fig. 6.1. Schematic of cell module 1 in OrCAD Capture.

The first requisite of the microcontroller is an ADC unit. It is required to obtain cell voltage value, which is one of the main tasks of the cell balancer module. The second requirement is a particular communication unit. It must be noted that all cells of the battery pack are connected in series which means that each cell module has its own ground reference and there is no common ground (here in some cases the negative terminal of the battery pack is considered the common ground). This brings up an issue that one cell module microcontroller cannot be directly connected to another cell module microcontroller for communication purposes. Additional circuitry to provide the correct voltage levels must be introduced for each communication line. Since one of the system objectives is to keep costs low, there is a clear understanding that less communication lines means fewer components and lower costs. All synchronous data transfer methods require a synchronisation signal line. However asynchronous data transfer uses only one line which performs both synchronisation and data exchange. For this reason, the microcontroller has to have a universal asynchronous receiver/transmitter (UART) peripheral module. One could argue that a standardized CAN bus should be used since it is widely used in automotive industry. Yet here the only device capable of using the rather specific and large data amount is the central battery management module which will perform data analysis and a CAN bus type communication might be used to send the produced battery pack and individual cell characteristic parameters to other devices. Here the UART will be used as an internal communication of the battery pack. Given the set requirements a microcontroller with lowest cost and good availability was selected. At the time of development, it was chosen to use an ultra-low power *MSP430G2153* microcontroller produced by *Texas Instruments*. It is a 16-bit microcontroller in a 32 pin QFN package with all the necessary peripherals.

The cell shunting block consists of two elements: string of excessive energy dissipation resistors and a solid-state switching element. The main performance of the dissipative shunting balancing topology is determined by the shunting resistor: the smaller the resistors resistance the more powerful the balancing is – balancing time is reduced. The main limit of the shunting resistor resistance from the low side is the resistor power rating and the solution of how to get rid of the produced heat. At some point the battery pack thermal management becomes an issue since LFP cells have a rather limited operational temperature range. For the first module prototype it was selected to use 2 W rated resistors R1 to R6 connected in series to obtain higher power rating and balancing current and thus better balancing performance. Six 1  $\Omega$  resistors were used which produces 633 mA shunting current at 3.8 V cell voltage. The resistors are rated 2 W at a temperature which is too high for overall system thermal integrity, which is why they are used at just about half their rated power. Once the resistors are selected it becomes quite an easy task to select the commutation element. The goal was to select a device that would be power efficient and with low conduction mode losses which in turn would mean that the device is physically small – an advantage since the board size is limited. A MOSFET was selected as the switch element VT1. It has reasonably low on state resistance and the SOT23 package makes it board area efficient. Another benefit is that this element is a logic level MOSFET – the gate threshold voltage is low enough to be provided by the microcontroller directly.

Power to the cell balancer module is supplied directly by the cell itself. Connectors CN1 and CN2 are used to connect to the cell. For the first cell balancer design the cell voltage was allowed to be from 2.8 to 3.8 V. The recommended supply voltage of the microcontroller is 3.6 V and absolute maximum voltage is 4.1 V. For safety reasons a 3.3 V Zener diode VD1 with a small value ballast resistor R9 was added to the circuit. A removable jumper J1 is used as a power switch of the balancer module. It is a necessary element since it is expected that the circuit will draw a certain amount of current from the cell at all times thus the cell will get discharged over time. If the battery pack is not intended to be used for a prolonged period, the jumper can be removed to save energy.

MSP430 series microcontrollers are equipped with internal voltage reference for the ADC. Two voltage levels: 1.5 V or 2.5 V can be selected as the reference. To provide higher noise level margin the 2.5 V internal reference was used. Yet even the lowest permissible cell voltage is higher than the reference. A resistor voltage divider consisting of resistors R7 and R8 was used to attenuate the voltage to the suitable range.

As previously mentioned, the cells of the battery pack are arranged in series. To decrease the amount of data cables between the master module and the cell balancers it was decided to connect all cell balancer data transmission lines in series as well thus forming a sort of daisy chain connection. The transmit pin of the microcontroller UART module is directly connected to the board communication output connector CONN2. A cable with this line and a corresponding return line is connected to the next module communication input connector CONN1. The transmit line of the first module is driving the input diode of the optocoupler VTO1 of the next module. The optocoupler secondary side transistor together with resistor R15 reproduces the signal which is then fed into the microcontroller UART receive pin. In this setup the optocoupler plays a critical role from two points of view. First it is an element of galvanic

isolation thus the second cell actually could be any cell of the string and the communication would still work. Second it is the element that limits the transmission speed of the UART communication because most generic optocouplers have a bandwidth in the vicinity of 50kHz. However, it was expected that quite low baud rates are acceptable since the data amount to be exchanged is not too large.

Additional module elements include two LEDs VD2 and VD3 which were intended to be used as indicators of program state during software design and debugging and cell state indicators during normal operation. The circuit features a full sized JTAG connector X1 which is used to program and debug MSP430 series microcontrollers.

After the circuit was designed in *OrCad Capture* it was time to design a PCB in *OrCad Layout*. In this case the main limit of the PCB is the board size which is limited by the cell size. Each cell balancer module is intended to be installed on the top of each cell. The balancer was designed in such a manner that the two main power connections (+ and -) of the board are located directly above the cell screw terminals. Two large pads were made on the PCB with 7 mm holes to suit the standard M6 screws used for the cell screw terminals. The cells in the battery pack will be arranged one next to another so the only available space for the board is a bit less than the top surface area of the cell which for the selected cells is 116×47 mm. While the PCB is made as a two-layer board, the components can be placed only on the top layer since the cell's relief occupies most of the bottom layer. An assembled developed board is shown on Fig. 6.2. It can be seen that the six shunting resistors were placed in a string around the edge of the board to conserve the more useful space in the middle of the board. An additional spacer was soldered to the bottom side of each power connector to provide some clearance between the board and cell connector and cell-to-cell connection bars.



Fig. 6.2. Top and bottom of assembled cell module 1.

### Development of data transfer

UART communication was used as the base for daisy chain communication implementation. During the initialization part of the cell balancer module microcontroller, the UART module is set to receive data. If a data package is received then the RX flag is set and the corresponding subroutine (Fig. 6.3) is activated. Once the program is in the subroutine the Watchdog Timer (WDT) is initiated. ADC is stopped and the last conversation result will be used as the data to be sent. If UART TX module is not busy then the cell voltage value is written to the transmit register. Value which was received is now saved as the cell voltage value to be sent during the next transmission. Since the ADC is stopped, this value will not be changed by the ADC subroutine. Afterwards the UART module is set to wait for the next RX data package and program exits interrupt subroutine.

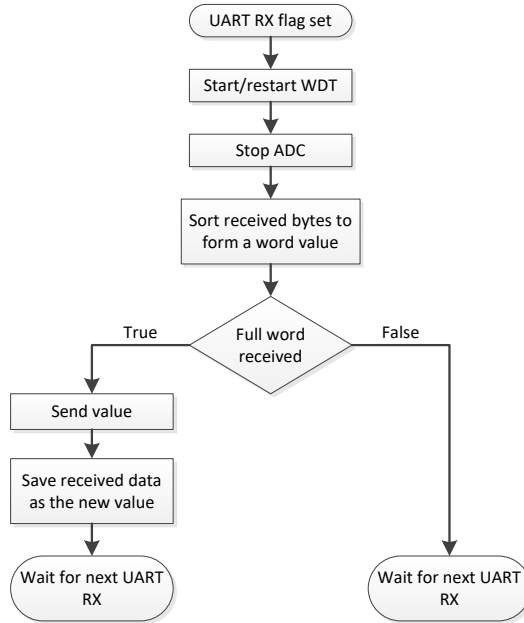


Fig. 6.3. UART receive subroutine.

If the next RX package is not received during certain amount of time then the WDT flag is automatically set and the program enters WDT subroutine. During this subroutine the ADC is initiated once again to continue cell voltage measurements and renew the voltage value in the corresponding processor register. After that the WDT is disabled and program continues its operation as set by the WDT subroutine.

In this program algorithm the WDT flag is set every time after all cell modules have sent their cell voltage values to the central master controller. This controller periodically checks all cell voltages to prevent cell overcharge or deep discharge which can lead to permanent failure of the cells. To initiate the daisy-chain data transfer, the higher controller sends a command byte to the first-of-the-chain cell balancer's RX input. Only one (first) cell balancer's RX input is connected to master controller. The last cell balancer's TX output is connected to the master

controller making a ring (daisy chain) communication line. Once the first command byte is sent, the master module waits for a data input from the last cell balancer, if the received data is not the same as the previously sent command byte then the received data is saved as a cell voltage value and another command byte is sent out by the master controller. Eventually through the daisy chain action all cell balancers have received a command byte and it is finally sent back to the master module. Once the controller receives a command byte, it stops transmitting new control bytes. All cell balancers have been successfully questioned for their cell voltage values and this cycle of information gathering has ended.

All the data is transferred one byte at a time. This leads to a problem how to distinguish a command byte from the data bytes. It is possible to select an appropriate unique command byte by analysing all the possible data byte values. If the measured cell voltage is 3.8V, the ADC produces the maximum value 906. If the measured voltage is 2.8V then the ADC produces a minimum value of 667. Both of these numbers are in two byte format. The most significant byte always takes values of 2 or 3. It was noticed that the least significant byte can take values from 0 to 139 and from 154 to 255. This leaves out a free region from 140 to 153. Generally any of these free values could be used as command bytes, but for increased confidence the middle value of 146 was used as command byte to initiate the data exchange by the master controller.

### **Development of the microcontroller program**

The first step to usefully exploit given ultra-low power microcontroller is to use interrupt routines. After the start-up, microcontroller ports are adjusted to perform the desired operations, the ADC, UART and WDT initialization parameters are set as well. ADC is set to acquire 50 kSPS to save extra power since the full conversion speed here is not essential. After all control variables are set, the CPU of the microcontroller is turned off to save power.

Two separate parts can be distinguished from the program operation point of view. The first part could be described as the main operation phase while the other part is used to perform the previously described data transfer. In the first part during the initialization ADC is set to perform sixteen cell voltage measurements and using the direct transfer controller save all measurements in the microcontroller RAM. After full measurement transfer is done, the ADC interrupt flag is set and the corresponding subroutine (Fig. 6.4) is activated. During this routine the sixteen measurements are sorted using bubble sort. After sorting the four lowest and highest values are removed from measurement stack. The remaining values are used to produce an average cell voltage value. If this value exceeds a certain previously defined higher or lower cut-off values then the program turns on one of the status indication LEDs. If the battery cell voltage has reached full charge then the green LED is lit and MOSFET is turned on to shunt the particular cell charging current thus prohibiting voltage increase of the cell. If the lower voltage value is reached then only the red LED is lit. The cell voltage value is saved in one of the processor registers for a quick access. Afterwards the ADC is set to perform the next sixteen measurements and program exits interrupt subroutine – CPU enters low power mode.

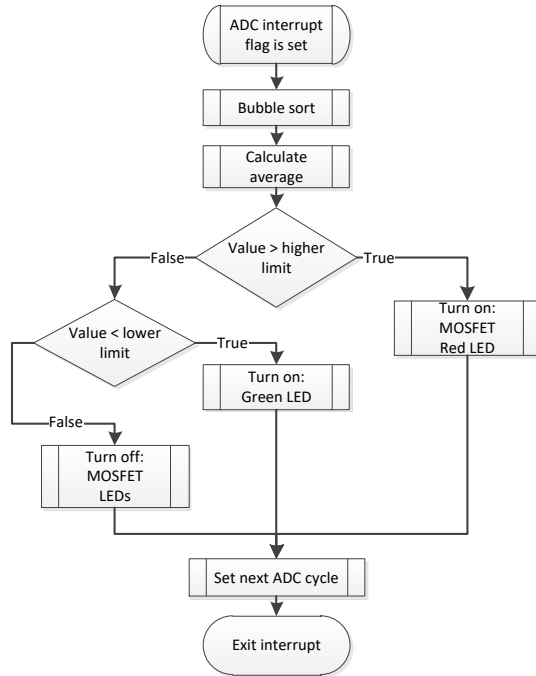


Fig. 6.4. ADC subroutine flowchart.

The second distinguished part (Fig. 6.5) of the program operation is started by an external event – the UART RX flag is set because the master module has initiated a data transfer. The operation of the daisy chain data transfer is described in the previous chapter. After the data transfer is complete the CPU once again enters low power mode while waiting for whether ADC or UART RX flag to be set.

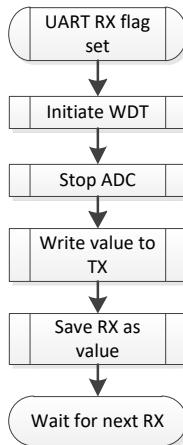


Fig. 6.5. UART subroutine flowchart.

### **Evaluation of cell module 1**

The first prototype version of the cell balancer module was made locally in two copies using a CNC PCB milling machine. All the parts were soldered and the program was written to the microcontroller.

It was quickly discovered that the board has some problematic issues. First, the actual connection to the cell was impossible since some of the through-hole component's pins on the bottom layer were making a contact with the cell terminals or the cell-to-cell connection copper bars. However, for initial testing the cell balancer module can be tested without the actual cell using a laboratory power supply.

The first test was verifying the operation of the shunting circuit. The applied voltage was varied to check whether microcontroller registers both high and low voltage thresholds and turns on the corresponding LEDs and the shunting resistor. It was noticed that the two assembled boards each had different ADC values at the same 2.8 V and 3.8 V used for the tests. This could indicate that the ADC with the built-in reference voltage generator varies from chip to chip. Once a voltage higher than 3.8V was applied to the cell balancer module, the shunting circuit MOSFET was turned on and the six resistors produced the set shunting current as expected. During the shunting operation the resistors reached temperature of 81.1 °C which is permissible by the resistor technical specification yet the resistors are heating up the whole board which could negatively affect such components as the microcontroller. Additionally, the high temperature raises a safety concern as it sufficient to cause a thermal burn if touched.

The data transfer function of the balancer board was tested as well. At the time of testing the master board was still not designed so for the test another specifically programmed microcontroller was used. The test setup can be seen in Fig. 6.6. The two cell balancer modules were connected one to another and the additional master module emulating microcontroller was directly connected to the first module optocoupler input and through an additional optocoupler to the second balancer module TX connector. The two cell balancers were operated automatically as defined by their program codes. The additional microcontroller was connected to a PC using a JTAG connection. It was set to transmit a command byte. After a brief moment the program was manually stopped to check what if anything the microcontroller UART module had received. This test was done with data transmission rate of 9600 kBaud and it was successful – the additional microcontroller received data as it was expected.

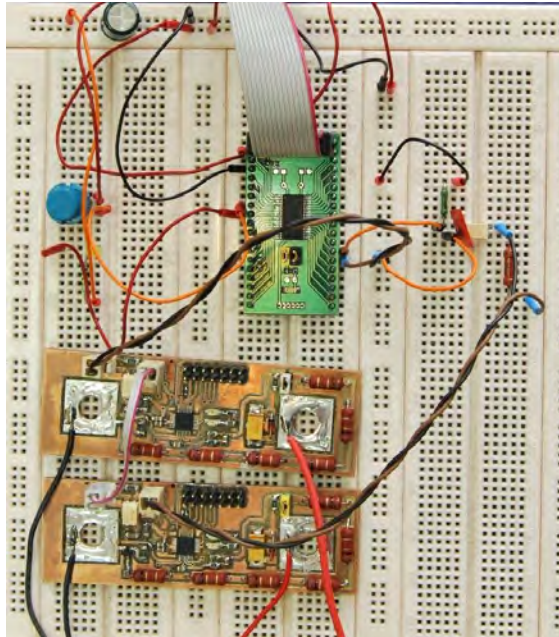


Fig. 6.6. Test setup for cell module 1 communication verification.

One of the relevant performance parameters of a battery-based systems is the power consumption. The current consumed by the cell balancer module during the normal operation (not exchanging data) was measured to be 2.865 mA at 3.2 V power supply which is the nominal cell voltage. At this current rate a fully charged cell would discharge in 582 days. After a brief inspection of the circuit it was decided to remove the Zener diode and measure the current again. It turned out to be 1.621 mA, which is 43 % less. The current consumption by the Zener diode can be easily explained by the current–voltage characteristic of the device. Both cell modules were tested with voltages as high as 4.0 V and it was found out that the microcontrollers were capable to operate at such levels. As a result, it was decided to remove the Zener diode from the next prototypes.

Based on the obtained overall results it was decided to redesign the cell balancer schematic and board to improve the power consumption and arrange all the elements in such a way that no pins could contact the previously mentioned cell interconnection tabs. Given the size of those tabs the available component space of the board was reduced to roughly 35×40 mm.

## 6.2. Cell module 2

The second prototype of the cell balancer module was designed to solve the problems associated with the board layout as well as to improve the circuit to increase the efficiency. Additionally, the software was updated to fix the problem with different module ADC precision. The goal of this revision was to produce a design that could be manufactured in the necessary numbers to assemble a functional battery pack.

### Improvements

The design of second prototype was started by the revision of the cell balancer module circuit. It was modified in three places. First, the Zener diode was removed from the circuit to improve the energy efficiency. Second the six shunting resistors were replaced with one 10 W rated heatsink encased wire wound power resistor thus saving extra space on the board. And third the standard JTAG connector was optimized. The *MSP430* standard programming JTAG connector has 14 pins out of which five pins are actually not connected and it has two Vcc pins – one for power and one for sense. To get a smaller and cheaper connector, the not-connected pins and the Vcc power pin were removed. The result is a custom pinout 8-pin one row connector that is more compact than the previous. Additionally, the pins were arranged in such a manner to ease the layout of the board. The same *OrCad* software was used for both the circuit and the new board design.



Fig. 6.7. Assembled cell module 2.

Fig. 6.7 shows the populated top side of the finished balancer module 2. All the parts are located in the middle section to not interfere with the cell connection tabs. Some surface mount elements are mounted to the bottom side of the board. The particular shunting resistor was selected due to the availability in the laboratory. Using a couple of screws and nuts the resistor was fixed at a 0.5 cm distance from the board to provide some thermal isolation to the board. The resistor resistance of 2.15  $\Omega$  provide 1.77 A shunting current at 3.8 V cell voltage. Fig. 6.8 shows a thermal image of the cell balancer module with a fully heated up shunting resistor. It can be seen that the resistor surface temperature reaches 197.6  $^{\circ}\text{C}$  while the microcontroller temperature goes up to 64.6  $^{\circ}\text{C}$ . Fortunately this temperature rise did not affect the performance of the microcontroller. The resistor temperature poses a burn risk if touched, however an alternative would be to use higher resistance resistor which would also increase balancing time.

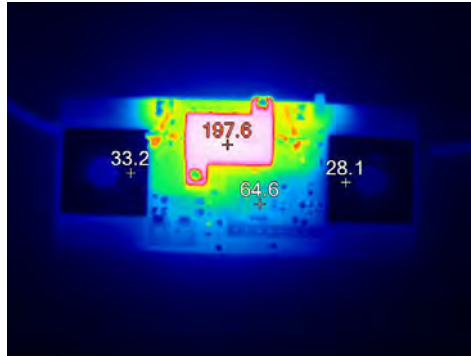


Fig. 6.8. Thermal image of cell module 2 during shunting.

For the final version the JTAG connector was not soldered into the board but a *pogo-pin* type programmer connector was used to program each board. Only a few boards were fitted with an on-board connector for easier debugging and testing purposes.

A simple BMS master board (Fig. 6.9) was designed with the main purpose to collect voltage readings from the cell module boards and display them on an LCD for easy access. Pushbuttons were added to scroll through the readings. A buzzer was added to sound an alarm if any of the readings are outside of safe operating area.

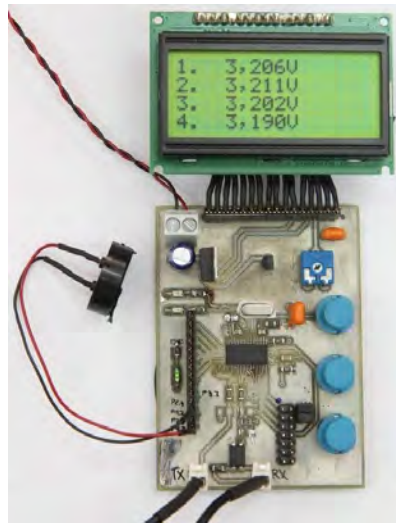


Fig. 6.9. First version of BMS master board.

### ADC calibration

Same as in the previous version of the cell balancer all the modules were designed with the same simple voltage resistor divider which consists of 1 % precision resistors. It is required to reduce the cell voltage to an appropriate level for the ADC. The testing of the first cell balancer prototype showed that the two initial boards produced different ADC results at the same

voltage. It is possible to calibrate each board so that it performs the necessary functions at the necessary voltages while having different ADC readings. However here the master module is intended to collect all cell balancer module ADC readings and store and analyse them. So that the analysis made a sense all the ADC readings have to on the same scale with the same reference point. While the second generation of cell balancer modules were produced in greater numbers it was decided to test the performance of each ADC and develop certain methods to overcome any problems.

Initially 20 cell balancer modules were assembled. All of the modules were tested to verify the uniformity of ADC measurements. A simple test was carried out: 3.8 V was applied to the cell balancer terminals and an averaged ADC output value was recorded. The obtained results are shown in Fig. 6.10. It can be seen that the dispersion of the group spans across 30 discreet values. 3.8 V was selected as it is the upper limit of the cell operational voltage while the lower voltage limit is 2.8 V which means that the measurable voltage range is 1 V. When this voltage is applied to the selected resistor divider and the 10-bit ADC, the result is with a resolution of 4 mV per bit and the permissible voltage range transforms to 244 values for the ADC output. It should be noted that the ADC full range spans across 1024 values, out of which three quarters are not used since the microcontroller can only provide positive reference voltage, which is referenced to the ground voltage. External op-amp circuitry could be used as well to scale the cell operational range voltage to the ADC range. Here the simple experiment showed that the ADC accuracy range spans 30 values – it means that the cell voltage measurement can have 12 % error from one chip to another, which cannot be allowed. Since as it previously was discussed it is not reasonable to correct the conversion error in the master board, two different approaches for the cell balancer ADC calibration were tested.

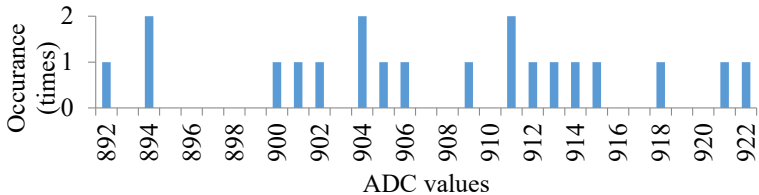


Fig. 6.10. ADC conversion values from 20 cell balancer modules.

**Levelling Out the ADC Measurements**

The first approach was to level out all the cell balancers so that all the ADCs produced the same value at one certain input voltage. The lowest cell voltage limit was selected as the calibration voltage. This particular value was selected because it corresponds to the limit beyond which the cell might be irreversibly damaged and the cell itself has the tendency to discharge and approach the lowest voltage. 2.8 V were applied to each cell balancer and the measured value was sent to the master board to be displayed on the LCD. A certain digital value was selected for the 2.8 V limit to be able to adjust all of the cell balancers. It was selected to be 685 because it is slightly smaller than the lowest ADC measurement at the set voltage and to obtain this value it is needed to add some calibration value to each cell balancer. Some small

amount of value is left as an extra in the case if some other microcontrollers ADCs will have even more shift. Since the cell balancer program code is composed in the assembler language then it is quite easy to add a calibration value to an ADC output value. Calibration value was stored in the microcontroller information memory to allow further program code modification without a risk to corrupt calibration data while performing programming of the chip.

Once all of the cell balancers were calibrated, they all were tested at three cell voltages: 2.798 V 3.298 V and 3.705 V. The readouts from the master board LCD were recorded and their relative values are shown in Fig. 6.11. It can be seen in Fig. 6.11(a) histogram that almost all balancers were successfully calibrated at 2.798 V. One could have wished that LCD showed 2.801 V since it is closer to the actual voltage but it is better for the LCD to show a smaller value because it gives extra mV reserve for the cell voltage minimum. In Fig. 6.11(b) histogram a collection of display output data is shown at 3.298 V. It can be noticed that the output values have some dispersion with a maximal shift of 18 mV down from the actual value. For the third test 3.705 V was applied to the same cell balancer modules. Display value histogram is shown in Fig. 6.11(c). In this case there is a strong dispersion with two stronger values closer to the actual voltage and multiple other values even 32 mV down from the actual voltage. This amount of dispersion in the high cell voltage region is too high if an accurate cell balancing is to be used.

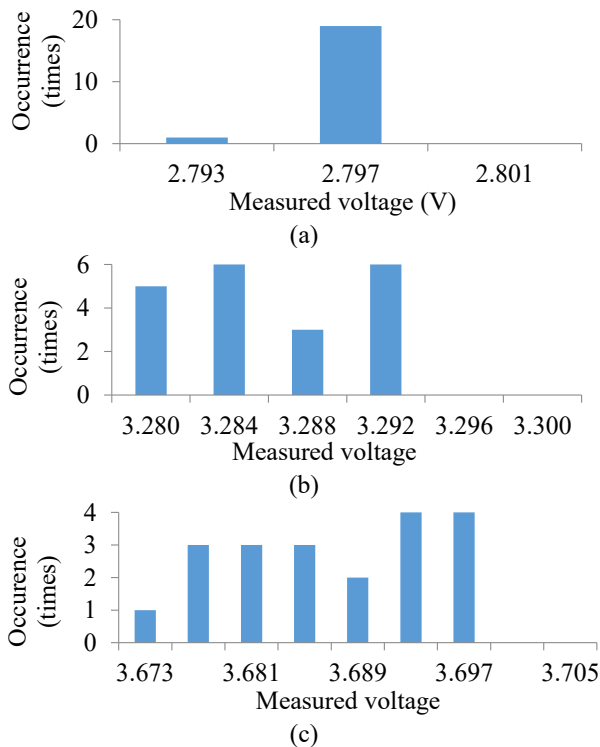


Fig. 6.11. Master BMS readouts after levelling at single value.

### Slope Equalization of the ADC

If the previous test results are carefully examined, then it can be noticed that the reason why balancer module ADCs produced good results at low voltage and bad results at higher voltages is because analog-to-digital conversion module has different output slopes varying from chip to chip.

To compensate for the different slopes, it is necessary to multiply the measured value by some calibration constant. The previously defined upper cell operational voltage value was used as the reference for the correct slope.

Each ADC output value was measured at 3.8 V cell voltage. The upper level value was divided by the obtained measurement values. For each cell balancer a fractional 15-bit binary number was obtained as the result. Each corresponding calibration constant was saved in the microcontroller information memory and later was used to compensate the measured values using software multiplication.

Voltage measurements were tested at 2.8 V 3.3 V and 3.8 V by collecting values from the master module display. Results are presented in Fig. 6.12. It can be seen that even at the calibration voltage of 3.8 V there is a shift in the readout by one discrete value. Here this might be a human error during the calibration process. The value shift can be seen at other voltages as well. Despite these minor deviations there is an explicit readout value group at each voltage which means that the slope calibration method can provide better results with less dispersion. It can be noted that as the cell voltage decreases the shift from the actual value increases. Once the lower limit is reached the display value has shifted down by two discrete values as can be seen in Fig. 6.12(a). This produces a certain error which leads to incomplete battery pack capacity utilization. To compensate for this effect a more complex ADC calibration routine could be designed, but it might not be reasonable because the shift by two discrete values produces just 0.8 % error which is sufficient for the current application. Additionally, the few millivolts of cell voltage at the lower operation voltage region have a rather small amount of energy.

A small calibration setup was designed to ease the ADC result tuning process. The primary purpose of the rack is to provide a stable calibration voltage to up to seven cell balancer modules. It serves its purpose by providing two functions: a stable regulated voltage and a module fixation mechanism. The voltage source was designed around an *LM317* adjustable linear regulator. A trimmer resistor was used to precisely adjust the voltage. An external laboratory power supply was used to power the board. The regulator board was attached to a piece of plywood. Module fixation screws with hand-tightenable were installed for easy replacement of modules. Only one voltage regulator was needed to supply all boards since the boards draw small power and the communication lines are optically isolated one from another. The master module was connected to the first and the last of the balancer modules communication connectors and was powered by another laboratory power supply. Fig. 6.13 shows the calibration setup: the calibration voltage source is in the right-hand corner and white breadboard is used to distribute voltage among cell module boards. Only four boards are installed without communication cables. Later the calibration setup was upgraded to support third version of cell module board which has a temperature sensor and lacks optical isolation,

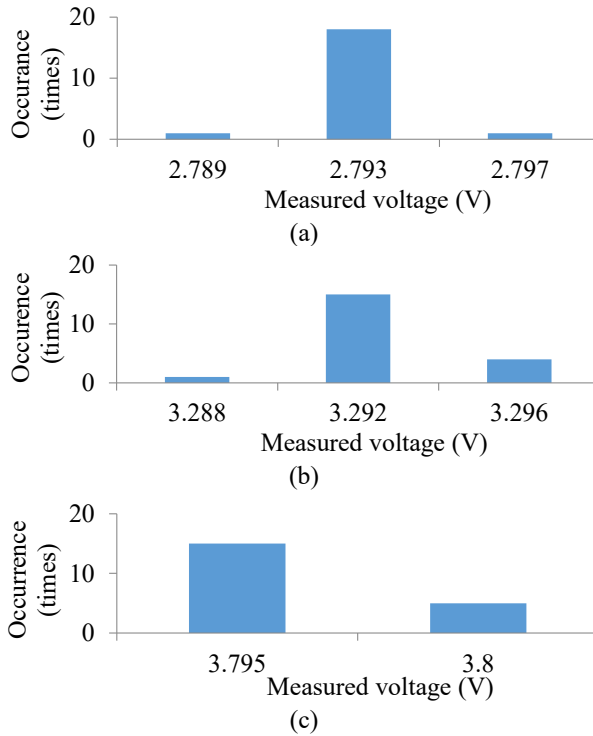


Fig. 6.12. Display readout dispersion with ADC slope compensation.

hence only one board could be calibrated at a time. However the setup was still useful for software development and debugging – the white breadboard is equipped with five isolated voltage sources which can be used to correctly power five cell modules.

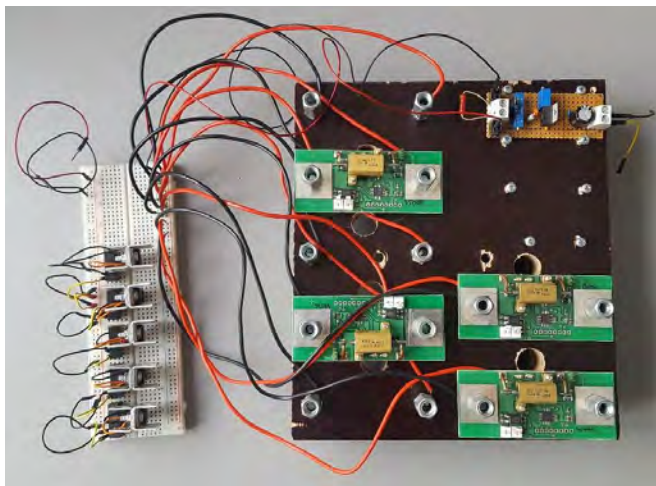


Fig. 6.13. Cell module calibration setup with four cell modules and a power supply.

### 6.3. Cell module 3

While cell module 2 was used in development of EV battery pack, the design was further improved in latter thesis period during development of stationary battery energy storage system within project *AREUS* [219]. Minor cell module improvements include utilization of less expensive shunting resistors with higher resistance to optimize temperature. Board cut-outs have been introduced around shunting resistor to reduce heat propagation to other parts of the PCB. All components have been moved to top layer and some packages have been changed to ease assembly. Two significant upgrades are addition of temperature measurement and removal of optocoupler.

A 10 k $\Omega$  NTC resistor has been added to the circuit to measure temperature of the corresponding cell. The NTC is soldered at the edge of the PCB so that it can be easily attached to the cell as shown in Fig. 6.14. The internal reference voltage of *MSP430G2553* was used to supply a resistor divider consisting of the NTC and 10 k $\Omega$  resistor as shown in Fig. 6.15. Additional calibration procedure was introduced to calibrate temperature measurements against normal room temperature.



Fig. 6.14. Cell module 3 installed on a 40 Ah LFP cell.

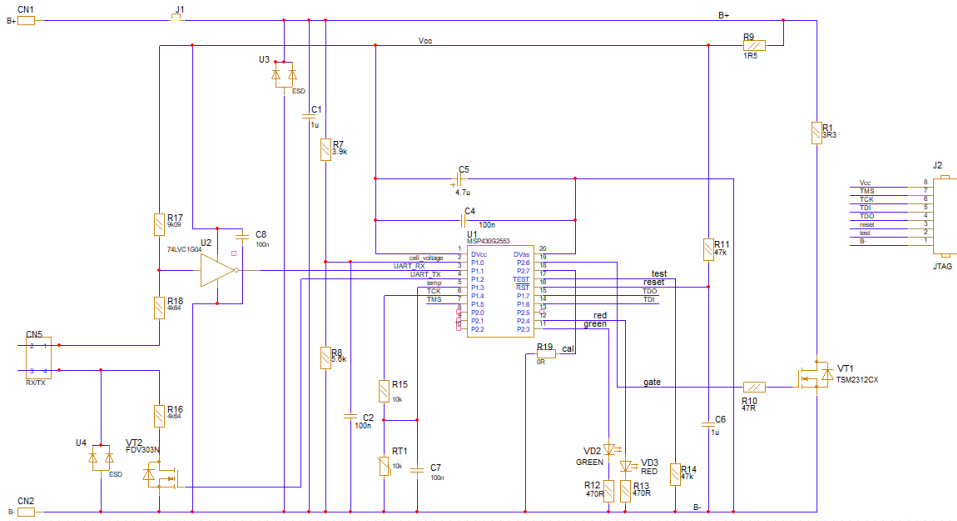


Fig. 6.15. Schematic of cell module 3 (middle) in *OrCAD Capture*.

The second significant upgrade concerns physical data transfer realization. The expensive and slow optocoupler has been replaced with a novel non-isolating circuit. The elements of the data transfer are shown in Fig. 6.15. The transmitting part consists of MOSFET VT2 and resistor R16. When a logic HIGH is sent, MOSFET pulls one side of R16 to ground. The other side of R16 goes to a connector which uses a single wire to connect to the next cell module of the stack. Let's assume that the receiving part of the next module consists of inverter U2 and resistor divider R17 and R18. The low pin of R18 goes to a connector connect to the high pin of R16 of previous board. Resistors R17, R18 and R16 produces a divider circuit which is attached to two series connected cells. When lower cell module is transmitting LOW bit, the MOSFET VT2 is not conducting, R18 low pin is floating and inverter U2 has high voltage at its input producing LOW output for the RX input of the microcontroller. When lower cell module is transmitting HIGH bit, the MOSFET VT2 is conducting and hence pulling R16 low which in turn pulls lower the lower pin of R18 of the higher cell module. The values of the resistors have been calculated using (6.1.) so that in this case the input of inverter U2 sees a legal LOW level which is translated as HIGH at the RX input of microcontroller U1.

$$\begin{cases} R_{R17} = (R_{R18} + R_{R16}) \cdot \left( \frac{U_{2cell}}{U_{inv\_low}} - 1 \right), \\ R_{R17} = R_{R18} + R_{R16} \end{cases} \quad (6.1.)$$

where  $R_{R17}$  – high side resistor of the divider,  $\Omega$ ;

$R_{R18}$  – half of low side resistor of the divider,  $\Omega$ ;

$R_{R16}$  – half of low side resistor of the divider,  $\Omega$ ;

$U_{2cell}$  – voltage of two neighbour cells, V;

$U_{inv\_low}$  – low level inverter input voltage, V.

The return current flows through both series connected cells, thus only one conductor cable is required for one-direction data transfer to the next cell. This data exchange principle is for *middle* cells. The first and last cell of the stack cannot use the same exact circuit due to high voltage differences. To overcome this and add galvanic isolation between the stack and BMS master controller, the first and last cell is equipped with different communication circuit. *Si8610AB* ultra-low power digital isolators from *Silicon Labs* have been used for this task. One side of the isolator is supplied by the cell while the other side is supplied by the BMS master controller. The three module boards are shown in Fig. 6.16. The middle board utilizes both sockets of the communication connector while first board utilizes only TX socket (RX data is obtained through digital isolator) and last board utilizes only RX socket (TX data is sent to master module through digital isolator).

A drawback for this cell module iteration is the requirement of three types of cell boards: one for first cell, one for last cell and one for remaining middle boards. One more drawback is the difference in current consumption: middle boards consume 0.943 mA, while first and last board consume 2.927 and 1.599 mA respectively. This current consumption difference will cause SOC mismatch in long-term. 200 hours are required to cause 1 % mismatch which is negligible for applications like EVs which charge almost daily. However, the cell modules should be disconnected if battery is not to be used for prolonged periods – months or more. It should be added that some of the engineering decisions have not been done to achieve lowest self-consumption. For example, the cell voltage measurement resistor divider (R7 and R8 in Fig. 6.15) will consume 0.34 mA at 3.2 V input voltage which is a considerable part of the total self-consumption current.

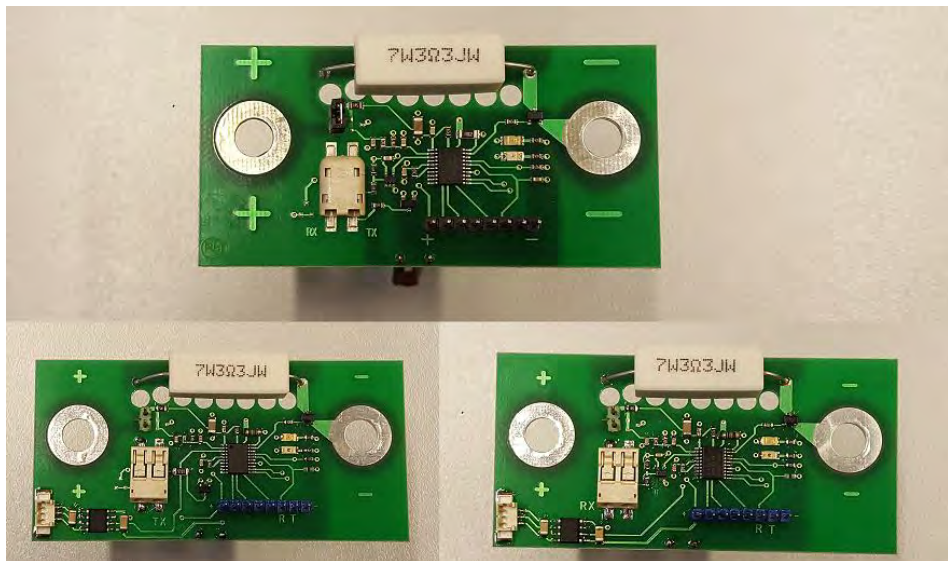


Fig. 6.16. Assembled cell modules 3. Left: first module; top: middle module; right: last module.

## 6.4. Development of the master module

As previously described some preliminary work to develop the master module was done during the design of the first cell balancer module prototype since a master controller was required to properly test the communication operational performance. A more complex second version master module was designed to provide the necessary functionality to reasonably test the battery pack and performance of cell modules.

The necessity to develop a master module was first commanded by the need to have a way to easily monitor cells voltages. For the first tests, a personal computer was used to directly read the memory of the master microcontroller. For the second cell module board, a simple master module with a four-line LCD was designed as shown in Fig. 6.9. For the testing of third cell module boards, a more integrated master module was designed.

### Hardware

The final version of finished master module is shown in Fig. 6.17. The master module block diagram is shown in Fig. 6.18. The central processing element is an *MSP430F2274* microcontroller. Its UART communication module with hardware associated with TX is used to transfer commands to the first cell balancing module while the hardware associated with RX is connected to the last cell balancer of the string. The other microcontroller built-in communication module is used in SPI mode to write the collected data to a micro SD card. An MMC/SD Flash memory card interfacing example [220] provided by *Texas Instruments* was adapted for use in this project to ease the program code development. Almost whole Port 4 is used to connect to the 4×16 character LCD display. All the control of the display is done in software. Four pins of Port 2 are used for user interface as buttons. This port was selected for its interrupt capability. One of the microcontroller timers is used to provide an alarm signal to the buzzer in situations when a cell voltage level exceeds its operational thresholds. An external 16 MHz crystal is used to generate the main microcontroller clock frequency. Since the master module is intended to save the cell voltages it is necessary to obtain them at precise time intervals. These intervals are set by an additional *MSP430G2221* microcontroller which operates just as a pulse generator which generates a pulse every 5 seconds.



Fig. 6.17. BMS master module.

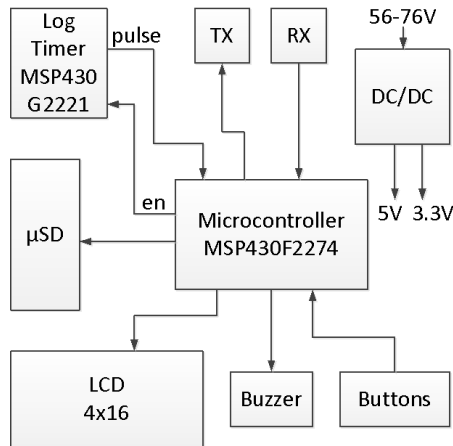


Fig. 6.18. Block diagram of BMS master module.

A received pulse starts data exchange phase. After a data exchange phase the master controller is in idle mode and it analyses if any of the cell voltages have reached the full or empty level. If one of these levels have been reached, then an appropriate output is generated which can be used to stop the charging or discharging of the battery pack. Additionally, during the idle phase master controller prints cell voltages to the four-line LCD display. The user can scroll through the values to check the individual cell voltages.

#### Communication

The *MSP430* UART module was used in cooperation with software control to perform 16bit data exchange between all the modules. Communication operates as follows. There are two operation phases: idle phase and data exchange phase. During the idle phase each cell balancer module measures and saves cell voltage value in memory buffer. Buffer value is constantly updated as a new cell voltage measurement is made. Once every five seconds the master sends a command word to the first cell balancer – this starts the data exchange phase. This exchange rate is selected for practical reasons. As the cell balancer receives any data word it stops cell voltage measurement. In the first step the cell module transmits its buffered data to the next cell module. In the second step the cell module saves the received word in the memory buffer and waits for more incoming data. If more data is received, then the operations are repeated – previous data are sent and the new are saved. If no more data have been received for a determined period, then the cell balancer returns to the idle phase and starts to refresh the memory buffer with actual measurements of the cell voltage.

As previously mentioned, the data exchange phase is initiated by the master board as it sends out a specific command word. As the first balancer receives the command word it sends first cell voltage word and saves command word. As the second balancer receives the first voltage word it sends second cell voltage word and saves first cell voltage. This pattern is repeated by all the cell balancers. The last cell balancer sends out its voltage data to the master board. Master board receives this data and since it is not the same specific command word previously sent, master controller saves this data in the cell voltage array and sends out another

specific command word. The operations are repeated until master board receives back the specific command word. Once the command word has been received the master stops to send out command words and after a brief moment the idle mode is once again active. Now the master module has the cell voltage values from all cell balancer modules. The developed master module was designed to be capable to operate with cell module 2 and cell module 3, only different software has to be downloaded into master controller to suit data differences caused by additional temperature readings of cell module 3.

The data in the micro SD card is stored as raw data, hence for further analysis it has to be pre-processed. The micro SD card content is copied using freeware hex editor *HxD*. Each group of readings is written in separate sectors of the card memory – most of the copied data is empty. The pre-processing includes deletion of these empty regions.

### 6.5. Testing of the developed switched resistor balancing system

The proposed balancing system is to be used for charging of electric kart lithium iron phosphate (LFP) battery. The kart is equipped with relatively low voltage traction motor with nominal voltage of 72 V and nominal current of 100 A. The previously described 40 Ah LFP cells will be used for the battery. It can be calculated that 23 cells are needed to achieve full 72 V but because of practical issues it was selected that one battery pack will consist of 20 cells. Total nominal voltage of battery pack is 64 V. If charged at 3.8 V then max voltage will reach 76 V – this voltage will be seen only briefly as voltage of LFP cells has a distinctive *knee* at the full SoC – during the discharge of the first few percent, the voltage per cell will drop to 3.2 V as seen in Fig. 4.2 and Fig. 4.3. Hence the voltage of the pack will be 66 V. A 20-cell battery with installed cell modules is shown in Fig. 6.19.



Fig. 6.19. 20-cell LFP battery pack with cell modules 2.

Prior to assembly, all cells were charged in parallel. For the first BMS test, the pack was discharged at a 20 A rate (0.5C). The discharging was stopped once the BMS registered a cell reaching 2.8 V limit. The micro SD card was removed from the BMS modules and data was downloaded to PC. The processing of obtained hex values was done in MatLab. The discharge voltage plot is shown in Fig. 6.20. The aforementioned voltage knee is seen explicitly at the very beginning of the discharge curve as voltage drops from ~3.33 V to 3.22 V. After this region the voltage decreases linearly. The difference in cells voltages becomes apparent quickly, however only during the last quarter the voltage of cell No.19 decreases rapidly indicating relatively lower capacity. Voltage of all cells increases after the discharge is stopped. This test indicates, that measurement and communication part of the developed system is functioning properly.

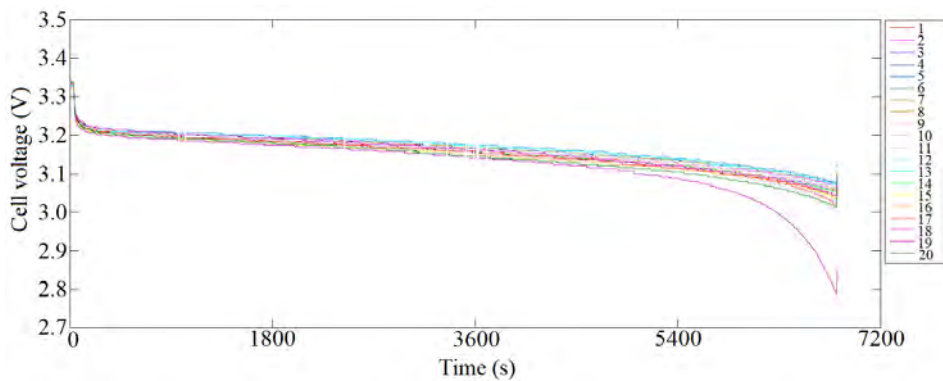


Fig. 6.20. Voltages of cells from BMS memory during discharging.

For the next test, the empty battery pack was charged with 11 A (limited by available charger). Fig. 6.21. Voltages of cells from BMS memory during charging. Fig. 6.21 shows the obtained graph of voltages. A distinctive knee can be seen at both ends of the voltage curve. It can be seen that during the final phase of the charging one of the cells reach 3.9 V while voltages of other cells fluctuate around 3.8 V. At this point the 11 A charging current is higher than the balancing current, and as the charging continues, the voltages of some (fuller) cells can rise above set 3.8 V limit. After the 3.9 V peak the charging current was manually decreased to 1.5 A, resulting in voltage decrease of all cells. However, soon afterwards the voltages of cells again reach 3.8 V limit as they have become fully charged. At this charging current, the balancing resistor is capable to limit the voltage to 3.8 V hence battery is eventually charged to 100 % SoC. This test concludes that the developed switched resistor balancing can perform balancing and overvoltage limitation if charging current is less than 1.77 A.

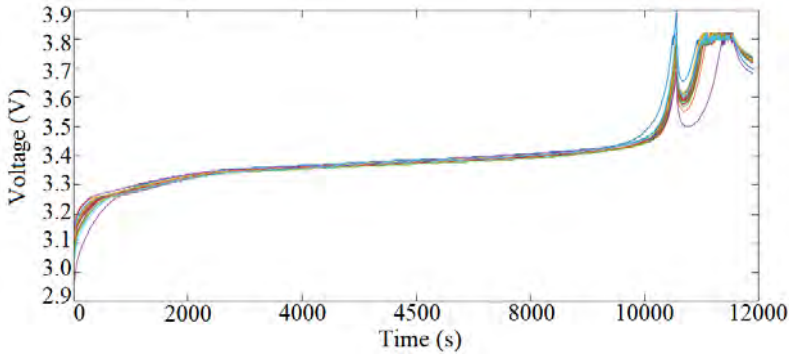


Fig. 6.21. Voltages of cells from BMS memory during charging.

Further system implementation activities were realized during research project *AREUS* – the developed switch resistor balancing system was used to design a 144-cell battery energy storage system [219]. The cell module 3 version was *mass produced* and installed on all cells. One communication test setup can be seen in Fig. 6.22. For fully functional BMS, the master module had to be designed using different microcontroller as the relatively high cell count requires more memory (RAM) for instant communication data storage.



Fig. 6.22. Testing of cell module 3 communication during project *AREUS*.

In additional BMS development step, a simple stand-alone coulomb counter was implemented using *MSP430F5172* microcontroller,  $2 \times 16$  LCD and *LEM HXS10-NP* current transducer as shown in Fig. 6.23. The primary goal of this step was to use this developed sub-system as the SOC estimator in the main BMS. Coulomb counter based SOC estimation is based on current integration (6.2):

$$SOC(t) = \frac{1}{C} \int_0^t I(p) dp, \quad (6.2.)$$

Generally, the counter was used as an energy measurement tool to evaluate the energy efficiency of the LFP battery and balancing system. It was measured that given LFP battery has 93 % efficiency over 10 charge/discharge cycles. Approximately 1.2 % of charging energy was lost during the switched resistor balancing. It can be concluded that under given circumstances (fresh cell which were equalized before assembly) the developed cell balancing system has miniscule losses while being simple and easy to implement in modular approach.

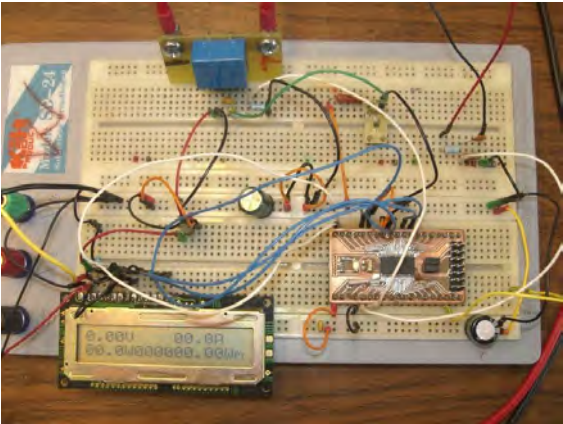


Fig. 6.23. Coulomb counter implementation.

## **7. DEVELOPMENT OF ADVANCED CELL BALANCING**

From the previous experiments, it could seem that switched resistor balancing is an optimal solution, however if the number of series connected cells is high then losses could significantly increase. This drawback could be minimized if cells of the battery are grouped in smaller groups and charged separately. Separate charging adds to system complexity in both circuitry and control as discussed in section “Battery balancing methods”. Grouped cells of a battery pack can be charged with a single multi-secondary winding transformer – this approach provides inherent charging current distribution according to cell group voltage. The performance of the BMS balancing system could be improved if both switched resistor balancing and multi-secondary winding transformer balancing were combined in a two-layer balancing scheme in which higher layer would utilize multi-secondary winding transformer to balance cell groups while lower layer would utilize switched resistor balancing to balance cells within one group. As switched resistor balancing system has already been designed in previous chapter, now the multi-secondary winding transformer approach has to be implemented and verified.

### **7.1. Development of multi-secondary winding transformer balancing**

As described in Battery balancing methods section, the multi-secondary winding transformer can be implemented as a standalone balancing topology if the primary side is supplied by the battery which is being balanced. Alternatively, the primary side can be supplied by an external power source – in this case the topology acts as self-balancing selective charging topology. A significant difference between the two is the power: plain balancing typically is low powered and thus has small transformer; on the other hand, charging function requires more power hence larger transformer must be used. In typical applications multi-secondary winding transformer is used for low series cells battery packs as the transformer can support limited secondary windings. However here the eventual goal is to combine two balancing methods where one method would be applied to cell level while the other would be applied to cell modules. If the number of modules is low, then a multi-secondary winding transformer topology could be implemented as a self-balancing selective charger. Additionally, this part could be implemented as a standalone charger which is removable from the battery pack. The previously described 20-cell LFP battery pack can be divided into 4 modules each consisting of 5 cells. The only required modification is the addition of three mid-point connections which should be easily connectable.

#### **Operation**

To verify the operation of the multi-secondary winding transformer, it was decided to build and test a three cell charger circuit with max charging current 10 A. It was decided to use supercapacitors instead of battery cells to decrease charging time and increase voltage range at the outputs of the balancing charger as supercapacitors are charged from 0 to 2 V while voltage range of LFP cells is 2.8 to 3.8 V. A half-bridge topology was selected for the primary side while each winding of the secondary side was equipped with a rectifier and an LC filter as

shown in Fig. 7.1. Filter input is shunted with freewheeling diode, to provide current path for LC filter inductor current during dead-time between transformer output pulses.

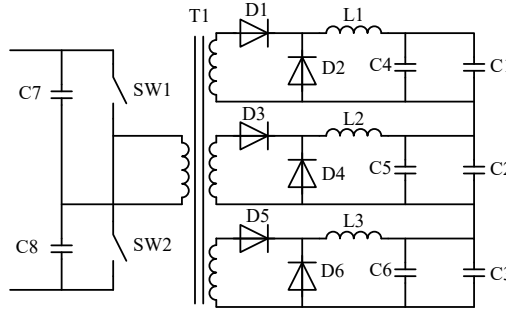


Fig. 7.1. Multi-secondary winding battery charger circuit for three cells.

A separate charger output is provided for each module/cell charging. Charger outputs are connected in series because cells in the module will be connected in series. The charger is capable of operation with both connected cells and completely isolated cells.

In order to describe charger balancing feature it is necessary to take a look at inductor current. During a pulse in secondary winding one of the rectification diodes goes into conduction. Current passes through inductor. It can be assumed that the inductor current increase is linear, and its change can be described (7.1.):

$$\Delta I(t)_+ = \frac{(V_{DC} \cdot k - v_o(t)) \cdot DT}{L} \quad (7.1.)$$

In (7.1.)  $V_{DC}$  is charger input voltage applied to capacitor C1 and  $k$  is transformer transformation coefficient.  $v_o(t)$  is output (supercapacitor cell) voltage at given time.  $D$  is duty cycle.  $L$  is filter inductance. Once secondary winding voltage is switched off, rectifier diodes stop conduction. Inductor current produces voltage that brings freewheeling diode into conduction. Inductor is discharged through filter capacitor and supercapacitor cell. During this phase inductor current can be described (7.2.):

$$\Delta I(t)_- = \frac{-v_o(t) \cdot (1-D)T}{L} \quad (7.2.)$$

By combining (7.1.) and (7.2.) into (7.3.) inductor current difference can be determined.

$$\Delta I(t) = \frac{V_{DC} \cdot k \cdot DT - v_o(t)T}{L} \quad (7.3.)$$

By analysing (7.3.) it can be noticed that inductor current depends on two variables: duty cycle and voltage on the cell's terminals. It can be assumed that practically all inductor current is diverted through battery cell. If duty cycle is kept constant then the cell current is inversely proportional to its voltage and thus its state of charge. Since all cells are in the same system, cell with the lowest voltage will have the largest current. Because of this effect this balancing technique is capable to balance cells without additional closed feedback loops [139].

## Testing

Experimental testing was performed using a laboratory prototype charger. Input voltage was supplied by a laboratory power supply with limited voltage which was adjusted according to the highest supercapacitor voltage.

The first test was done with equally discharged 1500 F supercapacitor cells connected to each charger output. Charging was done with constant 5 A current. It can be noticed in Fig. 7.2 that cap 1 voltage at worst situation was 100 mV less than cap 3. During final charging state the voltages equalize and difference is only 30 mV.

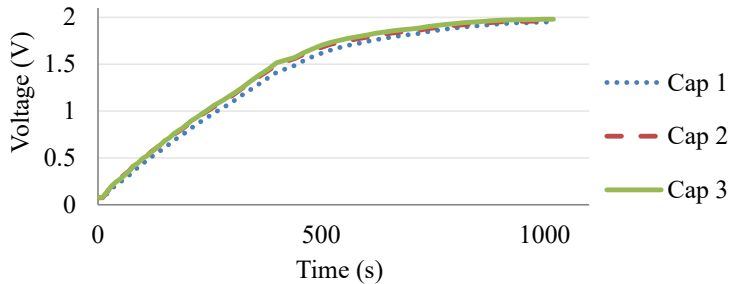


Fig. 7.2. Charging capacitor cells with the equal initial parameters.

For the second test (Fig. 7.3) double capacitance of 3000 F was used for cap 3. During initial charging cap 3 had voltage difference of 180 mV, but as cells reached charged state, voltage difference dropped to 58 mV.

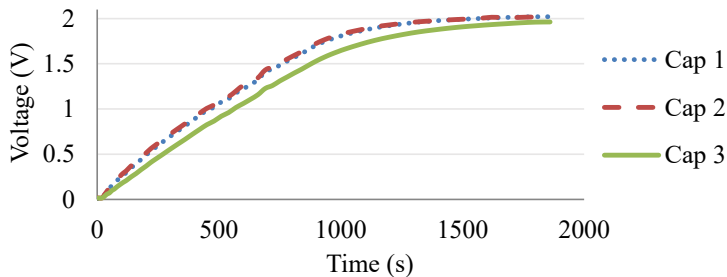


Fig. 7.3. Charging when cap 3 has double capacitance.

Third experiment (Fig. 7.4) was done with three equal 1500 F capacitances but with different initial voltages, 1.5 V, 1.0 V and 0.5 V respectively. For this case 10 A charging current was used. Cell with the lowest voltage had the highest current, while most charged cell had lowest. The self-balancing feature is depicted in the graph as all cells reach the same end voltage at the same time. It can be concluded that given multi-secondary winding transformer charger-balancer is a suitable choice for the top layer of proposed mixed multi-layer topology, as it has simple control and transformer can be designed to suit 4 secondary windings with relatively high current – suitable for charging.

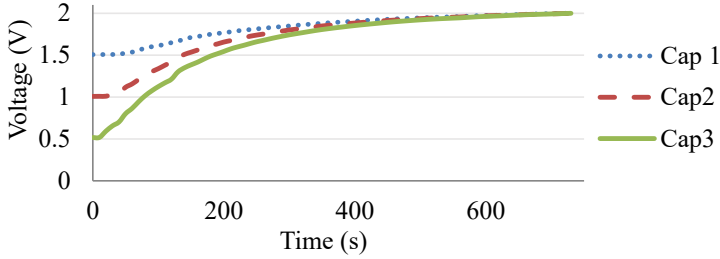


Fig. 7.4. Charging of capacitor cells with different initial voltages.

## 7.2. Energy Efficiency with Passive Balancing

Before proceeding with testing of two-layer mixed balancing system, a benchmark test of all-passive previously developed switched resistor balancing was performed. First all cells were connected in parallel then charged to 3.8 V and left for a few days to equalize the voltages. Afterwards the cells were arranged in series and equipped with cell balancer units. The pack was discharged with a constant 10 A current using an electronic load till one of the cells reached 2.8 V empty level. *N4L* precision power analyzer *PPA5530* was used to measure the energy drawn from the battery. The total energy was 2.45 kWh and additional measurement indicated that the battery was discharged for 38.7 Ah.

In the following day the pack was connected to the charger circuit. The setup is shown in Fig. 7.5. The converter was controlled to charge the battery with 10 A. Once one of the cells reached the 3.8 V full voltage level then the charging current was decreased to 2 A to prevent overcharge. The charging voltage was set to 76 V. During the charging the same power analyzer was used to measure the energy supplied to the charger circuit. The total amount of energy spent during the charging was 3.01 kWh. The energy used for the driver and control circuitry was not taken into account. For this system the energy efficiency can be found using (7.4.) and it is 81.4 %.

$$\eta = \frac{E_{\text{discharged}}}{E_{\text{charged}}} \cdot 100\%, \quad (7.4.)$$

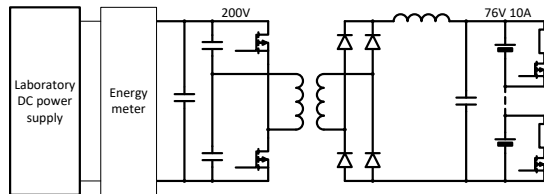


Fig. 7.5. The schematic of the charger with switched shunting resistor balancing function.

### 7.3. Test of battery efficiency with mixed two-layer balancing

A similar efficiency test was carried out with a mixed two-layer balancing topology. A charger/battery pack prototype setup was built to test the efficiency of the mixed two-layer balancing. The prototype setup consists of a DC laboratory power source, an energy meter, a half bridge charger circuit with four secondary windings, a 20-cell battery pack equipped with passive cell balancing units. The four secondary winding were connected to subpacks of the whole pack: each 5 cells of the pack constituted a subpack, hence battery was divided into four 5-cell subpacks. The schematic of the setup is shown in Fig. 7.6. The actual experimental test bench is shown in Fig. 7.7.

For the prototype setup experiment both switches of the half bridge converter primary side were operated at a constant 50 % duty cycle with a small dead time. The PWM signal for the switches was generated by a microcontroller. The DC laboratory power source output voltage was set to such a level to provide 10 A current for at least one of the battery subpacks. The charging current was limited to be no more than 10 A for any of the subpacks. The current adjustment was done manually by observing the measurements of multimeters which were connected in series with the battery subpacks. Once one of the cells reached full voltage 3.8 V, the charging current was gradually decreased until it reached 0.01 C or 400 mA level at which the cell charging was stopped. Then the system total energy consumption and the elapsed time measurement was recorded using the energy measurement device. The battery pack was fully discharged before the first measurement of the charging energy.

After a 20 hour rest period the battery pack was discharged. The discharge was done using an electronic load connected to an energy measurement device which in turn was connected to the battery terminals. The discharge was done with constant 10 A current. The discharge was stopped once one of the cells reached the empty voltage level 2.8 V. A battery management system was used to monitor all of the cell voltages. Then the system total energy consumption and the elapsed time measurement was recorded using the energy measurement device.

The experimentally obtained results are as follows: the energy required to fully charge the battery pack was measured to be 3.09 kWh and the process took 4 hours and 38 minutes; during the discharge the obtained energy amount was 2.43 kWh and the process took 3 hours and 50 minutes. During the discharge an additional battery pack capacity measurement was done and the battery pack measured to have 38.34 Ah capacity. From both measurements it can be calculated that the energy efficiency of the battery pack with charger and integrated mixed two-layer balancing is 78.6 %.

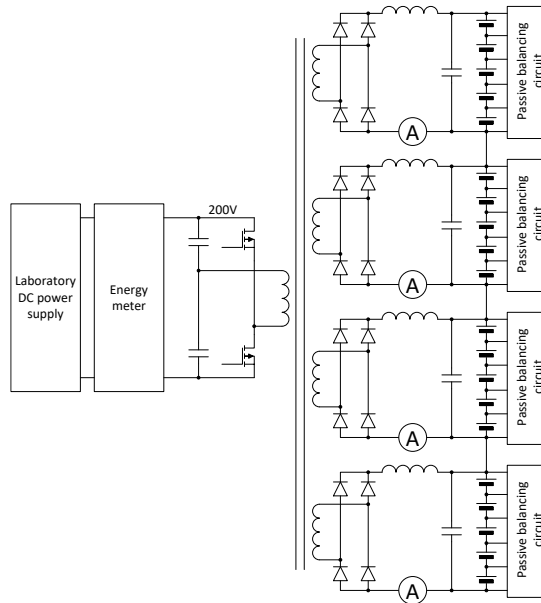


Fig. 7.6. The schematic of the charger with an integrated mixed balancing function.

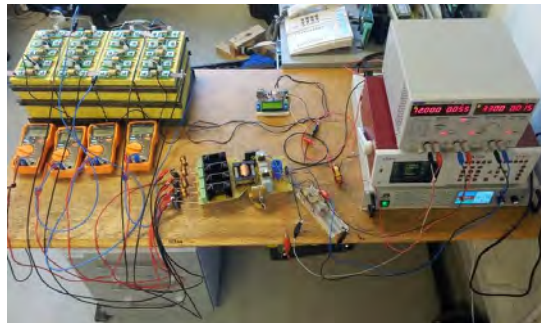


Fig. 7.7. The test setup of the energetic efficiency measurement.

#### 7.4. Discussion on performance of mixed two-layer balancing

The developed mixed balancing method is capable to successfully utilize a multi secondary transformer balancer for higher layer balancing while the switched shunting resistor balancing takes care of the lower layer balancing.

However, after the charge/discharge testing it was revealed that the overall system energy efficiency is 78.6 % while the previously tested efficiency of a simple switched shunting resistor balancing was 81.4 %. The introduction of additional windings and rectifiers have lowered the converter efficiency thus decreasing the energy efficiency measurement. From another perspective, the energy efficiency should increase due to split switched resistor balancing. The cells of the battery pack are split into 4 subpacks – the switched balancing losses should decrease as the number of cells to balance per subpack is smaller as discussed in section

3.2.2. where balancing losses of 20-cell pack with switched resistor balancing were plotted using random cell capacities with normal distribution and several standard deviation values. If the same randomly generated cell values are used for battery pack which is split into 4 subpacks then the switched balancing losses decrease as shown in Fig. 7.8. with line 4×5S (series connection of 4 subpacks each consisting of 5 series connected cells). It can be concluded that packs with higher cell capacity variation will benefit more from mixed balancing topology.

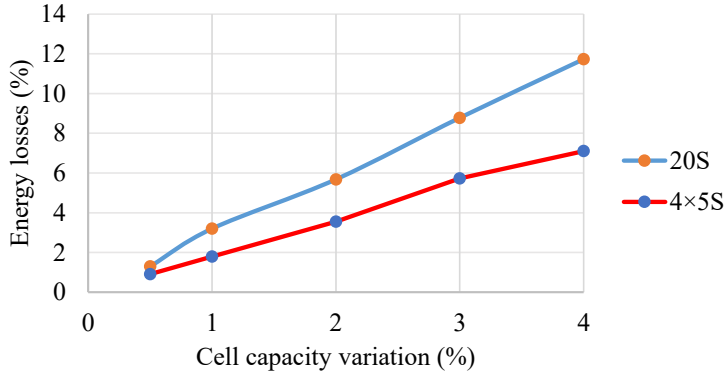


Fig. 7.8. Battery energy losses with full switched resistor balancing (20S) and split switched resistor balancing (4×5S).

If the achieved split switched resistor balancing loss improvement is larger than additional losses of multi secondary winding transformer (7.5.) then the mixed two-layer balancing will provide energy improvement over conventional switched resistor balancing:

$$E_{MST} < E_{SR\_full} - E_{SR\_split}, \quad (7.5.)$$

where  $E_{MST}$  – energy loss of multi secondary winding topology, Wh;

$E_{SR\_full}$  – energy loss of conventional switched resistor balancing, Wh;

$E_{SR\_split}$  – energy loss of split switched resistor balancing, Wh.

As the battery is split into more subpacks, the energy loss  $E_{SR\_split}$  is decreased and the advantage of multi secondary transformer introduction increases. The  $E_{SR\_split}$  value will decrease to 0 if an individual winding is used for each cell – the switched resistor balancing layer loses its purpose. However, it can be troublesome to achieve sufficiently low  $E_{MST}$  value as multi-secondary transformer topology related losses are generated throughout all charging procedure as opposed to switched resistor topology which generates losses only after the first cell has reached its full voltage. The losses of multi secondary transformer topology can be divided into three parts: primary side loss, secondary side loss and transformer core loss. The primary side and transformer core loss can be ignored in comparison as there would be the same losses in case of no multi secondary balancing – there would be a single secondary winding which would be used to provide charging current. Each extra winding of secondary side would add some copper losses and extra rectifiers would add semiconductor losses. Both of these losses should be optimized to achieve minimal losses at max transformer utilization to permit successful application of mixed two-layer balancing.

## CONCLUSIONS

The main hypothesis was formulated in the beginning of the Doctoral Thesis:

The balancing performance of a battery management system can be improved by combining two different balancing methods into a two-layer balancing solution.

However, the practical goal of this Thesis was to develop a BMS for small vehicles – PMVs. To achieve both goals, the work was started with the analysis of various electric vehicle battery systems. From the available material, it can be concluded that the voltage of the traction battery corresponds to the one of the drive system. On few occasions, a rudimentary BMS analysis was possible as images of BMS board was available – it yielded that switched resistor balancing method was used in all of reviewed cases.

Next, a review of state-of-art Li-ion battery technology was composed to achieve familiarity with the technology. Based on the obtained knowledge, further research literature analysis of BMS and balancing methods was conducted. A novel balancing method categorization was designed with three main sections: dissipative methods, selective charge/discharge methods, charge transfer methods. The first note one balancing methods is that dissipative (e.g. switched resistor) methods are regarded to as inefficient and hence they should be avoided although no proof with real world battery parameters were observed. Occasionally some extreme condition simulations were provided as a motivation. The second note is that no mixed multi-layer balancing methods were observed during literature review. There are some balancing methods which inherently use multi-layer structure (e.g. double tiered switched capacitor).

An experimental Li-ion battery performance analysis was carried out to obtain general performance indicators and more importantly to provide statistical data about cell parameter variance. The capacity analysis indicated that it is possible to achieve high initial cell capacity match (less than 0.2 % mismatch) if cells are sorted according to actual capacity. The capacity measurement is inherently time-consuming process although in some cases it could partially be replaced by much faster impedance measurement which correlates to capacity. It is planned to use obtained capacity and impedance data for further analysis of cell ageing.

In the BMS development process three iterations of cell balancing modules for 40 Ah LFP cells have been designed with gradually increased performance: voltage and temperature measurements, switched resistor balancing, daisy chain communication. Measurement calibration procedure have been developed and integrated in embedded system. The initial optocoupler-based communication chain has been optimized for energy efficiency. Two functional master BMS boards have been successfully developed to control monitor battery pack and log cell measurements for further analysis.

The performance of the designed BMS has been verified with a 20-cell LFP battery pack. The cells of the pack were properly balanced prior to pack assembly but no special batch selection was performed. After a full discharge, a charging cycle took 240 minutes of which the balancing lasted less than 16 minutes which indicate short balancing time. Further cell voltage measurement analysis showed that a single cell of the pack was the major reason for given balancing activity. Balancing requirement could have been decreased if cells were sorted prior to pack assembly.

The performance of a multi-secondary winding transformer balancing method has been experimentally validated using a 3-cell pack which used EDLCs for improved voltage range investigation. Further, a half bridge transformer topology with four secondary windings were used to test performance of mixed two-layer balancing topology. The 20-cell LFP battery was divided into four groups with switched resistor balancing modules for the lower layer. The energy efficiency of the whole system measured in at 78.6 % while the previously tested efficiency of just switched shunting resistor balancing was 81.4 %. From this a significant conclusion can be drawn: the combination of given two balancing methods does not provide higher energy efficiency at given cell capacity parameters. The defined hypothesis is true if loss improvement of split switched resistor pack is larger than additionally introduced multi secondary winding topology losses.

Future work includes continuation of work in the field of battery applications and their management systems. The developed BMS and 40 Ah LFP battery pack is to be used for educational electric kart project with multiple independent drives. The extended 144 cell 40 Ah LFP battery will be kept as an energy storage device for research and development of 600 VDC microgrid. The attained know-how was used to develop a removable 18650-size cell battery pack for a power assist wheelchair. It is planned to design battery packs for other PMV development projects. Another future research direction is related to the development of cell parameter measurement systems – to measure cell parameter change as they are being aged. The obtained statistical knowledge is to be used to develop model-based SoC and SoH estimators for future BMS.

## Author's publications

1. K. Vitols, "Selection of Power Supply Elements for Cow Rumen Smart Bolus," in *2020 IEEE 8th Workshop on Advances in Information, Electronic and Electrical Engineering (AIEEE)*, 2021, pp. 1–5.
2. R. Zemnieks and K. Vitols, "Automation of Battery Impedance Measurement Using Matlab," in *2020 IEEE 61st Annual International Scientific Conference on Power and Electrical Engineering of Riga Technical University, RTUCON 2020 - Proceedings*, 2020.
3. K. Vitols and A. Podgornovs, "Impact of battery cell configuration to powered wheelchair drive efficiency," *Arch. Electr. Eng.*, vol. 69, no. 1, pp. 203–213, 2020.
4. A. Zabasta et al., "Low-power wireless sensor network system for early diagnostic of subacute rumen acidosis in cows," in *2019 IEEE 7th IEEE Workshop on Advances in Information, Electronic and Electrical Engineering (AIEEE)*, 2019, pp. 1–6.
5. K. Vitols and E. Grinfogels, "Battery Batch Impedance Analysis for Pack Design," in *2019 IEEE 7th IEEE Workshop on Advances in Information, Electronic and Electrical Engineering (AIEEE)*, 2019, pp. 1–5.
6. K. Vitols and E. Poiss, "Development of Electric Scooter Battery Pack Management System," in *2018 IEEE 59th International Scientific Conference on Power and Electrical Engineering of Riga Technical University (RTUCON)*, 2018, pp. 1–5.
7. K. Vitols, E. Grinfogels, and D. Nikonorovs, "Cell Capacity Dispersion Analysis Based Battery Pack Design," in *2018 6th IEEE Workshop on Advances in Information, Electronic and Electrical Engineering (AIEEE)*, 2018, no. 1, pp. 1–5.
8. I. Galkin, A. Podgornovs, A. Blinov, K. Vitols, M. Vorobyov, and R. Kosenko, "Considerations Regarding the Concept of Cost-Effective Power-Assist Wheelchair Subsystems," *Electr. Control Commun. Eng.*, vol. 14, no. 1, pp. 71–80, 2018.
9. P. Apse-Apsitis, K. Vitols, E. Grinfogels, A. Senfelds, and A. Avotins, "Electricity meter sensitivity and precision measurements and research on influencing factors for the meter measurements," *IEEE Electromagn. Compat. Mag.*, vol. 7, no. 2, pp. 48–52, 2018.
10. K. Vitols and A. Podgornovs, "Concept of cost-effective power-assist wheelchair's electrical subsystem," in *2017 5th IEEE Workshop on Advances in Information, Electronic and Electrical Engineering (AIEEE)*, 2017, pp. 1–4.
11. K. Vitols, "Efficiency of LiFePO<sub>4</sub> battery and charger with a mixed two level balancing," in *2016 57th International Scientific Conference on Power and Electrical Engineering of Riga Technical University (RTUCON)*, 2016, pp. 1–4.
12. K. Vitols, "Efficiency of LiFePO<sub>4</sub> Battery and Charger with Passive Balancing," in *AIEEE 2015*, 2015.
13. K. Vitols, "Lithium ion battery parameter evaluation for battery management system," in *2015 56th International Scientific Conference on Power and Electrical Engineering of Riga Technical University (RTUCON)*, 2015, pp. 1–4.
14. K. Vitols, "Design considerations of a battery pack - DC grid interface converter," in *2015 IEEE 5th International Conference on Power Engineering, Energy and Electrical Drives (POWERENG)*, 2015, vol. 2015-Sept, pp. 476–479.
15. K. Vitols and I. Galkin, "Evaluation of cell balancing solution with a custom energy measurement device design," in *2014 55th International Scientific Conference on*

- Power and Electrical Engineering of Riga Technical University, RTUCON 2014*, 2014.
16. K. Vitols, "Redesign of passive balancing battery management system to active balancing with integrated charger converter," in *2014 14th Biennial Baltic Electronic Conference (BEC)*, 2014, pp. 241–244.
  17. K. Vitols, "Design of an embedded battery management system with passive balancing," in *2014 6th European Embedded Design in Education and Research Conference (EDERC)*, 2014, pp. 142–146.
  18. M. Vorobyov and K. Vitols, "Low-Cost Voltage Zero-Crossing Detector for AC-Grid Applications," *Electr. Control Commun. Eng.*, vol. 6, no. 1, pp. 32–37, Oct. 2014.
  19. M. Vorobjovs, K. Vitols, "High Precision Hardware/Software Zero Crossing Detection," in *14th International Symposium "Topical Problems in the Field of Electrical and Power Engineering. Doctoral School of Energy and Geotechnology II"*, Estonia, Pärnu, 13-18 January, 2014. Pärnu: Elektrijs, 2014, pp.154-157.
  20. K. Vitols, "Design Optimization of Passive Balancing Battery Management System," in *Riga Technical University 54th International Scientific Conference Materials. Section of Power and Electrical Engineering: Digest Book and Electronic Proceedings*, Latvia, Rīga, 14-16 October, 2013. Riga: RTU Publishing House, 2013, pp.26-28.
  21. M. Prieditis, K. Vitols, "Energy Flow Control System with Robot-Accumulator Interfacing Module," in *13th International Symposium "Topical Problems in the Field of Electrical and Power Engineering" and "Doctoral School of Energy and Geotechnology II": Topical Problems in the Field of Electrical and Power Engineering*, Estonia, Pärnu, 14-19 January, 2013. Pärnu: Elektrijs, 2013, pp.166-169.
  22. K. Vitols and I. Galkin, "Analysis of electronic differential for electric kart," in *2012 15th International Power Electronics and Motion Control Conference (EPE/PEMC)*, 2012, p. DS3a.2-1-DS3a.2-5.
  23. K. Vitols, "Use of Passive Cell Balancing for Electric Vehicle Battery Pack," in *Riga Technical University 53rd International Scientific Conference: Dedicated to the 150th Anniversary and the 1st Congress of World Engineers and Riga Polytechnical Institute / RTU Alumni: Electronic Proceedings of Power and Electrical Engineering of Subsection of Power Electronic Converters and Applications: Digest Book and Electronic Proceedings*, Latvia, Rīga, 11-12 October, 2012. Riga: RTU Publishing House, 2012, pp.68-70.
  24. K. Vitols, I. Galkins, Z. Skreija, "Electronic Differential Behaviour Analysis for Electric Kart," in *11th International Symposium "Topical Problems in the Field of Electrical and Power Engineering. Doctoral School of Energy and Geotechnology II"*, Estonia, Pärnu, 16-21 January, 2012. Tallinn: Elektrijs, 2012, pp.142-145.
  25. K. Vitols, "Design of Passive Balancing for Electric Kart Battery Pack," in *12th International Symposium "Topical Problems in the Field of Electrical and Power Engineering. Doctoral School of Energy and Geotechnology II"*, Estonia, Kuresäre, 11-16 June, 2012. Tallinn: Elektrijs, 2012, pp.60-64.
  26. K. Vitols, N. Reinberg, and I. Galkin, "PID Regulator Implementation for Electric Kart DC Motor Current Stabilization," *Electron. Electr. Eng.*, vol. 119, no. 3, Mar. 2012.

27. K. Vitols, N. Reinberg, I. Galkin, and A. Sokolovs, "Closed current loop regulator for electric kart DC motor torque stabilization," in *2011 7th International Conference-Workshop Compatibility and Power Electronics, CPE 2011 - Conference Proceedings*, 2011, pp. 377–381.
28. K. Vitols, N. Reinberg, I. Galkins, A. Andreiciks, "Implementation of Closed Current Loop Regulator Using MSP430," in *10th International Symposium "Topical Problems in the Field of Electrical and Power Engineering. Doctoral School of Energy and Geotechnology II": Proceedings*, Estonia, Pärnava, 10-15 January, 2011. Tallinn: Eesti Moritz Hermann Jacobi Selts, 2011, pp.17-20.
29. A. Andreiciks, I. Steiks, K. Vitols, L. Ribickis, "Current-Fed Double Inductor Push-Pull DC/DC Converter with Closed Loop Control System," in *10th International Symposium "Topical Problems in the Field of Electrical and Power Engineering. Doctoral School of Energy and Geotechnology II": Proceedings*, Estonia, Pärnu, 10-15 January, 2011. Tallinn: Estonian Society of Moritz Hermann Jacobi, 2011, pp.156-160.
30. K. Vitols, N. Reinberg, A. Sokolovs, and I. Galkin, "Drive selection for electric kart," in *Proceedings of EPE-PEMC 2010 - 14th International Power Electronics and Motion Control Conference*, 2010.
31. K. Vitols, N. Reinberg, I. Galkins, "Evaluation of Converter and Battery for Electric Kart," in *9th International Symposium "Topical Problems in the Field of Electrical and Power Engineering. Doctoral School of Energy and Geotechnology II"*, Estonia, Pärnu, 14-19 June, 2010. Tallinn: Estonian Society of Moritz Hermann Jacobi, 2010, pp.16-20.
32. A. Andreiciks, K. Vitols, O. Krievs, I. Steiks, "Current Fed Step-up DC/DC Converter for Fuel Cell Inverter Applications," *Power and Electrical Engineering*. Vol.25, 2009, pp.111-116.
33. A. Andreiciks, K. Vitols, O. Krievs, "Design of Current Source Step-up DC/DC Converter for Fuel Cell Applications," in *6th International Symposium "Topical Problems in the Field of Electrical and Power Engineering. Doctoral School of Energy and Geotechnology"*, Estonia, Kuressaare, 12-17 January, 2009. Tallinn: Estonian Society of Moritz Hermann Jacobi, 2009, pp.26-31.

# Appendix 1

## Abbreviations

ADC – analog to digital converter;  
ASIC – application specific integrated circuit;  
BES – battery energy storage;  
BEV – battery electric vehicle;  
BMS – battery management system;  
CAN – controller area network;  
CC – constant current;  
CCAV – constant current adaptive voltage;  
CCCV – constant current constant voltage;  
CGD – gate drain capacitance;  
CNC – computer numerical control;  
CPU – central processing unit;  
CSV – comma-separated values;  
CV – constant voltage;  
DC – direct current;  
DC/DC – direct current to direct current;  
DoD – depth of discharge;  
DSP – digital signal processing;  
EDLC – electric double layer capacitor;  
EIS – electrochemical impedance spectroscopy;  
EU – European Union;  
EV – electric vehicle;  
FET – field effect transistor;  
FOM – figure of merit;  
HEV – hybrid electric vehicle;  
HMI – human machine interface;  
IC – integrated circuit;  
IC – integrated circuit;  
ICE – internal combustion engine;  
JTAG – joint test action group;  
LCD – liquid crystal display;  
LCO – lithium cobalt oxide;  
LED – light emitting diode;  
LFP – lithium iron phosphate;  
LIB – lithium ion battery;  
LMO – lithium manganese oxide;  
LTO – lithium titanate;  
MMC – MultiMediaCard;  
MOSFET – metal-oxide-semiconductor field-effect transistor;

NCA – nickel cobalt aluminium;  
NiMH – nickel metal hydride;  
NMC – nickel manganese cobalt;  
NTC – negative temperature coefficient (resistor);  
OC – over current;  
OCV – open circuit voltage;  
OEM – original equipment manufacturer;  
OT – over temperature  
OV – over voltage  
PC – personal computer;  
PCB – printed circuit board;  
PCBA – printed circuit board assembly;  
PMOS – positive metal-oxide semiconductor;  
PMV – personal mobility vehicle;  
PPTC – polymeric positive temperature coefficient device / resettable fuse;  
PTC – positive temperature coefficient device;  
PWM – pulse width modulation;  
RUL - remaining useful life;  
RX – receiver;  
SC – short circuit;  
SD – Secure Digital;  
SEPIC – single ended primary inductor converter;  
SoC – state of charge;  
SoH – state of health;  
SoP – state of power;  
SPDT – single pole double throw;  
SPST – single pole single throw;  
SUV – sports utility vehicle;  
TX – transmitter;  
UV – under voltage;  
WDT – watchdog timer;

## Appendix 2

List of scooter parameters

Speed Km/h	Range km	Power W	Charging A	Voltage V	Energy Wh	Capacity Ah
8	10	130	2	24	48	2
14	10	130	4	21,6	55,08	2,55
16,09	25,90	100	4-8	24	108	4,5
16,09	25,90	120		24	108	4,5
25	15	150	2-4	21,6	129,6	6
23	8-11	250		24	144	6
24	17,5	250	2-3	25	150	6
25	10-20	250		25,2	151,2	6
16	40mins	300	2,5	36	158,4	4,4
20,92	33,67	300	3-6	24	168	7
19,31	40mins	200	12	24	168	7
25	14	250	3-5	36	180	5
30	20	250	3-4	24	180	7,5
20	20	250	3,5	36	183	5,1
20	22	300	3,50	36	184	5,1
25	25	300	3,5		187	
20	22	300		36	187	5,2
25	25	300	3,5	36	187	5,2
19,31	31,08	500	3,5		187	
24,94	40,14	300	3,5		187	
25	25	350	2-3	36	187,2	5,2
20	25	250	2	36	187,2	5,2
25	20	300	4-5	36	187,2	5,2
24	13-18	350	3	36	187,2	5,2
	20	250/500		36	187,2	5,2
28,97	46,62	350	2-3	24	192	8
23	20	250	3	36	208,8	5,8
25	25	300	4		215	5,96
25	15-20	350	3-4	36	216	6
25	20	350	3	36	230,4	6,4
25	20	350	2-3	36	230,4	6,4
25	30	350	4-6	36	230,4	6,4
28,97	46,62	250	2-3	36	237,6	6,6
24,14	38,85	250/600	3,25	36	237,6	6,6
25	22-25	250/350		36	237,6	6,6
24,14	38,85	400		24	240	10
25	20	350	4-6	36	262,8	7,3
29	19	350	4-6	36	262,8	7,3
25	28	350	4-5	36	270	7,5
25	28	250	4-5	36	270	7,5

25	25	350	4-6	36	270	7,5
25	30	350	4-6	36	270	7,5
25	25-30	300	3	36	270	7,5
24,14	38,85	350	4-6	36	270	7,5
29	16	300		36	270	7,5
25	30	250	5,5		275	7,65
25	30	250/500	5,5		280	
24,94	40,14	250	5		280	
25	30	250		36	280,8	7,8
30	25	380	2-6	36	280,8	7,8
24	16	250/450		36	280,8	7,8
25	30	250	3-4	36	280,8	7,8
32,19	51,80	350/700	3-5	36	288	8
32,19	51,80	250/600	4,5	36	288	8
32,19	51,80	250/600	4,5	36	288	8
31	23-36	350/500	2	36	309,6	8,6
29,77	47,91	250	5	36	313	8,7
35,41	56,98	500	3	36	314	8,7
30	40	350		36	345,6	9,6
25	25-30	350	4-5	36	360	10
25,75	41,44	350	4-6	36	360	10
24,14	38,85	750		36	360	10
25	45	350	5-6	36	360	10
25	30	350/500	5	36	360	10
25	30	350/500	5	36	360	10
25	45	300	7,5		368	10,2
30	45	300/800	7	36	374	10,38889
30,58	49,21	300	7	36	374	10,38889
28	30	350	4-6	36	374,4	10,4
28	30	350, max 800	4	36	374,4	10,4
30	30	350	4-6	36	374,4	10,4
35	32	500	6-7	36	374,4	10,4
34	24-32	350/650	4-5	36	374,4	10,4
28,97	46,62	350	4-8	48	384	8
38,62	62,16	1000		36	432	12
35	60	500		36	468	13
25	45	300	8,5	37	474	12,8
25	45	300/600	8-9		474	
25	45	300	9	37	474	12,8
40	35-40	500	3-5	48	480	10
32,19	51,80	500/750	3	48	480	10
40	40-26	500/700	4	48	499,2	10,4
40	35-22	600/1110	6	48	499,2	10,4
50	25-40	800	4-6	48	499,2	10,4
40	40-48	500	3-4	48	499,2	10,4

40	36,8	700	2,5	48	504	10,5
35,41	56,98	700	4,5	48	528	11
25	55	350	4-7	36	540	15
25	65	350	6	36	551	15,3
30	65		6		551	
29,76	35,2	350		36	552	15,33333
30	40	500 max800	4	48	556,8	11,6
30	40	500	4-6	48	556,8	11,6
36	40	500/800		48	556,8	11,6
25	45	500/800	6-7	36	568,8	15,8
35	35	600	5	48	576	12
32,19	51,80	1600	6-8	48	576	12
32,19	51,80	800	4-8	48	576	12
32,19	51,80	1000	4-8	48	576	12
40	48		2	48	614	12,79167
36,8	40	500 / 1000		48	614	12,79167
45	60	500	8	48	624	13
45	45	500			624	
30,6	38-45	450	7	48	624	13
40	32/40	500/800		48	624	13
40	30-45	600-1110	9	48	624	13
50	50	800	4-6	48,1	625,3	13
		2x500		48	633,6	13,2
40	32	1000		48	633,6	13,2
30	80	500			675	
25	45-55	500	5-6	48	720	15
45	40-70	1000/1600	3-8	48	720	15
45	40-70	2x500	3-8	48	720	15
42	60-70	2x500		48	720	15
42	35	2x500		48	720	15
55	85-100	500	6-8	48	748	15,6
45	48	1360	6	48	748	15,6
45	48	1360	6	48	748	15,6
48	48	500		48	748,8	15,6
25	45	800/1200	6-7	48	748,8	15,6
50	52	500	6-8	48	768	16
55	55	500/800	6,5	48	840	17,5
32,19	51,80	2000	6-8	60	900	15
40	44,8	2x500 / 2200		48	921	19,1875
50	60-45	1000/1300	9	52	936	18
64	40	2x1200	4-5	52	936	18
60	45-65	2000	7-9	48	960	20
25	60	1600/2400	6-7	48	960	20
65	70-75	2x1000		48	1008	21
60	60	3000	2,6-8,7	60	1050	17,5

52	55	1450	2,6-10	52	1050	17,5
45	45	2x600	5	48	1056	22
65	80	3200	6,5A	60	1077	18,2
32,19	51,80	2000	4-8	60	1080	18
60	60	3000	2,8-9	60	1092	18,2
55	85	2x800	10	48	1104	23
48	64	1000	2,5	52	1156	22,4
50	75	1600	12	48	1176	24,5
65	100	4000	5,5-11	52	1196	23
50	100	1000	6-8	48	1200	25
80	70-100	2x1600		60	1200	20
60	100	2400	6-8	60	1200	20
60	100	2400		60	1200	20
65	70	2x1000		52	1237,6	23,8
45	90-100	500	2-8	48	1248	26
70	80	3600	4-6	60	1248	20,8
65	60-80-110	2x1000		52	1248	24
64	80-50	2x1000 / 3600	10	52	1248	24
64	64	2x1000/1200	3	60	1260	21
45	52/72	800/1300	6-8/10-12	60	1260	21
64	60	2x1200 / 3600	10	60	1260	21
64	80	3400	3-12	60	1260	21
64	80	3600	3-12	60	1344	22,4
45	75-85/85-100	600/1500	9-10/11-12	52	1346	26
65	85	2000		52	1352	26
65	110	2400		52	1352	26
55	80	1600		52	1352	26
65	120	3600	3-13	59,2	1385,28	23,4
64	121	3600	4-13	60	1400	23,4
59,2	72	2x1000 / 3600		60	1404	23,4
85	90	3200		60	1440	24
59,2	64	2x650 / 3000		60	1470	24,5
64	48/72	2x1000	10-12/13-16	60	1470	24,5
55	100-120	1200	4-9	48	1536	32
45	90-120	1200		48	1536	32
65	50-120	2400	5-9	52	1560	30
64	80	2x800	12-14	60	1560	26
65	100-120	3600	3	67,2	1657	24,65774
64	80	2x800 / 3600		60	1658	27,63333
45		2000		60	1680	28
64	119	3600		60	1680	28
65	120	3600	3,4-16	59,2	1700	28
65	100-120	3200	5-12	60	1920	32

80	121	5400	5,3-20	60	1920	32
80	120	5400	4,2-20	59,2	2060	34,8
80	100-120	5400	5-17	60	2072	35
	110	2x1600	5-8	60	2100	35
80	150	2x1200	9/17h	60	2100	35
80	113	2x1200/5400	8	60	2100	35
32,19	51,80	2000	6-10	60	2160	36
100	129	6640	4,8-21	72	2268	31,5
96	128	2x1600	3	72	2520	35
85	100-130	2x2800	5-10	60	2520	42
100	140	6640	5-23	72	2520	35
85	120	2x1600		60	2760	46
89	150	6720	7,5	60	2940	49
95	100-120	6000		60	3000	50
120	90-120	7000		72	3240	45
25	36	350	4,5			
25	30	250	4,5			
25	30	250	5,5			
20	12	300	5	36		
20	40	500	4	36		
25	30	250	5,5			
21	20	250	3	36		
16	18,5	250	3	36		
16	40mins			22		
24	40mins			36		
18	60mins			24		
16	80mins			12		
16	60mins			12		
8	5		2-3			
65	110	2x1000	13,5			
30,6	45	450	7			
28	30	350, 750	6			
18	60mins			24		
13	8	150	3			
47	96	800	7,5			
34	38	350	5			
8	5		3	21,6		
25	8-10	300		36		4
19	40mins	250		24		
18	60mins			24		
30	30	350				7,5
25	30	250/500	5	36		
25	20	350	4-5			7,8
20	20	300				6
25	25-30	350				7,8

85	110	5600				32
90	90	3200				
40	60	1500/2000	4-5			21,8
85	110	5600/6000		60		
45	110	1200				26
65	120	3200				35
55	90-120	2400				32
90		5600				42
32,19	51,80	1000	8			20
32,19	51,80	1000	8			20
16,09	40mins	100	8	24		
22,53	36,26	201-400	8	24		
30,58	49,21	201-400	8			
24,14	38,85	250		24		
17,70	60mins	100	12	24		
16,09	80mins	90	8-12	12		
22,53	36,26	200				
33,80	54,39					
30	50	500				13
25	30	250/500	5h	36		

## Appendix 3

List of wheelchairs

Model	Range, km	Speed, km/h	Voltage, V	Capacity, Ah
Move Lite Folding Power Chair	24.1	9.7	24	12
Pride Go Chair	14.0	6.0	12	18
Golden LiteRider Envy	24.9	5.6	12	22
EZ Lite Cruiser Powerchair	24.1	8.0	24	15
Shoprider Jimmie Power Chair	16.1	6.0	12	12
Drive Cobalt X23 Standard Power Wheelchair	12.9	6.4	12	21
EZ Lite Cruiser Deluxe DX10 Powerchair	24.1	8.0	24	15
Shoprider Smartie Power Wheelchair	16.1	6.0	12	12
Pride Jazzy Sport Portable	20.6	6.4	12	12
Karman Tranzit Go Foldable Lightweight Power Wheelchair	19.3	6.0	24	10
CTM Portable Power Chair	8.4	7.2	12	14
Invacare Pronto P31 Power Wheelchair	20.9	6.4	12	30
EZ Lite Cruiser Deluxe DX8 Powerchair	24.1	8.0	24	15
Cirrus Plus Power Wheelchair	29.0	8.0	12	34
EZ Lite Cruiser Deluxe DX12 Powerchair	24.1	8.0	24	15
CTM HS-6200 Folding Power Chair with Drop-In Battery	19.3	8.0	12	36
Invacare Pronto Air PT Personal Transporter	16.1	7.2	12	17
Shoprider Vienna Electric Wheelchair	16.1	6.4	12	17
Travelux Venture Elevating Powerchair	19.3		24	33
Betterlife Aries Electric Wheelchair	32.2	6.4	24	36
Betterlife Capricorn Electric Wheelchair	9.7	6.4	12	18
Drive Cirrus Electric Wheelchair	24.1	6.4	24	34
Reno II Portable Electric Powerchair	20.1	6.4	24	22
Shoprider Sirocco Electric Wheelchair	40.2	6.4	24	36
Alpha Mid-Wheel Electric Powerchair	19.3	6.4	12	35
Drive Enigma Energi Electric Powerchair	24.1		24	34
Shoprider Marbella Electric Wheelchair	40.2	6.4	24	55
PCBL 1220/1420-SCRUBBY	25.0	12.0	24	50
W1018 LIMBER	25.0	10.0	24	38
PCBL 1600/1800	25.0	12.0	24	50
PCBL 1610/1810	20.0	10.0	24	50
W4029 - HANTER PLUS	40.0	14.0	24	75
W4025-RIDER II	30.0	12.0	24	40
W4028-CRUISER II	35.0	15.0	24	55

## Appendix 4

List of 18650 cells

Manufacturer	Model	Capacity, mAh	Price, €	Voltage, V	Weight, g	Cycles	Charging current	Discharge current	Cycle life threshold
Sony	US18650VTC2	1550	2.75	3.7	43.4	300	4.0	30.0	60%
Sony	US18650VTC5A	2500	5.25	3.6	47.1	300	6.0	35.0	70%
Sony	US18650VTC6	3000	5.75	3.6	46.5	500	4.0	20.0	60%
Sony	US18650VTC5	2500	4.45	3.6	44.3	300	4.0	20.0	70%
Sony	US18650VTC4	2000	3.35	3.7	45	500	4.0	30.0	60%
Sony	US18650V3	2150	2.8	3.7	43.6	500	2.2	10.0	88%
Sony	US18650VTC3	1500	3.95	3.7	45	500	4.0	30.0	60%
Sony	US18650NC1	2750	3.35	3.6	45.3	100	3.0	8.0	70%
LG	ICR18650-HB6	1500	2.45	3.65	48	400	4.0	30.0	60%
LG	ICR18650-HB2	1500	2.55	3.65	48	500	4.0	30.0	89%
LG	ICR18650-HE2	2500	2.99	3.6	48	300	4.0	20.0	60%
LG	INR18650-HG2	3000	4.75	3.6	47	300	4.0	20.0	70%
LG	INR18650-HG2	3000	4.84	3.6	47	300	4.0	20.0	70%
LG	INR18650MH1	3200	4.25	3.67	49	500	3.1	10.0	70%
LG	ICR18650-HE4	2500	3.45	3.6	47	300	4.0	20.0	60%
LG	INR18650-MJ1	3500	4.49	3.635	49	400	3.4	10.0	80%
LG	INR18650-MG1	2850	3.09	3.62	46	500	2.9	10.0	70%
LG	ICR18650-MF1	2150	2.6	3.65	44	500	2.2	10.0	70%
LG	ICR18650-B4	2600	2.35	3.6	48	300	2.5	5.0	80%
LG	ICR18650-E1	3200	3.5	3.75	49	300	2.2	4.7	75%
LG	ICR18650-S3	2200	2.5	3.6	47	300	2.2	3.2	80%
LG	ICR18650HD2C	2100	5.79	3.65	48	300	4.0	20.0	60%
LG	ICR18650D1	3000	5.95	3.75	48.5	300	2.9	5.8	75%
Samsung	INR18650-20R	2000	2.85	3.6	45	250	4.0	22.0	60%
Samsung	INR18650-15M	1500	2.4	3.6	45	250	4.0	23.0	60%
Samsung	INR18650-25R	2500	3.69	3.6	45	250	4.0	20.0	60%
Samsung	INR18650-30Q	3000	3.99	3.6	48	250	4.0	15.0	60%
Samsung	INR18650-20Q	2000	2.25	3.6	45	250	4.0	15.0	60%
Samsung	INR18650-35E	3350	4.25	3.6	50	500	2.0	8.0	60%
Samsung	ICR18650-22P	2150	2.75	3.62	44.5	500	2.2	10.0	70%
Samsung	INR18650-29E	2850	2.85	3.65	48	500	2.8	2.8	70%
Samsung	ICR18650-30A	3000	3.5	3.7	48	299	3.0	6.0	70%
Samsung	ICR18650-26F	2600	2.75	3.7	47	299	2.6	5.2	69%
Samsung	ICR18650-26H	2600	2.55	3.63	47	299	2.6	5.2	70%
Samsung	ICR18650-26J	2600	2.65	3.63	45	299	2.6	5.2	70%

Samsung	ICR18650-22F	2200	2.65	3.6	44.5	299	2.2	4.4	68%
Samsung	INR 18650 15L	1500	4.35	3.6	43	250	4.0	18.0	60%
Samsung	ICR18650 28A	2800	5.95	3.75	48	299	2.8	5.6	70%
Samsung	ICR18650-30B	3000	4.68	3.78	48	299	3.0	5.9	70%
Samsung	ICR18650-32A	3200	6.25	3.75	50	299	3.2	6.4	70%
Samsung	INR18650-32E	3200	6.5	3.65	50	500	3.2	6.4	70%
Sanyo	UR18650W2	1500	3.25	3.7	47	300	1.5	15.0	63%
Sanyo	UR18650NSX	2500	3.85	3.6	45.8	300	1.8	20.0	63%
Sanyo	NCR18650GA	3300	4.59	3.6	48	500	1.5	10.0	67%
Sanyo	UR18650AAN	2150	1.99	3.6	43	300	1.5	4.3	63%
Sanyo	NCR18650BF	3200	3.45	3.6	47.5	300	1.6	1.6	82%
Panasonic	NCR 18650A	2900	3.45	3.6	47.5	500	1.5	5.8	78%
Panasonic	NCR18650PF	2700	3.15	3.6	48	500	1.4	5.4	87%
Panasonic	NCR18650B	3350	3.65	3.6	48.5	500	1.6	6.4	70%
Panasonic	CGR18650 CH	2250	5.95	3.6	44	300	1.5	10.0	84%
Panasonic	CGR18650 CG	2250	4.95	3.6	45	500	1.5	4.3	78%
Sanyo	UR18650FM	2500	6.4	3.6	48	300	2.6	2.6	63%
Sanyo	NCR18650BL	3350	6.35	3.6	49	300	1.6	7.0	63%

## Appendix 5

Calculations of MOSFET losses @4.2 V

	IPT004N03L	FDMT80040DC	CSD16570Q5B	SiRA80DP	FDBL9401L-F085
FOM=	4.51E-02	1.06E-01	9.41E-02	5.88E-02	1.26E-01
Qg	1.22E+02	2.41E+02	1.92E+02	1.25E+02	2.69E+02
Udd	4.20E+00	4.20E+00	4.20E+00	4.20E+00	4.20E+00
Rdson	3.70E-04	4.40E-04	4.90E-04	4.70E-04	4.70E-04
Idon	8.90E+01	8.90E+01	8.90E+01	8.90E+01	8.90E+01
Cgd1	1.30E-09	1.00E-09	1.30E-09	1.50E-09	1.00E-09
Rg	5.00E+00	5.00E+00	5.00E+00	5.00E+00	5.00E+00
Udr	1.50E+01	1.50E+01	1.50E+01	1.50E+01	1.50E+01
Uplateau	2.20E+00	4.40E+00	2.50E+00	2.60E+00	2.90E+00
Cgd2	3.00E-09	2.00E-09	3.10E-09	3.00E-09	2.00E-09
tri	1.70E-08	6.20E-08	4.30E-08	2.30E-08	4.90E-08
tfi	3.70E-08	4.30E-08	7.20E-08	1.20E-08	7.90E-08
Qrr	1.00E-07	2.19E-07		1.44E-07	2.70E-07
Igon=	2.56E+00	2.12E+00	2.50E+00	2.48E+00	2.42E+00
tfu1=	2.12E-09	1.96E-09	2.16E-09	2.52E-09	1.72E-09
tfu2=	4.88E-09	3.93E-09	5.15E-09	5.03E-09	3.44E-09
tfu=	3.50E-09	2.94E-09	3.66E-09	3.77E-09	2.58E-09
Igoff=	4.40E-01	8.80E-01	5.00E-01	5.20E-01	5.80E-01
tru1=	1.23E-08	4.73E-09	1.08E-08	1.20E-08	7.17E-09
tru2=	2.84E-08	9.46E-09	2.58E-08	2.40E-08	1.43E-08
tru=	2.04E-08	7.09E-09	1.83E-08	1.80E-08	1.08E-08
EonMrr=	4.20E-07	9.20E-07	0.00E+00	6.05E-07	1.13E-06
Eon=	3.83E-06	1.21E-05	8.72E-06	5.00E-06	9.64E-06
Eoff=	1.07E-05	9.36E-06	1.69E-05	5.61E-06	1.68E-05
Psw=	1.4972	2.2420	2.5595	1.1214	2.7549
Pcm=	2.9308	3.4852	3.8813	3.7229	3.7229
Ptot=	4.4280	5.7272	6.4408	4.8443	6.4778

Calculations of MOSFET losses @8.4 V

	IPT004N03L	TPHR6503PL	SiRA20DP	FDMS8050	SiDR140DP	TPWR8004PL
FOM=	4.51E-02	4.51E-02	6.43E-02	1.02E-01	6.10E-02	6.70E-02
Qg	1.22E+02	1.10E+02	1.34E+02	2.04E+02	1.13E+02	1.03E+02
Udd	8.40E+00	8.40E+00	8.40E+00	8.40E+00	8.40E+00	8.40E+00
Rdson	3.70E-04	4.10E-04	4.80E-04	5.00E-04	5.40E-04	6.50E-04
Idon	4.50E+01	4.50E+01	4.50E+01	4.50E+01	4.50E+01	4.50E+01
Cgd1	9.00E-10	3.50E-10	7.00E-10	4.00E-10	6.00E-10	1.20E-10
Rg	5.00E+00	5.00E+00	5.00E+00	5.00E+00	5.00E+00	5.00E+00
Udr	1.50E+01	1.50E+01	1.50E+01	1.50E+01	1.50E+01	1.50E+01
Uplateau	2.20E+00	7.50E+00	2.20E+00	2.80E+00	2.20E+00	3.00E+00
Cgd2	3.00E-09	1.10E-09	2.40E-09	1.20E-09	1.80E-09	6.00E-10
tri	1.70E-08	1.20E-08	2.40E-08	2.20E-08	9.00E-09	1.30E-08
tfi	3.70E-08	1.00E-08	9.00E-09	1.60E-08	9.00E-09	1.40E-08
Qrr	1.00E-07	7.00E-08	8.70E-08	1.41E-07	1.00E-07	7.00E-08

Igon=	2.56E+00	1.50E+00	2.56E+00	2.44E+00	2.56E+00	2.40E+00
tfu1=	2.95E-09	1.96E-09	2.29E-09	1.37E-09	1.96E-09	4.19E-10
tfu2=	9.82E-09	6.15E-09	7.85E-09	4.12E-09	5.89E-09	2.09E-09
tfu=	6.39E-09	4.05E-09	5.07E-09	2.75E-09	3.93E-09	1.26E-09

Igoff=	4.40E-01	1.50E+00	4.40E-01	5.60E-01	4.40E-01	6.00E-01
tru1=	1.71E-08	1.96E-09	1.33E-08	5.98E-09	1.14E-08	1.67E-09
tru2=	5.72E-08	6.15E-09	4.57E-08	1.80E-08	3.43E-08	8.37E-09
tru=	3.72E-08	4.05E-09	2.95E-08	1.20E-08	2.28E-08	5.02E-09

EonMrr=	8.40E-07	5.88E-07	7.31E-07	1.18E-06	8.40E-07	5.88E-07
Eon=	4.42E-06	3.03E-06	5.49E-06	4.68E-06	2.44E-06	2.69E-06
Eoff=	1.40E-05	2.66E-06	7.28E-06	5.29E-06	6.02E-06	3.60E-06

Psw=	1.9275	0.6277	1.3505	1.1147	0.9301	0.6878
Pcm=	0.7493	0.8303	0.9720	1.0125	1.0935	1.3163
Ptot=	2.6767	1.4580	2.3225	2.1272	2.0236	2.0040

Calculations of MOSFET losses @12.6 V

	TPHR6503PL	FDMS8050	SIDR140DP	CSD16556Q5B	SIRC16DP	BSC009NE2LS5I
FOM=	4.51E-02	1.02E-01	6.10E-02	3.24E-02	5.52E-02	1.36E-02
Qg	1.10E+02	2.04E+02	1.13E+02	3.60E+01	6.90E+01	1.70E+01
Udd	1.26E+01	1.26E+01	1.26E+01	1.26E+01	1.26E+01	1.26E+01
Rdson	4.10E-04	5.00E-04	5.40E-04	9.00E-04	8.00E-04	8.00E-04
Idon	3.00E+01	3.00E+01	3.00E+01	3.00E+01	3.00E+01	3.00E+01
Cgd1	3.50E-10	2.10E-10	5.00E-10	2.20E-10	3.50E-10	1.10E-10
Rg	5.00E+00	5.00E+00	5.00E+00	5.00E+00	5.00E+00	5.00E+00
Udr	1.50E+01	1.50E+01	1.50E+01	1.50E+01	1.50E+01	1.50E+01
Uplateau	7.50E+00	2.90E+00	2.30E+00	2.40E+00	2.50E+00	2.40E+00
Cgd2	1.10E-09	1.20E-09	9.00E-10	1.00E-09	1.15E-09	6.00E-10
tri	1.20E-08	2.20E-08	9.00E-09	3.40E-08	2.10E-08	5.00E-09
tfi	1.00E-08	1.60E-08	9.00E-09	1.30E-08	9.00E-09	4.00E-09
Qrr	7.00E-08	1.41E-07	1.00E-07	8.40E-08	4.70E-08	5.00E-09

Igon=	1.50E+00	2.42E+00	2.54E+00	2.52E+00	2.50E+00	2.52E+00
tfu1=	2.94E-09	1.09E-09	2.48E-09	1.10E-09	1.76E-09	5.49E-10
tfu2=	9.23E-09	6.24E-09	4.46E-09	4.99E-09	5.78E-09	2.99E-09
tfu=	6.08E-09	3.67E-09	3.47E-09	3.04E-09	3.77E-09	1.77E-09

Igoff=	1.50E+00	5.80E-01	4.60E-01	4.80E-01	5.00E-01	4.80E-01
tru1=	2.94E-09	4.56E-09	1.37E-08	5.76E-09	8.80E-09	2.88E-09
tru2=	9.23E-09	2.60E-08	2.46E-08	2.62E-08	2.89E-08	1.57E-08
tru=	6.08E-09	1.53E-08	1.91E-08	1.60E-08	1.89E-08	9.30E-09

EonMrr=	8.82E-07	1.78E-06	1.26E-06	1.06E-06	5.92E-07	6.30E-08
Eon=	3.42E-06	4.85E-06	2.36E-06	7.00E-06	4.68E-06	1.28E-06
Eoff=	3.04E-06	5.92E-06	5.32E-06	5.48E-06	5.27E-06	2.51E-06

Psw=	0.7340	1.2543	0.8937	1.3536	1.0541	0.3857
Pcm=	0.3690	0.4500	0.4860	0.8100	0.7200	0.7200
Ptot=	1.1030	1.7043	1.3797	2.1636	1.7741	1.1057

Calculations of MOSFET losses @16.8 V

	CSD18502Q5B	STL190N4F7AG	STL210N4F7AG	NVMF55C423NL	BSC014N04LS
FOM=	9.36E-02	6.89E-02	5.59E-02	8.00E-02	3.41E-02
Qg	5.20E+01	4.10E+01	4.30E+01	5.00E+01	3.10E+01
Udd	1.68E+01	1.68E+01	1.68E+01	1.68E+01	1.68E+01
Rdson	1.80E-03	1.68E-03	1.30E-03	1.60E-03	1.10E-03
Idon	2.30E+01	2.30E+01	2.30E+01	2.30E+01	2.30E+01
Cgd1	2.30E-11	9.00E-11	8.00E-11	8.00E-11	2.00E-10
Rg	5.00E+00	5.00E+00	5.00E+00	5.00E+00	5.00E+00
Udr	1.50E+01	1.50E+01	1.50E+01	1.50E+01	1.50E+01
Uplateau	2.50E+00	5.80E+00	5.80E+00	3.10E+00	2.50E+00
Cgd2	4.00E-10	5.30E-10	4.50E-10	8.00E-10	1.00E-09
tri	6.80E-09	6.40E-09	6.00E-09	7.40E-09	9.00E-09
tfi	4.00E-09	6.50E-09	6.00E-09	8.10E-09	7.00E-09
Qrr	8.80E-08	4.30E-08	7.10E-08	2.90E-08	9.80E-08

Igon=	2.50E+00	1.84E+00	1.84E+00	2.38E+00	2.50E+00
tfu1=	1.54E-10	8.20E-10	7.29E-10	5.63E-10	1.34E-09
tfu2=	2.68E-09	4.83E-09	4.10E-09	5.63E-09	6.71E-09
tfu=	1.42E-09	2.82E-09	2.42E-09	3.10E-09	4.03E-09

Igoff=	5.00E-01	1.16E+00	1.16E+00	6.20E-01	5.00E-01
tru1=	7.71E-10	1.30E-09	1.16E-09	2.16E-09	6.71E-09
tru2=	1.34E-08	7.66E-09	6.51E-09	2.16E-08	3.35E-08
tru=	7.09E-09	4.48E-09	3.83E-09	1.19E-08	2.01E-08

EonMrr=	1.48E-06	7.22E-07	1.19E-06	4.87E-07	1.65E-06
Eon=	1.59E-06	1.78E-06	1.63E-06	2.03E-06	2.52E-06
Eoff=	2.14E-06	2.12E-06	1.90E-06	3.86E-06	5.24E-06

Psw=	0.5208	0.4626	0.4718	0.6379	0.9404
Pcm=	0.9522	0.8887	0.6877	0.8464	0.5819
Ptot=	1.4730	1.3513	1.1595	1.4843	1.5223

Calculations of MOSFET losses @21 V

	BSC027N06LS5	BSC034N06NS	SiR688DP	TPN2R805PL	AON6152	SiR608DP
FOM=	5.52E-02	9.24E-02	1.28E-01	8.58E-02	9.90E-02	1.11E-01
Qg	2.40E+01	3.30E+01	4.40E+01	3.90E+01	1.10E+02	1.11E+02
Udd	2.10E+01	2.10E+01	2.10E+01	2.10E+01	2.10E+01	2.10E+01
Rdson	2.30E-03	2.80E-03	2.90E-03	2.20E-03	9.00E-04	1.00E-03
Idon	1.80E+01	1.80E+01	1.80E+01	1.80E+01	1.80E+01	1.80E+01
Cgd1	5.00E-11	5.00E-11	9.00E-11	5.00E-11	1.00E-10	1.10E-10
Rg	5.00E+00	5.00E+00	5.00E+00	5.00E+00	5.00E+00	5.00E+00
Udr	1.50E+01	1.50E+01	1.50E+01	1.50E+01	1.50E+01	1.50E+01
Uplateau	2.90E+00	4.70E+00	2.90E+00	9.00E+00	3.00E+00	3.00E+00
Cgd2	1.00E-09	5.40E-10	4.00E-10	8.00E-10	9.00E-10	9.00E-10
tri	4.80E-09	5.00E-09	8.00E-09	7.40E-09	6.00E-09	1.00E-08
tfi	5.40E-09	5.00E-09	8.00E-09	1.20E-08	6.50E-09	8.00E-09
Qrr	3.60E-08	6.50E-08	3.70E-08	2.70E-08	7.40E-08	7.10E-08

Igon=	2.42E+00	2.06E+00	2.42E+00	1.20E+00	2.40E+00	2.40E+00
tfu1=	4.33E-10	5.08E-10	7.79E-10	8.73E-10	8.74E-10	9.62E-10
tfu2=	8.66E-09	5.49E-09	3.46E-09	1.40E-08	7.87E-09	7.87E-09
tfu=	4.55E-09	3.00E-09	2.12E-09	7.42E-09	4.37E-09	4.41E-09

Igoff=	5.80E-01	9.40E-01	5.80E-01	1.80E+00	6.00E-01	6.00E-01
tru1=	1.81E-09	1.11E-09	3.25E-09	5.82E-10	3.50E-09	3.85E-09
tru2=	3.61E-08	1.20E-08	1.44E-08	9.32E-09	3.15E-08	3.15E-08
tru=	1.90E-08	6.57E-09	8.85E-09	4.95E-09	1.75E-08	1.77E-08

EonMrr=	7.56E-07	1.37E-06	7.77E-07	5.67E-07	1.55E-06	1.49E-06
Eon=	1.77E-06	1.51E-06	1.91E-06	2.80E-06	1.96E-06	2.72E-06
Eoff=	4.61E-06	2.19E-06	3.18E-06	3.20E-06	4.53E-06	4.85E-06

Psw=	0.7129	0.5065	0.5874	0.6572	0.8048	0.9065
Pcm=	0.7452	0.9072	0.9396	0.7128	0.2916	0.3240
Ptot=	1.4581	1.4137	1.5270	1.3700	1.0964	1.2305

Calculations of MOSFET losses @25.2 V

	BSC065N06LS5	CSD18563Q5A	SiS184DN	BSC014N06NS	BSC016N06NS	SiR180DP
FOM=	9.54E-02	8.55E-02	9.87E-02	1.07E-01	9.94E-02	9.86E-02
Qg	1.80E+01	1.50E+01	2.10E+01	8.90E+01	7.10E+01	5.80E+01
Udd	2.52E+01	2.52E+01	2.52E+01	2.52E+01	2.52E+01	2.52E+01
Rdson	5.30E-03	5.70E-03	4.70E-03	1.20E-03	1.40E-03	1.70E-03
Idon	1.50E+01	1.50E+01	1.50E+01	1.50E+01	1.50E+01	1.50E+01
Cgd1	1.80E-11	1.30E-11	2.00E-11	6.00E-11	6.00E-11	5.00E-11
Rg	5.00E+00	5.00E+00	5.00E+00	5.00E+00	5.00E+00	5.00E+00
Udr	1.50E+01	1.50E+01	1.50E+01	1.50E+01	1.50E+01	1.50E+01
Uplateau	3.10E+00	3.30E+00	3.70E+00	4.30E+00	4.30E+00	3.80E+00
Cgd2	4.10E-10	1.40E-10	3.00E-10	1.30E-09	1.00E-09	6.00E-10
tri	3.00E-09	6.30E-09	6.00E-09	1.00E-08	9.00E-09	8.00E-09
tfi	3.00E-09	1.70E-09	6.00E-09	1.10E-08	9.00E-09	7.00E-09
Qrr	1.40E-08	6.30E-08	3.20E-08	1.39E-07	7.80E-08	8.30E-08

Igon=	2.38E+00	2.34E+00	2.26E+00	2.14E+00	2.14E+00	2.24E+00
tfu1=	1.90E-10	1.40E-10	2.22E-10	7.06E-10	7.06E-10	5.62E-10
tfu2=	4.33E-09	1.50E-09	3.34E-09	1.53E-08	1.18E-08	6.74E-09
tfu=	2.26E-09	8.21E-10	1.78E-09	8.00E-09	6.24E-09	3.65E-09

Igoff=	6.20E-01	6.60E-01	7.40E-01	8.60E-01	8.60E-01	7.60E-01
tru1=	7.29E-10	4.95E-10	6.79E-10	1.76E-09	1.76E-09	1.66E-09
tru2=	1.66E-08	5.33E-09	1.02E-08	3.81E-08	2.93E-08	1.99E-08
tru=	8.67E-09	2.91E-09	5.43E-09	1.99E-08	1.55E-08	1.08E-08

EonMrr=	3.53E-07	1.59E-06	8.06E-07	3.50E-06	1.97E-06	2.09E-06
Eon=	9.94E-07	1.35E-06	1.47E-06	3.40E-06	2.88E-06	2.20E-06
Eoff=	2.21E-06	8.71E-07	2.16E-06	5.84E-06	4.63E-06	3.36E-06

Psw=	0.3552	0.3805	0.4438	1.2747	0.9479	0.7652
Pcm=	1.1925	1.2825	1.0575	0.2700	0.3150	0.3825
Ptot=	1.5477	1.6630	1.5013	1.5447	1.2629	1.1477

Calculations of MOSFET losses @29.4 V

	SiR180DP	BSC016N06NS	BSC065N06LS5	SiS184DN	FDMS86500L	SiR662DP
FOM=	9.86E-02	9.94E-02	9.54E-02	9.87E-02	2.46E-01	1.40E-01
Qg	5.80E+01	7.10E+01	1.80E+01	2.10E+01	1.17E+02	6.35E+01
Udd	2.94E+01	2.94E+01	2.94E+01	2.94E+01	2.94E+01	2.94E+01
Rdson	1.70E-03	1.40E-03	5.30E-03	4.70E-03	2.10E-03	2.20E-03
Idon	1.30E+01	1.30E+01	1.30E+01	1.30E+01	1.30E+01	1.30E+01
Cgd1	5.00E-11	6.00E-11	1.80E-11	2.00E-11	4.00E-11	1.40E-10
Rg	5.00E+00	5.00E+00	5.00E+00	5.00E+00	5.00E+00	5.00E+00
Udr	1.50E+01	1.50E+01	1.50E+01	1.50E+01	1.50E+01	1.50E+01
Uplateau	3.80E+00	4.30E+00	3.10E+00	3.70E+00	5.00E+00	3.00E+00
Cgd2	6.00E-10	1.00E-09	4.10E-10	3.00E-10	5.00E-10	7.50E-10
tri	8.00E-09	9.00E-09	3.00E-09	6.00E-09	1.60E-08	1.10E-08
tfi	7.00E-09	9.00E-09	3.00E-09	6.00E-09	7.80E-09	1.10E-08
Qrr	8.30E-08	7.80E-08	1.40E-08	3.20E-08	8.40E-08	8.80E-08

Igon=	2.24E+00	2.14E+00	2.38E+00	2.26E+00	2.00E+00	2.40E+00
tfu1=	6.56E-10	8.24E-10	2.22E-10	2.60E-10	5.87E-10	1.71E-09
tfu2=	7.87E-09	1.37E-08	5.05E-09	3.89E-09	7.34E-09	9.18E-09
tfu=	4.26E-09	7.28E-09	2.64E-09	2.08E-09	3.97E-09	5.45E-09

Igoff=	7.60E-01	8.60E-01	6.20E-01	7.40E-01	1.00E+00	6.00E-01
tru1=	1.93E-09	2.05E-09	8.52E-10	7.93E-10	1.17E-09	6.85E-09
tru2=	2.32E-08	3.42E-08	1.94E-08	1.19E-08	1.47E-08	3.67E-08
tru=	1.26E-08	1.81E-08	1.01E-08	6.34E-09	7.93E-09	2.18E-08

EonMrr=	2.44E-06	2.29E-06	4.12E-07	9.41E-07	2.47E-06	2.59E-06
Eon=	2.34E-06	3.11E-06	1.08E-06	1.54E-06	3.82E-06	3.14E-06
Eoff=	3.74E-06	5.18E-06	2.51E-06	2.36E-06	3.01E-06	6.26E-06

Psw=	0.8522	1.0584	0.3997	0.4843	0.9291	1.1995
Pcm=	0.2873	0.2366	0.8957	0.7943	0.3549	0.3718
Ptot=	1.1395	1.2950	1.2954	1.2786	1.2840	1.5713

Calculations of MOSFET losses @33.6 V

	AON6278	BSC037N08NS5	BSZ075N08NS5	BSC070N10NS5	IPP052N08NS5
FOM=	1.69E-01	1.56E-01	1.49E-01	1.80E-01	1.93E-01
Qg	6.15E+01	4.60E+01	2.40E+01	3.00E+01	4.20E+01
Udd	3.36E+01	3.36E+01	3.36E+01	3.36E+01	3.36E+01
Rdson	2.75E-03	3.40E-03	6.20E-03	6.00E-03	4.60E-03
Idon	1.20E+01	1.20E+01	1.20E+01	1.20E+01	1.20E+01
Cgd1	5.00E-11	3.30E-11	2.00E-11	4.00E-11	3.00E-11
Rg	5.00E+00	5.00E+00	5.00E+00	5.00E+00	5.00E+00
Udr	1.50E+01	1.50E+01	1.50E+01	1.50E+01	1.50E+01
Uplateau	4.00E+00	4.80E+00	4.60E+00	4.80E+00	5.20E+00
Cgd2	2.50E-10	8.00E-10	4.00E-10	5.00E-10	7.00E-10
tri	6.00E-09	1.00E-08	4.00E-09	5.00E-09	7.00E-09
tfi	7.00E-09	7.00E-09	4.00E-09	6.00E-09	7.00E-09
Qrr	1.74E-07	3.60E-08	3.90E-08	8.90E-08	9.20E-08
Igon=	2.20E+00	2.04E+00	2.08E+00	2.04E+00	1.96E+00
tfu1=	7.63E-10	5.43E-10	3.22E-10	6.57E-10	5.13E-10
tfu2=	3.81E-09	1.32E-08	6.45E-09	8.22E-09	1.20E-08
tfu=	2.29E-09	6.85E-09	3.38E-09	4.44E-09	6.25E-09
Igoff=	8.00E-01	9.60E-01	9.20E-01	9.60E-01	1.04E+00
tru1=	2.10E-09	1.15E-09	7.29E-10	1.40E-09	9.68E-10
tru2=	1.05E-08	2.80E-08	1.46E-08	1.75E-08	2.26E-08
tru=	6.29E-09	1.46E-08	7.65E-09	9.43E-09	1.18E-08
EonMrr=	5.85E-06	1.21E-06	1.31E-06	2.99E-06	3.09E-06
Eon=	1.67E-06	3.40E-06	1.49E-06	1.90E-06	2.67E-06
Eoff=	2.68E-06	4.35E-06	2.35E-06	3.11E-06	3.78E-06
Psw=	1.0197	0.8953	0.5148	0.8004	0.9546
Pcm=	0.3960	0.4896	0.8928	0.8640	0.6624
Ptot=	1.4157	1.3849	1.4076	1.6644	1.6170

Calculations of MOSFET losses @37.8 V

	BSC037N08NS5	BSC072N08NS5	BSZ075N08NS5	BSC061N08NS5	BSC052N08NS5
FOM=	1.56E-01	1.49E-01	1.49E-01	1.40E-01	1.41E-01
Qg	4.60E+01	2.40E+01	2.40E+01	2.70E+01	3.20E+01
Udd	3.78E+01	3.78E+01	3.78E+01	3.78E+01	3.78E+01
Rdson	3.40E-03	6.20E-03	6.20E-03	5.20E-03	4.40E-03
Idon	1.00E+01	1.00E+01	1.00E+01	1.00E+01	1.00E+01
Cgd1	2.70E-11	1.50E-11	1.50E-11	1.50E-11	2.00E-11
Rg	5.00E+00	5.00E+00	5.00E+00	5.00E+00	5.00E+00
Udr	1.50E+01	1.50E+01	1.50E+01	1.50E+01	1.50E+01
Uplateau	4.80E+00	5.00E+00	4.60E+00	4.90E+00	4.90E+00
Cgd2	8.00E-10	4.00E-10	4.00E-10	4.50E-10	5.10E-10
tri	1.00E-08	7.00E-09	4.00E-09	6.00E-09	7.00E-09
tfi	7.00E-09	5.00E-09	4.00E-09	5.00E-09	5.00E-09
Qrr	3.60E-08	3.70E-08	3.90E-08	3.70E-08	3.50E-08

Igon=	2.04E+00	2.00E+00	2.08E+00	2.02E+00	2.02E+00
tfu1=	5.00E-10	2.83E-10	2.72E-10	2.80E-10	3.74E-10
tfu2=	1.48E-08	7.55E-09	7.26E-09	8.41E-09	9.53E-09
tfu=	7.66E-09	3.92E-09	3.76E-09	4.34E-09	4.95E-09

Igoff=	9.60E-01	1.00E+00	9.20E-01	9.80E-01	9.80E-01
tru1=	1.06E-09	5.66E-10	6.15E-10	5.78E-10	7.71E-10
tru2=	3.15E-08	1.51E-08	1.64E-08	1.73E-08	1.96E-08
tru=	1.63E-08	7.83E-09	8.51E-09	8.96E-09	1.02E-08

EonMrr=	1.36E-06	1.40E-06	1.47E-06	1.40E-06	1.32E-06
Eon=	3.34E-06	2.06E-06	1.47E-06	1.96E-06	2.26E-06
Eoff=	4.40E-06	2.42E-06	2.36E-06	2.64E-06	2.87E-06

Psw=	0.9095	0.5887	0.5306	0.5991	0.6457
Pcm=	0.3400	0.6200	0.6200	0.5200	0.4400
Ptot=	1.2495	1.2087	1.1506	1.1191	1.0857

Calculations of MOSFET losses @42 V

	FDMC86184	FDMS86182	BSC110N15N55	BSC093N15N55	FDWS86068-F085
FOM=	1.34E-01	1.53E-01	2.52E-01	2.61E-01	1.61E-01
Qg	2.10E+01	2.60E+01	2.80E+01	3.30E+01	3.10E+01
Udd	4.20E+01	4.20E+01	4.20E+01	4.20E+01	4.20E+01
Rdson	6.40E-03	5.90E-03	9.00E-03	7.90E-03	5.20E-03
Idon	9.00E+00	9.00E+00	9.00E+00	9.00E+00	9.00E+00
Cgd1	2.00E-11	2.00E-11	3.10E-11	4.00E-11	2.50E-11
Rg	5.00E+00	5.00E+00	5.00E+00	5.00E+00	5.00E+00
Udr	1.50E+01	1.50E+01	1.50E+01	1.50E+01	1.50E+01
Uplateau	4.80E+00	4.80E+00	5.80E+00	5.70E+00	5.20E+00
Cgd2	2.00E-10	2.00E-10	3.00E-10	3.10E-10	2.10E-10
tri	4.00E-09	4.00E-09	3.30E-09	4.30E-09	6.00E-09
tfi	4.00E-09	4.00E-09	2.90E-09	3.80E-09	7.00E-09
Qrr	9.60E-08	1.16E-07	4.60E-08	5.80E-08	5.60E-08

Igon=	2.04E+00	2.04E+00	1.84E+00	1.86E+00	1.96E+00
tfu1=	4.11E-10	4.11E-10	7.06E-10	9.02E-10	5.35E-10
tfu2=	4.11E-09	4.11E-09	6.83E-09	6.99E-09	4.49E-09
tfu=	2.26E-09	2.26E-09	3.77E-09	3.94E-09	2.52E-09

Igoff=	9.60E-01	9.60E-01	1.16E+00	1.14E+00	1.04E+00
tru1=	8.74E-10	8.74E-10	1.12E-09	1.47E-09	1.01E-09
tru2=	8.74E-09	8.74E-09	1.08E-08	1.14E-08	8.47E-09
tru=	4.81E-09	4.81E-09	5.98E-09	6.44E-09	4.74E-09

EonMrr=	4.03E-06	4.87E-06	1.93E-06	2.44E-06	2.35E-06
Eon=	1.18E-06	1.18E-06	1.34E-06	1.56E-06	1.61E-06
Eoff=	1.66E-06	1.66E-06	1.68E-06	1.93E-06	2.22E-06

Psw=	0.6880	0.7720	0.4947	0.5929	0.6180
Pcm=	0.5184	0.4779	0.7290	0.6399	0.4212
Ptot=	1.2064	1.2499	1.2237	1.2328	1.0392

## REFERENCES

- [1] CSDD, “Statistics of registered vehicle.” [Online]. Available: <https://www.csdd.lv/en/vehicles/statistics-of-registered-vehicle> .
- [2] “A European Green Deal | European Commission.” [Online]. Available: [https://ec.europa.eu/info/strategy/priorities-2019-2024/european-green-deal\\_en](https://ec.europa.eu/info/strategy/priorities-2019-2024/european-green-deal_en). [Accessed: 29-Oct-2021].
- [3] N. Smith, “Beyond Energy: The Main Offenders [Climate Change Energy],” *Eng. Technol.*, vol. 15, no. 10, pp. 30–33, Nov. 2020.
- [4] “Electric Race Car Design & Engineering — Drive eO.” [Online]. Available: <https://driveeo.com/>. [Accessed: 01-Nov-2021].
- [5] “Electric Racing Karts - Blue Shock Race Electric karts.” [Online]. Available: <https://blushockrace.com/electric-racing-karts/>. [Accessed: 01-Nov-2021].
- [6] “e-up! for everyone – new generation of the electric e-up! with a long range to be launched at a low price | Volkswagen Newsroom.” [Online]. Available: <https://www.volkswagen-newsroom.com/en/press-releases/e-up-for-everyone-new-generation-of-the-electric-e-up-with-a-long-range-to-be-launched-at-a-low-price-5318>. [Accessed: 27-Jun-2020].
- [7] “Build Your Own Toyota | Toyota Configurator.” [Online]. Available: <https://www.toyota.com/configurator/build/step/model/year/2020/series/prius>. [Accessed: 27-Jun-2020].
- [8] “2018 Nissan Leaf battery technology, a deep dive.” [Online]. Available: [https://www.greencarreports.com/news/1117928\\_2018-nissan-leaf-battery-technology-a-deep-dive](https://www.greencarreports.com/news/1117928_2018-nissan-leaf-battery-technology-a-deep-dive). [Accessed: 27-Jun-2020].
- [9] “BMS and contactor box - AEVA Forums.” [Online]. Available: <https://forums.aeva.asn.au/viewtopic.php?t=4278>. [Accessed: 27-Jun-2020].
- [10] “Bmw i3 bms | DIY Electric Car Forums.” [Online]. Available: <https://www.diyelectriccar.com/threads/bmw-i3-bms.198547/>. [Accessed: 01-Jul-2020].
- [11] “BMW i3 electric car battery balancing circuit (BMS) - Imgur.” [Online]. Available: <https://imgur.com/gallery/wdk7o/comment/1046244385>. [Accessed: 01-Jul-2020].
- [12] “Tesla Motors Begins Regular Production of 2008 Tesla Roadster | Tesla.” [Online]. Available: <https://www.tesla.com/blog/tesla-motors-begins-regular-production-2008-tesla-roadster>. [Accessed: 27-Jun-2020].
- [13] “A Bit About Batteries | Tesla.” [Online]. Available: <https://www.tesla.com/blog/bit-about-batteries>. [Accessed: 27-Jun-2020].
- [14] G. Berdichevsky, K. Kelty, J. B. Straubel, and E. Toomre, “The Tesla Roadster Battery System Tesla Motors,” 2007.
- [15] “Tesla Model S 90D (2016-2017) price and specifications - EV Database.” [Online]. Available: <https://ev-database.org/car/1063/Tesla-Model-S-90D>. [Accessed: 27-Jun-2020].
- [16] “Pics/Info: Inside the battery pack | Page 14 | Tesla Motors Club.” [Online]. Available: <https://teslamotorsclub.com/tmc/threads/pics-info-inside-the-battery-pack.34934/page-14#post-755546>. [Accessed: 27-Jun-2020].
- [17] “Tesla BMS Module - Front.jpg (6798×3415).” [Online]. Available:

- [http://files.wizkid057.com/teslapack/update2/Tesla BMS Module - Front.jpg](http://files.wizkid057.com/teslapack/update2/Tesla_BMS_Module_-_Front.jpg). [Accessed: 27-Jun-2020].
- [18] “Tesla Model 3 - NextGen Battery - EVT Motor Verks.” [Online]. Available: <http://evtv.me/2018/05/tesla-model-3-gone-battshit/>. [Accessed: 27-Jun-2020].
- [19] “LTC6813-1 18-Cell Battery Monitor with Daisy Chain Interface.” Analog Devices, pp. 1–86, 2019.
- [20] P. Hummel *et al.*, “Q - Series Tearing down the heart of an electric car: Can batteries provide an edge, and who wins?,” 2018.
- [21] “Tesla Model Y Battery Pack Is Different From Model 3: Check Out How It Differs.” [Online]. Available: <https://insideevs.com/news/414440/tesla-model-y-battery-different-model-3s/>. [Accessed: 01-Jul-2020].
- [22] I. Tsiropoulos, D. Tarvydas, and N. Lebedeva, “Li-ion batteries for mobility and stationary storage applications,” 2018.
- [23] H. Cui and G. Xiao, “Fuel-efficiency technology trend assessment for LDVs in China : Hybrids and electrification,” 2018.
- [24] G. Park, S. Lee, S. Kim, M. Jung, and H. Kang, “Automatic restarting methods of electric forklifts in the free running state,” in *2013 World Electric Vehicle Symposium and Exhibition (EVS27)*, 2013, pp. 1–8.
- [25] C. W. Seitz, “Industrial battery technologies and markets,” *IEEE Aerosp. Electron. Syst. Mag.*, vol. 9, no. 5, pp. 10–15, May 1994.
- [26] “E-Force One AG - EF26 KSF.” [Online]. Available: <https://www.eforce.ch/en/products/ef26-ksf>. [Accessed: 11-Jul-2020].
- [27] “BYD ELECTRIC VEHICLES.”
- [28] “8 electric truck and van companies to watch in 2020 | Greenbiz.” [Online]. Available: <https://www.greenbiz.com/article/8-electric-truck-and-van-companies-watch-2020>. [Accessed: 31-Jul-2020].
- [29] “2019 BYD 8TT - Cut Sheet 190306.” [Online]. Available: <https://www.californiahvip.org/wp-content/uploads/2019/07/2019-BYD-8TT-Cut-Sheet-190306.pdf>. [Accessed: 31-Jul-2020].
- [30] “BYD Europe.” [Online]. Available: <https://bydeurope.com/pdp-bus-coach>. [Accessed: 31-Jul-2020].
- [31] “Omnibus Magazine: The strategy for the battery – Mercedes-Benz Buses.” [Online]. Available: [https://www.mercedes-benz-bus.com/en\\_DE/brand/omnibus-magazin/ecitaro-battery-technology.html](https://www.mercedes-benz-bus.com/en_DE/brand/omnibus-magazin/ecitaro-battery-technology.html). [Accessed: 31-Jul-2020].
- [32] “Mercedes eCitaro, Daimler Buses puts the battery on its best seller. Story of the electric bus - Sustainable Bus.” [Online]. Available: <https://www.sustainable-bus.com/electric-bus/mercedes-ecitaro-daimler-buses-puts-the-battery-on-its-best-seller-story-of-the-electric-bus/>. [Accessed: 03-Aug-2020].
- [33] “OPPORTUNITY CHARGE M2 ELECTRIC MINIBUS.” [Online]. Available: [https://emobility.lv/wp-content/uploads/2017/10/Emobility\\_Bus\\_Buklets\\_2\\_Fin-1.pdf](https://emobility.lv/wp-content/uploads/2017/10/Emobility_Bus_Buklets_2_Fin-1.pdf). [Accessed: 21-Oct-2020].
- [34] European Commission, “Regulation (EU) No 168/2013 of the European Parliament,” pp. 0–112, 2019.
- [35] “The largest and most affordable Online E-Bike Battery Shop!” [Online]. Available:

- <https://hollandbikeshop.com/en-gb/bicycle-parts-electric-bicycle/e-bike-battery-parts/e-bike-battery/>. [Accessed: 17-Aug-2020].
- [36] “Batteries for EBikes – EbikeMarketplace.” [Online]. Available: <https://ebikemarketplace.com/collections/lithium-batteries>. [Accessed: 18-Aug-2020].
- [37] “The Battery Doctor - YouTube.” [Online]. Available: <https://www.youtube.com/channel/UCxgrR15ORCLx7JI2MKqnmWw/videos>. [Accessed: 21-Aug-2020].
- [38] “PCB/BMS/CMB/UPS.” [Online]. Available: <https://www.batteryspace.com/PCB/BMS/CMB/UPS.aspx>. [Accessed: 24-Aug-2020].
- [39] “Xiaomi M365 Battery Issues - Diagnose And Repair - YouTube.” [Online]. Available: <https://www.youtube.com/watch?v=uUEI9BMblfc>. [Accessed: 12-Oct-2020].
- [40] P. Kurzweil, “HISTORY | Secondary Batteries,” in *Encyclopedia of Electrochemical Power Sources*, Elsevier, 2009, pp. 565–578.
- [41] “Lithium-ion Battery Market Size and Share | Industry Analysis by 2027.” [Online]. Available: <https://www.alliedmarketresearch.com/lithium-ion-battery-market>. [Accessed: 19-Nov-2020].
- [42] C. A. Vincent, “Lithium batteries: A 50-year perspective, 1959-2009,” *Solid State Ionics*, vol. 134, no. 1–2, pp. 159–167, Oct. 2000.
- [43] Olof Ramström, “Scientific Background on the Nobel Prize in Chemistry 2019 LITHIUM-ION BATTERIES,” 2019.
- [44] C. Gustafsson, G. von Heijne, S. S. Linse, and the N. C. for Chemistry, “The Nobel Prize in Chemistry 2019: They developed the world’s most powerful battery,” *R. Swedish Acad. Sci.*, p. 8, 2019.
- [45] G.-A. Nazri and G. Pistoia, Eds., *Lithium Batteries*. Boston, MA: Springer US, 2003.
- [46] M. Yoshio, R. J. Brodd, and A. Kozawa, Eds., *Lithium-Ion Batteries*. New York, NY: Springer New York, 2009.
- [47] A. Bindra, “Electric Vehicle Batteries Eye Solid-State Technology: Prototypes Promise Lower Cost, Faster Charging, and Greater Safety,” *IEEE Power Electron. Mag.*, vol. 7, no. 1, pp. 16–19, Mar. 2020.
- [48] L. Zhou, W. Utetiwabo, R. Chen, and W. Yang, “Layer by Layer Assemble of Colloid Nanomaterial and Functional Multilayer Films for Energy Storage and Conversion,” in *Comprehensive Nanoscience and Nanotechnology*, Elsevier, 2019, pp. 255–278.
- [49] Y. Abu-Lebdeh and I. Davidson, Eds., *Nanotechnology for Lithium-Ion Batteries*. Boston, MA: Springer US, 2013.
- [50] I. Buchmann, *Batteries in a Portable World: A Handbook on Rechargeable Batteries for Non-Engineers*, 3rd editio. Cadex Electronics Inc., 2011.
- [51] O. Kyung Su, “INR18650 MJ1 Product Specification,” 2014.
- [52] “US18650VTC6,” 2015.
- [53] “A Behind the Scenes Take on Lithium-ion Battery Prices | BloombergNEF.” [Online]. Available: <https://about.bnef.com/blog/behind-scenes-take-lithium-ion-battery-prices/>. [Accessed: 04-Dec-2020].
- [54] “AMP20m1HD-A,” 2011.
- [55] “LT34 Power cell.”

- [56] “Lithium Ion Batteries Technical Handbook Japanese / International English,” vol. June. Panasonic, 2007.
- [57] W. Xie *et al.*, “Challenges and opportunities toward fast-charging of lithium-ion batteries,” *J. Energy Storage*, vol. 32, no. August, p. 101837, Dec. 2020.
- [58] Toshiba, “Toshiba SCiB™ Product catalouge,” no. July. Toshiba, 2017.
- [59] “Volkswagen e-Golf price and specifications - EV Database.” [Online]. Available: <https://ev-database.org/car/1087/Volkswagen-e-Golf>. [Accessed: 04-Dec-2020].
- [60] S. Gantenbein, M. Schönleber, M. Weiss, and E. Ivers-Tiffée, “Capacity Fade in Lithium-Ion Batteries and Cyclic Aging over Various State-of-Charge Ranges,” *Sustainability*, vol. 11, no. 23, p. 6697, Nov. 2019.
- [61] P. G. Balakrishnan, R. Ramesh, and T. Prem Kumar, “Safety mechanisms in lithium-ion batteries,” *J. Power Sources*, vol. 155, no. 2, pp. 401–414, Apr. 2006.
- [62] F. Leng, C. M. Tan, and M. Pecht, “Effect of Temperature on the Aging rate of Li Ion Battery Operating above Room Temperature,” *Sci. Rep.*, vol. 5, no. 1, p. 12967, Oct. 2015.
- [63] S. Xiang, G. Hu, R. Huang, F. Guo, and P. Zhou, “Lithium-Ion Battery Online Rapid State-of-Power Estimation under Multiple Constraints,” *Energies*, vol. 11, no. 2, p. 283, Jan. 2018.
- [64] J. D. Welsh, “A Comparison of Active and Passive Cell Balancing Techniques for Series / Parallel Battery Packs,” Ohio State University, 2009.
- [65] S. Moore and P. Schneider, “A Review of Cell Equalization Methods for Lithium Ion and Lithium Polymer Battery Systems,” in *SAE World Congress*, 2001, p. Doc. 2001-01-0959.
- [66] M. Daowd, N. Omar, P. Van Den Bossche, and J. Van Mierlo, “Passive and active battery balancing comparison based on MATLAB simulation,” in *2011 IEEE Vehicle Power and Propulsion Conference*, 2011, vol. 6, no. 7, pp. 1–7.
- [67] J. Gallardo-Lozano, E. Romero-Cadaval, M. I. Milanés-Montero, and M. A. Guerrero-Martinez, “Battery equalization active methods,” *J. Power Sources*, vol. 246, pp. 934–949, 2014.
- [68] J. Gallardo-Lozano, E. Romero-Cadaval, M. I. Milanés-Montero, and M. a. Guerrero-Martinez, “Battery Equalization Control Based on the Shunt Transistor Method,” *Electr. Control Commun. Eng.*, vol. 7, no. 1, 2014.
- [69] C. H. Kim, M. Y. Kim, H. S. Park, and G. W. Moon, “A modularized two-stage charge equalizer with cell selection switches for series-connected lithium-ion battery string in an HEV,” *IEEE Trans. Power Electron.*, vol. 27, no. 8, pp. 3764–3774, 2012.
- [70] J. Cao, N. Schofield, and A. Emadi, “Battery balancing methods: A comprehensive review,” in *2008 IEEE Vehicle Power and Propulsion Conference, VPPC 2008*, 2008, pp. 3–8.
- [71] J. Gallardo-Lozano, A. Lateef, E. Romero-Cadaval, and M. I. Milanés-Montero, “Active Battery Balancing for Battery Packs,” *Electr. Control Commun. Eng.*, vol. 2, no. 1, pp. 40–46, 2013.
- [72] A. Baughman and M. Ferdowsi, “Double-tiered capacitive shuttling method for balancing series-connected batteries,” in *2005 IEEE Vehicle Power and Propulsion Conference, VPPC*, 2005, vol. 2005, pp. 50–54.

- [73] Z. G. Kong, C. B. Zhu, R. G. Lu, and S. K. Cheng, "Comparison and evaluation of charge equalization technique for series connected batteries," in *PESC Record - IEEE Annual Power Electronics Specialists Conference*, 2006.
- [74] A. M. Imtiaz and F. H. Khan, "'Time shared flyback converter' based regenerative cell balancing technique for series connected li-ion battery strings," *IEEE Trans. Power Electron.*, vol. 28, no. 12, pp. 5960–5975, 2013.
- [75] M. J. Isaacson, R. P. Hollandsworth, P. J. Giampaoli, F. A. Linkowsky, A. Salim, and V. L. Teofilo, "Advanced lithium ion battery charger," in *Fifteenth Annual Battery Conference on Applications and Advances (Cat. No.00TH8490)*, 2000, pp. 193–198.
- [76] W. C. Lee, D. Drury, and P. Mellor, "Comparison of passive cell balancing and active cell balancing for automotive batteries," in *2011 IEEE Vehicle Power and Propulsion Conference, VPPC 2011*, 2011.
- [77] A. Affanni, A. Bellini, G. Franceschini, P. Guglielmi, and C. Tassoni, "Battery choice and management for new-generation electric vehicles," *IEEE Trans. Ind. Electron.*, vol. 52, no. 5, pp. 1343–1349, 2005.
- [78] V. L. Teofilo, L. V. Merritt, and R. P. Hollandsworth, "Advanced lithium ion battery charger," in *The Twelfth Annual Battery Conference on Applications and Advances*, 1997, pp. 227–231.
- [79] V. L. Teofilo, L. V. Merritt, and R. P. Hollandsworth, "Advanced lithium ion battery charger," *IEEE Aerosp. Electron. Syst. Mag.*, vol. 12, no. 11, pp. 30–36, 1997.
- [80] B. S. D. Letkeman, "A low cost Lithium Ion battery management system for a multi-cell , high voltage battery pack," 2008. [Online]. Available: [http://www.zanthic.com/images/A\\_low\\_cost\\_Lithium\\_Ion\\_battery\\_management\\_system.pdf](http://www.zanthic.com/images/A_low_cost_Lithium_Ion_battery_management_system.pdf). [Accessed: 01-Jan-2015].
- [81] S. Wen, "Cell balancing buys extra run time and battery life," *Analog Appl.*, pp. 14–18, 2009.
- [82] S. Munwaja, B. Tanboonjit, and N. H. Fuengwarodsakul, "Development of cell balancing algorithm for LiFePO4 battery in electric bicycles," in *2012 9th International Conference on Electrical Engineering/Electronics, Computer, Telecommunications and Information Technology*, 2012, pp. 1–4.
- [83] L. Hu, M. L. Zhao, X. B. Wu, and J. N. Lou, "Cell balancing management for battery pack," in *ICSICT-2010 - 2010 10th IEEE International Conference on Solid-State and Integrated Circuit Technology, Proceedings*, 2010, pp. 339–341.
- [84] J. Gallardo-lozano and E. Romero-cadaval, "A Battery Cell Balancing Method with Linear Mode Bypass Current Control," in *2014 14th Biennial Baltic Electronic Conference (BEC)*, 2014, pp. 245–248.
- [85] T. Kim, W. Qiao, and L. Qu, "Series-connected self-reconfigurable multicell battery," in *Conference Proceedings - IEEE Applied Power Electronics Conference and Exposition - APEC*, 2011, pp. 1382–1387.
- [86] A. Manenti, A. Abba, A. Merati, S. M. Savaresi, and A. Geraci, "A new BMS architecture based on cell redundancy," *IEEE Trans. Ind. Electron.*, vol. 58, no. 9, pp. 4314–4322, 2011.
- [87] T. Kim, W. Qiao, and L. Qu, "A series-connected self-reconfigurable multicell battery capable of safe and effective charging/discharging and balancing operations," in *Conference Proceedings - IEEE Applied Power Electronics Conference and Exposition*

- *APEC*, 2012, pp. 2259–2264.
- [88] H. Shibata *et al.*, “Management of serially-connected battery system using multiple switches,” in *4th IEEE International Conference on Power Electronics and Drive Systems. IEEE PEDS 2001 - Indonesia. Proceedings (Cat. No.01TH8594)*, 2001, vol. 2, pp. 508–511.
- [89] F. Baronti, G. Fantechi, R. Roncella, and R. Saletti, “Design of a module switch for battery pack reconfiguration in high-power applications,” *IEEE Int. Symp. Ind. Electron.*, pp. 1330–1335, 2012.
- [90] E. Chatzinikolaou and D. J. Rogers, “Cell SoC Balancing Using a Cascaded Full-Bridge Multilevel Converter in Battery Energy Storage Systems,” *IEEE Trans. Ind. Electron.*, vol. 63, no. 9, pp. 5394–5402, Sep. 2016.
- [91] C. M. Young, N. Y. Chu, L. R. Chen, Y. C. Hsiao, and C. Z. Li, “A Single-phase multilevel inverter with battery balancing,” *IEEE Trans. Ind. Electron.*, vol. 60, no. 5, pp. 1972–1978, 2013.
- [92] S. D’Arco, L. Piegari, and P. Tricoli, “A modular converter with embedded battery cell balancing for electric vehicles,” in *Electrical Systems for Aircraft, Railway and Ship Propulsion, ESARS*, 2012.
- [93] F. Altaf, L. Johannesson, and B. Egardt, “Performance evaluation of Multilevel Converter based cell balancer with reciprocating air flow,” in *2012 IEEE Vehicle Power and Propulsion Conference, VPPC 2012*, 2012, pp. 706–713.
- [94] A. Gholizad and M. Farsadi, “A Novel State-of-Charge Balancing Method Using Improved Staircase Modulation of Multilevel Inverters,” *IEEE Trans. Ind. Electron.*, vol. 63, no. 10, pp. 6107–6114, Oct. 2016.
- [95] S. Chakraborty, A. K. Jain, and N. Mohan, “Novel converter topology and algorithm for simultaneous charging and individual cell balancing of multiple Li-ion batteries,” in *INTELEC 2004. 26th Annual International Telecommunications Energy Conference*, 2004.
- [96] S. Chakraborty and N. Mohan, “A comparative study of various single stage PFC converters in implementing novel converter topology for simultaneous charging and individual cell balancing of multiple Li-ion batteries,” in *INTELEC, International Telecommunications Energy Conference (Proceedings)*, 2005, pp. 251–256.
- [97] M. Y. Kim, C. H. Kim, J. H. Kim, D. Y. Kim, and G. W. Moon, “Switched capacitor with chain structure for cell-balancing of lithium-ion batteries,” in *IECON Proceedings (Industrial Electronics Conference)*, 2012, pp. 2994–2999.
- [98] J. Jang, J. Nam, and J. Yoo, “Cell balancing circuit implementation with DC/DC converters using super capacitor equivalent circuit parameters,” in *VPPC 2007 - Proceedings of the 2007 IEEE Vehicle Power and Propulsion Conference*, 2007, pp. 646–653.
- [99] F. Baronti, G. Fantechi, R. Roncella, and R. Saletti, “High-efficiency digitally controlled charge equalizer for series-connected cells based on switching converter and super-capacitor,” *IEEE Trans. Ind. Informatics*, vol. 9, no. 2, pp. 1139–1147, 2013.
- [100] Z. Nie and C. Mi, “Fast battery equalization with isolated bidirectional DC-DC converter for PHEV applications,” in *5th IEEE Vehicle Power and Propulsion Conference, VPPC '09*, 2009, pp. 78–81.
- [101] D. B. W. Abeywardana, M. a M. Manaz, M. G. C. P. Mediwaththe, and K. M. Liyanage,

- “Improved shared transformer cell balancing of Li-ion batteries,” in *2012 IEEE 7th International Conference on Industrial and Information Systems, ICIIIS 2012*, 2012.
- [102] Y. Barsukov, “Battery cell balancing: what to balance and how,” *Texas Instruments*, 2005. [Online]. Available: [http://focus.ti.com/download/trng/docs/seminar/Topic 2 - Battery Cell Balancing - What to Balance and How.pdf](http://focus.ti.com/download/trng/docs/seminar/Topic_2_-_Battery_Cell_Balancing_-_What_to_Balance_and_How.pdf). [Accessed: 01-Jan-2015].
- [103] C. Pascual and P. T. Krein, “Switched capacitor system for automatic series battery equalization,” in *Proceedings of APEC 97 - Applied Power Electronics Conference*, 1997, vol. 2, no. c, pp. 848–854.
- [104] Y. C. Hsieh, Z. X. Cai, and W. Z. Wu, “Switched-capacitor charge equalization circuit for series-connected batteries,” in *2014 International Power Electronics Conference, IPEC-Hiroshima - ECCE Asia 2014*, 2014, pp. 429–432.
- [105] A. Baughman and M. Ferdowsi, “Analysis of the double-tiered three-battery switched capacitor battery balancing system,” in *2006 IEEE Vehicle Power and Propulsion Conference, VPPC 2006*, 2006.
- [106] A. C. Baughman and M. Ferdowsi, “Double-tiered switched-capacitor battery charge equalization technique,” *IEEE Trans. Ind. Electron.*, vol. 55, no. 6, pp. 2277–2285, 2008.
- [107] H. S. Park, C. H. Kim, and G. W. Moon, “Charge equalizer design method based on battery modularization,” in *2008 IEEE International Conference on Sustainable Energy Technologies, ICSET 2008*, 2008, pp. 558–563.
- [108] Hong-Sun Park, Chol-Ho Kim, Ki-Bum Park, Gun-Woo Moon, and Joong-Hui Lee, “Design of a Charge Equalizer Based on Battery Modularization,” *IEEE Trans. Veh. Technol.*, vol. 58, no. 7, pp. 3216–3223, Sep. 2009.
- [109] M. Daowd, N. Omar, P. van den Bossche, and J. van Mierlo, “A review of passive and active battery balancing based on MATLAB/Simulink,” *Int. Rev. Electr. Eng.*, vol. 6, no. 7, pp. 2974–2989, 2011.
- [110] Y.-S. Lee and M.-W. Cheng, “Intelligent Control Battery Equalization for Series Connected Lithium-Ion Battery Strings,” *IEEE Trans. Ind. Electron.*, vol. 52, no. 5, pp. 1297–1307, 2005.
- [111] Y.-S. L. Y.-S. Lee, M.-W. C. M.-W. Chen, K.-L. H. K.-L. Hsu, J.-Y. D. J.-Y. Du, and C.-F. C. C.-F. Chuang, “Cell equalization scheme with energy transferring capacitance for series connected battery strings,” in *2002 IEEE Region 10 Conference on Computers, Communications, Control and Power Engineering. TENCOM '02. Proceedings.*, 2002, vol. 3, pp. 2042–2045.
- [112] Y.-S. L. Y.-S. Lee and C.-W. J. C.-W. Jao, “Fuzzy controlled lithium-ion battery equalization with state-of-charge estimator,” in *SMC'03 Conference Proceedings. 2003 IEEE International Conference on Systems, Man and Cybernetics. Conference Theme - System Security and Assurance (Cat. No.03CH37483)*, 2003, vol. 5, pp. 4431–4438.
- [113] M. Borne and S. Wen, “Power up your battery design with cell balancing,” *EE Times-Asia*, pp. 1–5, 2009.
- [114] J. Moran, “PowerPump™ Balancing,” 2011.
- [115] T. H. Phung, J.-C. Crebier, A. Chureau, A. Collet, and V. Nguyen, “Optimized structure for next-to-next balancing of series-connected lithium-ion cells,” in *2011 Twenty-Sixth Annual IEEE Applied Power Electronics Conference and Exposition (APEC)*, 2011, vol. 29, no. 9, pp. 1374–1381.
- [116] D. Lewis, “Bidirectional current pump for battery charge balancing,” US5631534, 1997.

- [117] N. H. Kutkut and D. M. Divan, "Dynamic equalization techniques for series battery stacks," in *International Telecommunications Energy Conference*, 1996, pp. 514–521.
- [118] A. Stanislav and R. pod Radhoštem, "Active Cell Balancing in Battery Packs," 2012.
- [119] T. H. Phung, A. Collet, and J. C. Crebier, "An optimized topology for next-to-next balancing of series-connected lithium-ion cells," *IEEE Trans. Power Electron.*, vol. 29, no. 9, pp. 4603–4613, 2014.
- [120] F. Mestrallet, L. Kerachev, J. C. Crebier, and A. Collet, "Multiphase interleaved converter for lithium battery active balancing," *IEEE Trans. Power Electron.*, vol. 29, no. 6, pp. 2874–2881, 2014.
- [121] X. Lu, W. Qian, and F. Z. Peng, "Modularized buck-boost + Cuk converter for high voltage series connected battery cells," in *Conference Proceedings - IEEE Applied Power Electronics Conference and Exposition - APEC*, 2012, pp. 2272–2278.
- [122] Y. S. Lee and G. T. Cheng, "Quasi-resonant zero-current-switching bidirectional converter for battery equalization applications," *IEEE Trans. Power Electron.*, vol. 21, no. 5, pp. 1213–1224, 2006.
- [123] C. H. Lin, H. Y. Chao, C. M. Wang, and M. H. Hung, "Battery management system with dual-balancing mechanism for LiFePO<sub>4</sub> battery module," in *IEEE Region 10 Annual International Conference, Proceedings/TENCON*, 2011, pp. 863–867.
- [124] Y. C. Hsieh, C. S. Moo, I. S. Tsai, and J. C. Cheng, "Dynamic charge equalization for series-connected batteries," in *Proceedings of the IEEE International Conference on Industrial Technology*, 2002, vol. 1, pp. 444–449.
- [125] C. S. Moo, Y. C. Hsieh, and I. S. Tsai, "Charge equalization for series-connected batteries," *IEEE Trans. Aerosp. Electron. Syst.*, vol. 39, no. 2, pp. 704–710, Apr. 2003.
- [126] C. S. Moo, Y. C. Hsieh, I. S. Tsai, and J. C. Cheng, "Dynamic charge equalisation for series-connected batteries," *IEE Proc. - Electr. Power Appl.*, vol. 150, no. 5, p. 501, 2003.
- [127] S. H. Park, T. S. Kim, J. S. Park, G. W. Moon, and M. J. Yoon, "A new battery equalizer based on buck-boost topology," in *7th International Conference on Power Electronics, ICPE '07*, 2008, pp. 962–965.
- [128] S. H. Park, T. S. Kim, J. S. Park, G. W. Moon, and M. J. Yoon, "A new buck-boost type battery equalizer," in *Conference Proceedings - IEEE Applied Power Electronics Conference and Exposition - APEC*, 2009, pp. 1246–1250.
- [129] J. Reynaud, C. Carrejo, O. Gantet, and P. Aloïsi, "Active balancing circuit for advanced lithium-ion batteries used in photovoltaic application," in *International Conference on Renewable Energies and Power Quality - ICREPQ11*, 2010.
- [130] J. H. Gao, L. F. Jia, Y. Y. Li, and J. Tang, "The design of a non-energy-consuming balance system for lithium-ion batteries," in *Proceedings - International Conference on Electrical and Control Engineering, ICECE 2010*, 2010, pp. 4403–4405.
- [131] M. Uno and K. Tanaka, "Single-switch equalization charger using multi-stacked buck-boost converters for series-connected energy storage cells," in *Power Electronics and ECCE Asia (ICPE & ECCE), 2011 IEEE 8th International Conference on*, 2011, pp. 2990–2996.
- [132] M. Uno and K. Tanaka, "Single-switch constant-power equalization charger based on multi-stacked buck-boost converters for series-connected supercapacitors in satellite power systems," in *2011 IEEE Ninth International Conference on Power Electronics*

- and Drive Systems*, 2011, no. December, pp. 1158–1165.
- [133] M. Uno and K. Tanaka, “Single-Switch Multioutput Charger Using Voltage Multiplier for Series-Connected Lithium-Ion Battery/Supercapacitor Equalization,” *IEEE Trans. Ind. Electron.*, vol. 60, no. 8, pp. 3227–3239, Aug. 2013.
- [134] M. Uno and K. Tanaka, “Single-switch single-inductor equalization charger using a voltage multiplier for series-connected energy storage modules,” in *8th International Conference on Power Electronics - ECCE Asia*, 2011, pp. 2985–2989.
- [135] M. Uno and A. Kukita, “Double-switch single-inductor resonant cell equalizer using voltage multiplier for series-connected supercapacitors,” in *Conference Proceedings - 2012 IEEE 7th International Power Electronics and Motion Control Conference - ECCE Asia, IPEMC 2012*, 2012, vol. 3, pp. 1990–1997.
- [136] M. Uno and A. Kukita, “Single-Switch Single-Transformer Cell Voltage Equalizer Based on Forward-Flyback Resonant Inverter and Voltage Multiplier for Series-Connected Energy Storage Cells,” *IEEE Trans. Veh. Technol.*, vol. 63, no. 9, pp. 4232–4247, Nov. 2014.
- [137] M. Uno and A. Kukita, “Single-switch equalization charger integrating SEPIC and equalizer using series-resonant voltage multiplier for series-connected energy storage cells/modules,” in *2013 IEEE ECCE Asia Downunder*, 2013, pp. 297–303.
- [138] C. H. Kim, Y. Do Kim, G. W. Moon, and H. S. Park, “Individual cell voltage equalizer using selective two current paths for series connected li-ion battery strings,” in *2009 IEEE Energy Conversion Congress and Exposition, ECCE 2009*, 2009, pp. 1812–1817.
- [139] C. H. Kim, M. Y. Kim, and G. W. Moon, “A modularized charge equalizer using a battery monitoring ic for series-connected li-ion battery strings in electric vehicles,” *IEEE Trans. Power Electron.*, vol. 28, no. 8, pp. 3779–3787, 2013.
- [140] A. M. Imtiaz, F. H. Khan, and H. Kamath, “A low-cost time shared cell balancing technique for future lithium-ion battery storage system featuring regenerative energy distribution,” in *Conference Proceedings - IEEE Applied Power Electronics Conference and Exposition - APEC*, 2011, pp. 792–799.
- [141] M. Y. Kim, J. W. Kim, C. H. Kim, S. Y. Cho, and G. W. Moon, “Automatic charge equalization circuit based on regulated voltage source for series connected lithium-ion batteries,” in *8th International Conference on Power Electronics - ECCE Asia: “Green World with Power Electronics”, ICPE 2011-ECCE Asia*, 2011, pp. 2248–2255.
- [142] M. Y. Kim, C. H. Kim, J. H. Kim, and G. W. Moon, “A modularized BMS with an active cell balancing circuit for lithium-ion batteries in V2G system,” in *2012 IEEE Vehicle Power and Propulsion Conference, VPPC 2012*, 2012, pp. 401–406.
- [143] H. S. Park, C. E. Kim, G. W. Moon, J. H. Lee, and J. K. Oh, “Two-stage cell balancing scheme for hybrid electric vehicle lithium-ion battery strings,” in *PESC Record - IEEE Annual Power Electronics Specialists Conference*, 2007, pp. 273–279.
- [144] Y.-N. Chang, Y.-S. Shen, H.-L. Cheng, and S.-Y. Chan, “Design of active balance circuit for lithium battery pack,” in *Future Energy Electronics Conference (IFEEEC), 2013 1st International*, 2013, pp. 109–114.
- [145] H. S. Park, C. E. Kim, C. H. Kim, G. W. Moon, and J. H. Lee, “A modularized charge equalizer for an HEV lithium-ion battery string,” *IEEE Trans. Ind. Electron.*, vol. 56, no. 5, pp. 1464–1476, 2009.
- [146] H. S. Park, C. E. Kim, G. W. Moon, J. H. Lee, and J. K. Oh, “Charge equalization with

- series coupling of multiple primary windings for hybrid electric vehicle Li-Ion battery system,” in *PESC Record - IEEE Annual Power Electronics Specialists Conference*, 2007, pp. 266–272.
- [147] C. H. Kim, M. Y. Kim, and G. W. Moon, “Individual cell equalizer using active-clamp flyback converter for Li-ion battery strings in an electric vehicle,” in *2012 IEEE Vehicle Power and Propulsion Conference, VPPC 2012*, 2012, pp. 327–332.
- [148] R. H. Park, “Method of equalizing the voltages of the individual cells of storage batteries,” US4331911, 1982.
- [149] H. L. W. Deepakraj M. Divan, Nasser H. Kutkut, Donald W. Novotny, “Battery charging using a transformer with a single primary winding and plural secondary windings.pdf,” 5659237, 1997.
- [150] N. H. Kutkut, D. M. Divan, and D. W. Novotny, “Charge Equalization for Series Connected Battery Strings,” *IEEE Trans. Ind. Appl.*, vol. 31, no. 3, pp. 562–568, 1995.
- [151] N. H. Kutkut, H. L. N. Wiegman, D. M. Divan, and D. W. Novotny, “Design considerations for charge equalization of an electric vehicle battery system,” *IEEE Trans. Ind. Appl.*, vol. 35, no. 1, pp. 28–35, 1999.
- [152] N. H. Kutkut, H. L. N. Wiegman, D. M. Divan, and D. W. Novotny, “Design considerations for charge equalization of an electric vehicle battery system,” in *Proceedings of 1995 IEEE Applied Power Electronics Conference and Exposition - APEC’95*, 1995, vol. 35, no. 1, pp. 96–103.
- [153] C.-C. Hua, Y.-H. Fang, and P.-H. Li, “Charge equalisation for series-connected LiFePO<sub>4</sub> battery strings,” *IET Power Electron.*, vol. 8, no. 6, pp. 1017–1025, 2015.
- [154] M. Y. Kim, C. H. Kim, S. Y. Cho, and G. W. Moon, “A cell selective charge equalizer using multi-output converter with auxiliary transformer,” in *8th International Conference on Power Electronics - ECCE Asia: “Green World with Power Electronics”, ICPE 2011-ECCE Asia*, 2011, pp. 310–317.
- [155] T. Gottwald, Z. Ye, and T. Stuart, “Equalization of EV and HEV batteries with a ramp converter,” *IEEE Trans. Aerosp. Electron. Syst.*, vol. 33, no. 1, pp. 307–312, 1997.
- [156] T. Gottwald, Z. Ye, and T. Stuart, “Equalization of EV and HEV batteries with a ramp converter,” *IEEE Trans. Aerosp. Electron. Syst.*, vol. 33, no. 1, pp. 307–312, 1997.
- [157] M. Tang and T. Stuart, “Selective buck-boost equalizer for series battery packs,” *IEEE Trans. Aerosp. Electron. Syst.*, vol. 36, no. 1, pp. 201–211, 2000.
- [158] Z. Ye and T. A. Stuart, “Sensitivity of a ramp equalizer for series batteries,” *IEEE Trans. Aerosp. Electron. Syst.*, vol. 34, no. 4, pp. 1227–1236, 1998.
- [159] C.-C. Hua and Y.-H. Fang, “Design of a charge equalizer based on multi-winding transformer,” in *2014 International Conference on Information Science, Electronics and Electrical Engineering*, 2014, vol. 58, no. 7, pp. 446–449.
- [160] Y.-C. Hsieh, J.-L. Wu, and X.-H. Chen, “Class-E-based charge-equalisation circuit for battery cells,” *IET Power Electron.*, vol. 5, no. 7, p. 978, 2012.
- [161] C.-C. Hua, Y.-L. Chen, and Y.-H. Fang, “Modified rectifications for improving the charge equalisation performance of series-connected battery stack,” *IET Power Electron.*, vol. 9, no. 9, pp. 1924–1932, 2016.
- [162] C. Bonfiglio and W. Roessler, “A cost optimized battery management system with active cell balancing for lithium ion battery stacks,” in *5th IEEE Vehicle Power and Propulsion*

- Conference, *VPPC '09*, 2009, pp. 304–309.
- [163] M. Einhorn, W. Roessler, and J. Fleig, “Improved performance of serially connected Li-ion batteries with active cell balancing in electric vehicles,” *IEEE Trans. Veh. Technol.*, vol. 60, no. 6, pp. 2448–2457, 2011.
- [164] S. Hanxin, Z. Wenlong, and C. Wenxiang, “Charge equalization for series connected lithium-ion batteries,” in *ICEMI 2009 - Proceedings of 9th International Conference on Electronic Measurement and Instruments*, 2009, pp. 41032–41037.
- [165] S. Li, C. Mi, and M. Zhang, “A high efficiency low cost direct battery balancing circuit using a multi-winding transformer with reduced switch count,” in *Conference Proceedings - IEEE Applied Power Electronics Conference and Exposition - APEC*, 2012, pp. 2128–2133.
- [166] S. H. Park, K. B. Park, H. S. Kim, G. W. Moon, and M. J. Youn, “Cell-to-cell charge equalization converter using multi-winding transformer with reduced number of windings,” in *8th International Conference on Power Electronics - ECCE Asia: “Green World with Power Electronics”, ICPE 2011-ECCE Asia*, 2011, pp. 285–290.
- [167] T. H. Kim, N. J. Park, R. Y. Kim, and D. S. Hyun, “A high efficiency zero voltage-zero current transition converter for battery cell equalization,” in *Conference Proceedings - IEEE Applied Power Electronics Conference and Exposition - APEC*, 2012, pp. 2590–2595.
- [168] Tae-Hoon Kim, Nam-Ju Park, Rae-Young Kim, and Dong-Seok Hyun, “Low cost multiple zero voltage/zero current switching battery equalization circuit with single soft-switching resonant cell,” in *2012 IEEE Vehicle Power and Propulsion Conference*, 2012, pp. 419–424.
- [169] J. Ewanchuk, D. Yague, and J. Salmon, “A modular balancing bridge for series connected Li-ion batteries,” in *2011 IEEE Energy Conversion Congress and Exposition*, 2011, pp. 2908–2915.
- [170] J. Ewanchuk and J. Salmon, “A modular balancing bridge for series connected voltage sources,” *IEEE Trans. Power Electron.*, vol. 29, no. 9, pp. 4712–4722, 2014.
- [171] A. Tavakoli, S. A. Khajehoodin, and J. Salmon, “Switching pattern of a modular voltage balancing circuit for battery cells,” *ECCE 2016 - IEEE Energy Convers. Congr. Expo. Proc.*, pp. 1–8, 2016.
- [172] A. Tavakoli, I. Smith, S. A. Khajehoodin, and J. Salmon, “Performance comparison of two controllers for a modular voltage balancing circuit,” *Conf. Proc. - IEEE Appl. Power Electron. Conf. Expo. - APEC*, pp. 1667–1674, 2017.
- [173] A. Tavakoli, S. Ali Khajehoddin, and J. Salmon, “Control and Analysis of a Modular Bridge for Battery Cell Voltage Balancing,” *IEEE Trans. Power Electron.*, vol. 33, no. 11, pp. 9722–9733, 2018.
- [174] B. T. Kuhn, G. E. Pitel, and P. T. Krein, “Electrical properties and equalization of lithium-ion cells in automotive applications,” in *2005 IEEE Vehicle Power and Propulsion Conference, VPPC*, 2005, vol. 2005, pp. 55–59.
- [175] Samsung, “INR18650-35E.” Samsung SDI, 2015.
- [176] “(No Title).” [Online]. Available: <https://shop.gwl.eu/docs/pdf/Winston-OperatorManual.pdf>. [Accessed: 17-Dec-2020].
- [177] “Types of Lithium-ion Batteries – Battery University.” [Online]. Available: [https://batteryuniversity.com/index.php/learn/article/types\\_of\\_lithium\\_ion](https://batteryuniversity.com/index.php/learn/article/types_of_lithium_ion). [Accessed:

- 17-Dec-2020].
- [178] “Shenzhen Smart Lion Power Battery Limited.” [Online]. Available: [http://en.winston-battery.com/index.php/products/power-battery/item/wb-lyp40aha?category\\_id=182](http://en.winston-battery.com/index.php/products/power-battery/item/wb-lyp40aha?category_id=182). [Accessed: 10-Dec-2020].
- [179] A. Cuadras and O. Kanoun, “SoC Li-ion battery monitoring with impedance spectroscopy,” in *2009 6th International Multi-Conference on Systems, Signals and Devices*, 2009, pp. 1–5.
- [180] B. G. Carkhuff, P. A. Demirev, and R. Srinivasan, “Impedance-Based Battery Management System for Safety Monitoring of Lithium-Ion Batteries,” *IEEE Trans. Ind. Electron.*, vol. 65, no. 8, pp. 6497–6504, 2018.
- [181] Panasonic, “Specifications for NCR18650GA.” Panasonic.
- [182] H. Wang, K. Dong, G. Li, and F. Wu, “Research on the consistency of the power battery based on multi-points impedance spectrum,” *2010 Int. Forum Strateg. Technol. IFOST 2010*, pp. 1–4, 2010.
- [183] Z. Xia and J. A. A. Qahouq, “An online battery impedance spectrum measurement method with increased frequency resolution,” *Conf. Proc. - IEEE Appl. Power Electron. Conf. Expo. - APEC*, vol. 2018-March, no. 1, pp. 1930–1933, 2018.
- [184] W. Zhang, L. Jiao, and X. Zhang, “An Online Fast Battery Impedance Measurement Method,” *Proc. - 2018 IEEE Int. Power Electron. Appl. Conf. Expo. PEAC 2018*, pp. 1–3, 2018.
- [185] Thanh-Tuan Nguyen, Van-Long Tran, and Woojin Choi, “Development of the intelligent charger with battery State-Of-Health estimation using online impedance spectroscopy,” in *2014 IEEE 23rd International Symposium on Industrial Electronics (ISIE)*, 2014, pp. 454–458.
- [186] Y. F. Pulido, C. Blanco, D. Ansean, M. Gonzalez, J. C. Viera, and V. M. Garcia, “Effect of aging on C/LFP battery impedance: Operating conditions to which the impedance has minimal variations,” in *2017 IEEE International Conference on Environment and Electrical Engineering and 2017 IEEE Industrial and Commercial Power Systems Europe (EEEIC / I&CPS Europe)*, 2017, vol. 7, pp. 1–5.
- [187] D. A. Howey, V. Yufit, P. D. Mitcheson, G. J. Offer, and N. P. Brandon, “Impedance measurement for advanced battery management systems,” *2013 World Electr. Veh. Symp. Exhib. EVS 2014*, pp. 1–7, 2014.
- [188] R. Hasan and J. Scott, “Impedance Measurement of Batteries under load,” pp. 1–5, 2019.
- [189] L. Zhao, Q. Fu, and Z. Liu, “An electrochemical impedance spectroscopy measurement system for electric vehicle batteries,” *Chinese Control Conf. CCC*, vol. 2016-Augus, pp. 5050–5055, 2016.
- [190] Z. Xia and J. A. Abu Qahouq, “Adaptive and Fast State of Health Estimation Method for Lithium-ion Batteries Using Online Complex Impedance and Artificial Neural Network,” in *2019 IEEE Applied Power Electronics Conference and Exposition (APEC)*, 2019, vol. 2019-March, pp. 3361–3365.
- [191] R. Koch, R. Kuhn, I. Zilberman, and A. Jossen, “Electrochemical impedance spectroscopy for online battery monitoring - Power electronics control,” *2014 16th Eur. Conf. Power Electron. Appl. EPE-ECCE Eur. 2014*, 2014.
- [192] A. Christensen and A. Adebuisoyi, “Using on-board electrochemical impedance spectroscopy in battery management systems,” in *2013 World Electric Vehicle*

- Symposium and Exhibition (EVS27)*, 2013, vol. 6, no. 3, pp. 1–7.
- [193] K. Vitols, E. Grinfogels, and D. Nikonorovs, “Cell Capacity Dispersion Analysis Based Battery Pack Design,” in *2018 6th IEEE Workshop on Advances in Information, Electronic and Electrical Engineering (AIEEE)*, 2018, no. 1, pp. 1–5.
- [194] P.-C. Chen and Y.-F. Koh, “Residual traveling distance estimation of an electric wheelchair,” in *2012 5th International Conference on BioMedical Engineering and Informatics*, 2012, no. Bmei, pp. 790–794.
- [195] R. Hou, X. Shi, and M. Krishnamurthy, “Design and implementation of a novel power assisted drivetrain for a wheelchair,” in *2012 IEEE Transportation Electrification Conference and Expo (ITEC)*, 2012, pp. 1–6.
- [196] Y.-P. Yang, H.-C. Lin, F.-C. Tsai, C.-T. Lu, and K.-H. Tu, “Design and integration of dual power wheels with rim motors for a powered wheelchair,” *IET Electr. Power Appl.*, vol. 6, no. 7, p. 419, Dec. 2012.
- [197] M. Vorobyov and I. Galkin, “Development and optimization of adjustable vibration source for investigation of prosthesis-to-human feedback of intellectual artificial limb,” in *2014 IEEE 2nd Workshop on Advances in Information, Electronic and Electrical Engineering (AIEEE)*, 2014, vol. 21, pp. 1–4.
- [198] “1800wheelchair.com.” [Online]. Available: [www.1800wheelchair.com](http://www.1800wheelchair.com). [Accessed: 01-Jan-2017].
- [199] “Betterlife from Lloyds Pharmacy.” [Online]. Available: <http://www.betterlifehealthcare.com>.
- [200] “ALTER AL.” [Online]. Available: <http://www.alteral.lv/>.
- [201] A. Di Napoli and A. Ndokaj, “Auxiliary power buffer based on ultracapacitors,” in *SPEEDAM 2012 - 21st International Symposium on Power Electronics, Electrical Drives, Automation and Motion*, 2012, pp. 759–763.
- [202] R. a. Cooper and Changfeng Tai, “Feasibility of flywheel batteries for electric powered wheelchairs,” in *Proceedings of the 20th Annual International Conference of the IEEE Engineering in Medicine and Biology Society. Vol.20 Biomedical Engineering Towards the Year 2000 and Beyond (Cat. No.98CH36286)*, 1998, vol. 5, no. 5, pp. 2261–2263.
- [203] J. H. Aylor, A. Thieme, and B. W. Johnson, “A Battery State-of-Charge Indicator for Electric Wheelchairs,” *IEEE Trans. Ind. Electron.*, vol. 39, no. 5, pp. 398–409, 1992.
- [204] G. Zaleskis, V. Brazis, and L. Latkovskis, “Estimation of Traction Drive Test Bench with Energy Storage System Operation in Regenerative Braking Mode,” *Electr. Control Commun. Eng.*, vol. 1, no. 1, pp. 40–45, 2012.
- [205] R. Rahulanker and V. Ramanarayanan, “Battery assisted wheel chair,” in *Proceedings of India International Conference on Power Electronics, IICPE 2006*, 2006, no. 3, pp. 167–171.
- [206] K. Vitols and A. Podgornovs, “Concept of cost-effective power-assist wheelchair’s electrical subsystem,” in *2017 5th IEEE Workshop on Advances in Information, Electronic and Electrical Engineering (AIEEE)*, 2017, pp. 1–4.
- [207] “Home page | NKON.” [Online]. Available: <https://eu.nkon.nl/>. [Accessed: 20-Dec-2021].
- [208] “akkuteile.de.” [Online]. Available: <https://www.akkuteile.de/>. [Accessed: 20-Dec-2021].

- [209] N. Hanini, B. Tabbache, A. Kheloui, and T. Roubache, "Sizing methodology of EV drive system based on optimal power efficiency," in *2008 International Symposium on Power Electronics, Electrical Drives, Automation and Motion*, 2008, pp. 1043–1048.
- [210] A. M. Omara and M. A. Sleptsov, "Efficient electric traction drive configuration for battery electric vehicles," in *2017 International Conference on Industrial Engineering, Applications and Manufacturing (ICIEAM)*, 2017, no. 1, pp. 1–5.
- [211] I. P. Kopilov, *Design of Electrical Machines*, 4th ed. Yurayt-Izdat, 2011.
- [212] P. Salminen, J. Pyrhonen, H. Jussila, and M. Niemela, "Concentrated Wound Permanent Magnet Machines with Different Rotor Designs," in *2007 International Conference on Power Engineering, Energy and Electrical Drives*, 2007, pp. 514–517.
- [213] V. A. Lifanov, "Calculation of low-power electric machines with excitation from permanent magnets." Publishing Center, Chelyabinsk, p. 164, 2010.
- [214] D. Graovac, M. Pürschel, and A. Kiep, "MOSFET Power Losses Calculation Using the Datasheet Parameters," no. July. Infineon, pp. 1–23, 2006.
- [215] Vishay, "Power MOSFET Basics: Understanding Gate Charge and Using it to Assess Switching Performance." Vishay Siliconix, Malvern, p. 6, 2016.
- [216] G. Lakkas, "MOSFET power losses and how they affect power-supply efficiency," *Analog Appl. J.*, vol. 1, pp. 22–26, 2016.
- [217] I. Galkin, A. Blinov, I. Verbytskyi, and D. Zinchenko, "Modular Self-Balancing Battery Charger Concept for Cost-Effective Power-Assist Wheelchairs," *Energies*, vol. 12, no. 8, p. 1526, Apr. 2019.
- [218] *ISO 7176-25:2013*, vol. 2013. International Organization for Standardization, 2013.
- [219] K. Vitols, "Design considerations of a battery pack - DC grid interface converter," in *2015 IEEE 5th International Conference on Power Engineering, Energy and Electrical Drives (POWERENG)*, 2015, vol. 2015-Septe, pp. 476–479.
- [220] "Interfacing MSP430™ MCUs With MMC or SD Flash Memory Cards Application Report Interfacing MSP430™ MCUs With MMC or SD Flash Memory Cards," 2005.